Contents

CAPACITANCE BASED STUDIES OF DEFECTS IN DEEP BURIED LAYERS PRODUCED BY MeV HEAVY IONS IN SILICON

by

PRAVAT KUMAR GIRI

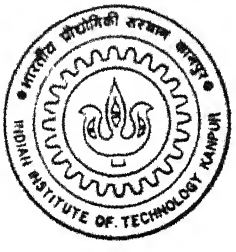

DEPARTMENT OF PHYSICS

Indian Institute of Technology Kanpur

OCTOBER, 1997

CAPACITANCE BASED STUDIES OF DEFECTS IN DEEP BURIED LAYERS PRODUCED BY MeV HEAVY IONS IN SILICON

A Thesis Submitted
in Partial Fulfilment of the Requirements
for the Degree of
DOCTOR OF PHILOSOPHY

by
PRAVAT KUMAR GIRI

to the

DEPARTMENT OF PHYSICS

Indian Institute of Technology Kanpur

OCTOBER, 1997

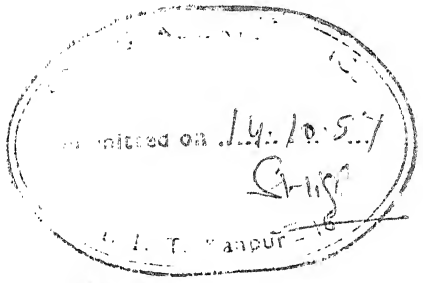

CERTIFICATE

It is certified that the work contained in the thesis entitled **Capacitance based studies of defects in deep buried layers produced by MeV heavy ions in silicon** *by* **Mr. Pravat Kumar Giri**, has been carried out under my supervision and has not been submitted elsewhere for a degree.

October, 1997

Dr. Y.N. Mohapatra
Department of Physics
Indian Instutute of Technology
Kanpur

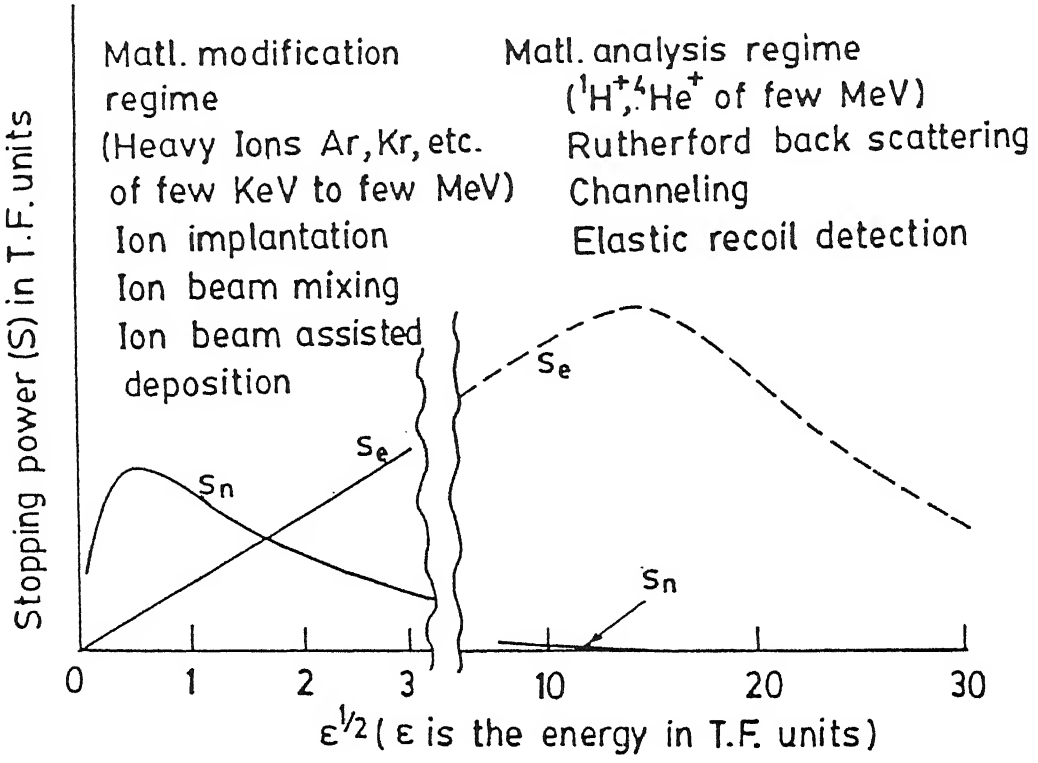

Figure 1.1: Universal stopping power vs. ion energy plot in solid in Thomson-Fermi (T.F.) unit as predicted by LSS theory. S_n and S_e are the nuclear and electronic stopping powers respectively (after ref. [14]).

between swift ions and the target nuclei is small. Therefore, stopping power goes through a maximum at intermediate energies. Typical ranges of application for different energy ranges are also mentioned in the figure.

There are other energy loss mechanisms, which are not so significant in the energy and mass regime of conventional ion implantation, such as elastic collisions with free electrons, inelastic collision with nuclei resulting from Cerenkov radiation etc [14].

Knowledge of energy loss mechanisms help determine the path that an implanted ion takes before coming to a halt. The ion trajectories being a statistical process, the resulting ion profile is a distribution, often assumed to be a Gaussian for low implant energies of

Dedicated to my Parents
&
to my Teachers

in electron and neutron irradiated silicon. Lee *et al.* [39] argue that the divacancy , A-center and divacancy-oxygen $[V_2 + O]$ are equally probable in electron irradiated high oxygen content Si below 350°C. These anneal above 350°C giving the (divacancy + 2 oxygen) $[V_2 + O_2]$ and (trivacancy + oxygen) $[V_3 + O]$ centers. These in turn anneals out at 400°C yielding the (trivacancy + 2 oxygen) $[V_3 + O]$ and (trivacancy + 3 oxygen) $[V_3 + O]$ centers. Lee *et al.* have provided a comprehensive list of all such defects [39].

1.4.1.3 Self-interstitials

Self-interstitial is one of the most interesting defects in silicon because of its nearly athermal migration and ability to form pairs with impurities. Experiments to study directly the self-interstitial in silicon have not yielded much information on it's configuration. Using EPR, Lee and Corbett found evidence for self-interstitial in neutron irradiated intrinsic Si at room temperature [40]. It appeared to be stable in a$\langle 100 \rangle$ di-interstitial configuration. Interstitial silicon atoms have been found to be highly mobile at 4.2K under electron irradiation in p-Si [41]. In n-Si, its presence has been detected below 175K, though migration properties are less clear. In the absence of direct experimental observation of isolated interstitials, most of its properties are based on theoretical calculation. It is predicted to be a negative U center state binding two electrons deeply with first ionization state at E_c-0.8 eV and second one at E_c-0.4 eV. The self-interstitials readily form pairs with impurities such as B, Al, Ga, C, P and O [42]. A number of EPR centers has been attributed to interstitial related defects (P6, A5, B3 and O2) [43] and their annealing characteristics are roughly established. Figure 1.4 shows schematic of thermal stability of several such interstitial related defect in Si as identified with EPR technique [44].

There has been resurgence of interest in silicon interstitial in order to account for defect processes quantitatively under irradiation conditions. We review some of these phenomena related to interstitial clusters later. In this section, in the context of the work described

Acknowledgements

As working for the satisfaction of the teacher is the secret of success for a student, working for a thesis upto the satisfaction of my supervisor was a privilege for me. I take this opportunity to express my deep sense of gratitude to my thesis supervisor Dr. Y. N. Mohapatra for providing me an opportunity to work in an atmosphere of dignity & confidence and extending various kinds of help during the course of this work. His everlasting enthusiasm in physics research has kept me alive with physics for such a long time and I do not have sufficient words to appreciate his endeavours. His interest and faith in me have taken me long way in my career. His invaluable guidance, moral and intellectual support, meticulous observations and critical analysis have contributed enormously to my academic potentiality.

I am grateful to Dr. V. N. Kulkarni for providing me all the experimental facilities for sample preparation. His constant support and encouragement were of great help. I am thankful to Dr. B. N. Deb and other members of Palletron accelerator facility, Institute of Physics, Bhubaneswar, for their invaluable help in gold ion irradiation of samples. Special thanks to Mr. B. Sundaravel for his selfless help at times during the course of this work.

I am profoundly indebted to Prof. R. Sharan for his stimulating discussions and valuable suggestions at times. Thanks are also due to Dr. J. Narayan for not only providing valuable training in his laboratory in the preliminary stages but also for his frequent help in experimental requirements.

Special thanks to Prof. V. A. Singh and Prof. S. C. Agarwal for their keen interest in my work and providing valuable suggestions from time to time. I wish to acknowledge the background help provided by Prof. A. K. Mazumder for motivating me in doing good physics. Thanks are also due to Dr. Satyendra Kumar, Dr. Alok Dutta, Prof. J. Kumar, Prof. D. C. Agarwal, Prof. K. Shahi for their valuable help at different stages. I must also thank Dr. Sandeep Agarwal for extending expert help and suggestions in setting up of electrical characterization facilities here.

I wish to thank all the staff members of Physics department office for their invaluable help at times. Special thanks to Pandaji, Srivastavji and Lalluji for the care and interest taken by them. Thanks are due to Viswanathji and Sharmaji of ACMS for their help

of species. Gold ions are used as comparatively more massive particle than argon, and processing temperatures are kept well below that required for electrical activation. The issues that depletion layer capacitance based methods can illuminate best are also the ones least studied in such samples. We seek to study those aspects of defect phenomena which would complement simulational and structural studies through electrical signatures of defects created due to heavy ions. The questions and issues that these studies can potentially address are grouped below.

- Are the electrically active defects created due to heavy ions in silicon, same as well-characterized point defects observed with light particle irradiation apart from being in larger concentration ? Or are distinctly new ones created ? Does agglomeration lead to change in the spectrum of density of states ? Do electrically active defect behave like point defects in such cases ? Which of these control compensation ?

- Electrically active defects are sensitive to inhomogeneities in their environment. Does the damage in the environment of the defects lead to their energy broadening? Are they also sensitive to relaxation of the damaged layer brought about by say thermal treatment ?

- The physics of the defects are best studied by monitoring trapping / detrapping kinetics, which also provide information on relaxation mechanisms. It is only to be expected that the disorder created by MeV heavy ions can sustain metastable states of defects. There are several such not so well understood cases of metastabilities reported in the literature in implanted silicon as we point out in more detail in chapter 6. Transient based spectroscopic methods are highly suitable to explore the nature of defect relaxation and metastabilities. We planned this work with the expectation that high energy, high fluence implants would be ideal laboratories for such studies. This was hoped to be specifically relevant to charge relaxation

and cordial behaviour. I also wish to appreciate the efforts of all the members of Physics Workshop especially Mr. Bahadur Singh who worked with interest and designed various things for my work.

I am greatly indebted to Dr. Sankar Dhar and Topobrata Som for their expert help in ion irradiation and sample fabrication processes. I take this opportunity to thank Subhasis Basu Mazumder for his valuable help.

I also wish to acknowledge the support and nice company of my friends Gautam, Swapan, Nazrul, Anil, Subhas Chand, Yoginder, Manju and Renu. I also take pleasure in thanking many other friends who maintained a cordial and lively environment and made my stay at IITK a cherishable and memorable one.

Words are insufficient to express my gratitude to my parents and sister who encouraged and inspired me under all circumstances. I am deeply grateful to my teacher Dhananjoybabu who brought me up with so much care. I am also deeply grateful to my Mama and Mamima for their encouragement and support at every stage. Thanks to Bhola, Mili, Mithu, Tutu and Boudi for their love and affection towards me. I am thankful to Mrs. Mohapatra and sweet Stuti for providing me a homely atmosphere in IITK. I also wish to thank Sonia for her care and assistance in many important activities.

May Supreme Lord Sri Krishna be glorified for His causeless mercy upon me in my insignificant endeavour to understand nature with so much mystery. Though knowledge comes from within, all those who contributed immensely to rediscover myself need be mentioned. I am thankful to Sudipto, Snehansu, Mishraji, Kamlesh, Paritosh, Monoranjan, Asish, Mahesh, Varun and others for their invaluable company and guidance.

IIT Kanpur *Pravat Kr. Giri*

curves are simulated for Q=0, 0.88, 1.16, 1.46 and 1.73 where $Q=\omega r_s C_s$. Note that for Q¡1, the effect of series resistance is negligible. This effect becomes severe with Q≥1. Consequently, wrong carrier concentration profile will be obtained from these curves. When series resistance is not negligible, then there is additional phase shift ϕ between the *ac* voltage applied and *ac* current flowing through the device for capacitance measurement.

Assuming that the diode being profiled can be represented by a simple RC equivalent circuit, if one measures the phase angle ϕ during profiling, true doping profile N is given by [88]

$$N(\omega) = \frac{C_m^3}{q\epsilon A^2}[\sin^2\phi(\frac{dC_m}{dV} + 2C_m \cot\phi\frac{d\phi}{dV})]^{-1} \tag{2.4}$$

with

$$\omega = \frac{\epsilon A \sin^2\phi}{C_m} \tag{2.5}$$

If there is also shunt resistance in the equivalent circuit, the analysis becomes more complicated. Although shunt resistance does not affect capacitance measurement, it cause changes in the phase angle which could invalidate Eqns. 2.4 and 2.5. In practice, shunt resistance is easily detectable by monitoring the *dc* leakage current during profiling. In presence of high density of traps, the analysis is more complicated since both will have similar effect in C-V profiling.

There are several possible ways to reduce the effect of series resistance since its presence is felt through the product $(2\pi f r_s C)^2$. One could reduce the capacitance C by using test diode of smaller area. Because of importance of edge-effect, stray capacitance correction and difficulty in measuring small area accurately, it is not practical to use diode areas below 10^{-4} cm^2. The measurement frequency could be reduced to reduce the product, but the signal to noise ratio becomes worse at lower frequencies. In any case the frequency must be kept high compared to the relaxation times of the any traps present in the material. Series resistance can be altogether avoided by using a feedback circuit to keep the capacitance constant and measure the corresponding voltage. We have used this

SYNOPSIS

Heavy ions accelerated to MeV energies are finding increasing use in semiconductor device technology. Their use is likely to emerge as a standard industrial process for their ability to introduce, at distances larger than several microns from the surface, controlled modifications in doping, conductivity, lifetime, composition and degree of amorphization. The success in the use of MeV heavy ions is closely linked to development of coherent understanding of defects and defect related phenomena accompanying these processes.

Though study of defects produced by energetic particle irradiation in semiconductors has been a field of intense research for many decades, there has been a recent upsurge in interest specific to heavy ions both from fundamental and technological point of view. The primary electrical defects produced by irradiation of light particles, such as electron, have been well characterized with various magnetic resonance spectroscopy and electrical techniques such as deep level transient spectroscopy (DLTS). On the other hand, defects and lattice damage induced by MeV heavy ions with high dose are comparatively much less understood. Our present knowledge of heavy ion induced damage is mostly limited to studies related to structural tools. For example, transmission electron microscopy has been extensively used to study evolution of structural defects during post-implantation annealing, and often complimentary information is obtained by Rutherford backscattering spectrometry studies.

The use of conventional electrical characterization in heavy ion damaged semiconductors, however, have been mostly limited to resistivity studies. Some recent studies have utilized DLTS technique to characterize defects in case of low dose implantation or in samples subjected to post-implantation annealing at high temperatures. *This thesis attempts to study electrically active defects in deep buried layers produced by MeV heavy ions in Si prior to removal of damage by high temperature annealing.* A variety of capacitance based techniques including transient spectroscopies such as DLTS, novel methods of isothermal spectroscopic techniques such as time analyzed transient spectroscopy (TATS), and their suitable extension for meaningful extraction of defect parameters, have been used to study

2.6.1 DLTS lineshape analysis

DLTS lineshape is dependent on both temperature and energy of the trap for a chosen value of r. For an exponential transient, DLTS signal is given by

$$S = C_0[e^{-e_n t_1} - e^{-e_n t_2}]$$

where $e_n = AT^2 exp(-E_T/kT)$. S goes though a peak at temperature T_m. If T_1 and T_2 are temperatures corresponding to the half maxima positions of the DLTS peak then

$$e^{-e_n t} - e^{-2e_n t} = \frac{1}{8}$$

for a choice of $r = \frac{t_2}{t_1} = 2$.

Solving the quadratic equation for $e_n t$ we get

$$ln(e_{n_1}) - ln(e_{n_2}) = 2.496$$

$$2\, ln(\frac{T_1}{T_2}) - \frac{E_T}{k}(\frac{1}{T_1} - \frac{1}{T_2}) = 2.496 \qquad (2.21)$$

Thus, for DLTS signal the linewidth can be defined by Eqn. 2.21 which depends on E_T, T_1, T_2 and r factor. A prior knowledge of activation energy is required to verify the deviation from non-exponentiality from the observed spectra using Eqn. 2.21. This is a major limitation of DLTS in applying it for lineshape analysis. In deriving this equation, we have assumed that C_o is not changing with temperature. For temperature dependent prefactor C_o in Eqn. 2.9 , lineshape is not defined by Eqn. 2.21. Hence, lineshape analysis is not straightforward in case of DLTS.

Usually, the first term in Eqn. (2.23) is negligible for exponential transients. In that case from the knowledge of T_1 and T_2, calculation of activation energy is straightforward from a single spectra. However, lineshape analysis is quite easy using isothermal spectroscopic techniques such as time analyzed transient spectroscopy which is discussed in a later section.

deep buried layers.

In order to separate out effects due to heavy ion damage alone from electrical activity of implanted species, we have used noble gas Ar^+ ions, with energies around 1.45 MeV and doses 10^{13}-10^{14} cm^{-2} to produce buried layers in both n and p-type epitaxial silicon. Samples implanted with heavier Au^+ ions at 4.5 MeV and dose 5×10^9 cm^{-2}, but not annealed to avoid electrical activation, have also been studied for comparison. Irradiation doses are chosen to be below amorphization threshold but comparatively higher than used by most other workers. Conventional Schottky barrier diodes are fabricated for characterization using capacitance based techniques. Both as-implanted and low temperature annealed samples have been studied to monitor progressive changes in electrically active defects. Use of a variety of electrical spectroscopic techniques yield interesting physics of defect phenomena related to migration, clustering and carrier kinetics at deep levels. Specifically, defects primarily responsible for carrier compensation have been identified in both n-Si and p-Si. Origin of many interesting phenomena have been traced to the trapping kinetics of these defects within the depletion layer.

The work has been presented in **eight** chapters. The first three Chapters deal with review and motivation, principle and critique of techniques employed, and experimental details respectively. Chapter 4, 5, and 6 present results on n-type samples, and Chapter 7 is devoted to p-type samples for comparison. Chapter 8 summarizes salient conclusions of this work. In what follows, we summarize contents of each chapter.

Chapter 1 provides a brief introduction to the field of irradiation induced defects, defect processes and damage in Si with specific focus on MeV implantation. With this perspective, the motivation of the present study and its regimes of interest have been defined.

Chapter 2 discusses principles behind use of various conventional experimental techniques and their extensions to analyze complex situations relevant to our present work. Limitations of standard use of capacitance-voltage (C-V) techniques and various factors affecting capacitance measurements are discussed. Common origin of nonexponentialities

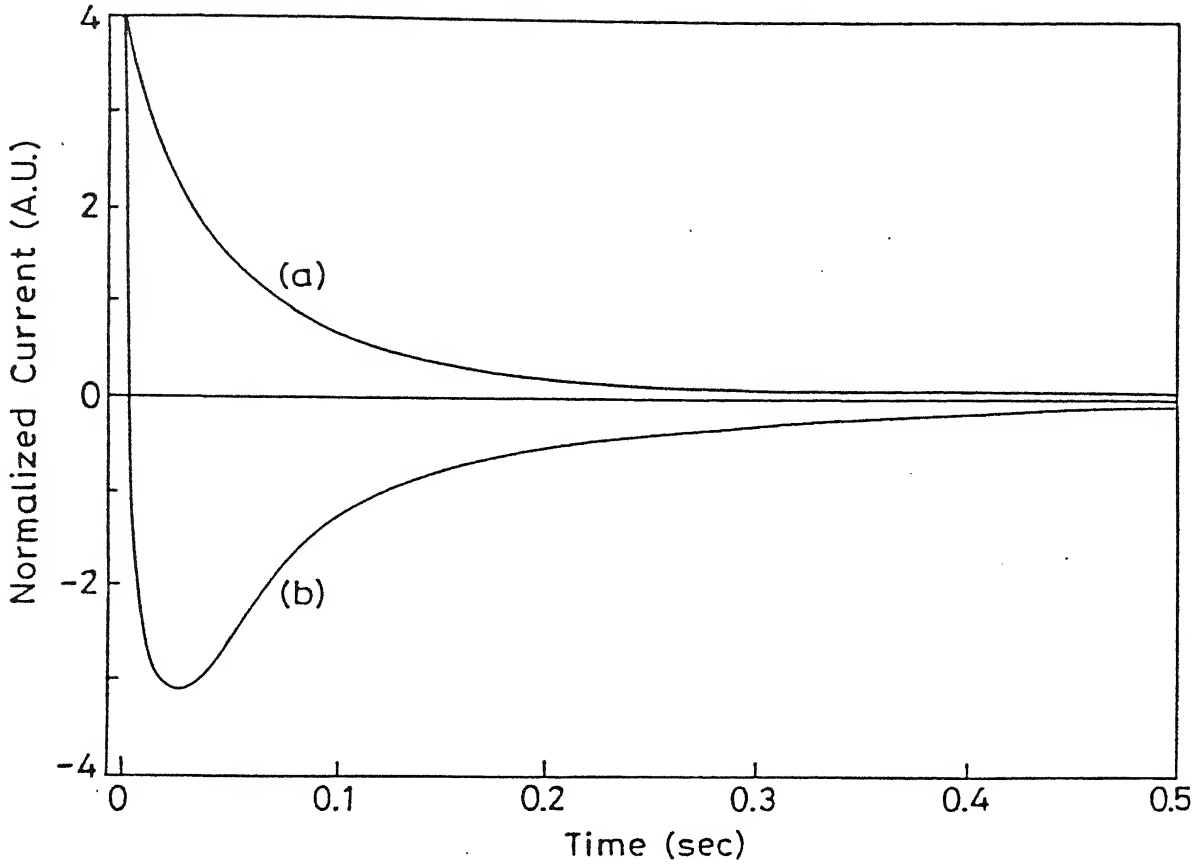

Figure 2.7: Typical photocurrent transients in SI-GaAs samples : (a) decaying current at 174.9K, (b) rising current at 293.2K.

believe that the current dipping to a minimum before rising is an essential part of the whole transient and this major deviation from exponentiality needs to be explained. Any analysis of this phenomena which focuses only on the later rising part, as has been done in the literature, can be misleading.

The most popular way of characterizing traps in these materials has been PITS. The decaying transients give rise to positive peaks in PITS spectra. Transients such as given in curve (b) of Fig. 2.7 results in negative peak feature in such spectra and has been widely discussed in literature. Figure 2.8 shows conventional PITS spectra in the higher temperature regime where the negative feature is clearly observed. This figure also shows

in capacitance transients and their effect on trap parameter evaluation from conventional deep level spectroscopies are assessed.

The critical role of spectroscopic lineshape analysis of transient signals in the study of defect phenomena is emphasized and suitability of different spectroscopic techniques from this point of view is analyzed. Specifically, use of time analyzed transient spectroscopy (TATS), an isothermal spectroscopic technique, is shown to provide cleaner interpretations and better insights into nonexponential transients which indeed manifest in various forms in our experiments. A brief case study involving analysis of experimental data of photo-induced current transients in semi-insulating gallium arsenide has been presented to demonstrate superiority of TATS in analyzing nonexponential transients. Brief account of principles of other well known techniques which have been used for the present work is also included.

Chapter 3 gives details of sample preparation, experimental setup and measurement procedures. Various steps in sample preparation including Schottky diode fabrication, MeV ion implantation and thermal annealing are described. Design of cryostat and experimental setups developed and automated in-house have been described.

In **Chapter 4** we present results on steady state capacitance-voltage (C-V) measurements on Schottky diodes of n-Si containing damaged buried layers. Occurrence of a flat voltage-independent region in $1/C^2 - V$ plot, for low reverse bias, is common to all irradiated devices. C-V measurements also show hysteresis which is dependent on voltage sweep rate. This in addition to temperature dependence of C-V curves is strongly indicative of trap controlled nature of observed phenomena. In as-implanted device, zero bias depletion width is seen to be very large compared to the control device. It is observed to be several microns larger than the range of ions predicted from Monte Carlo simulations using TRIM, and it is also larger for higher irradiation doses. The experimental features in C-V curves have been simulated using model charge profiles taking into account crossing of Fermi level with a midgap trap within the depletion layer. The simulations suggest that the irradiation damage seem to produce two regions : (i) a compensated region with

ity of our model to mimic these essential features of the data opens up new possibilities as regards study of underlying mechanisms. We have assumed that e_n is the dominant thermally controlled parameter. However, it is possible that even the rate of conversion r is temperature dependent and hence the energy measured through Arrhenius plot is an effective energy associated with this combined process. The existence of metastable states with involvement of slow relaxation processes has often been invoked in relation to deep levels, as in the case of EL2 in GaAs, DX centers in AlGaAs and M center in InP. The occurrence of complex transient forms can be taken as possible indicator of involvement of metastable states even at such relatively high temperatures in these materials.

In summary, we have demonstrated the efficacy of TATS in comparison to PITS, a temperature scanning spectroscopic technique, in analyzing nonexponential transients in SI-GaAs. Different kinds of nonexponentiality playing role at different temperature range are estimated using TATS. A phenomenological model to account for the observed nonexponentiality at higher temperature rising transients has been proposed.

We will use TATS operated in constant capacitance mode (CC-TATS) to study a range of defect phenomena observed in heavily ion damaged layers in Si. CC-TATS will be an obvious choice to eliminate nonexponentiality due to series resistance effect and high trap concentration. Though we will use TATS and DLTS both to analyze data, CC-TATS will be used to study nonexponentiality due to other reasons than those discussed above.

most dopants being deactivated, and (ii) a sharp negatively charged defect profile with large concentration close to the depletion edge which is much larger than expected range of ions. Our experimental observations lend support to recent results of molecular dynamic simulations according to which primary defects such as vacancies and interstitials migrate and form clusters and complexes.

A clear proof of occurrence of a defect-controlled near intrinsic region comes from measurements of forward current-voltage (I-V) characteristics of the irradiated device in which crossover from ohmic conduction to square law space charge limited conduction regime is observed. A nearly vertical rise in current at a voltage corresponding to trap filled limit is an indicator that the associated defect is a discrete level.

C-V characteristics of samples after vacuum annealing of irradiated samples are also presented. They show progressive reduction in zero bias depletion width with isochronal (30 minutes) annealing upto 600°C. Reduction in depletion width on annealing is accompanied with dopant activation in the damaged region. The nature of variations in charge profile with annealing has been shown using simulations of progressive changes in C-V characteristics.

Chapter 5 deals with deep level spectroscopic investigation of defects in the buried layers. Some of the interesting and unusual features observed in transient response are first described. This includes occurrence of a 'spike' in capacitance response during capture of carriers, small difference between reverse-bias and zero-bias depletion width following capture, large magnitude emission transient and its premature termination. These features are shown to be consequences of trap filling giving rise to large negative charge density within the depletion layer and are discussed in the light of crossing between quasi-Fermi level and the major trap controlling these phenomena. DLTS, in spite of its inadequacy in this situation to provide reliable defect parameters through standard analysis, has been useful as a survey technique, and does provide helpful guide to further experimentation. Both DLTS and thermally stimulated capacitance (TSCAP) spectra in the range 90K-320K reveal occurrence of mainly two discrete trap levels of which one is the well known

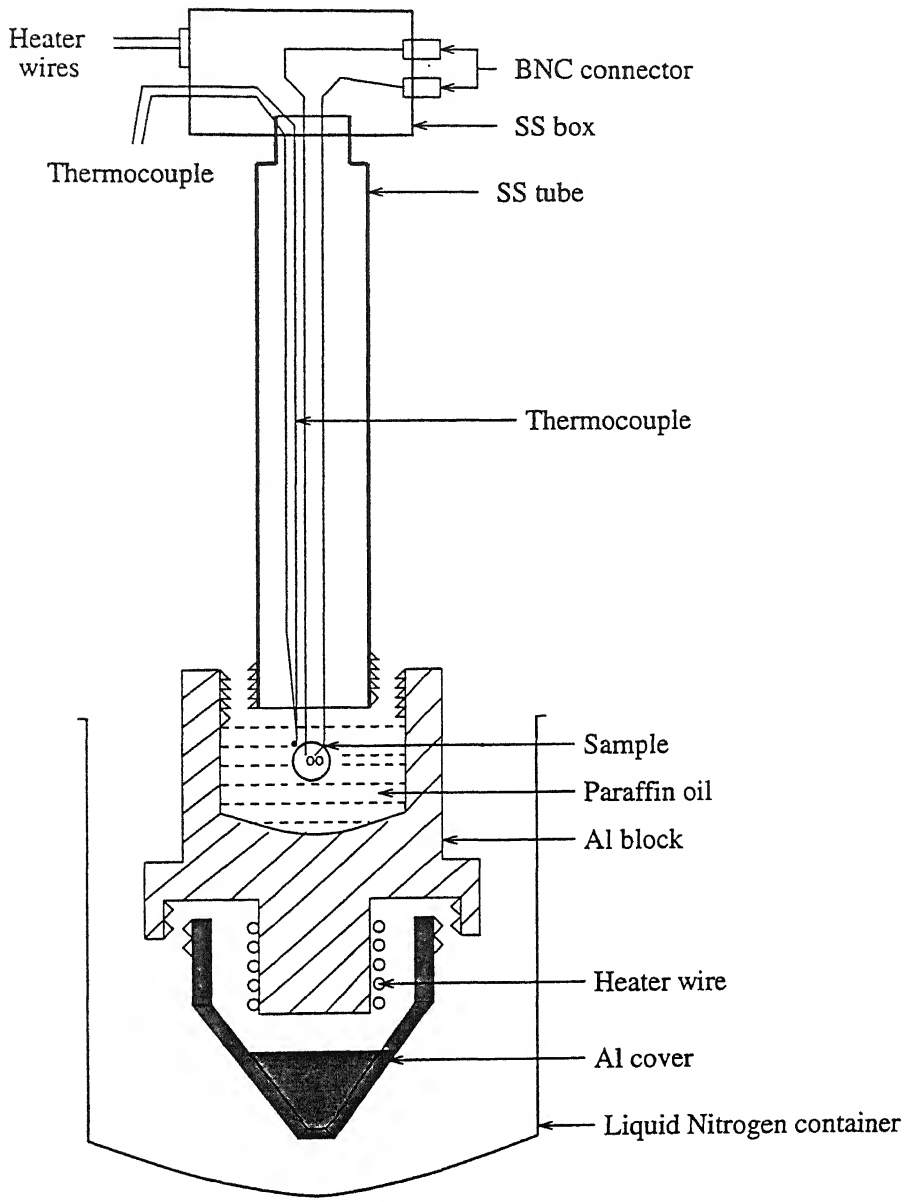

Figure 3.5: Layout of the home-made dipstic cryostat used for electrical measurement in the temperature range 80K-350K.

Chapter 4

Steady State Capacitance and Current Characteristics

In this chapter, our central concern would be ways of obtaining useful information from the study of capacitance-voltage (C-V) characteristics of Schottky barriers containing damage due to implantation in the depletion width. In chapter 2, we have given a brief account of usefulness of conventional C-V measurements, also indicating major factors that influence such characteristics. Here we first present unusual and interesting features of results obtained from C-V measurements, and then describe their dependence on temperature and sweep rate of measurement, and different stages of annealing. We also present current - voltage (I-V) characteristics data to the extent needed as support for interpretation of C-V data. In the last section we present a discussion of the view that emerges from these results regarding the nature and role of defects in the damage layer, band bending and charge profile. The discussion is supplemented with results of model simulations using simple physically consistent assumptions to reproduce all the major observed features in the data.

4.1 C-V Characteristics

4.1.1 Typical C-V Characteristics

A number of sets of Schottky diodes were made on unimplanted and implanted wafers using procedures described in Chapter 3. All the results presented in this chapter deal with n-type Si implanted with 1.45 MeV Ar^+ ions and 4.6 MeV Au^+ ions. The samples

divacancy center ($V_2^{-/0}$, E_c-0.42 eV) and the other is a newly found midgap trap level. This new trap level is the dominant trap occurring in very large concentrations in all our MeV irradiated samples and is responsible for controlling hysteresis in C-V and space charge limited conduction in forward I-V characteristics. In order to study the nature of nonexponentiality and proper evaluation of defect parameters, we resort to isothermal transient spectroscopic analysis in time domain using TATS. To avoid known sources of nonexponentiality due to large trap concentrations and series resistance, transient measurements for time domain analysis are performed in constant capacitance mode.

TATS lineshape corresponding to the major trap is seen to be broad for low temperatures and, narrow and skewed at high temperatures. The peak shape narrowness is linked to occurrence of premature termination of transients which in turn is explained on the basis of time evolution of quasi-Fermi level and its crossing with the trap level within the depletion layer. It is possible to estimate the true time constant and peak height associated with these skewed peaks from a careful fitting of the useful part of the lineshape. The signature of the dominant trap is obtained from such analysis for various samples. The emission energy of the dominant trap is observed to vary from E_c-0.49 eV to E_c-0.56 eV depending on processing conditions such as low temperature oven annealing and irradiation dose. This sensitivity of the defect parameters seem to be characteristic of pramorphized regions and is due to varying degree of relaxation of disorder in its environment. At low temperatures, in the absence of skewness in lineshape due to premature termination, the damage related peak for high dose samples shows a Gaussian broadening in energy with FWHM of 25 meV. This broadening is disorder induced since it is observed to be only 6 meV for low dose samples. The capture cross-section values are typical of neutral trapping center. The possible origin of this defect has been discussed, most likely candidates being dangling bonds, higher order vacancy complexes or interstitial clusters. However, consistent with our observation of involvement of migrating species and in accordance with mounting evidence from recent studies on involvement of interstitials, di-interstitials or their clusters seem to be responsible for the dominant damage

related trap. High temperature furnace annealing studies show near complete removal of the dominant trap on heat treatment at 600 C for 30 minutes. In annealed samples minority carrier related traps could also be observed possibly due to mild inversion in the damaged layer.

Chapter 6 is devoted to the study of trapping kinetics by monitoring relative occupancies of multiple traps after allowing filling of traps for different duration over 5-6 orders of magnitude in time. Surprisingly we observe two distinct mechanisms which could be isolated at different temperature regimes in different group of samples. At lower temperatures, filling time dependence of TATS peaks corresponding to multiple traps show nonmonotonic change in trap occupancy. With filling time evolution it was possible to recognize that the peak attributed to divacancy alone, in reality, constitutes contributions from two distinct emitting centers. The resolution of peak structure has been clearly demonstrated using higher order implementations of TATS. The progressive evolution of occupancies over many orders of magnitude in time reveals coupling in capture kinetics. We show that this coupled kinetics is due to *charge redistribution* among multiple traps, in which deeper states gain at the cost of shallower states with time. Broad experimental features in occupancy as a function of filling time could be reproduced by solving coupled rate equations with charge redistribution constraint. However, closer match with experiment is obtained when in addition a configurational interdependence of two traps is assumed. The mechanism of charge redistribution had been invoked earlier to explain charge relaxation in amorphous silicon, though it was considered controversial in that context due to lack of unambiguous experimental proof. This mechanism is expected to be operative whenever number of trapping sites are larger than availability of carriers for capture.

Evidence of a novel defect relaxation mechanism was encountered during the course of studies on filling time dependence of occupancies for low dose implanted samples (Au^+ at dose 5×10^9 cm^{-2}) and for partially relaxed Ar^+ irradiated samples - presence of a preamorphised region with comparatively lesser degree of disorder being common to

rate not sufficiently fast and partly due to saturation in trap filling. The occurrence of negative slopes in these curves is indicative of profile in the trap concentration. Consider, for example, the filling curve denoted by solid lines during voltage change from reverse toward forward bias. Around zero bias, an increase in forward bias leads to so much of increase in negative trapped charge that the depletion width is forced to widen at the same bias to uncover additional positive charge at the edge. Hence the slopes are due to combined effect of trap occupation in the depletion layer and dopant charges at the edge of the depletion layer.

The observation of hysteresis with different degree of filling and various sweep rates establish that C-V is controlled by large trap concentration due to irradiation damage in these samples. We go on to show their manifestation in I-V measurements in the following section.

4.2 I-V Characteristics

I-V measurements are useful for understanding the transport properties across junction of different materials. In our irradiated devices, a major deviation from conventional Schottky barrier (our control diode) behaviour occurs due to the presence of damaged layer. Such behavior is seen in both Ar^+ and Au^+ irradiated device.

4.2.1 Typical I-V Characteristics

Figure 4.8 shows typical forward and reverse I-V characteristics at room temperature for Ar^+ implanted Schottky diodes. For irradiated device, both the forward and reverse current are significantly smaller compared to corresponding currents in the unirradiated device. This also confirms the presence of a compensating region in the depletion region of the device. For bias voltages corresponding to low forward bias, the magnitude of current

dynamics of defect occupation. In case of a depletion layer without deep traps, voltage changes across the device are accommodated through changes at the depletion layer edge. However, in case of large trap concentration, changes of occupancy at the E_T-E_F crossing would control the total depletion width.

From the experimental results it is abundantly clear that the occupied dominant traps produce charges opposite in sign to the background doping i.e. they get negatively charged after capture of electron. Hence, when reverse bias is increased (from, say, zero bias) the extra voltage drop can be accommodated either by increasing the depletion width, which leads to uncovering of positive charges at the edge, or by emitting electrons from the traps thereby increasing net effective positive charge in the depletion layer. The former process would occur within the time constant of dielectric relaxation time while the later would be controlled by trap emission rate. At sufficiently high temperature, if the trap emission rate is faster than voltage sweep rate, detrapping at the crossing would itself accommodate the voltage change. The width of the depletion layer and hence capacitance would remain constant even when bias is being changed causing the feature of flatness. For larger biases the trap concentration may not be sufficient to do so and width would also increase in part. This would continue till Fermi level loses contact with trap level. Beyond this the C-V would reflect the background concentration giving rise to conventional linearity in $1/C^2$ vs. V curve. In this sense, E_T-E_F crossing is the primary determinant in studies involving high dose implanted samples, while it is only a minor irritant in conventional depletion capacitance studies.

This explanation of major features in C-V characteristics is fully consistent with (or can be viewed as derived from) the occurrence of hysteresis and temperature dependence. Hysteresis arises from the fact that the traps get occupied by a fast capture process at the crossing point during decreasing bias cycle while on the increasing cycle the capacitance change is dependent on slower emission process from the traps. Similarly, when temper-

these set of samples. The phenomenon, as described below, could most conveniently be studied for temperatures above 270K. When filling time is increased at a particular temperature, TATS emission spectra shows a distinct new peak whose time constant is strongly dependent on the duration of filling. The time constant varies in a typical case from 7ms to 14s (corresponding to energy deepening of 180 meV) for filling times in the range 20ms-60s, showing a power law dependence on filling time. This dependence of emission characteristics on history, in terms of waiting time, is a strong indicator of a non-Markovian process of relaxation occurring during capture. The height of the new evolving peak remains almost constant for all filling times. Further, free energy changes seem to involve an entropy-like term since the emission time constant is nearly temperature independent for a particular filling time. All these features suggest that the relaxation mechanism follows a hierarchically constrained dynamics as proposed for glassy systems. A closely similar defect relaxation mechanism has been invoked to explain capacitance transient data in hydrogenated amorphous silicon though it is more involved in that case due to presence of broad density of states. We discuss plausible scenario in which such a hierarchical mechanism may be operative in our case.

In **Chapter 7** we have discussed the case of p-type silicon under irradiation conditions (MeV Ar^+ and Au^+ ions) similar to n-type. C-V characteristics showed similar features as n-type though the increase in depletion width due to damage was to a lesser extent. Conventional thermally stimulated capacitance (TSCAP) and constant capacitance TSCAP studies reveal two trap levels in irradiated samples : one is due to well known C_iO_i (carbon interstitial-oxygen interstitial pair) complex related hole trap and other is damage related trap newly found by us. Conventional DLTS studies showed three majority carrier trap related peaks and one minority carrier related peak. Major peak in this case is due to damage related trap and the DLTS peak shape is broader than peak expected from exponential transients. Trap emission time constants, capture cross-section and trap concentration are determined using constant capacitance TATS analysis. The major trap is located at E_v+0.52 eV having a large capture cross-section of 9.9×10^{-14}

cm^2.

Carrier capture rate at this major trap is seen to be surprisingly slow and thermally activated. From DLTS-like processing of capture transients as well as from variable filling pulse width TATS measurements, capture barrier was estimated to be 0.66 eV which is quite large compared to the emission barrier mentioned above. A part of this barrier is associated with a macroscopic barrier for holes to reach the trap levels at the damaged layer. With a high macroscopic barrier, a mild inversion is the most probable source of filling of minority carrier traps which show up as negative peak in CC-TATS spectra. The time constant of the major negative peak matches with that of damage related majority carrier peak in n-Si. Thus the dominant majority carrier trap in n-type and dominant minority carrier trap in p-type Si is of same origin and it acts as an efficient recombination center in heavy ion damaged Si. The majority carrier peaks in p-type also seem to have origin in interstitials and their clusters.

High temperature furnace annealing of damaged p-Si upto 600°C showed appearance of new traps in DLTS and TSCAP spectra. In contrast to the case of n-Si, large concentration of secondary defects are found in p-Si on annealing and their characterization would require more systematic studies than envisaged in this work.

In **Chapter 8** summary and conclusions of this work are collated highlighting their implications for study of MeV heavy ion induced defects, and defect dominated semiconductors in general. At the end of this chapter, we suggest directions in which this work can be extended.

Part of this work has been communicated to various journals and presented in conferences as listed next.

related question of how is one able to change the interface between trap-dominated and trap free region through irradiation dose, annealing and even long duration storage.

Any residual channeling in spite of misorientation of the surface with respect to the beam, cannot lead to observation of huge concentration of traps so far away from the location of the nuclear damage. We have confirmed this in another set of experiments [135], not included in this thesis, in which n-Si samples were implanted with very heavy dose of 1.5 MeV He ions at an angle as large as 60^o to the surface normal so as to keep range of these light ions to approximately 1-1.5μm. In these experiments also the total depletion width turned out to be larger than that predicted from TRIM simulations.

We propose that the dominant compensating deep acceptor traps have their origin in species which can migrate over large distances from the source of their creation even at room temperature. As migration occurs, these species would tend to form clusters rendering them immobile. This process of migration and cluster/complex formation can indeed lead to a sharp profile moving deeper into the sample.

We go on to show that the pieces of supporting evidence for such a mechanism is increasing in some recently reported experimental and theoretical studies. Recently Privitera et al [51] demonstrated room temperature migration of Si interstitials over several microns. In these experiments interstitials generated at the surface migrated deeper into the sample to interact with preexisting damage induced defects.[1] Similarly, Larsen *et al.* [50], in study of migration of Si self interstitials at room temperature using spreading resistance technique, detected dopant deactivation upto depth of several microns beyond the region directly modified by the ions. High fluence MeV implants, specifically with heavy ions, have usually been reported to result in very wide spatial distribution of defects (2-4μm) in contrast to TRIM predictions of FWHM of only a fraction of micron [51, 141].

Jaraiz *et al.* [52] have recently reported a set of significant results from molecular

[1]Note that these experiments were done with low fluences and low energy ions and clustering is not expected to limit the range of migration in this case.

List of Publications

In international Journals

1. **P.K. Giri** and Y.N. Mohapatra

   Nonexponentiality in photoinduced current transients in undoped semi-insulating gallium arsenide.

   J. Appl. Phys. 78, 262 (1995).

2. **P.K. Giri**, S. Dhar, V.N. Kulkarni and Y.N. Mohapatra

   Electrically active defects due to end-of-ion range damage in silicon irradiated with MeV Ar^+ ion.

   Nucl. Instr. & Meth. B 111, 285 (1996).

3. **P.K. Giri**, S. Dhar, V.N. Kulkarni and Y.N. Mohapatra

   Electrically active defects in as-implanted deep buried layers in p-type silicon.

   J. Appl. Phys. 81, 260 (1997).

4. **P.K. Giri**, S. Dhar, V.N. Kulkarni and Y.N. Mohapatra

   Characterization of deep level defects in Si irradiated with MeV Ar^+ ions using constant capacitance time analyzed transient spectroscopy.

   Bull. of Mater. Sci. 20, 417 (1997).

5. **P.K. Giri** and Y.N. Mohapatra

   Compensating defect in deep buried layers produced by MeV heavy ions in n-silicon.

   Appl. Phys. Lett. 71, p... (1997).

Papers presented in Conferences / Workshops

1. **P. K. Giri** and Y.N. Mohapatra

   Time analyzed transient spectroscopy analysis of photo-induced current transients in semi-insulating gallium arsenide.

   National conference on Recent advances in Semiconductors, New Delhi, India, June 20-22, 1995.

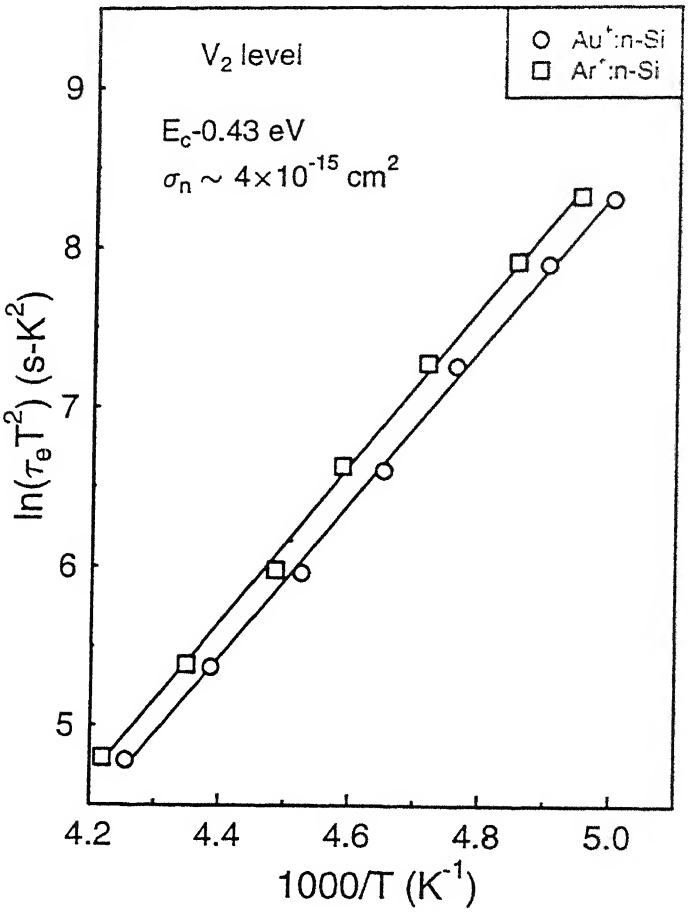

Figure 5.3: Arrhenius plot for peak V_2 obtained from DLTS spectra of Ar^+ and Au^+ irradiated n-Si.

has also been detected [20]. However, we do not see any detectable density of this level as production density is smaller for heavier mass [20]. As the density of V_2 is smaller, nonexponentiality corresponding to its emission in transients is insignificant. This enables standard use of Arrhenius plot for estimation of trap energy and capture cross-section. Arrhenius plot shown in Fig. 5.3 yields activation energy and capture cross-section of E_c-0.43 eV and 4×10^{-15} cm^2 respectively for V_2 level. These results are in good agreement with the reported values in the literature [20, 21, 23].

2. **P.K. Giri**, S. Dhar, V.N. Kulkarni, and Y.N. Mohapatra

   Electrically active defects due to end-of-ion range damage in silicon irradiated with MeV Ar ion.

   National conference on Recent advances in Semiconductors, New Delhi, India, June 20-22, 1995.

3. **P.K. Giri** and Y.N. Mohapatra

   Electrically characterization of deep defects induced by MeV irradiation in semiconductors.

   Workshop on Material Research with Ion beam facilities at IOP, Bhubaneswar, India, July 27-28, 1995.

4. **P.K. Giri**, S. Dhar, V.N. Kulkarni, and Y.N. Mohapatra

   Characterization of deep level defects in Si irradiated with MeV Ar^+ ions using constant capacitance time analyzed transient spectroscopy

   International Conference on Defects in Condensed Media, Kalpakkam, India, 20-22 September, 1995.

5. **P.K. Giri**, S. Dhar, V.N. Kulkarni, and Y.N. Mohapatra

   Trapping characteristics of MeV ion implanted buried layers in silicon.

   DAE Solid State Physics Symposium, Mumbai, India, Dec 27-31, 1996.

Papers to be Published

1. **P.K. Giri**, S. Dhar, V.N. Kulkarni and Y.N. Mohapatra

   Charge redistribution among discrete defect levels due to pre-amorphization damage in silicon.

   Phys. Rev. Lett. (Under Review).

2. **P.K. Giri** and Y.N. Mohapatra

   Evidence for a novel defect relaxation process in preamorphized silicon produced by

situations where faster processes progressively appear at later times are highly unlikely to occur. Our theoretical simulation shows that it's possible to get narrow peaks in TATS due to simultaneous trapping and detrapping at the depletion edge with inclusion of a time dependent capture term in rate equation. However, it is difficult to visualize such a mechanism in our case where complication occurs due to large density of localized traps. Without proper knowledge of the nature of nonexponentiality, calculation of the activation energy from these apparent peak position may involve substantial error.

Analysis of nonexponential transients, following an external perturbation, has been an exciting field of research in semiconductors due to it's connection with fundamental processes occurring in the material. In chapter 2 we have discussed many possible cases of nonexponentiality observed in physical systems where they have given rise to peaks in TATS or DLTS broader than exponential case. However, we have a distinct case here where peaks are narrower than exponential case.

In Fig. 5.8(a) we have plotted two constant capacitance voltage transient in logarithm of time scale and corresponding CC-TATS spectra are shown in Fig. 5.8(b). The sudden flatness of the transient towards the end of the transient can be noted from the figure. In analogy with DLTS analysis, in TATS signal construction when the time windows is chosen such that t_1 is on falling part of the transient and t_2 on the flat part of the transient, a peak skewed at right side will occur as shown in bottom figure. Considering the apparent peak as the true peak, an exponential peak is fitted with dotted line in Fig. 5.8(b) and the broken line corresponds to the exponential fit only considering the left side of the peak. The dotted line shows that the experimental peaks are considerably narrower than corresponding exponential transient, especially for 160°C annealed samples. As the apparent peak is an artefact of premature termination of the transient as already seen in DLTS spectrum (Fig. 5.2), it is only the later fitting by broken line which is meaningful. Note that for low temperature annealed sample, D1 peak height is more and

more defects are activated with time and defect seem to be relaxing to deeper and stable states even at room temperature. The V_2 related peak has not changed as they are thermally stable upto 350°C. Prior to these measurements, the samples were kept at room temperature for few months before devices were made on the irradiated wafers. Hence, room temperature annealing may not be alone responsible for this behaviour and it could have been induced by some intended process cycling during measurements. In earlier studies with alpha irradiated n-Si, room temperature transformation of the defect are reported [27], though no specific reasons have been assigned to it. In a recent study of defect stability on ion damaged n-Si using I-V measurement, it was reported that typical decay time of defects lies within 2-3 days after implantation [148].

Effect of relatively low temperature oven annealing at 160°C for 30 minutes is shown as curve 3 in Fig. 5.13. In this case spectra from as-implanted sample and annealed sample are different in many respects. Firstly, the V_2 related peak height seem to have reduced with annealing and D1 peak is shifted toward higher temperatures. This is attributed to relaxation of the damaged layer where defects D1 find a more stable configuration upon such low temperature annealing. The broad feature H1 does not seem to be entirely due to minority carrier related trap.

Effect of further annealing at 160°C for the irradiated sample is shown in curve 4 of the same figure. It shows increased peak (D1) height with small shift in peak position. Note that this peak is substantially narrow compared to the as-implanted case (curve 1 of Fig. 5.13). We have discussed the cause of such narrow peaks in DLTS or TATS spectra. Minority carrier related peak height is increased in longer duration annealed sample. Thus low temperature annealing of the damaged layer shows more electrically active defects, and the emission energy of the dominant defect goes deeper into the gap with annealing. Note that lower dose implanted samples have larger concentration and similar defect parameters as 160°C annealed samples. The gradual change in energy with

MeV heavy ions.

(To be communicated to Phys. Rev. Lett.).

3. P.K. Giri and Y.N. Mohapatra

Capacitance based studies of defect profile in deep buried layers in preamorphized silicon.

(To be communicated to J. Appl. Phys.).

Chapter 6

Trapping kinetics of defect states in n-Si

6.1 Introduction

In the previous chapter we have shown the presence of discrete trap levels of which divacancy and the major damage induced traps are dominant and that the latter occurs in large concentrations with energy approximately at the middle of the bandgap.

In this chapter, we use variable pulse-width filling experiments to monitor occupancy changes as is normally done to obtain a direct measure of capture cross-sections. However, due to the special characteristics of these materials, which we discuss later in the chapter, such measurements yield some interesting new physics of defects instead of providing a routine method of obtaining capture cross-sections. Significantly, these experiments shed light on a long debated question of how does charge relaxation occur in disorder semiconductors. This has been of paramount concern in amorphous and glassy systems. We avoid amorphous regime of silicon, by choosing ion doses smaller than the threshold dose, as has been mentioned earlier. Our choice of implantation parameters yield embedded damaged regions which have been referred to in the literature as 'preamorphized silicon' [1]. Therefore, the contents of this chapter can be viewed as an investigation into mechanism of charge relaxation in preamorphized silicon, which turns out to be a cleaner

[1]The term 'preamorphized' has been used in the literature in two distinct senses. Some use it to denote that a sample is amorphized prior to further implantations, or is 'amorphous to start with'. Other use it to mean that the induced damage is heavy but below amorphization limit. We have used this term in the second sense meaning 'damage below amorphization threshold'.

where n_{Ti} is the occupied states for i-th level with e_i and c_i its emission rate and capture rate constants and N_{Ti} its total concentration. We have numerically solved the above set of equations with $m = 3$ using model parameters for N_{Ti} and c_i and experimental emission time constants. For three independent trap levels with roughly equal concentrations, the occupancy behaviour is shown in Fig. 6.5(a).

A distinct feature of the independent model is that the final equilibrium concentration of the fastest trap is not as low as seen in experiments. We have checked that this feature is not merely dependent on the choice of capture and emission parameters, but is integral characteristics of these set of equations. This suggests that the fast peak (P1A) and the slowest peak (D1) may not be independent. Hence we modify the above model to include the assumption that P1A and D1 are two different configurations of the same defect. This additional constraint modifies the equations above as follows :

$$\frac{dn_{T1}}{dt} = -e_1 n_{T1} + c_1 n(N_{T1} + N_{T3} - n_{T1} - n_{T3}) \tag{6.3}$$

$$\frac{dn_{T2}}{dt} = -e_2 n_{T2} + c_2 n(N_{T2} - n_{T2}) \tag{6.4}$$

$$\frac{dn_{T3}}{dt} = -e_3 n_{T3} + c_3 n(N_{T1} + N_{T3} - n_{T1} - n_{T3}) \tag{6.5}$$

with the constraint on number of electrons as,

$$n = N_{T1} + N_{T2} + N_{T3} - n_{T1} - n_{T2} - n_{T3}. \tag{6.6}$$

Figure 6.5(b) shows the occupancy behaviour in such case assuming the same emission and capture time constant as in the earlier case. Here, we have assumed that $N_{T1} + N_{T3} = 0.45N_T$ and $N_{T2} = 0.55N_T$.

This indeed reproduce features close to experimental occupancy behaviour, particularly for reduction of occupancy of P1A. Here there is substantially large reduction of occupancy of P1A compared to the earlier case and this resembles more the experimental observation. Thus P1A peak can be considered as unstable configuration of D1 related

As mentioned in the beginning of this chapter, relaxation phenomena with similar characteristic features have been reported through a series of papers by Cohen and coworkers [159, 165] using junction capacitance measurements and modulated photocurrents in lightly n-type and intrinsic amorphous silicon. Since a broad density of states is clearly involved in the case of amorphous silicon, the corresponding capacitance transients are highly nonexponential [159] in contrast to our case. The defect spectra in preamorphized damage Si is dominated by discrete density of states making observation and analysis simpler. They report temperature independence of relaxation time for initial few orders of magnitude in filling time and usual activation once time constant ceases to change with further increase in t_f. In our case, the filling time needed to go over to the activation regime is very large and experimental limitations prevents access to this regime at convenient temperature of investigation. Su and Farmer [160] had sought to explain the experimental features in observations of Cohen and coworkers by charge redistribution among a broad density of states. They reproduced the features of progressive deepening of emission energy, nonexponential decay and temperature independence of τ for initial filling time t_f. However, they had to invoke a very specific form (exponential) of density of states to fit the data. In our case, we have got rid of broad density of states by choosing the fluence to be below amorphization threshold and further have observed near exponential decay spectroscopically. Hence there is no room for interpretation involving charge redistribution in this case. The fact that charge redistribution would occur in presence of large concentration of multiple states vying for capture of small number of carriers has been demonstrated in separate temperature regime in our samples.

Though the mechanism which drives this novel relaxation is not clear, a plausible physical scenario as visualized by Cohen and coworkers [159] can be described. With capture of a carrier a positive polarization cloud in the vicinity of the defect deepens the potential well and emission is monitored from this deepened state in absence of capture.

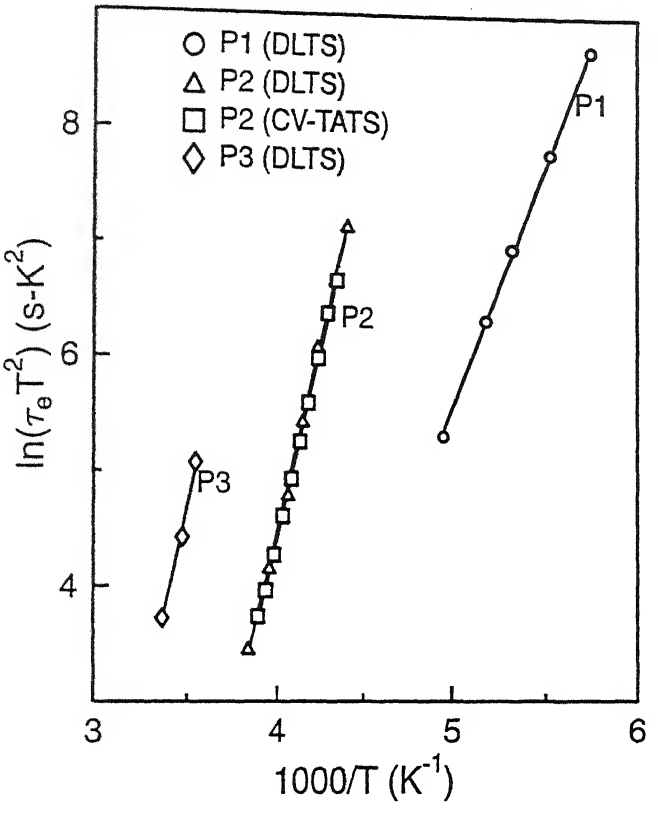

Figure 7.5: Arrhenius plot for peaks (P1, P2 and P3) obtained from DLTS spectra. For major peak (P2) data from CV-TATS is also shown for comparison.

in this case, the change in capacitance is too large for conventional (constant voltage) capacitance transient to be exponential. It is known that in case there exists a source of high series resistance in the sample, DLTS peak shifts in temperature and displays narrower width along with reduction in peak height. Further, lattice strain in the damaged region may be responsible for broadening of energy level. As argued previously, we rely on proper lineshape analysis using TATS, with constant capacitance implementation overcoming nonexponentiality due to high trap density and high series resistance.

The feature marked P4 in Fig. 7.4 shows a signal in the positive direction, indicating possible emission from minority carrier traps. Its presence also contributes to line shape distortion to the majority carrier peaks (P2 and P3). Definite conclusions regarding traps

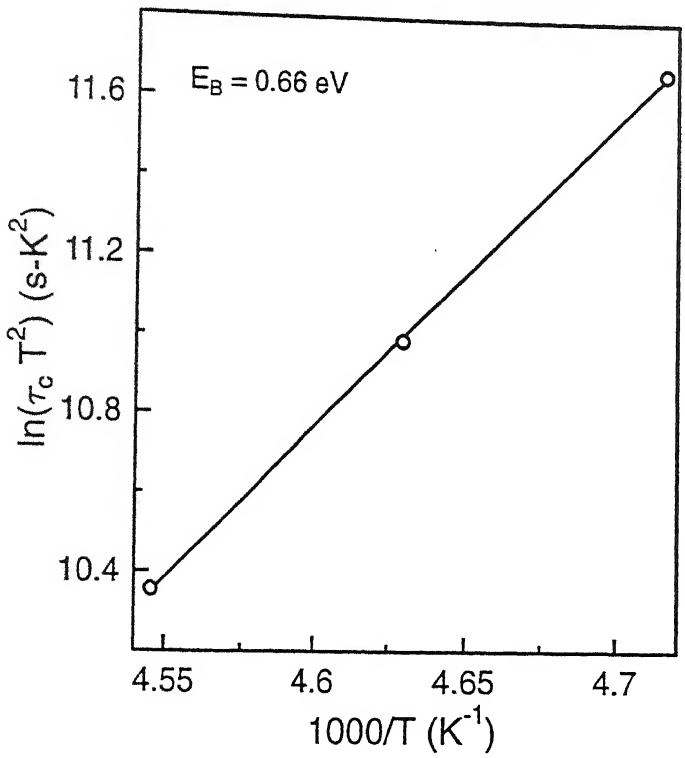

Figure 7.12: Arrhenius plot of the capture time constants of the major trap obtained from CC-TATS measurements at different temperatures.

7.4 Minority Carrier Related Traps

In Fig. 7.4 we have shown the presence of a negative peak P4 along with conventional majority carrier related positive peaks. Occurrence of the negative peak (P4) in the CC-TATS spectra cannot be ascribed to the series resistance of the damaged layer created by Ar^+ ions since a high *dc* resistance does not distort transients in the CC mode of operation. A careful evaluation of time constants of this negative peak shows that this trap corresponds to major trap observed in n-type Si. Hence, the major damage related trap in both n-type and p-type Si seems to be of common origin acting as an efficient recombination center.

It is somewhat unusual to observe minority carrier traps using Schottky diode. Under

annealed samples have been studied to monitor progressive changes in electrically active defects.

In addition to conventional techniques of steady-state capacitance-voltage (C-V), deep level transient spectroscopy (DLTS) and thermally stimulated capacitance (TSCAP), novel methods of transient based isothermal spectroscopic techniques such as time analyzed transient spectroscopy (TATS) have been extensively utilized. Implementation of constant capacitance (CC) mode of operation in spectroscopic characterization overcomes interpretational difficulties. Complimentary methods of electrical of characterization such as impedance analysis and current-voltage (I-V) measurements have also been used in this study.

The major contributions of the present work are summarized below.

A. Methodological Contributions

A proper appreciation of limitations of standard use of defect characterization techniques and various factors affecting capacitance measurements have been central to this work. Common origin of nonexponentialities in capacitance transients and their effect on trap parameter evaluation from conventional deep level spectroscopies have been assessed critically. Spectroscopic lineshape analysis of transient signals in the study of defect phenomena plays important role and determines suitability of spectroscopic techniques. Specifically, use of time analyzed transient spectroscopy (TATS), an isothermal spectroscopic technique, is shown to provide cleaner interpretations, and better insights into nonexponential transients which indeed manifest in various forms in our experiments. A brief case study involving analysis of experimental data of photo-induced current transients in semi-insulating gallium arsenide (SI-GaAs) has been presented to demonstrate superiority of TATS in analyzing nonexponential transients. Our work shows that TATS should be the preferred method in the study of physics of defects in defect dominated

List of Figures

[25] J. Krynicki, M. Toulemonde, J.C. Muller, and P. Siffert, *Mater. Sci. Eng. B* **2**, 105 (1989).

[26] P. Mary, P. Bogdanski, G. Nouet, and M. Toulemonde, *Appl. Surf. Sci.* **43**, 102 (1989).

[27] M. Asghar, M. Zafar Iqbal, and N. Zafar, *J. Appl. Phys.* **73**, 3698 (1993).

[28] K.L. Wang, *Appl. Phys. Lett.* **36**, 48 (1980).

[29] S. D. Brotherton, J. R. Ayres, J. B. Clegg, and J. P. Gowers, *J. Electron. Mater.* **18**, 173 (1989).

[30] E.G. Sieverts, S. H. Muller, and C. A. J. Ammerlann, *Phys. Rev. B* **18**, 6834 (1978).

[31] J. G. deWit, E.G. Sieverts, and C. A. J. Ammerlaan, *Phys. Rev. B* **14**, 3494 (1976).

[32] G.D. Watkins and J.W. Corbett, *Phys. Rev.* **138**, A543 (1965).

[33] J. Makinen, E. Punkka, A. Vehanen, P. Hautojarvi, J. Keinonen, M. Hautala, and E. Rauhala, *J. Appl. Phys.* **67**, 990 (1990).

[34] L. Sealy, R. C. Barklie, K. J. Reeson, W. L. Brown, and D. C. Jacobson, *Nucl. Instrum. Methods* **B62**, 384 (1992).

[35] G.D. Watkins, *Phys. Rev.* **134**, A1359 (1967).

[36] L.C. Kimerling, *Radiation Damage in Semiconductors*, - 1976 (Edited by N.B. Urli and J. W. Corbett), *Inst. Phys. Conf. Ser.* **31** p221. London (1977).

[37] L.C. Kimerling, H.M. DeAngelis and J.W. Diebold, *Solid St. Comm.* **16**, 171 (1975).

[38] G.D. Watkins and J.W. Corbett, *Phys. Rev.* **121**, 1001 (1961).

[39] Y. H. Lee and J. W. Corbett, *Phys. Rev. B* **13**, 2653 (1976).

[177] S.D. Brotherton and J. Bicknell, *J. Appl. Phys.*, **49**, 667 (1978).

[178] Daniel B. Jackson and C. T. Sah, *J. Appl. Phys.* **58**, 1270 (1985).

[179] S. Hahn, T. Hara, T. Maekawa, N. Satoh, Y.-K. Kwon, K.-I. Kim, Y.-H. Bae, W.-J. Chung, E.K. McIntyre, W.L. Smith, L. Larson and R. Meinecke, *Nucl. Intr. Methods*, **B 74**, 275 (1993).

[180] M. Asghar, M. Zafar Iqbal, and N. Zafar, *J. Appl. Phys.* **73**, 4240 (1993).

List of Tables

List of Symbols and Abbreviations

Symbol	Description
a-Si	Amorphous silicon
A	Diode area
C	Capacitance
CMOS	Metal oxide semiconductor capacitor
C-V	Capaciatnce vs. Voltage
DLTS	Deep level transient spectroscopy
DOS	Density of states
EPR	Electron paramagnetic resonance
E_{bi}	Binding enegy of interstitial clusters
E_c	Conduction band edge
E_F	Fermi energy
E_T	Trap enegy
E_v	Valence band edge
ϵ_o	Permitivity of the free space
f	Frequency
HREM	High resolution electron microscopy
IR	Infrared
FWHM	Full width at half maximum
I-V	Current vs. voltage
J	Current density
JFET	Junction field effect transistor
J_{leak}	Leakage current density
κ	Relative dielectric constant
λ	Width of transition region

MIS	Metal insulator semiconductor
MOS	Metal oxide semiconductor
MOSFET	MOS field effect transistor
M-S-I-S	Metal-semiconductor-insulator-semiconductor
N_d	Doping concentration
N_T	Trap concentration
N_c	Effective density of states at the conduction band
ν	Attempt to escape frequency
PATS	Paired temperature spectroscopy
r_s	Series resistance
RBS	Rutherford backscattering
ρ_d	Dopant charge density
ρ_t	Trap charge density
SCL	Space charge limited
σ	Capture cross-section
SI-GAAS	Semi-insulating gallium arsenide
SRH	Schokley-Read-Hall
TATS	Time analyzed transient spectroscopy
τ_c	Time constant for capture
τ_e	Time constant of emission
TED	Transient enhanced diffusion
TEM	Transmission electron microscopy
TRIM	Transport of ions in matter
TSCAP	Thermally stimuted capacitance
t_f	Trap filling time
U_{eff}	Effective correlation energy
V_{TFL}	Trap filled limit voltage
v_{th}	Thermal velocity of carriers
XTEM	Cross-sectional TEM

Chapter 1
Introduction

1.1 Preamble

Ion beams as instrument for modification and analysis of semiconductors have contributed in large measure to the remarkable progress during last decades in semiconductors. The success of ion implantation as an industrial process are due to its many advantages which include precision, speed and reproducibility. This is achieved through accurate control of energy, dose and species of ion beams. It has become indispensable in standard device technology mainly as a method of introducing dopants at desired depths, at temperatures lower than that needed for diffusion and with less stringent requirements on purity of the source. The application of ion beams in silicon processing and characterization has been recently reviewed [1]. One of the primary disadvantages of the method, however, is that it creates radiation damage requiring high temperature annealing to repair the crystal and to activate the dopants by moving them to substitutional sites. The need to understand the nature of damage and defects created in the implantation process and their evolution under processing conditions have spawned a vast literature over many decades [2]. The remarkable progress in this field has not only helped in optimization of process, but also has enriched fundamental understanding of a whole range of solid state phenomena [3]. The technological benefits of this knowledge are now being reaped in increasingly large number of applications involving ion beams to an extent that the field has come to be recognized as 'defect engineering'.

However, most of these developments have centered around applications of low to

medium energy ions, or light particles such as electron, protons and neutrons mainly to understand the nature of radiation induced defects. It is only recently that there has been an increasing interest in the use of heavy ions in the MeV energy range driven primarily by the technological demands of ability to modify semiconductor materials at distances larger than several microns below the surface. The problems and issues arising out of use of high energy heavy ions are in many ways different from that of their keV counterparts. The present work is an attempt to contribute to this new emerging area of studies on defect phenomena due to MeV heavy ion implantation primarily through electrical studies. We postpone a more comprehensive statement of our objectives and scope to a later section in this chapter. We first give a brief review of issues in MeV ion implantation with primary focus on defect related studies of relevance to this work.

1.2 Technological Significance of MeV Ion Implantation

Though there are several potential applications of MeV ion beams, they have mostly been used in three distinct areas : (i) deep implantation of dopants to fabricate retrograde wells or tubs, (ii) production of buried dielectric layers such as silicon dioxide in silicon or semi-insulating isolation in III-V compounds, (iii) introduction of controlled gettering sites to remove harmful impurities such as iron [1]. Of these, MeV technology is already in use for over a decade in the fabrication of retrograde wells for DRAM, CCD and CMOS applications [4, 5] which would otherwise need lengthy high temperature dopant diffusion. This has led to the increasing importance of studies on defects and the interaction between multiple implants in new processing protocols. Production of buried dielectric layers has focused on implantation of oxygen in silicon and the efforts has been towards reduction of defect density levels to acceptable limits. Similar techniques of isolation is being adopted in III-V processing by implanting impurities or engineering defects which led to deep

compensated layers [6]. These applications typically need high energy and high dose implants. Effective gettering of detrimental impurities have been demonstrated by using intrinsic implant induced damage, nanocavities and high energy carbon implants. Commercial exploitation of these gettering techniques is imminent if the process is understood in sufficient detail [1].

Apart from these, there are several emerging applications involving mechanical and optical patterning using ion microbeams to form optical waveguides and cavities and selective disordering of superlattices [7]. Ion beam induced synthesis of desirable compounds such as sillicides and germanides using heavy ion implantation has also shown in potential contact technologies [8]. MeV heavy ion implantation has been shown to be an effective way of obtaining pure amorphous layers which is essential for technologies involving solid phase epitaxy. The growth of applications has been stimulated by availability of purpose-built MeV ion accelerators.

There are many additional advantages that accrue with the use of MeV implantation technology in processing. Some of the important ones include : (i) increased yield and shorter design cycle time due to simplification of process steps, (ii) reduction in thermal budget, (iii) avoidance of warping in large diameter wafers owing to low temperature processing. In DRAM fabrication technology, improvements have been reported in several device characteristics such as lower offset error rates, latch-up immunity, increased RAM retention time, improved low voltage operation etc.

With so many emerging applications, high energy implants are likely to become an integral part of semiconductor processing technologies, just as low energy implanters are standard industrial and laboratory tools today [9]. The key to the success of these applications and their widespread adoption hinges on our ability to predict process effects through a detailed understanding of defect related issues in each case. We can illustrate the importance of defect issues by citing another example apart from those mentioned

above. There has been a concerted effort over the recent years to introduce rare earth into silicon[1] and other semiconductors using MeV ions to take advantage of optical transitions in rare earth atoms within a semiconductor host [10, 11]. There has been a recent breakthrough in obtaining room temperature electroluminiscence at telecommunication wavelength of 1.5 μm using MeV Er and O co-implantation in silicon [12]. It is believed that the mechanism of excitation is mediated by deep levels defects, though the defect issues arising out of these implantations are little understood at present [13].

1.3 MeV Implantation : Energy Deposition and Range

The production of range and distribution of implanted ions is based on knowledge of processes through which the projectile looses energy in the medium. The two most important mechanisms of energy loss are [14] : (i) electronic stopping, in which ion looses energy by inelastic collisions with bound electrons in solid, and (ii) nuclear stopping, in which part of the kinetic energy is transferred to a nuclei in near elastic collision. The relative importance of the two stopping mechanisms depends on the energy and mass of the implanted ions, and the atomic density of the solid. The cross-section of stopping S associated with each mechanism is represented as

$$S_{e,n} = -\frac{1}{N}\left[\frac{dE}{dx}\right]_{e,n} \quad eV.cm^{-2} \tag{1.1}$$

where $\frac{dE}{dx}$ is the energy loss per unit distance for either electronic or nuclear stopping and N is the atomic density of solid. Figure 1.1 shows a schematic of these stopping power as a function of energy [14]. For low energy ions typically used for shallow junction formation, the nuclear stopping is the dominant mechanism. The nuclear stopping power is small for low energies since electronic screening reduces the effective atomic number of target nuclei, and it becomes again small at very high energies since interaction time

[1]Rare earth doped semiconductors has become a field in itself at present.

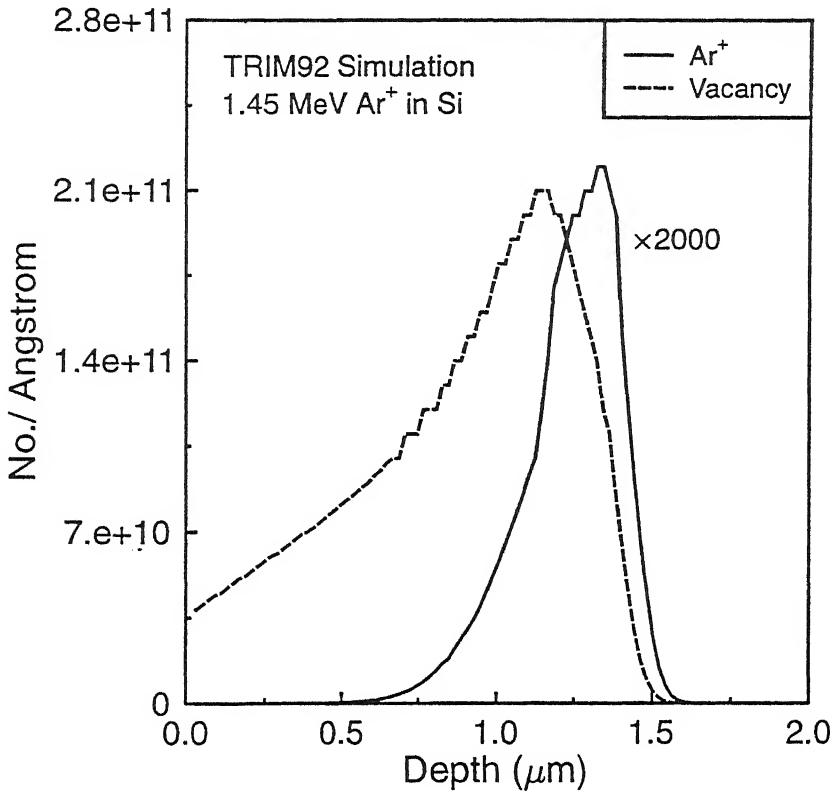

Figure 1.2: Vacancy and ion profile for 1.45 MeV Ar^+ ions (dose 5×10^{13} cm^{-2}) in Si using TRIM simulation.

approximately the range of the ion divided by its velocity. The thermal spikes created by ionization and excitation along ion track decays away by $\sim 10^{-12}$ s after entry of the ions, and many of the vacancies also created along the ion track and the tracks of the cascading secondaries recombine in $\sim 10^{-9}$ secs. *Light ions* tend to leave tracks characterized by relatively small amount of damage. They slow down by electronic stopping process initially with little displacement damage. Eventually nuclear stopping becomes predominant at the end of their range where they undergo collisions involving large scattering angles. Thus there is little lattice damage to the crystal except near the end of the ion range.

Heavy ions by contrast may create damage clusters along their path, as shown in Fig. 1fig3. These ions undergo a relatively higher degree of nuclear stopping than the light

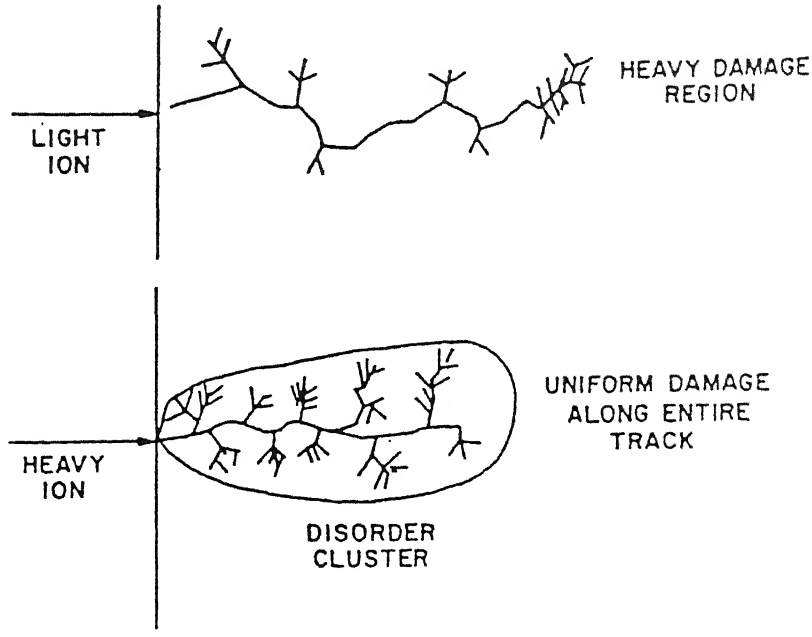

Figure 1.3: Schematic of the ion track in solid and associated damage for a light ion (top) and a heavy ion (bottom) (after ref.[6]).

ions, displacing target atoms right from the surface inwards. Large density of collision cascades give rise to considerable lattice damage within relatively small volume. For both light and heavy ion damage, the volume of the crystal in which the ion energy is deposited is usually larger than the volume in which lattice damage occurs. Much of the ion energy is transferred to the lattice as a localized thermal spike.

There has been a large number of studies dealing with implantation of dopants at MeV energies. The focus of these studies were on the issue of electrical activation of these dopants and damage evolution upon annealing. Here again resistivity, secondary ion mass spectrometry (SIMS) and transmission electron microscopy (TEM) studies have been the main tools. The annealing studies get often complicated by the fact that the implanted ions are substitutional electrically active dopants. Also in-situ dynamic annealing have been found to influence defect introduction. Even a reverse temperature dependence of annealing has been reported at high dose rates due to overlapping cascades in time [18].

The role of damage induced purely by ballistic processes and species dependant effects of damage appear simultaneous in each studies. The effects are due only to damage induced by massive projectiles can be separated from species dependent effects using noble gas ions which are ultimately electrically inactive in silicon. However, studies in this direction has been rare.

The nature of final disorder depends on a variety of factors such as ion mass, energy, dose, dose rate, temperature of implantation. For light particles and low fluences only point defects are produced while for high fluences of heavy particles one encounters the other extreme of amorphous layers. These are the two extreme regimes of MeV implants that have been intensively studied in recent years though with different methods. The point defect regime has been studied mostly using electrically sensitive techniques and magnetic resonance methods, whereas heavy damage and their evolution has been studied using structural tools such as cross-sectional transmission electron microscopy (XTEM). It is the middle regime of the damage, below amorphization but much above point defect regime, that is least studied. In fact, a recent study christens this regime of damage as 'missing link' [19]. We review recent results in each of these regimes for MeV implantation.

1.4.1 Point defects

The regime of low damage, specially with light particles such as electrons, neutrons and protons, only point defects seem to be generated. These defects have been studied in great detail in the past and it would be impossible to review this vast area within the scope of this work. It is only recently that there have been studies on similar point defects generated by heavy ions in MeV range by keeping the fluence of the ion very small ($< 10^9$ cm^{-2}) [20]. An impressive list of many defects have been studied using spectroscopic techniques such as infrared (IR), electron paramagnetic resonance (EPR) and transient based spectroscopies such as deep level transient spectroscopy (DLTS). In this regime of

defects, identification of electrical signature of the defects have played a central role in determining their nature and properties. The information is generally sought in terms of trapping and detrapping parameters such as energy, capture cross-section and relaxation mechanisms, and mechanisms of formation, diffusion, and interaction with other impurities. The actual defects produced in any given experimental situation depends critically on a number of parameters such as implant temperatures, ion species and energy, dose, dose rate, conductivity type, impurity present, annealing conditions etc. Such variability has contributed to continuing interest in this field. We will limit ourselves only to those well known aspects which are relevant to this work.

The hierarchy of stable defects generated from primary defects such as frenkel pairs, vacancies and interstitials have been most thoroughly studied for electron irradiation. These intrinsic defects pair among themselves or with commonly found impurities such as carbon, oxygen or with dopants. The most of these simple point defects pair anneal at well characterized temperature below 450°C. Some of the well known interstitial complexes are $C_s - C_i$, $C_i - O_i$, $B_i - B_s$, while vacancy complexes include divacancy (V_2), V-O, V-P. Many different interaction mechanisms between them have been proposed to explain relative concentration of these defects under different experimental situations. Though a wealth of data has been generated, a coherent picture of mechanisms is yet to emerge. Most commonly detected defects in ion irradiated n-Si are oxygen vacancy pair (V-O) or A center, two different charge state of the divacancy (V_2^{2-} and V_2^{-}) and phosphorus vacancy (P-V) or E-center. A summary of energy and capture cross-section of reported defect levels in as-implanted n-Si is presented in Table 1.1.

In p-type Si, the assignment of defect identification has been less straightforward. This difficulty may be attributed to a general lack of consensus in the literature regarding the identity of similar defect levels observed in electron irradiated p-Si. Hence it is difficult to tabulate defect levels for p-Si. Nevertheless, divacancy and interstitial-carbon-interstitial-

Table 1.1: Comparison of reported defect levels due to various ion in n-Si

Reference	Ions	O.V	V_2^{2-}	V_2^-/P.V	Unknown(?)
Wang [28]	H^+, He^+, B^+, P^+	E(0.18)	E(0.23)	E(0.41)	
Troxell [21]	H^+, B^+, Si^+	E(0.16)	E(0.23) *3×10^{-16}	E(0.43) 2×10^{-15}	
Hallen [22]	H^+, He^+	E(0.18) 23×10^{-15}	E(0.24) 2.6×10^{-15}	E(0.42) 1.7×10^{-15}	E(0.32), E(0.45 E(0.5)
Svensson [20]	H^+, He^{2+}, O^{4+} S^{7+}, Br^{8+}, I^{10+}	E(0.17) 2×10^{-14}	E(0.23)	E(0.42) 2×10^{-15}	E(0.35)
Palmetshofer [23]	H^+, D^+ He^+	E(0.17) 8×10^{-15}	E(0.21) 1×10^{-16}	E(0.41) 2×10^{-16}	E(0.30), E(0.35 E(0.39)
Indusekhar [24]	He^{2+}	E(0.18) 1.2×10^{-15}		E(0.48) 5.3×10^{-13}	E(0.28) E(0.51)
Krynicki [25]	C			E(0.41)	E(0.63)
Mary [26]	U	E(0.17) 2×10^{-14}	E(0.22) 7×10^{-16}	E(0.44) 7×10^{-15}	
Zafar [27]	He^{2+}	E(0.17) 2×10^{-13}	E(0.20) 2.2×10^{-13}	E(0.43) 3.4×10^{-15}	E(0.26),E(0.31) 1.7×10^{-14}
Benton [19]	Si^+	E(0.18)	E(0.23)	E(0.40,0.44)	

* Capture cross-section in cm^2

oxygen (C_iO_i) have been observed in most of the works [21, 28] with hole traps at 0.23 eV and 0.36 eV respectively above valence band. Other interstitial related defect such as B_iC_s at E_v+0.26 eV and clusters are sporadically noted in the literature [29].

1.4.1.1 Divacancy

Among radiation induced defects in silicon, divacancy (V_2) is the most ubiquitous and therefore is also one of the most well studied centers. Unlike monovacancy, the divacancy is stable and immobile at room temperature. As far as electrical activity is concerned, divacancy introduce deep levels corresponding to multiple charge states ranging from singly positive to doubly negative in heavily doped n-type Si. The level scheme for divacancy

Table 1.2: Charge state transition and energy level scheme for divacancy trap in silicon

Charge state	Transition	Energy level
$V_2^{0/+}$	emission of electron from neutral state	E_v+0.25 eV
$V_2^{-/0}$	electron emission to become neutral	E_c-0.42 eV
$V_2^{2-/-}$	electron emission to become singly charged	E_c-0.23 eV

that has emerged from several DLTS studies are given in Table 1.2 [20].

There have been controversies regarding whether E_c-0.23 eV level and E_c-0.42 eV level are indeed the two charge states of the same defect or not. The concentration of the two levels do not show one to one correspondence in many cases. For example, irradiations using MeV proton and alpha particles in n-Si showed difference in dose dependence of the two levels [22]. Recently, Svensson *et al.* studied the two levels in n-Si irradiated with a series of high energy particles starting from light particles to very heavy ions (electron, $^1H^+$, $^4He^{2+}$, $^{16}O^{4+}$, $^{32}S^{7+}$, $^{79}Br^{8+}$ and $^{127}I^{10+}$ [20]. Though the concentration of the two levels are same in electron irradiated material, their ratio was dependent on depth in case of ion bombardment. From a study of depth profile it was concluded that the concentration of level corresponding to E_c-0.42 eV is significantly larger than that of E_c-0.23 eV level in regions of large damage most probably due to strain favouring one state over the other. The E_c-0.42 eV peak in DLTS studies seemed to be broader for increasing projectile mass. Observations such as these and other properties have been sought to be explained on the basis of a model which invokes motional averaging of the two states at higher temperatures. The absence of E_c-0.23 eV level in MeV heavy ion implants is attributed to hindrance in reorientation among states at low temperature due to internal lattice strain associated with damage [20]. However, unresolved issues in terms of relative concentration of these two oft-observed levels persist and require more

studies by complimentary techniques. The divacancy is paramagnetic in the two charge state V_2^+ and V_2^-. There has been several thorough studies using EPR, IR and ENDOR spectroscopies by several workers [30, 31]. The defect has a point group symmetry D_{3d} with four equivalent orientation in $< 111 >$ directions. However, in its '+', '0' and '-' charge states, presence of Jann-Teller distortion lowers the symmetry to C_{2h}, a fact that has been confirmed by EPR observations below 20K. For higher temperatures, the defect does not relax to lower symmetry configurations, rather a motionally averaged D_{3d} state appears making V_2 a six-silicon atom center. This electronic bond switching was first observed by Watkins and Corrbett [32] and subsequently confirmed by Sieverts and coworkers [30, 31]. The symmetry of V_2^- state should be D_{3d} since no Jann-Teller distortion is expected. However this symmetry state is not observable since it is EPR inactive.

The formation mechanism of divacancy has also been controversial. Pairing of single vacancies due to bombardment in neighboring sites has been considered improbable. A more likely mechanism is that two single vacancies, created directly through primary knock-ons or indirectly in recoiling atom collisions migrate and subsequently agglomerate to form the more stable V_2 state. These defects anneal in the temperature range 300-350°C in low oxygen content silicon. Involvement of oxygen has been suspected in annealing kinetics by comparison of results for float zone and Chrochralski silicon.

The observed divacancy concentration in MeV implanted samples is much smaller than that would be predicted by a simulational package such as TRIM because of dynamic annealing and recombination. It has also been reported that divacancy concentration saturates for high dose implantations, the saturation value being one order of magnitude larger close to the surface compared to the deeper region ($> 1\mu$m for MeV implant) [33]. Interestingly, no divacancy centers are detected through EPR measurements in amorphous silicon [34]. The reasons for observed low concentrations of divacancy in high

fluence implantations needs further systematic studies.

1.4.1.2 Other vacancy associated defects

Vacancies produced in silicon during a room temperature irradiation are mobile and have been shown to combine with dopant atoms [35]. This combination appears to be the result of a Coulombic interaction. Formation of such a pair is more efficient in n-Si compared to p-Si.

The vacancy-phosphorus (P.V) center or E-center is a well understood defect and has an acceptor level 0.44 eV below the conduction level [36] and have capture cross-section $\sim 10^{-15}\ cm^2$. It has been observed to form even in p-type doubly doped silicon. The E-center has been shown to have a charge-state dependent annealing [37]. In DLTS spectra, E-center related peak is overlapped by the presence of V_2^- related peak as they have similar trap parameters. The overlapping nature of the two peaks in DLTS has been a source of controversy as regards the relative concentration of the two levels. However, differences in annealing behavior is used to differentiate between E-center and divacancy peak. E-centers are annealed out at $\sim 150°C$ whereas V_2 centers are stable upto 300°C. In moderately doped (phosphorus) Si, E-center concentration is reported to be only $< 20\%$ of the divacancy concentration in low dose MeV ion implanted n-Si [18]. However, in GeV heavy ion implanted Si, presence of E-center in full concentration has been reported by Mary *et al.* [26].

The vacancy - oxygen center (A-center) is a fairly well understood defect [36, 38] with an acceptor level at $E_c - 0.17$ eV. It occurs even in low oxygen content silicon. This defect is formed when a vacancy is trapped by interstitial oxygen atom. This trap level exhibits a very large capture cross-section for electrons, $\sigma_n \sim 1 \times 10^{-14}$ cm^2 [36]. The oxygen - vacancy pair has been reported to be stable upto $\sim 350°C$ [36].

A large number of oxygen plus multivacancy defects have been observed and studied

1.4.2 Defect Migration and Clustering

Studies on diffusion of impurities in semiconductors has been of central importance for both fundamental and technological reasons. This has led to a wealth of data on high temperature diffusivities and various mechanisms of diffusion [48]. Without attempting to review these, we only focus on the recent interest in migration and agglomeration of intrinsic point defects such as silicon self-interstitials and vacancies.

Since point defects in crystalline silicon generally occur in low equilibrium concentrations, measurements of their diffusive properties have been fraught with uncertainties. For example, high temperature diffusion data show very large discrepancies from different experiments. This has been illustrated by Gosele and Tan [49] by collating information from several authors. Extrapolation of defect diffusivities determined from high temperature measurement, to room temperature shows that vacancies should show no room temperature migration (with diffusivities $< 10^{-30}$ cm/s). There has also been a long-held view in the literature that defect evolution in Si under irradiation is fully determined by recombination and clustering within the damaged region. However, as mentioned earlier, long distance migration even at cryogenic temperature have been shown from EPR experiments and DLTS. From these experiments room temperature diffusion coefficients for vacancies and interstitial have been estimated to be $D_I = 3.4 \times 10^{-4}$ cm^2/s and D_v=4.2$\times 10^{-9}$ cm^2/s, respectively. These large discrepancies could be attributed to either change in structures at high temperature or ionization enhanced migration under irradiation condition. However, there are several recent studies which show long range room temperature migration of these defects. Larsen *et al.* [50] have shown the importance of long-range trap limited diffusion for self-interstitials using spreading resistance measurements on heavy ion irradiated silicon. Coffa *et al.* [51] have provided evidence of room temperature migration of self-interstitials over several microns through specially designed experiments. The interstitial and vacancy diffusivities being used for quantita-

tive prediction of phenomena in simulation at present are $D_I = 0.01exp(-0.9/kT)$ and $D_v = 0.001exp(-0.43/kT)$ [52].

The ion generated interstitials and vacancies, being mobile at room temperature, are most likely to end up in clusters if they escape recombination. Though presence of such clusters have been invoked in many studies, direct correlation between their occurrence and electrical activity is still lacking. The vacancy clusters have been grown in the past by cooling down as-grown crystals and were reported to be electrical inactive [53, 54]. Early observations of interstitial type cluster had come from electron microscopy in relation to formation of dislocations. There has been so far no easy effective experimental way of bridging the gap between observations of simple point defects as in EPR and DLTS on the one hand, and electron microscopic investigations of observable extended defects on the other hand. It is for this reason that intermediate defect configuration between two such clusters have not been studied in the literature.

There has been recently attempts to simulate the effects of migration and clustering and indirectly infer their properties from matching with experiments [55, 56]. The number of point defects produced due to ion bombardment depends on ion species, energy and vary over large orders of magnitude per ion. A survey of literature does suggest that clustering is predominant when the projectiles are heavy and doses are high most probably because long-lived excess interstitials are available under such conditions [52].

The binding energies of interstitial clusters have been estimated from molecular dynamics (MD) simulations [57], and from smooth fit to the data are given by $E_{bi}(n) = 2.1 - 1.45(\sqrt{n} - \sqrt{n-1})$ where n is the number of interstitials. Similarly, the cluster binding energies for vacancies have been estimated to be $E_{bv}(n) = 3.65 - 5.15[n^{2/3} - (n-1)^{2/3}]$. Jaraiz *et al.* [52] have shown from MD calculations that a fraction of interstitial population remain free to migrate, annihilate and agglomerate even after three hours of irradiation at room temperature for a dose of 5×10^{13} cm^{-2} of Si. The depth distributions

of interstitials were shown to peak at twice the implant range which was attributed to momentum transfer from the implant and profile distortion due to initial annihilation at the surface. In annealing studies, clusters are believed to undergo Ostwald ripening process eventually dissolving at high temperature at the surface. The simulation in particular predict continual formation of interstitial atomic cluster with increasing size at room temperature. In our view, a careful study of this regime is essential at present in order to enable corrections among a variety of phenomena.

The electrical activity corresponding to these clusters is a largely unexplored area. Benton *et al.* [19] have recently associated two hole levels at 0.29 eV and 0.48 eV with clusters in p-type Si. They also argue that DLTS peaks correspond to cluster smaller than 50Å. However, it is surprising that one observes very well defined point defects like signature in the presence of expected distribution in sizes of these clusters.

1.4.3 Extended defects

When ion damaged materials in the dose regime $> 10^{14}$ cm^{-2} are annealed, extended defects have been observed to form. There have been fairly large number of studies on extended defect formation using cross-sectional TEM as the principal instrument. On annealing in the range of 670-800°C following high dose and high energy implants, the damage is known to evolve into rod-like interstitial agglomerates large enough to be observed by TEM and are known as {311} defects [56]. These intermediate defect configurations can either dissolve giving rise to self-interstitials or provide a nucleation site for the generation of full blown dislocation loops. The concentration of these agglomerates decreases while sizes increase on continued heat treatment as in Ostwald ripening process.

The nature of evolution of damage in this range of extended defect formation has been systematically categorized by Jones *et al.* [58] on the basis of TEM studies of a very large number of implanted samples under varying conditions. There has also been an effort to

determine a threshold dose below which extended defect formation would not occur on annealing [59]. This dose is believed to be below the amorphization threshold, but the parameters that determine it are not so well known [60].

The electrical signature of extended defects in DLTS studies, remains controversial in spite of several studies especially in plastically deformed silicon. Generally, a DLTS signature is attributed to an extended defect if it is a broad signal corresponding to a many-electron center. A characteristics of such many-electron center is believed to be slow increase in occupancy (logarithmic in time), due to changing Coulombic barrier during capture. However, such increase can be due to various other reasons such as local macroscopic barriers or coupled kinetics in multi-trap situation. Hence careful interpretation of conventional DLTS spectra are needed in such cases [61]. In high dose ion implanted Si, a commonly observed level at 0.5 eV is generally associated with an extended defect [29]. However, systematic correlations leading to definitive identification is still lacking.

Injection of interstitials from extended defects at high temperatures and issues of interstitial migrations and clustering are being studied extensively in relation with a technologically important phenomena of transient enhanced diffusion (TED) of dopant in Si. TED is the phenomena of large nonequilibrium of diffusion of dopants in implanted samples at about 800°C. The non-equilibrium diffusion vanishes at large times. It is by now well established [46, 62] that the anomalous diffusion arises from excess silicon self-interstitials that are generated from extended agglomerates, such as {311} defect, though consensus regarding mechanisms of diffusion is yet to emerge. A recent article by Stolk *et al.* [46] discusses many aspects of these phenomena in great details and provide an agenda for researches in this field. Significantly many of the issues raised deal with defect migration and clustering and interstitial injection kinetics.

In this work, in a bid to study as-implanted damage , we have avoided the regime of

extended defects by limiting ourselves to processing temperatures below 650°C.

1.4.4 Defects and amorphization by irradiation

It is well known that ion-beam induced damage for sufficiently high dose, can give rise to amorphization. Though it is possible to make estimates of dose requirement from simple considerations, experimentally amorphization tends to depend on many parameters. The total number of atoms displaced by an incoming ion can be estimated as [63]

$$N_d \sim \frac{E_n}{2E_d}$$

where E_n is the total energy loss of a particle in primary and secondary nuclear collisions, and E_d is the displacement energy of a lattice atom. Typically, E_d is ~15 eV in semiconductors. The number of displaced atoms, for example, with a 1.4 MeV Ar ion in Si is ~3400. Thus at doses near 10^{14} cm^{-2} the displacement disorder concentration is approximately equal to the Si atom density, leading to amorphization.

If one assumes all target atoms must be displaced to form an amorphous layer, then the critical dose for its formation is [14]

$$\phi_m = \frac{2E_d N}{(dE/dx)_n}$$

This relation always underestimates the critical dose because of self-annealing or dynamic annealing of vacancies and interstitials. Some attempts have been made to take this into account by including defect diffusion and recombination processes. The critical dose for amorphization depends strongly on the temperature of the implantation [64]. With an increase in the dose rate, the critical dose usually decreases because the damage is able to accumulate before it self-anneals. For very high dose rates however, the sample can be heated by irradiation, and dynamic annealing of the damage occurs. In this case an amorphous layer may never form. The critical dose for creation of an amorphous layer in Si for room temperature Ar^+ implant has been shown to be $\sim 1.2 \times 10^{14}$ cm^{-2} [65]. The

annealing of point defects and locally amorphous zones occurs by defect diffusion and recombination at elevated temperatures. The energy deposition increases with nuclear energy loss $(\frac{dE}{dx})_n$ which in turn increases with projectile mass as in modified Kinchin-Pease model. The earliest model of ion beam induced amorphization was by Morehead and Crowder [66] who attributed it to sufficient overlap of the amorphized cylindrical cascades. This is viewed as a heterogeneous mechanism of amorphization.

However, there has been homogeneous amorphization models, proposed initially by Swanson *et al.* [67] and more recently by Holland *et al.* [68], according to which amorphization is a phase transition induced by sufficient number of defects in crystalline silicon. Motooka *et al.* [55] have also proposed a model of homogeneous amorphization using molecular dynamic calculations in which accumulation of divacancy and di-interstitial pairs beyond a threshold value lead to amorphization. However, empirical evidence of identity of accumulating defect is still lacking.

Apart from process of amorphization, implant induced pure amorphous silicon (a-Si), in contrast to hydrogenated a-Si, has also aroused interest and it has been studied by a variety of methods [69, 70]. It has been shown that pure a-Si undergoes structural relaxation due to kinetics of point defects. Both structural relaxations (i.e. short range ordering) in a-Si and defect annihilation in crystalline silicon is found to obey bimolecular relaxation kinetics. The nature of short range ordering in pure a-Si, as obtained from ion implantation, turns out to be different from that obtained in usual hydrogenated a-Si, where creation of metastable defects and their annealing dominates.

In spite of the realization that most phenomena in implant induced a-Si can be understood within the framework of a defect mediated structural relaxation, the nature of participating defects is unclear. This is mainly due to difficulties in establishing clear connection between structural studies and defect spectroscopic techniques. In our view, such correlations can be best done using proper choice of regimes of controlled disorder.

The choice of dose for heavy ion implantation in this work is motivated by this consideration. The doses are kept below amorphization threshold but sufficiently high to create conditions of large disorder in crystalline Si with the hope that it would enable possible identification of dominant defects. We show in a later chapter that the study of charge relaxation mechanisms in samples so disordered can provide significant insights into relaxation mechanisms in a-Si in general. However, we postpone a review of related issues to a more appropriate context in Chapter 6 where these results are presented.

1.5 Motivation and Focus of The Present Work

The foregoing review shows that there are many unresolved issues in our understanding of radiation induced damage in case of high fluence, MeV heavy ion implantation in silicon, though earlier studies with light particle irradiation provide a relatively firm basis. It is not clear as to which aspects and to what extent our understanding of light particles, low energy and low dose implantation can be carried over to the cases with combinations of parameters such as high energy, heavy ion and high fluence. The inherent differences are primarily due to nature of disorder created due to high density collisional cascades, and complexities arising out of movement and agglomeration of large concentration of defects. There is a lack of studies on electrical manifestation of phenomena such as defect migration and agglomeration. The empirical support to test results of recent molecular dynamic simulational studies [52] are inadequate. The connection between damage as studied by structural tools such as cross-sectional transmission electron microscopy (XTEM) and defects controlling electrical characteristics such as compensation and trapping are missing. This is primarily because electrical characterization has been used for limited purposes in this regime of parameters. In fact, studies involving electrical characterization of point defects deliberately avoid complexities attributable to heavy damage in order to preserve validity of the techniques used and simplicity of interpretations. Hence the power of spec-

troscopic electrical defect characterization techniques has so far been grossly underutilized in the study of phenomena related to damage created by heavy ions.

The principal motive of this work is to study electrical manifestation of damage created in deep buried layers using MeV heavy ions and relate them to the nature of dominant electrical defects created. It was essential therefore to critically evaluate validity of standard electrical methods of characterization for these cases. The sources of difficulties in electrical studies are many. Firstly, the concentration of defects are large invalidating straightforward use of popular characterization methods such as DLTS. Secondly, their spatial distribution is highly nonuniform leading to inhomogeneous modification of the host. Thirdly, the damage layer of interest is located deep within the sample. Though transport studies would certainly be intrinsically interesting in these samples, we deliberately avoid them as methods of characterization since transport parameters typically constitute contribution in varying degree from many different mechanisms. Hence we limit the scope of this study to capacitance based techniques. Characterization techniques based on depletion layer capacitance provide a degree of control unavailable in transport measurement in terms of defect depth from the surface and spectroscopic character. Capacitance based techniques, specially transient based spectroscopic methods, have been highly successful in the study of point defects in the well characterized regime of radiation induced damage (as for example, in the case of electron irradiation). A running theme of this work has been to suitably extend and modify these techniques keeping in view anticipated difficulties such as various sources of non-exponentiality of transients.

With this in focus, the damaged layers of interest are created using MeV heavy ions (Ar^+ and Au^+) within the depletion layers of Schottky devices, which serve as laboratory for all defect studies in this work. The doses are kept below amorphization threshold. The choice of Ar^+ ion has been motivated by the need to avoid issues of electrical activation of the implanted ion so as to focus only on damage induced by heavy ion irrespective

Chapter 2

Principles of Experiments and Techniques of Data Analysis

2.1 Introduction

Defects and impurities in crystalline semiconductors introduce states in their otherwise forbidden gap. Substitutional dopants give rise to shallow states (states close to band edges) which control carrier concentration, while deeper states control carrier lifetime. Hence electrical characterization of these states has been both convenient and appropriate for most applications. Among electrical measurements the use of capacitance based techniques has several advantages over transport measurements. One of the principal advantages is the wide availability of robust instrumentation for carrying out sensitive capacitance measurements. Further, in the context of semiconductor devices, space charge regions in a wide variety of structures provide convenient laboratories for implementing capacitance based techniques to study defects in environments most suitable from application point of view. The use of capacitance-voltage (C-V) measurements is one of the most popular methods of profiling shallow dopants. The experimental study of deep levels in semiconductors was revolutionized following introduction of capacitance based methods. In fact we owe much of our present understanding of deep levels and the huge amount of information collected over the last two decades to transient based capacitance techniques.

The electrical characterization of deep level defects is normally carried out in terms of phenomenological parameters of these levels provided by Shokley-Read-Hall (SRH) model

of trapping and recombination processes. The basic information that one seeks from such measurements include thermal activation energy (E_T), carrier capture cross-sections (σ), concentration (N_T) profile etc. of traps. With the advent of transient spectroscopic methods such as deep level transient spectroscopy (DLTS) [71], easy electrical recognition of defects through their emission signatures made a large number of dynamical studies possible. There are number of excellent books, monographs and reviews devoted to the subject in the literature [72, 73, 74, 75, 76]. We confine ourselves in this chapter to brief discussions of only those aspects which are relevant to our study of deep levels in ion induced buried layers.

In this chapter, at the outset we discuss in presence of high trap density and series resistance in a Schottky diode, validity of standard C-V profiling. The effect of series resistance, leakage current, high defect concentration ($N_T/N_d \geq 1$, N_T is trap concentration and N_d is shallow doping concentration), on capacitance transients are examined in this chapter. Their effect on trap parameter estimation is analyzed in detail. A variety of nonexponential transients are encountered in the study of defects in the ion-damaged materials. Critical comparison between temperature scanning techniques such as DLTS and isothermal techniques such as time analyzed transient spectroscopy (TATS) are made as regards their suitablity for quantitative evaluation of nonexponentiality and to understand underlying physics of defects. Nonexponentiality in transients are estimated from lineshape analysis of the DLTS and TATS spectra. A case study is presented with experimental evidence of different kinds of nonexponentilaity in different temperature regime in case of semi-insulating gallium arsenide (SI-GaAs). Superiority of TATS over conventional DLTS kind of analysis in this case is demonstrated with this example. Limitations and advantages of various techniques and methodologies used in this work are discussed.

2.2 Defect Study by C-V Technique

Techniques using depletion capacitance rely on the fact that the width of a reverse biased space-charge region (scr) of a semiconductor junction device depends on the applied voltage. The C-V profiling method has been used with Schottky barrier diodes using metal and liquid electrolyte contacts, *pn* junctions, metal oxide semiconductor (MOS) capacitors, and metal oxide semiconductor field effect transistors (MOSFET).

We first recall the principles behind profiling semiconductors for the majority carrier distribution by the C-V technique. In the case of a Schottky barrier diode, a reverse bias produces a space charge region of width W in the semiconductor side of the junction. The capacitance ($\frac{dQ}{dv}$) is determined by superimposing a small-amplitude *ac* voltage v on the dc voltage V. The *ac* voltage typically varies at a frequency of 1 MHz with an amplitude of 10-100 mV. The capacitance of the Schottky diode is

$$C = A\sqrt{q\epsilon/2}\sqrt{N_{scr}/(V_{bi} - V)} \tag{2.1}$$

where N_{scr} is the ionized impurity concentration in the space charge region. It is also assumed that potential drop due to leakage current is small and all the reverse biasing potential V drops across the depletion layer. It is assumed that diffusion capacitance is negligibly small compared to the depletion capacitance and no transverse non-uniformities exist.

2.2.1 Defect profile in presence of uniformly distributed traps

It is known that special analyses are required for the interpretation of junction capacitance measurements on semiconductors containing deep traps [77, 78, 79, 80, 81]. A deep trap is generally defined [1] as a trap whose energy is located below Fermi level in n-type

[1]Though a srtict definition does not exist, magnitude of ionization energies and their pressure coefficients can be used as distinguishing characteristics between deep and shallow levels. From a theoretical point of view, defect levels whose properties cannot be described by hydrogenic effective mass theory are

material or above the Fermi level in p-type material. Particularly, deep traps have been found to greatly influence apparent free carrier profiles determined by C-V measurements [79, 81, 82].

Under the assumption of one sided step junction, Fig. 2.1(a) and 2.1(b) shows the resulting band bending of the junction at a given reverse bias V for the case of deep donors and deep acceptors, respectively. The unique feature of a structure with deep traps in the region (x-y) in which generation-recombination processes are active in determining the equilibrium occupation of the traps. The more general case is exemplified by the rest of the depletion region, 0¡W¡y which is fully depleted of mobile carriers, and in which trap occupation is controlled only through emission processes. The existence of these two regions results in a space-charge nonuniformity. This nonuniformity is represented in Fig. 2.1 by a staircase function [83]. This transition region has a 'Debye tail' of majority carrier which spills into the depletion region. This carrier concentration acts to give a finite equilibrium population probability of deep traps in that portion of the depleted region. In addition, this fuzziness of the depletion width boundary serves to limit the spatial resolution of C-V profiles to about a Debye length [84] even in materials without deep traps. To find majority carrier profile for uniformly doped substrate, Eqn. 2.1 can be written in the form

$$N_{scr}(x) = \frac{2}{qK_s\epsilon_o A^2[\frac{d(1/C^2)}{dV}]} \tag{2.2}$$

with $x = K_s\epsilon_o A/C$. The trap profile can be extracted from the knowledge of background profile.

deep levels.

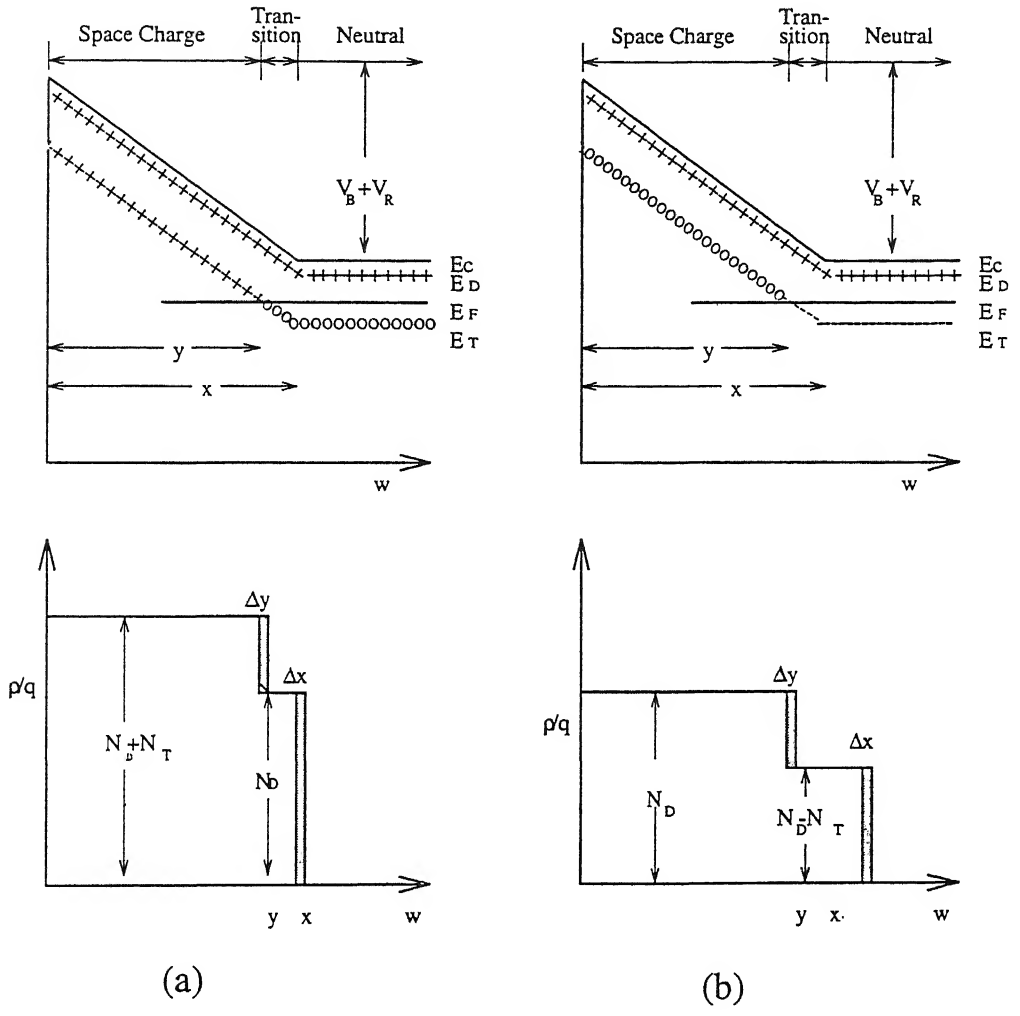

Figure 2.1: Band diagram of a Schottky diode under reverse bias with one deep trap. V_B is the junction barrier height, V_R is the applied reverse bias, E_c is the energy position of the conduction band edge, E_D is the shallow donor level, E_F is the Fermi level, E_T is the trap level, y is the point at which E_F and E_T intersect and x is the edge of the depletion region. Deep donor traps are shown in (a) and deep acceptor traps are in (b). (after ref. [83])

2.2.2 Defect profile in presence of nonuniform distribution of traps

The shape of the profile in the presence of a nonuniform distribution of deep levels is now considered. A discussion of the C-V technique applied to nonuniform distribution of trap have been considered by Kimerling [83] and by Schulz [85]. It has been shown that great care must be taken in capacitance measurement of free carrier distribution in semiconductors containing deep traps. Kimerling [83] has shown that spatial distribution derived from C-V can be anomalous unless measured conditions such as temperature and frequency of the measurements are carefully determined based on the junction structure and the electronic nature of the traps. Schulz [85] has shown that when large concentration of deep donors/acceptors are present in a certain region of space charge layer, one measures an 'apparent' profile which is shifted from the actual profile of the defect. In case of deep donors this profile appears broad and for deep acceptor it appears sharp compared to the actual trap profile. This is due to crossing of the Fermi level with the trap level which causes occupation change deep inside the depletion region where defect are present. In such cases, a knowledge of the defect profile helps in determining the energy level of the deep traps by locating the cross-over point of Fermi level and trap level.

In case of heavy damage in the semiconductor due to ion implantation, presence of an insulating layer may make a Schottky diode behave more like an Metal-insulator-semiconductor (MIS). In case of buried oxide layers, for example, C-V characterization is carried out modelling the structure as M-S-I-S [86]. The doping profile can be obtained in such a case from appropriate modifications to standard MIS analysis. With combined measurements of capacitance at high and low frequency in regions of inversion, depletion and accumulation, a number of parameters such as thikness of the insulating layer and interface traps density can be inferred.

2.2.3 Factors affecting C-V profiling technique

C-V measurements can be affected by many factors which include (i) series resistance, (ii) diode edge and stray capacitance, (iii) excess leakage current, (iv) minority carrier and interface traps, (v) Debye length, and (vi) voltage breakdown etc. We discuss below some of these factors relevant to the present work.

2.2.3.1 Series resistance

A simple equivalent circuit for a *pn* junction or Schottky diode consists of a junction capacitance C, a junction conductance G, and a series resistance r_s. Conductance determines the junction leakage current and can be varied by processing conditions. The series resistance depends on the bulk wafer resistivity and on the contact resistance. Capacitance meter assumes the device to be represented by the parallel circuit in Fig. 2.2, where C_m and G_m are measured capacitance and conductance. Comparing the two circuits allows C_m to be written as [87]

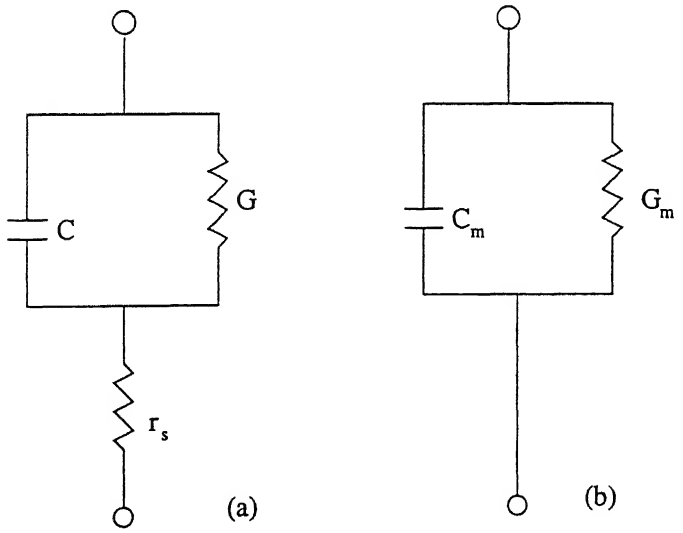

Figure 2.2: (a) Actual circuit with a series resistance r_s and (b) capacitance meter equivalent circuit for a *pn* junction or Schottky diode.

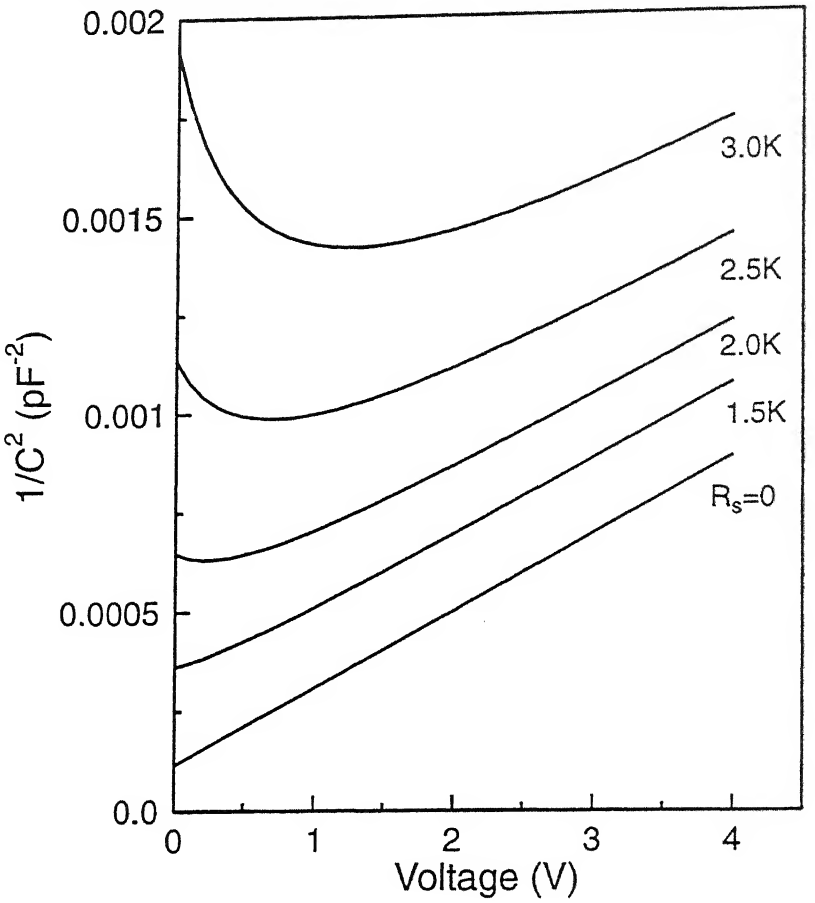

Figure 2.3: Effect of series resistance on the C-V plot in a Schottky device. Simulation parameters : Doping $N_D = 1 \times 10^{15}$ cm^{-3}, Diode area A=7.85×10^{-3} cm^2, measurement frequency f=1 MHz.

$$C_m = \frac{C}{(1 + r_s G)^2 + (2\pi f r_s C)^2} \tag{2.3}$$

For the measured capacitance to be approximately equal to the true capacitance, it is necessary that $r_s G \ll 1$ and $(2\pi f r_s C)^2 \ll 1$. For junction with low leakage current, $r_s G \ll 1$ is satisfied. But, $(2\pi f r_s C)^2 \ll 1$ is not always satisfied. For example, if the true capacitance is 100 pF measured at f=1 MHz then r_s should be less than 160 Ω for 1% accuracy in capacitance measurement. In this way, series resistance interferes with capacitance measurement. In Fig. 2.3 the effect of series resistance on the $1/C^2$ vs. V plot is shown for various values of series resistance in a Schottky diode. These

2.3 Current-Voltage (I-V) Characteristics

I-V studies are very important for complimentary information on carrier transport behaviour in ion-damaged materials. Current transport in a Schottky device under forward bias constitutes four basic processes [90] namely, (i) thermionic emission, (ii) tunneling, (iii) carrier recombination in depletion region and (iv) minority carrier injection. When the diode is forward biased, the current raises exponentially with voltage and in presence of series resistance, the part of the applied voltage drops across it for larger current at high voltage. The series resistance and ideality factor of the diode can be estimated from an iterative fitting of I-V data. However, in presence of an insulating/semi-insulating layer between metal and semiconductor contact, the current conduction is determined by a number of processes namely, (i) Schottky emission, (ii) Poole-Frenkel emission, (iii) Tunnel or field emission, (iv) space charge limited, (v) Ohmic and (vi) ionic conduction. In particular, we are concerned with the case of space charge limited current in the case of $p - i - n$ type device. Space charge limited current for a unipolar trap free case is proportional to the square of applied voltage (i.e. $J \propto V^2$). At low voltage and high temperature, current is ohmic with exponential dependence on temperature. In presence of high concentration of trap, on the log-log plot of current versus voltage, there is a nearly vertical section in the characteristics. This is attributed to the filling of a discrete set of traps. The voltage at which this vertical transition occurs, is known as trap-filled-limit voltage (V_{TFL}) [91].

Trap filled limit voltage measures that fraction of the total concentration of trap that is empty in thermal equilibrium. From the knowledge of dimension of the insulator region, trap concentration is estimated as [91]

$$N_T = \frac{1.1 \times 10^6 \kappa V_{TFL}}{L^2} cm^{-3} \tag{2.6}$$

where κ is the relative static dielectric constant, L is in cm. For distributed trap states,

the distribution can be extracted from fitting of I-V characteristics. However, in MIS structure, presence of metal-insulator and insulator-semiconductor junction can have contribution to the total current making the analysis difficult. Apart from N_T estimation, one can determine trap energy (E_T) from the relation [91]

$$E_c - E_T = kT \ln(N_c/\theta g N_T) \tag{2.7}$$

where $g \approx 2$, N_c is conduction band effective density of states and θ is determined from the knowledge of κ and μ (mobility). In materials with high degree of structural disorder, even though chemically very pure, one may expect multiple trap levels distributed in energy. A distribution in energy of trap in an insulator would reflect in the sharpness of current rise at V_{TFL}. In principle, energy distribution can be recovered from observations of I-V curve in such cases. We show later that our samples do show trap limited space-charge conduction when forward biased.

2.4 Thermally Stimulated Capacitance (TSCAP)

In this method, a reverse biased junction or Schottky diode is cooled to sufficiently low temperatures so that thermal emission rates of carriers is negligible. A non-equilibrium occupancy of deep levels is then induced with zero bias pulse of duration long enough to fill the traps. As the sample temperature is increased, the deep levels relax to their equilibrium occupancy. The steady state capacitance is measured as a function of temperature. Capacitance steps are observed as traps emit their carriers. The midpoint of the TSCAP step in temperature (T_m) is related to the activation energy E_e by [92]

$$E_e = kT_m \ln\left[\frac{\nu k T_m^2}{\beta(E_e + 2kT_m)}\right] \tag{2.8}$$

where β is the heating rate and ν is attempt to escape frequency. Trap concentration is estimated from the step height of TSCAP curve. Activation energy is determined from an

Arrhenius plot of $\ln(T_m^2/\beta)$ versus $1/T_m$ for varying heating rate (β). One can distinguish between majority and minority carrier trap by noting sign of the capacitance change.

The technique works well for $N_T > 0.1N_D$ and $E_e \geq 0.3$ eV i.e. its sensitivity is much less than the spectroscopic techniques described earlier. TSCAP measurement is less influenced by diode quality. Baseline determination in TSCAP data without trap filling is necessary to know the TSCAP step height. Often, there is a large change in capacitance during heating cycle even without filling. This is mostly due to Fermi level movement with temperature which causes the effective change in depletion width. In terms of convenience of use and interpretation, TSCAP is less convenient than DLTS and TATS due to requirement of controlled thermal scan rate.

2.5 Capacitance Transient

The junction capacitance in a semiconductor diode is related to the trapped charge concentration. If nonequilibrium occupancy of deep traps can be induced, the equilibrium can be monitored through measurements of capacitance consisting of capacitance transients [93]. Under reverse bias, the traps in the part of the depletion region are unoccupied since trap level is above the Fermi level. A non-equilibrium situation is created typically by applying a forward bias or zero bias for short duration, during which the depletion width reduces. This duration is called filling time, t_f. Under filling condition, a trap level (say, an electron trap) goes below the Fermi level and the unoccupied traps capture conduction band electrons. On reapplication of reverse bias, the carriers emitted from the trap subsequently are swept out of the depletion region. As already shown in Fig. 2.1, there can be a region within depletion width where the traps are occupied till the point trap level crosses the Fermi level. In case of high trap concentration, consideration of this region can play an important role.

2.5.1 Exponential transient

The measured capacitance transient would be exponential if the change in capacitance is small as compared to the steady state capacitance and can be expressed as

$$C(t) = C_0 \left[1 - \left(\frac{n_T}{2N_d}\right) exp(-t/\tau_e)\right] \tag{2.9}$$

where C_0 is steady state capacitance value at reverse bias, n_T is occupied trap concentration and N_d is shallow doping concentration, τ_e is characteristic emission time constant of trap. The condition that change in capacitance should be small as compared to C_o is same as the condition $N_T/N_d \ll 1$ i.e. for small trap concentration. Use of constant capacitance voltage transient does not have any limitation on trap density. This has been discussed in the next section. The emission time constant τ_e in the above equation has an Arrhenius dependence on temperature given by

$$\frac{1}{\tau_e} = \sigma_n < v_{th} > N_c exp(-E_T/kT) \tag{2.10}$$

where E_T is the activation energy of the trap and σ_n is the capture cross-section of the trap. Other symbols have their usual meaning. Hence, monitoring of capacitance transients at various temperature allows determination of τ_e as a function of temperature and hence the trap parameter E_T and σ_n. Experimental characterization is performed by use of Arrhenius plot to obtain the activation energy and attempt to escape frequency from the slope and intercept, respectively.

2.5.2 Nonexponential transient

The capacitance transient signal represented in Eqn. 2.9 is an exponential. However, nonexponential capacitance transient may occur when (i) trap density is of the same order as that of shallow dopants, (ii) several trap levels decay with similar emission rates, and (iii) emission rate is field dependent. There are large number of papers in which

attempts have been made to take into account non-exponentiality due to each of these reasons in interpretation of data [94, 95]. There have been also varieties of experimental ways of avoiding nonexponentiality [96]. There are large variety of methods available for extracting the trap parameters of exponential signals [97].

The nonexponentiality due to high trap density can be avoided by performing the transient measurement in constant capacitance (CC) mode. In this method capacitance or the depletion width is held constant during the carrier emission measurement by dynamically varying the applied voltage through a feedback circuit [96, 98, 99]. The voltage transient in that case is expressed as

$$V(t) = \frac{q\epsilon A^2}{2C^2}[N_d - N_T exp(-t/\tau_e)] + V_{bi} \tag{2.11}$$

without any restriction on $\frac{n_T}{N_d}$ ratio. Equation 2.11 shows V(t) response to be exponential in time. One of the limitation of the CC transient measurement is its slower circuit response due to feedback circuit. Initial part of the transient can be affected due to carrier capture even during the emission process [100]. Some of the sample dependent causes of nonexponential transient may include series resistance effect and leakage current effect in the device.

2.5.2.1 Series resistance effect

Distortion in capacitance transient due to series resistance is also well known [101, 102]. Carrier freezeout or trap compensation may lead to temperature dependent series resistance. For non-leaky devices with series resistance r_s, measured capacitance transient C_m(t) is related to the sample capacitance C_s(t) by

$$C_m(t) = \frac{C_s(t)}{1 + \omega^2 r_s^2 C_s^2(t)} \tag{2.12}$$

where ω is the test signal frequency of the capacitance meter.

It is clear from Eqn. 2.12 that C_m(t) will go through a maxima when $\omega^2 r_s^2 C_s^2 > 1$. At this point of inversion (time t_m) of the nonmonotonic transient, t_m is such that the condition $\omega r_s C_s(t_m) = 1$. This is easily obtained by differentiating Eqn. 2.12 with respect to time and setting it to zero. Hence,

$$r_s = \frac{1}{\omega C_s(t_m)} = \frac{1}{2\omega C_m(t_m)} \tag{2.13}$$

Evaluating r_s for a particular temperature (in case of isothermal transient), we get from Eqn. 2.12,

$$C_s = 2C_m \frac{1-\sqrt{1-x^2}}{x^2} \qquad for\ t < t_m \tag{2.14}$$

$$C_s = 2C_m \frac{1+\sqrt{1-x^2}}{x^2} \qquad for\ t > t_m \tag{2.15}$$

where $x = 2\omega r_s C_m(t)$. The presence of series resistance in the transient is first detected by noting peak shape in the transient and the actual transient is constructed using Eqn. 2.14 and 2.15 [103].

The applicability of this method relies on the fact that series resistance should be appreciably high such that $\omega^2 r_s^2 C_s^2 \geq 1$ is satisfied. If r_s is not so high, one can add external resistance in series with the device to fulfill the condition stated above. However, when both majority carrier and minority carrier traps occur at the same time, nonmonotonic transient may also result. One may mistakenly attribute such occurrence to series resistance. It is advisable to cross-check the presence of series resistance from current-voltage characteristics of the device as well as from impedance and loss measurement. Therefore, independent estimate of series resistance and prior knowledge of types of traps (majority or minority carrier) are needed. We have already discussed ways of obtaining series resistance, in section 2.2.4.1. Particularly, we use impedance and loss measurement in our device to estimate the effect of series resistance in capacitance measurement.

Series resistance effect in transient can be reduced by reducing the measurement frequency ω [104]. However, it severely restricts the range of usable time constants, also low

frequency measurement gives rise to noisy data. In presence of defect/damaged region in the device, at lower frequencies one normally observes increase in capacitance which in turn does not help in reducing the quantity $\omega^2 r^2 C_s^2$. The use of constant capacitance (CC) mode in which C_s is kept fixed during transient overcome the series resistance problem altogether [105]. Since *dc* resistance does not affect the CC mode of operation, voltage transient carries trap information alone.

2.5.2.2 Leakage current

Device prepared under poor vacuum condition and surface preparation, ion implanted devices often exhibit high reverse leakage current. If the capture of the leakage related carriers in the space charge layer is larger than the thermal emission rate from a particular gap state to the band, then the apparent emission rate is given by [106]

$$e_{app} = e_n + \frac{J_{leak}}{q}\sigma_n \tag{2.16}$$

where e_n is true emission rate, J_{leak} is leakage current, σ_n is capture cross-section. Particularly, for the case of broad density of states, leakage current has dramatic effect on capacitance transient [107]. A correction scheme for leakage current effect on the capacitance transient has been proposed by Dmowski *et al.* [106].

2.6 Deep Level Transient Spectroscopy (DLTS)

Though several methods are known for extracting time constant from the capacitance transient directly, the advantages of spectroscopy in transient analysis was first realized by D.V. Lang [71] who introduced the rate window concept in the form of DLTS to deep level characterization. DLTS converts the exponential transient signal into a spectrum which is amenable to standard spectroscopic interpretation. The signal S(T) is constructed from

the capacitance transient C(t,T), at a fixed rate window $\{t_1, t_2\}$:

$$S(T) = C(t_1, T) - C(t_2, T) \tag{2.17}$$

S(T) has a maximum at a temperature T_m. For an exponential transient, emission rate e_n at temperature T_m is given by

$$e_n = \frac{ln(\frac{t_2}{t_1})}{t_2 - t_1} \tag{2.18}$$

and peak value of the signal f(r) is given as

$$f(r) = C_0 \frac{N_T}{2N_d} (\frac{1}{r})^{\frac{r}{r-1}} (r - 1) \tag{2.19}$$

where

$$r = \frac{t_2}{t_1} \tag{2.20}$$

Note that the signal height depends on strength of the transient C_0 and trap concentration n_T. From different choice of rate windows, the dependence of emission rate on temperature can be obtained in a single temperature scan. The ratio r in Eqn. 2.20 is chosen to optimize the signal/noise ratio and peak shape resolution. Along with high sensitivity, DLTS provides a quick and simple way to identify all the traps in the depletion layer of a diode provided one is able to change trap occupation by external excitation such as voltage pulse. From the lineshape of the spectrum, extent of nonexponentiality can be judged.

Nonexponentiality due to high trap density is avoided by implementing the DLTS measurement in constant capacitance mode (CC-DLTS) of operation where voltage transient instead of capacitance transient is recorded as a function of temperature [108] and processed. However, we do not perform CC-DLTS measurement in this work due to large change of capacitance with temperature.

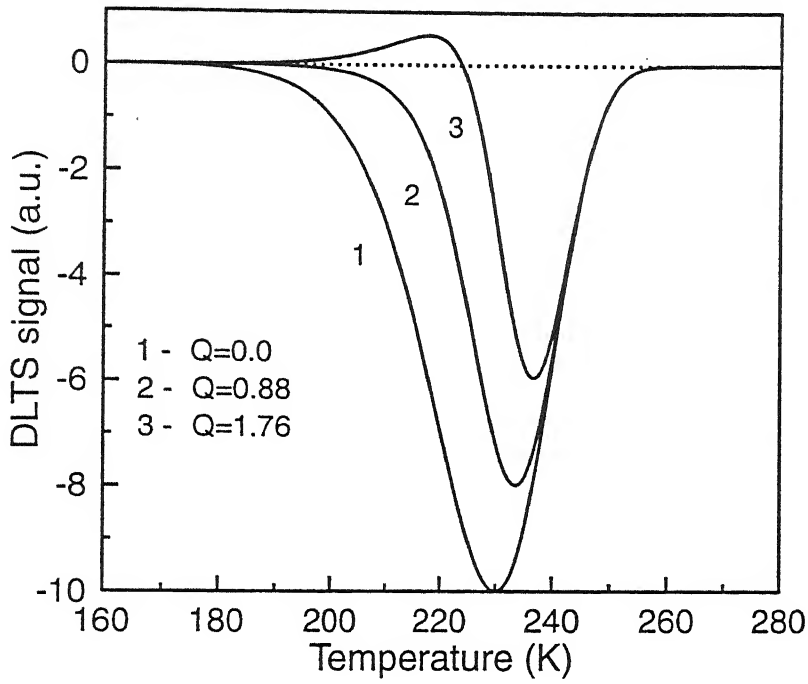

Figure 2.4: Effect of series resistance on DLTS spectra for different Q values. Simulated peak corresponds to a trap with E_T=0.5 eV, $\sigma = 1 \times 10^{-15}$ cm^2, C=40 pF; t1=7ms, t2=14ms.

DLTS signal will assume complicated form in presence of very large trap concentration in the depletion layer [110].

2.6.3 Trap parameter extraction

In case of exponential transient, DLTS signal peak temperatures corresponding to different rate windows will follow an Arrhenius relationship. Slope of $ln(e_n/T^2)$ versus $1/T$ plot yields activation energy of the trap and intercept gives capture cross-section (σ). The cross-section determined in this way may be affected by electric field, degeneracy of the level and temperature dependent capture rate. More direct estimation of σ is done by varying pulse width technique in which fraction of occupancy for a particular level is monitored as a function of fill pulse duration t_f [98, 111]. Trap concentration is estimated

from DLTS signal peak height (using Eqn. 2.22) for a chosen value of t_2/t_1 ratio. However, this relation holds only for small trap concentration compared to the backgraound doping. For larger trap concentration, trap density can be estimated from CC-DLTS method or from transient amplitude measured in constant capacitance mode of operation. Concentration profiling of traps in DLTS measurement is done by selecting the region of interest through appropriate changes in magnitude of majority carrier pulse for different scans in temperature.

Broadening in energy for capture barrier or emission energy is determined from the broadening in DLTS peak shape. A broad peak may results from continuously distributed states in the band gap as in the case of amorphous Si. Majority and minority carrier trap can be distinguished from the sign of the peak.

Many variants of the conventional DLTS have been proposed for characterization of semiconductors including frequency scanned DLTS, Laplace transform DLTS, Fourier transform DLTS, optical and scanning DLTS, interface trapped charge DLTS, lockin DLTS etc. [112]. In the next section, we will describe a variant of frequency scanned DLTS technique which we have used extensively in our work.

2.7 Time Analyzed Transient Spectroscopy (TATS)

This is an isothermal spectroscopic technique where time window is varied keeping the temperature constant unlike DLTS where temperature is varied keeping the time window fixed. Isothermal spectroscopic techniques have been used in the literature in various forms [113, 114, 115]. TATS is one such isothermal spectroscopic technique based on difference signal in time window. The TATS signal is given by

$$S(t) = C(t,T) - C(t+\gamma t, T) \tag{2.23}$$

where C represent isothermal capacitance transient at temperature T and γ is an experimentally chosen constant. For exponential transient of time constant τ_e, S(t) has a maximum when plotted against $ln(t)$ and maximum occurs at time t_m given by the relation

$$\tau_e = \frac{\gamma t_m}{ln(1+\gamma)} \tag{2.24}$$

The peak value of the TATS signal is given by

$$S_{max} = C_0 \frac{N_T}{2N_d} \frac{\gamma}{1+\gamma} (1+\gamma)^{-\frac{1}{\gamma}} \tag{2.25}$$

where C_0 is the prefactor of the transient C(t,T).

There are several advantages of TATS analysis over DLTS. TATS is a spectroscopy in the time domain alone and therefore possible temperature dependence of the transient prefactor containing occupancy etc. does not occur. Additionally, in methods involving temperature scanning such as DLTS, the lineshape is dependent on trap parameters and the temperature regime of observation.

In contrast, the width of the TATS peak depends only on the parameter γ, which is chosen to optimize resolvability and signal to noise ratio. The full width half-maximum (FWHM) of the TATS lineshape is a constant given by [116]

$$FWHM = ln(t_+) - ln(t_-) = 2.496 \tag{2.26}$$

for $\gamma = 1$, t_+ and t_- being the times corresponding to the half maximum of the TATS peak. This can be obtained in the same manner as Eqn. 2.21 was derived for DLTS lineshape. Because of this, it is very easy to detect and estimate the degree of nonexponentiality from TATS lineshape. A convenient way of characterizing nonexponentiality is to represent it by a stretched exponential transient of the form

$$C \sim C_0 exp\left[-(\frac{t}{\tau_e})^{\beta}\right], \quad \beta \leq 1 \tag{2.27}$$

where β is the stretching factor. This form of transient, also known as William-Watts decay [117], has been invoked in many physical systems including defect analysis [118, 119]. Constructing the TATS signal for transient of Eqn. 2.27, it can be shown by differentiation that signal goes through a peak at t_m given by

$$(\frac{t_m}{\tau_e})^\beta = \frac{\beta \ln(1+\gamma)}{(1+\gamma)^\beta - 1} \tag{2.28}$$

which reduces to the expression in Eqn. 2.24 for $\beta = 1$. Simple calculation shows that the peak position in time t_m does not change appreciably on lowering β. Specifically, for $\gamma = 1$, the peak position $(\frac{t_m}{\tau_e})$ is 0.990 times the perfect exponential case even for a β as low as 0.5. Hence, estimation of the time constant is independent of the stretching factor β in most cases. The experimental inaccuracies are much larger than expected due to nonexponentiality factor β.

Nonexponentiality in transient normally shows up as broadening of the lineshape. If we use Eqn. 2.28 for peak position t_m, then the FWHM of the TATS signal is proportional to $(1/\beta)$ for the case of $\gamma = 1$. Hence, a quantitative measure of nonexponentiality is obtained simply by inspection of TATS spectral lineshape. For more precise determination of the β factor, one can use precomputed values of FWHM as a function of β. For example, for the case of $\gamma = 1$, we have simulated the FWHM of the TATS lineshape for various values of β, which fits into the following straight line formula :

$$\frac{1}{\beta} = \frac{FWHM - 0.078}{2.417} \tag{2.29}$$

for determination of β correct upto three decimal places. In many cases, it is more meaningful to give a physical interpretation to the broadened peak in DLTS or TATS spectra. A distribution in deep energy levels can give rise to nonexponential transient of the form [120, 121]

$$C(t) = \int_0^{E_g} g(E_{a_i}) C_0 exp([-e_n(E_{a_i})t] dE_{a_i} \tag{2.30}$$

where the distribution function often assumed to be Gaussian around the mean energy value E_{a_0} is

$$g(E_{a_i}) = \frac{1}{S\sqrt{2\pi}} exp[-\frac{(E_{a_i} - E_{a_0})^2}{2S^2}] \tag{2.31}$$

Here, $2S\sqrt{2\ln 2}$ is the FWHM of the broadening of the energy level. This situation arise in case of alloy semiconductors and defect located in strain field as in the case of less perfect crystal. From TATS lineshape fitting, exact value of E_{a_0} and $g(E - a_i)$ can be estimated. In case of DLTS lineshape fitting, other temperature dependent factors may complicate the analysis.

For better resolution of emission time constants, TATS can be performed using higher order spectroscopies [122, 123, 124, 125]. For any gamma value, TATS signal of different orders are given as

$$1st \quad order: \quad S_1(t) = C(t) - C((1+\gamma)t) \tag{2.32}$$

$$2nd \quad order: \quad S_2(t) = C(t) - 1.5C((1+\gamma)t) + 0.5C((1+\gamma)^2 t) \tag{2.33}$$

$$3rd \quad order: \quad S_3(t) = C(t) - \frac{7}{4}C((1+\gamma)t) + \frac{7}{8}C((1+\gamma)^2 t) - \frac{1}{8}C((1+\gamma)^3 t) \tag{2.34}$$

A hierarchy of higher order spectroscopies can be used, where suitability is dictated by signal to noise ratio. In case of large signal, higher order TATS is very useful in resolving close peaks as shown in Fig. 2.5. Here two peaks with τ_2/τ_1=4 which are not so well resolved in first order spectra is resolved clearly in 3rd order spectra. We have taken advantages of such higher order analysis for our studies in this work. The formalism can be applied to the case of other spectroscopies namely DLTS, PATS [126] and TWTS [125]. Although we have mentioned many advantages of TATS over DLTS, it should be pointed out that for TATS analysis, data is required over very wide time scales for a given temperature. For example, peaks occurring in the temperature range 80K-250K in DLTS will have time constant variation in the range of 10^6 sec - 10^{-6} sec for a particular temperature within the above mentioned temperature range. However, it should be noted

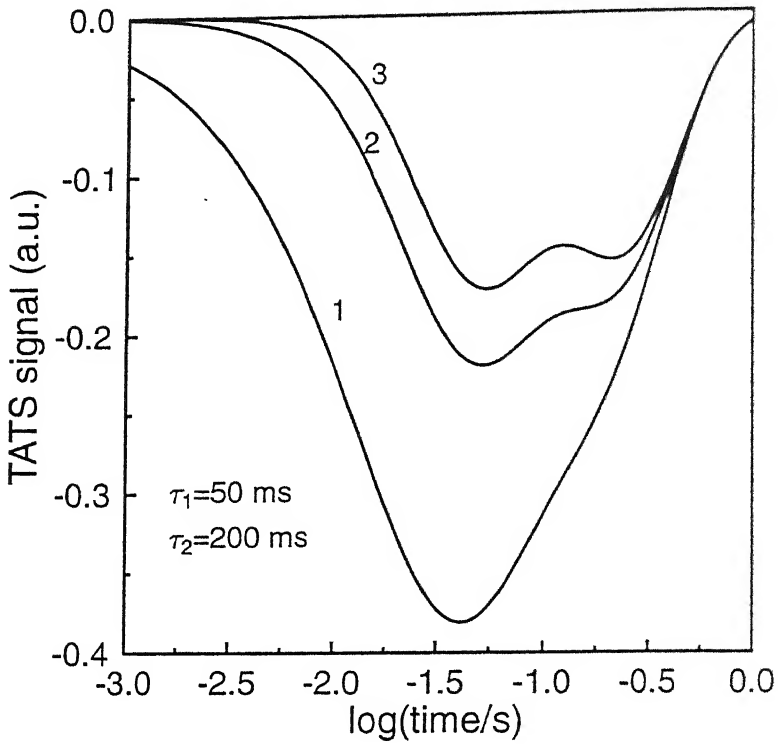

Figure 2.5: Comparison of different orders of TATS to resolve two closely spaced peaks : (1) first order TATS, (2) second order TATS, and (3) third order TATS.

that while DLTS is used for surveying defects, TATS can be used for detailed analysis of defect phenomena related to a particular defect or defects lying close in energy. In particular, TATS is more versatile in analyzing different kinds of nonexponentiality of transients encountered in this work.

2.7.1 Analysis of nonexponentiality : A case study

We present here a case study in analyzing nonexponentiality of photo-induced current transients in undoped semi-insulating GaAs (SI-GaAs). The superiority of TATS over conventionally used photoinduced transient spectroscopy (PITS) [127], which is based on DLTS like analysis, is demonstrated in this section using our own experimental data [2].

[2]This case study involves current transients instead of capacitance transients. Only commonality of techniques with the rest of this work is emphasized.

In SI-GaAs, at the end of an intrinsic light pulse, normally one expects to observe decaying photocurrent transient leading to positive peak in PITS spectra. However, most often negative peak arising out of rising current transient have also been observed in these materials. In spite of inherent nonexponential nature of the photoinduced current transients, several workers have attempted to fit multiple exponentials [128, 129] for the observed transient.

For acquiring experimental data, we have used commercial undoped SI-GaAs sample cut from 400-μm thick wafer. We used the planar structure with electrical contacts in the form of strips on front surface by evaporating Au/Ge alloy in vacuum. The metal contacts are annealed at 450°C in flowing forming gas. The samples were mounted on a liquid nitrogen cooled cold-finger type cryostat with temperature controlled to within $\pm$0.1K in the temperature range 90K-350K. A copper-constantan thermocouple was mounted on the sample holder close to the device. Light pulses were provided from the He-Ne laser source (λ=6328 $\AA$) with the help of a mechanical chopper with cut off times less than 0.2 ms. The current transients are digitized at each temperature with the help of Keithley Source Measure Unit (Model 236). The complete setup, shown in Fig. 2.6, is PC controlled except for temperature control. Each acquired transient is then used for further analysis using TATS. The time constants are calculated using Eqn. 2.24 and stretching factor or nonexponentiality is estimated using Eqn. 2.29.

2.7.1.1 Typical current transients and PITS

Typical photocurrent decay curves are shown in Fig. 2.7 for two different temperatures. In SI-GaAs both these types of transients are commonly observed. In our discussion, we will refer to transients labelled as (a) in Fig. 2.7 as decaying transients and to curves of type (b) as rising transients. Decaying photocurrent transient in these materials is interpreted to be due to slow thermal release of carriers from traps filled during light pulse. Most of

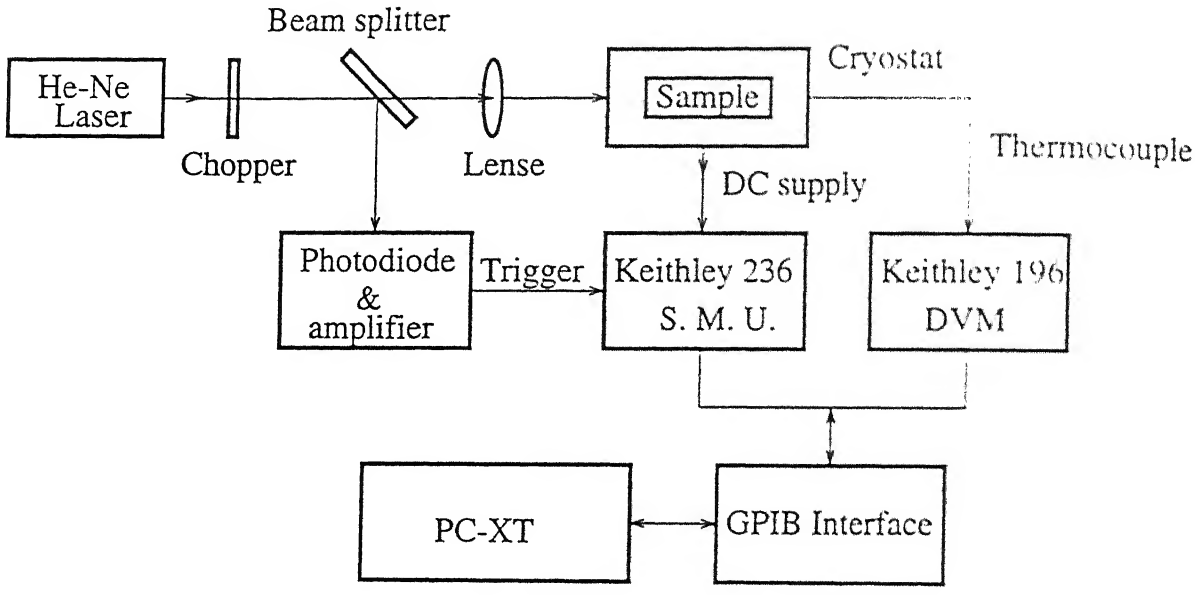

Figure 2.6: Schematic of photocurrent transient measurement setup.

the excess carriers would have recombined at a much faster rate normally due to band to band recombination. Hence the slow decaying transient carries information regarding the emission rate of carriers from the defect center. However a 'clean' interpretation of rising transients such as curve (b) has not been possible and many models have been advanced mainly through photoinduced current transient spectroscopy (PITS) studies [127, 128, 130].

As far as transients of type (b) are concerned, note that in most earlier studies only the rising part of the transients have been analyzed. However our data clearly shows that all such transients also have a slow decaying component reaching a minimum and then rising to a saturation. We have taken care to confirm that the decaying component is not related to any artefact of experiment such as time constant of chopper or R-C circuit response. This is further borne out by the fact that the slow decaying component is highly temperature dependent and is always observed along with negative transient. Hence we

PITS analysis questionable. Hence, PITS is not well suited for detailed studies involving questions of phenomena, though it can be used as a general purpose survey technique. Specifically, it fails miserably in trying to understand negative peaks or rising transients in SI-GaAs.

2.7.1.2 TATS of positive peak

As has already been pointed out in section (2.7), there are several advantages associated with TATS analysis, it being a completely isothermal technique. To demonstrate its efficacy we choose at first to analyze the decaying transients which lead to positive peak in PITS spectra in the temperature range 165-200K. In Fig. 2.9(a), we show TATS signals for these transients at several temperatures. The emission time constant is obtained from the peak position using Eqn. 2.24. The corresponding Arrnenius plot is shown in Fig. 2.9(b) which yields an activation energy of 0.41 eV with corresponding capture cross-section of 6.1×10^{-13} cm^2. This can be attributed to the level called EL6 reported in the literature [130].

As discussed in section (2.5), inspection of the TATS spectra directly show that transients are nonexponential. This is clearly shown in Fig. 2.10 where experimental TATS points are shown by symbols and a perfect exponential of time constant corresponding to the maximum (t_m) is shown as a dashed curve. From experimental FWHM, the stretching factor β is obtained using Eqn. 2.29 and the corresponding TATS spectra is shown by bold line in the same figure. This clearly shows the power of TATS in determining degree of nonexponentiality of transients in a straightforward way. Similarly, stretching factor determined at different temperatures range between 0.67-0.90, the lower value being obtained at lower temperatures. The significance of this systematic deviation from exponentiality with temperature is not clear to us but it could be related to recapture of carriers. The height of TATS peak at different temperatures do not scale with $(1/t_m)$

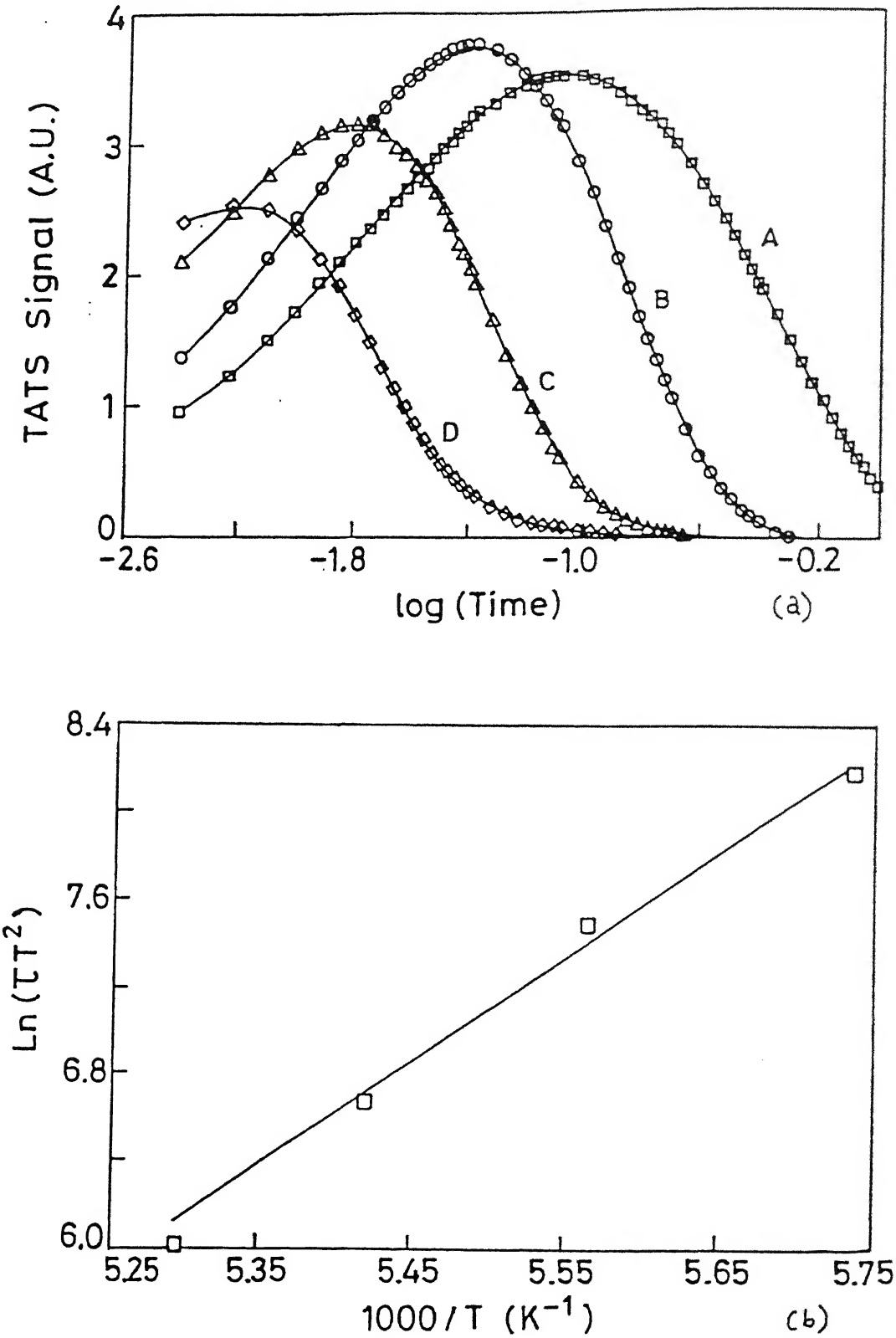

Figure 2.9: (a) A series of TATS spectra in a SI-GaAs sample at different temperatures : (A) 174.3K, (B) 179.7K, (C) 184.5K, and (D) 188.8K. (b) Arrhenius plot for deep trap corresponding to positive TATS peak shown in (a).

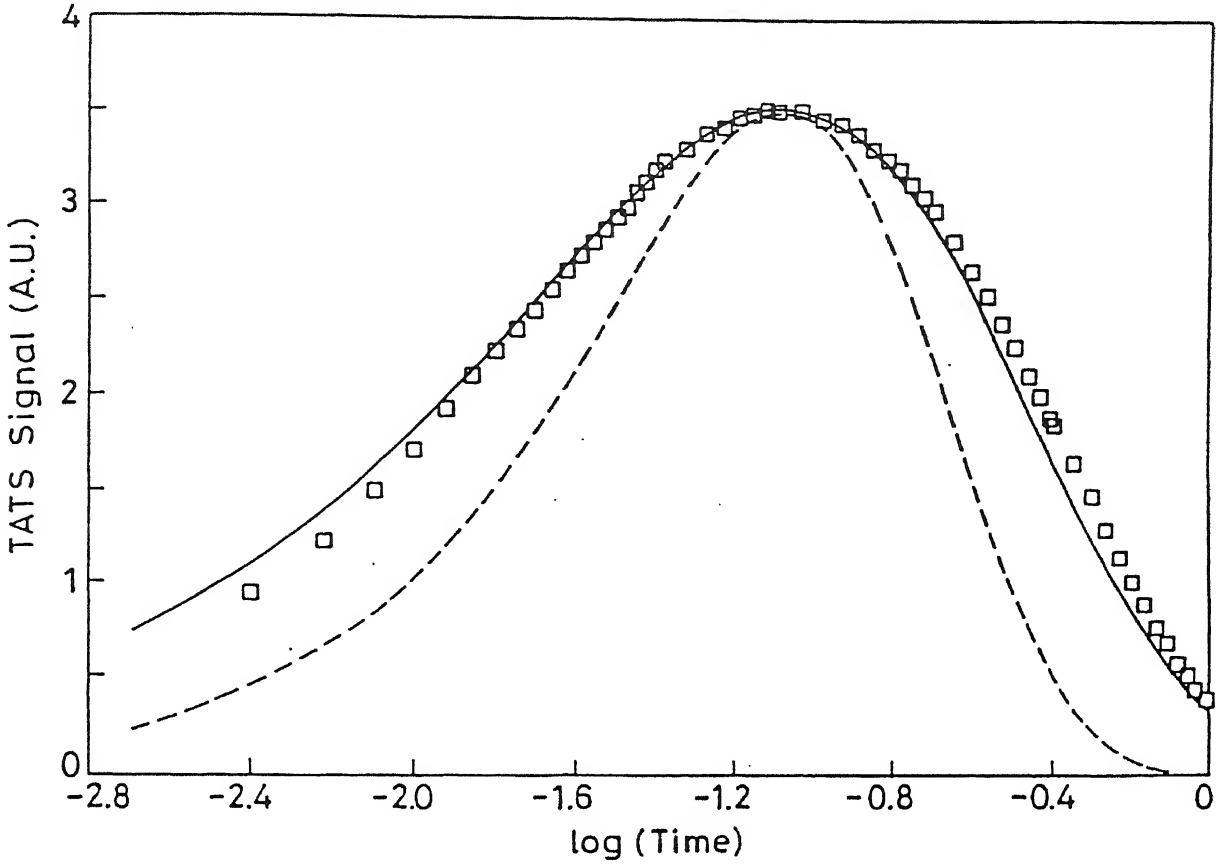

Figure 2.10: Comparison of experimental spectra with calculated ones to demonstrate the degree of nonexponentiality. The experimental spectra (with symbols) are broader than the spectrum corresponding to perfect exponential (dotted) line. The bold line corresponds to a stretched exponential with β=0.668 determined from the FWHM of the experimental curve.

as current transient prefactor includes e_n, emission rate of trap. This is mainly due to the change in the degree of occupancy achieved for a fixed exposure time at different temperatures. Normally this would contribute to lineshape distortion in PITS spectra.

2.7.1.3 TATS of negative peak

We use TATS to analyze the nature of nonexponentiality of rising transients (Fig. 2.7) observed at higher temperature. As in PITS spectra, rising transients lead to negative peaks in TATS spectra for several temperatures. Note that the sample shows two negative

peaks shown in Fig. 2.11(a) as opposed to what is usually observed in PITS spectra. This is possibly due to the fact that the smaller negative peak gets submerged in already highly distorted PITS lineshape.

The dominant negative peak in TATS spectra is due to the rising part of the current transient as shown in curve (b) of Fig. 2.7. Note that the TATS signal falls to zero sharply on the faster side of the peak. In fact it is initially positive corresponding to the decaying part of the transient. The TATS signal goes through zero at a time approximately corresponding to the minimum of the transient. Hence, it is clear that by no stretch of imagination the transient corresponding to the negative peak can be considered exponential or mildly non-exponential by choosing to focus only on the later rising part of such transients.

However, for thermally stimulated relaxation processes, use of Arrhenius plots to estimate the approximate energy involved is a robust procedure not withstanding nonexponentiality. Hence, we treat the TATS peak shifts with temperature as indicator of shift in time constant and hence plot an Arrhenius plot given in Fig. 2.11(b). The activation energy so obtained is 0.79 eV with an estimate of capture cross section from the intercept as 2.3×10^{-11} cm^2. The activation energy of negative peaks found in earlier works [130, 131] normally range between 0.65 to 1.2 eV. Therefore, it has always been attributed to midgap centers, though a definite identification has remained controversial. It has been suggested earlier that presence of large dark current plays a crucial role in giving rise to negative peak [128]. In contrast, note that we have observed negative peaks even at temperature well below room temperature where the dark currents are negligibly small.

Figure 2.12 shows TATS of transients at a particular temperature (290K) for various values of filling time i.e. the time for which the laser light is on. Change in height of TATS peak of the main negative peak is an indicator of slow increase in the corresponding filled trap concentration. However, it is seen that the second negative peak height remains

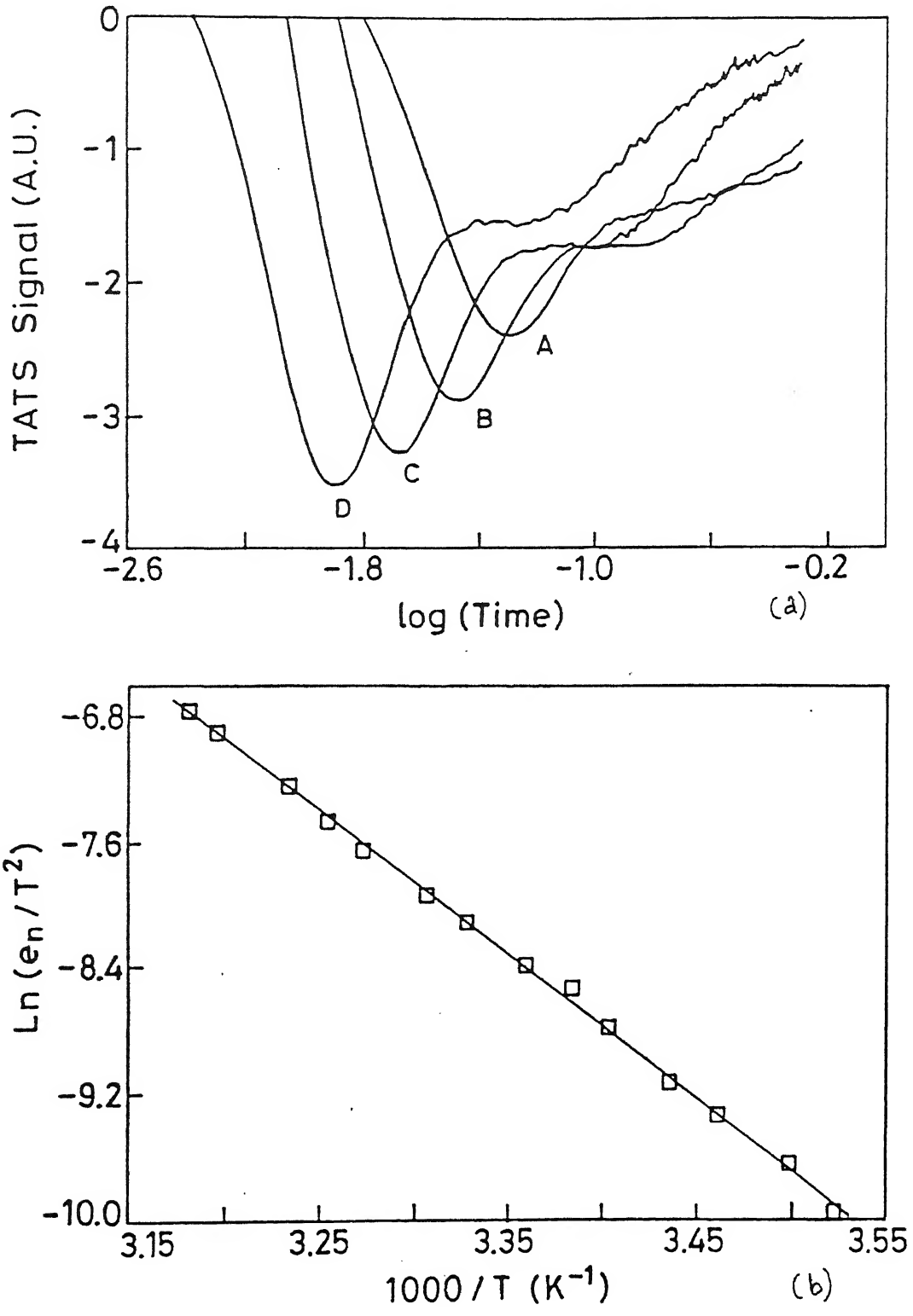

Figure 2.11: (a)TATS spectra with γ=1 in SI-GaAs samples at different temperatures : (A) 293.9 K, (B) 297.7 K, (C) 302.5K, and (D) 307.4 K showing two negative peaks. (b) Arrhenius plot for the dominant negative peak of (a).

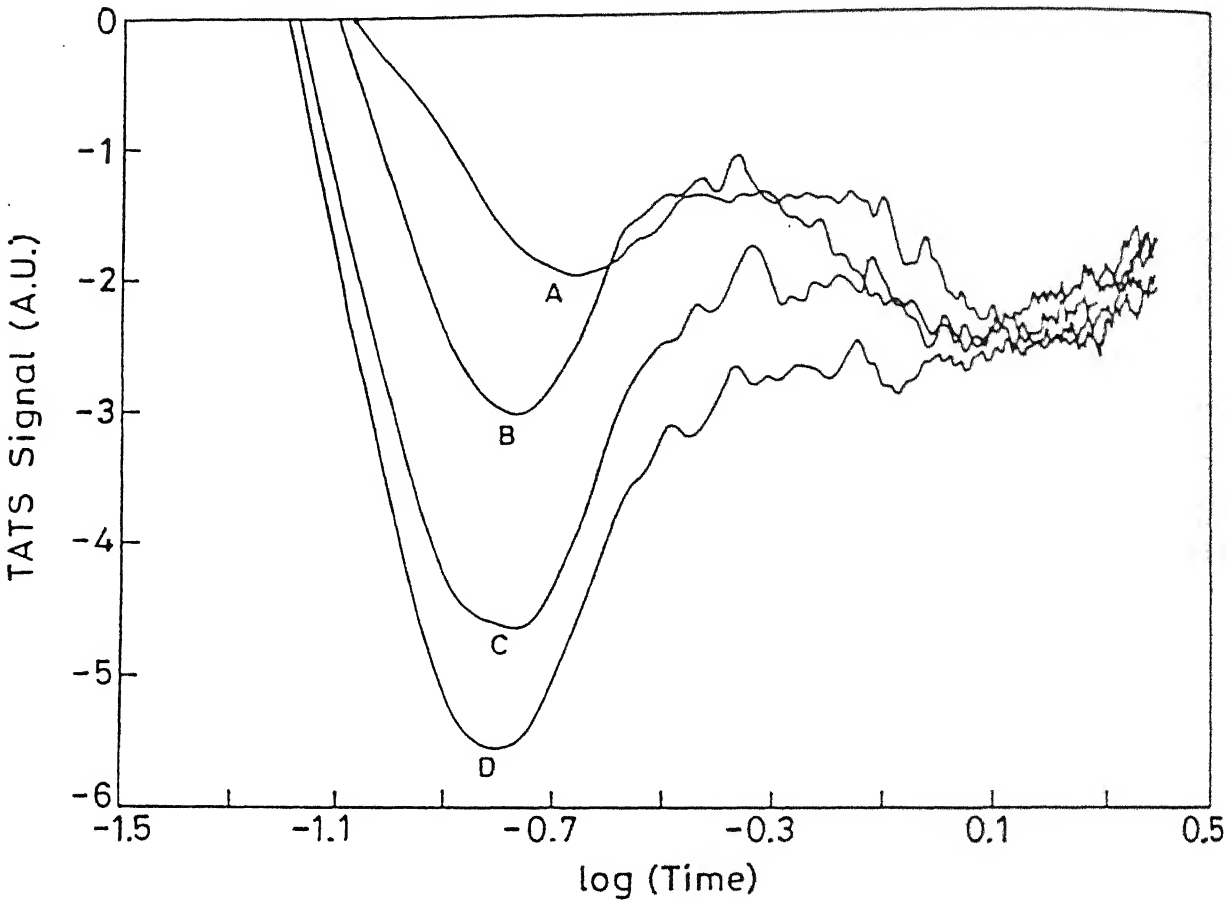

Figure 2.12: TATS spectra for SI-GaAs at temperature 290 K for different filling times : (A) 20 ms, (B) 70 ms , (C) 100 ms, and (D) 200 ms.

constant indicating that saturation of the peak occurs in time scale faster than the shortest filling time scale used in these experiments. The extent of trap filling is found to be highly temperature dependent and studying filling behavior is rewarding by an isothermal spectroscopy such as TATS. It also demonstrates that the height of conventional PITS peaks cannot be considered as healthy indicator of extent of filling.

To explain such kind of nonexponentiality revealed from TATS, we have proposed a simple kinetic model [105] without attempting to pinpoint any physical mechanism. The most significant feature of our model is to introduce a new rate process which acts as a delay between capture of a carrier and its emission. For simplicity, we will assume that

only one dominant electron trap and one band, say, conduction band is involved in the process. An electron gets captured at an empty trap taking the defect to a metastable state from which it must relax to the ground state. It can then finally emit the carriers to the band. We can write down the rate equations as follows :

$$\frac{dA^+}{dt} = -A^+A^+C + e_nA^0 \tag{2.35}$$

$$\frac{dA^*}{dt} = A^+A^+C - rA^* \tag{2.36}$$

with the constraint that $A^0 + A^* + A^+ = 1$, where A^+, A^*, A^0 are the concentration of empty, occupied metastable state and occupied ground state respectively, r is the rate of conversion from A^* to A^0 and C is the product of capture cross section (σ), average thermal velocity (v_{th}) and the total trap concentration. It is also assumed that the concentration of electrons in the band is equal to the concentration of empty traps, an assumption mostly valid in these materials in the dark. The rate equations are written with all concentrations normalized with respect to the total trap concentration. The desired delay between capture and emission is introduced by the negative term in the Eqn. 2.36 where it is treated like an emission term in so far as it depends only on the concentration of the metastable state. The rate equations can conveniently be summarized in a state transition diagram as is given in inset of Fig. 2.13 [116].

These rate equations are solved numerically on a personal computer. The choice of parameter e_n is taken from the experimental Arrhenius plot, normalized capture coefficients and initial concentrations are chosen to correspond approximately to EL2 parameters in SI-GaAs. The rate r is chosen so as to produce qualitative features of our data. Figure 2.13 shows the TATS of a particular solution obtained numerically and compares it with a typical experimental TATS curve for negative peak. The ability of any model to mimic cusp like behavior of the transient or positive to negative crossover in TATS spectrum puts severe restriction on the class of models that need be considered. The abil-

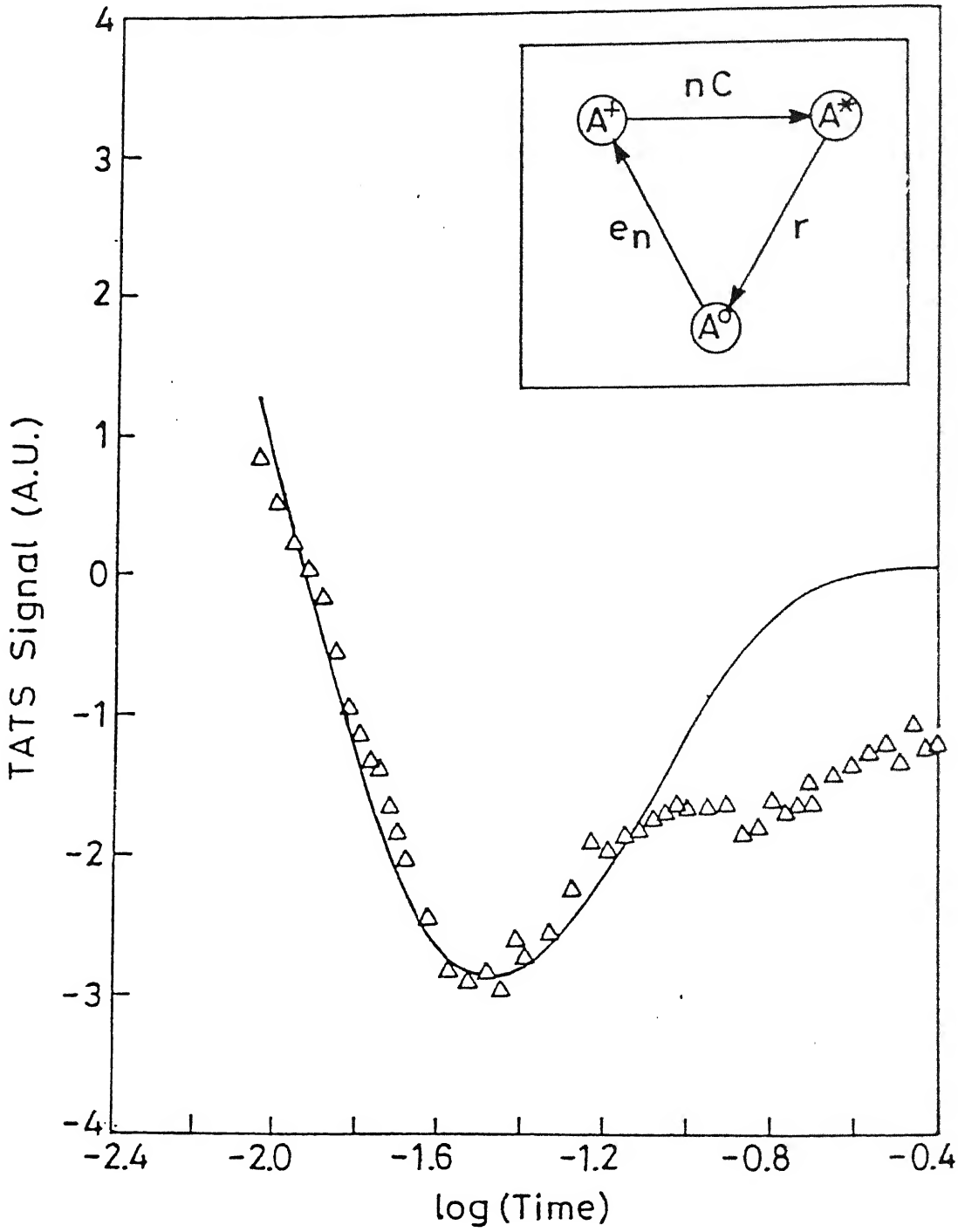

Figure 2.13: TATS spectra for the experimental data (symbols) and calculated data (bold line) from the proposed model with EL2 parameters. The chosen parameters as defined in Eqs. 2.36 and Eqs. 2.37 are : e_n=19.5 s^{-1}, C=1×10^4 s^{-1}, r_c=1, $A^+(0)$=0.011, $A^*(0)$=0.96.

Wafer →	n^+n-Si	p^+p-Si
Orientations :	[100]	[111]
Epilayer thickness :	22 μ m	22 μ m
Doping concentration :	1.2×10^{15} P /cc	1.5×10^{15} B /cc
Back contact (Ohmic) :	Al	Al
Schottky contact :	Au	Al, Pd
Implanted species :	Ar^+, Au^+	Ar^+, Au^+
Respective energy (MeV) :	1.45 , 4.6	1.45, 4.6
Ar^+ ion doses (cm^{-2}) :	$5\text{-}10\times10^{13}$	$1\text{-}5\times10^{14}$
Au^+ ion doses (cm^{-2}) :	5×10^9	5×10^9
Annealing (Post Imp.) :	160-600°C	160-600°C

Table 3.1: Details of sample preparation conditions.

ion irradiation. 3MV Tandem Van de Graaff accelerator facility at Institute of Physics, Bhubaneswar, India, was used for Au^+ ion implantation.

3.2.1 Schottky diode fabrication

For the present study, epitaxially grown silicon wafers of both n-type and p-type were used. Details of the device preparation conditions are listed in Table 3.1. The wafers are cleaned in ultra pure trichloroethylene (TCE), acetone and methanol sequentially in an ultrasonic cleaner for few minutes at room temperature. Then the wafer is etched in buffer hydrofloric acid (HF) solution for few seconds to remove surface oxide and then cleaned in deionized water thoroughly and dried. The cleaned wafers are put immediately in a vacuum chamber for deposition of Al (thickness $\sim 1500\AA$) on the back side of the wafer for making ohmic contact. The metal is deposited using a thermal evaporation system. In case of non-epitaxial wafers i.e. CZ wafers, back contact is annealed at 485°C for 30 minutes in vacuum for ohmic contact formation.

The wafers with ohmic contact on back side are then put into an electron beam

evaporation system for deposition of gold on n-type Si, and aluminium/palladium on p-type Si for Schottky contact formation. This evaporation system is equipped with a liquid nitrogen trap to have a clean vacuum in the deposition chamber. The evaporation is done under 10^{-6} Torr pressure and about 2000$\AA$ thickness of metal is deposited on the front side (mirror finished) of the wafer. The thickness is monitored using a quartz crystal controlled digital thickness monitor during deposition. High purity (99.99 %) gold wires and aluminium from ingot are used for deposition of Schottky contact. Metal masks each having many circular holes of 1 mm diameter were used during metal deposition for defining Schottky diode area. The wafers are scribed to obtain pieces of convenient size.

Ion irradiation (described in the next section) are performed on finished devices or on bare wafers from front side of the wafer. For n-type Si samples, irradiation is done prior to any contact formation and for p-type Si, irradiation is done on finished devices and on bare wafers which are cut into pieces. In case of Schottky diodes prepared after ion irradiation, the wafer is carefully degreased and subsequently cleaned in buffer HF solution for oxide removal. The wafers are cut into small pieces having one/two Schottky diode(s) on each piece and mounted on standard TO5 header for measurements. The contact from metal side of each Schottky diode is taken with fine gold wire (25 μm diameter) bonded with polymer based conductive silver paste (A and B compound, Elteck Corp., India). Other terminal is pasted with the body of the header. The epoxy contact is cured in oven at 70^oC for 30 minutes for proper strength of the bonding. A cap is put onto the header for protection from mechanical damage. All the devices underwent this low temperature heat treatment for curing prior to any measurement and these devices will be referred to as as-implanted.

3.2.2 MeV ion implantation

High energy Ar^+ and Au^+ ions are used for implantation on silicon. High energy Ar^+ ions are produced using Van de Graaff accelerator. It is a widely used and commonly available electrostatic accelerator. A schematic diagram of the accelerator system is shown in Fig. 3.1 This accelerator (Model AN-2000) is a precision 2-MeV, high intensity source of positive ions. The accelerator produces a beam of ions which is intense, homogeneous, stable and controllable over a wide range of energies. It is provided with three gas bottles and presently they are filled up with He, Ar and Kr gases. An r.f. ion source is used to produce positive ions.

The mass and energy analysis of the accelerated ion beam is done by an analyzing magnet. The analyzing magnet system consists of a 16 KGauss electro-magnet coupled with a d.c. regulated (0-30 V) power supply. During operation the magnet is cooled to 280K by circulating chilled water through the coils. The stainless steel switching chamber has five ports at angles 0^o, $\pm 20^o$ and $\pm 45^o$. The energy and the mass analyzed beam can be directed to the experimental chamber through any one of the five ports.

The accelerated ions obtained from the accelerator reach the experimental chamber through a clean and highly evacuated beam line. The ion beam after leaving the analyzing magnet passes through beam stopper followed by a beam profile monitor. The beam profile monitor is used to monitor the position, shape and uniformity of the beam. The beam then passes through a specially designed beam defining X-Y slit arrangement mounted on a double cross chamber which is used for selecting a uniform portion of beam of required size onto the target placed in the irradiation chamber.

The heavy ion (Ar) irradiation chamber (shown in Fig. 3.2) is mounted on a turbo molecular pump to obtain a hydrocarbon free clean vacuum. In the center of the chamber a vertically movable sample holder is placed on which many samples can be mounted at a time. The holder is electrically isolated from the rest of the chamber. A current integrator

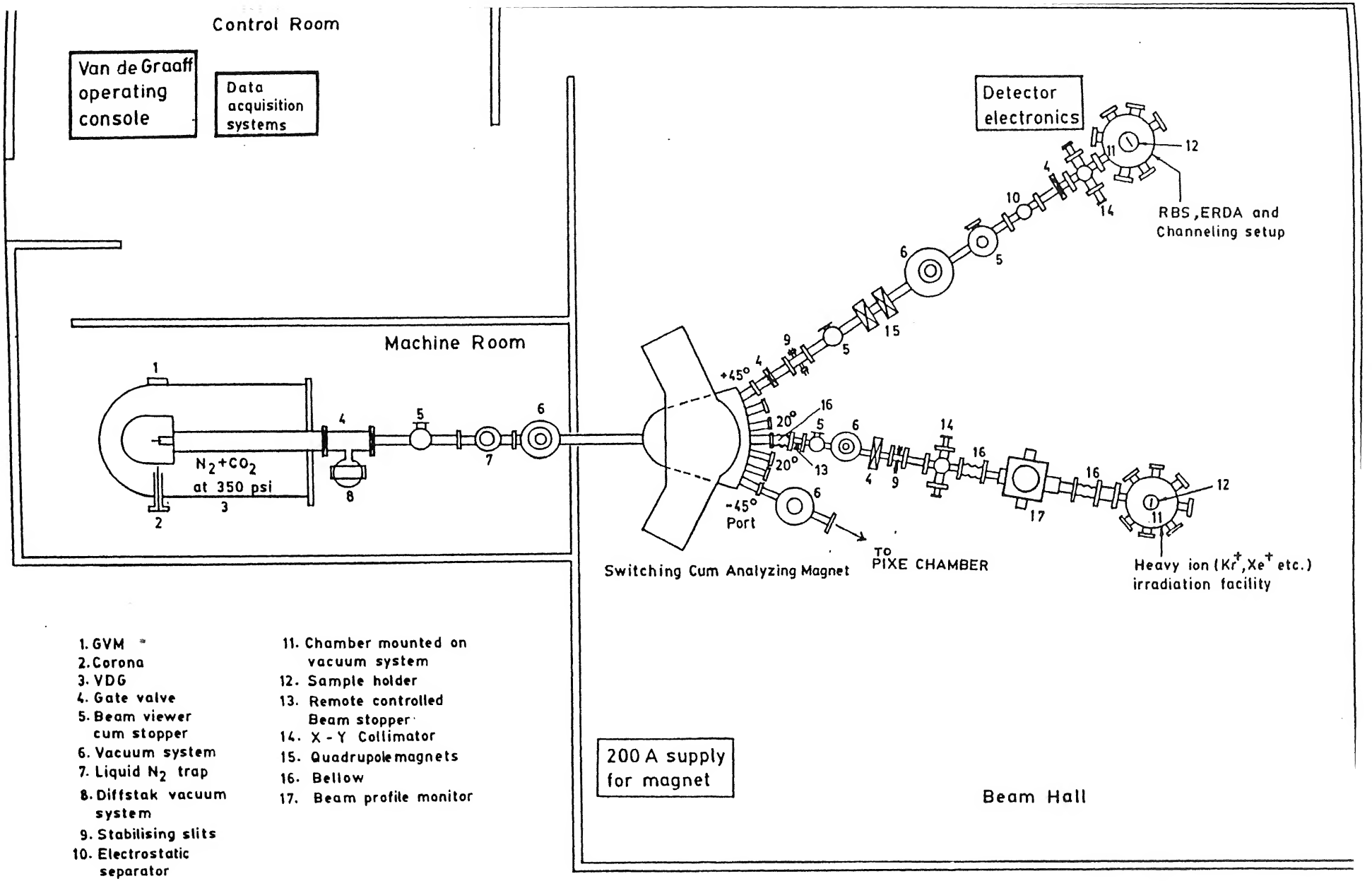

Figure 3.1: Schematic diagram of the 2 MeV Van de Graaff accelerator system.

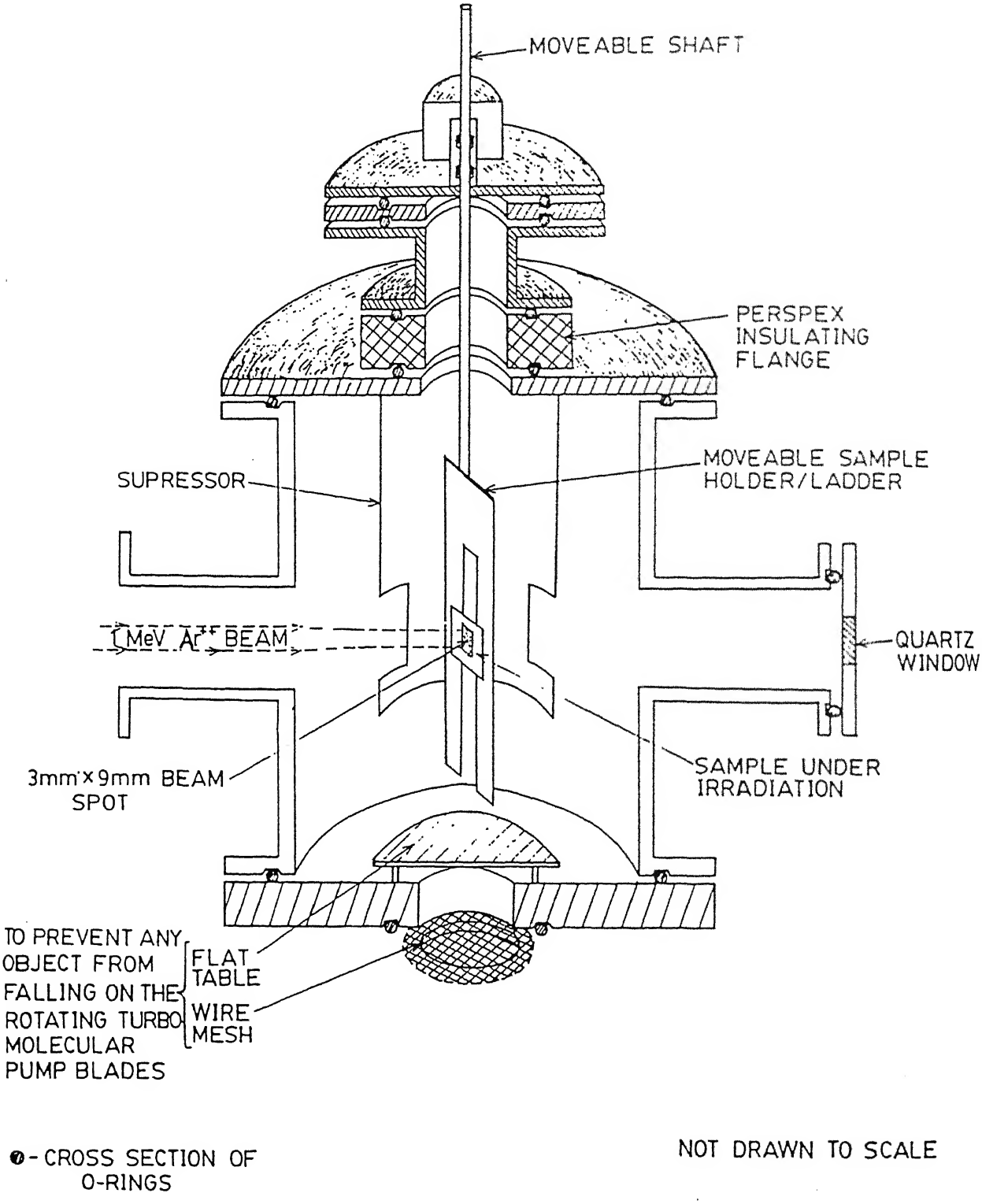

Figure 3.2: Schematic diagram of the heavy ion irradiation chamber.

(ORTEC Model 439) which measures the total charge accumulated during irradiation is connected to the sample holder. A cylinder made up of aluminium sheet surrounding the sample holder acts as secondary electron emission (from sample) suppressor.

For Au^+ ions irradiation, 3 MV tandem Van de Graaff accelerator facility at Institute of Physics, Bhubaneswar, India was used. The irradiation was performed on cleaned n-type and p-type Si wafers at room temperature at an energy of 4.6 MeV with beam current of 0.2 nA for 60 seconds. This resulted in a dose of 5×10^9 cm^{-2} in both n-Si and p-Si. With the help of a beam scanner, an area of 10mm×5mm was exposed to Au^+ ions. The irradiation was performed 2-4^o off surface normal on Si for avoiding channeling.

1.45 MeV Ar^+ ions are irradiated at a dose rate 5×10^{12} cm^{-2} s^{-1} for various duration resulting in total doses of 5×10^{13} cm^{-2} & 1×10^{14} cm^{-2} for n-type Si and 1×10^{14} cm^{-2} & 5×10^{14} cm^{-2} for p-type Si. The current was chosen such that negligible beam heating occurs during irradiation. The irradiation is performed at normal incidence to the surface of the wafer which have 4^o misalignment cut to avoid channeling. An area of 3.5×3.5 mm^2 uniform beam was falling on the sample at normal incidence.

3.2.3 Thermal annealing

For high temperature annealing of the irradiated samples, the irradiated wafers after ultrasonic cleaning with TCE, acetone and methanol are kept in a quartz tube which is evacuated by diffusion pump equipped with a liquid nitrogen trap. The furnace used for annealing has a ceramic tube, wound with nichrome wire and insulated with asbestos powder. A uniform temperature with control of ±2K could be obtained in the central portion of the furnace. The furnace is kept in a horizontal movable platform (see Fig. 3.3). After annealing, the cooling of the sample was done under room temperature. As-implanted wafers are annealed in vacuum for $\frac{1}{2}$ hour at temperatures 400^oC and 600^oC. For low temperature annealing, the finished devices (ion irradiated) are kept in oven set at 160^oC

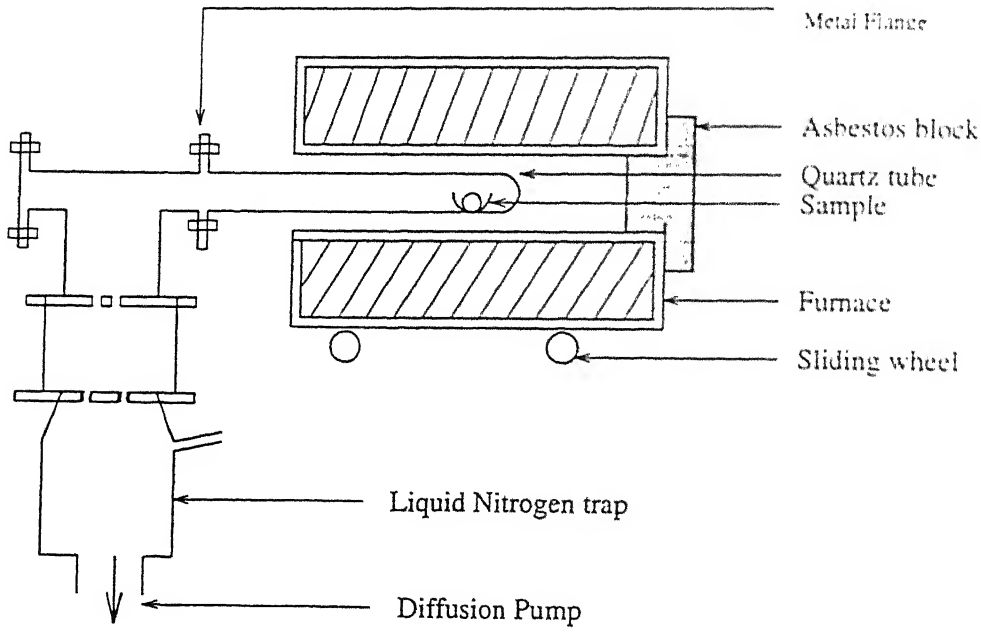

Figure 3.3: Schematic of the furnace used for vacuum annealing at high temperatures.

for $\frac{1}{2}$ hour, 1 hour and 2 hours in sequence. Few samples were stored at room temperature ($20°C$-$35°C$) for more than one year and some of these samples were used for studying possible annealing due to room temperature storage.

3.3 Experimental Setup and Measurements

This work involves capacitance measurements as a function of temperature, time and voltage. The same setup is used for transient as well as steady state measurements. Except for temperature programming, the setup is made fully computer controlled for a variety of measurements. A block diagram of capacitance measurement setup is shown in Fig. 3.4 In the following subsections various parts of measurement setups and procedure are described.

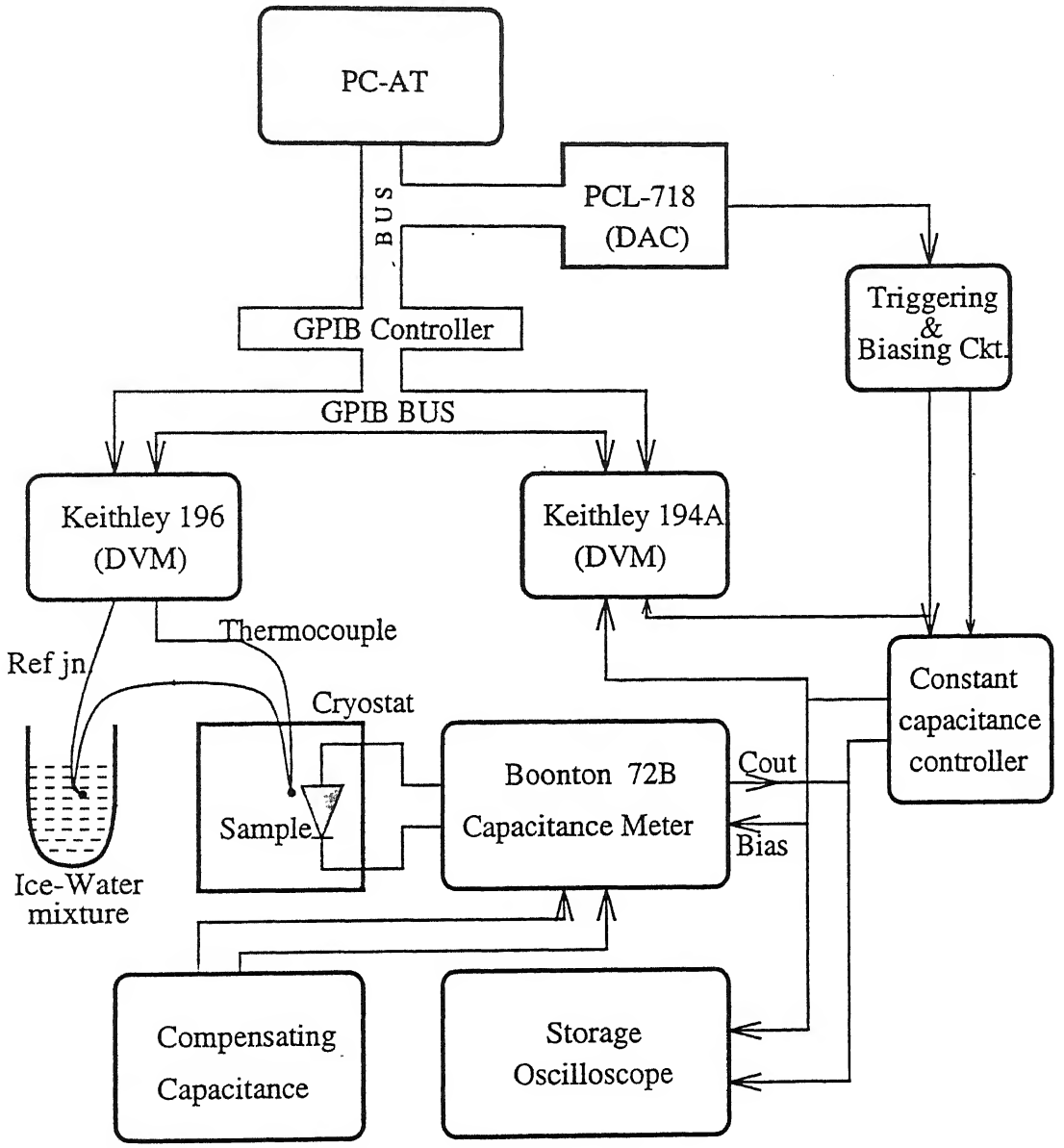

Figure 3.4: Block diagram of the capacitance/voltage transient and DLTS/TATS measurement system.

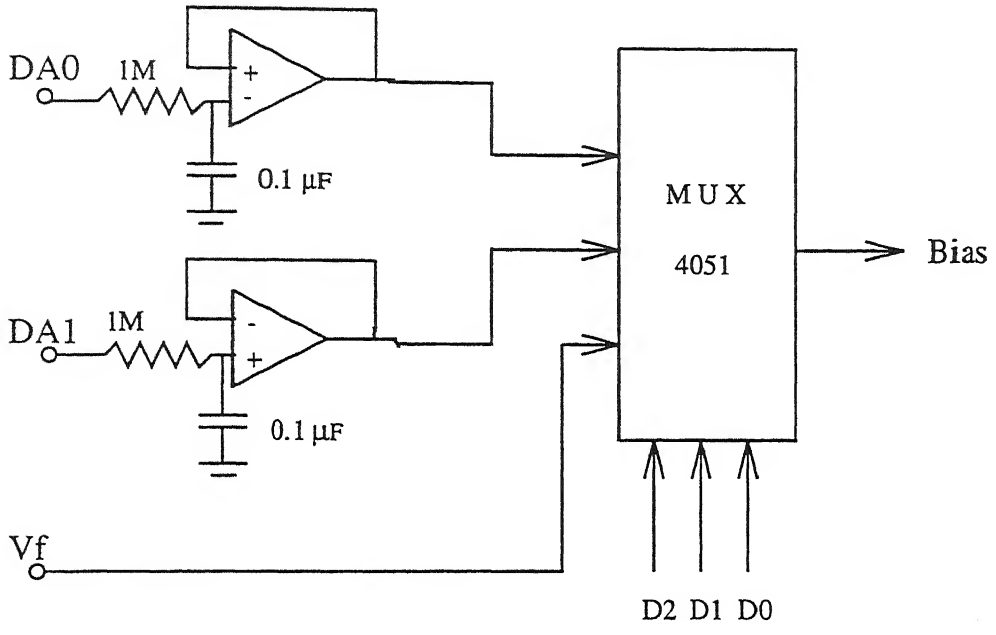

Figure 3.7: Schematic of bias pulsing and triggering circuit.

the capacitance range is chosen as 1 pF or 3 pF, respectively or its multiple of 10. For a typical C-V measurement, at first temperature is monitored and voltmeter is triggered (internal) to measure the applied voltage and capacitance simultaneously in two channels of the high speed voltmeter. The control is done through IEEE-488 interface bus. The set up is fully computer controlled except temperature control. The data is transferred from internal buffers of the high speed voltmeter to the computer for further processing.

3.3.3 Capacitance transient measurements

The sample is kept under reverse bias, and a desired temperature is achieved through proper control of heater current in the cryostat and liquid nitrogen level. Bias voltage pulses and trigger pulses (for synchronous measurements) are generated from the PCL 718 card along with the help of a multiplexer (Fig. 3.7). Since the analog outputs from

plug-in boards in the computer are very noisy, a simple trick is used to obtain clean pulses with programmable voltage levels and duration. The noisy software programmable analog outputs from the card are heavily filtered and fed to the various inputs of a multiplexer (e.g 4051). Bias voltage pulse is generated by switching analog channels. The selection of multiplexer channel is controlled by setting digital outputs of the same board (D0, D1, D2). Filling pulse widths down to few micro seconds could be easily achieved. The trigger pulse for synchronization are also obtained from the digital outputs of the plug-in board. The capacitance meter (Boonton 72B) had a fast response time option of 50 μs installed in it. For capacitance transients, the analog output of the capacitance meter is digitized using high speed voltmeter Keithley 194A with 16-bit accuracy.

For each transient, a maximum of 30,000 data points are stored at sampling rates ranging from 1 μs to 1 s. An acquired transient with 30,000 data points at equal intervals covers about $4\frac{1}{2}$ orders of magnitude in time. For longer durations, two transients are acquired with different sampling rates. The data is generally compressed and stored in binary format. A typical transient measurement consists of the following sequence of operations :

1. Device is kept under reverse bias to ensure emptying of traps above Fermi level (E_F) in the depletion region.

2. Temperature is stabilized in the cryostat to the desired degree of accuracy.

3. Filling pulse is applied leading to partial or complete occupancy of traps in the depletion region.

4. The high speed voltmeter (Keithley 194A) is triggered for data acquisition at the end of the fill pulse.

5. The acquired data is transferred from Keithley 194A to the PC for further processing at the end of the emission transient.

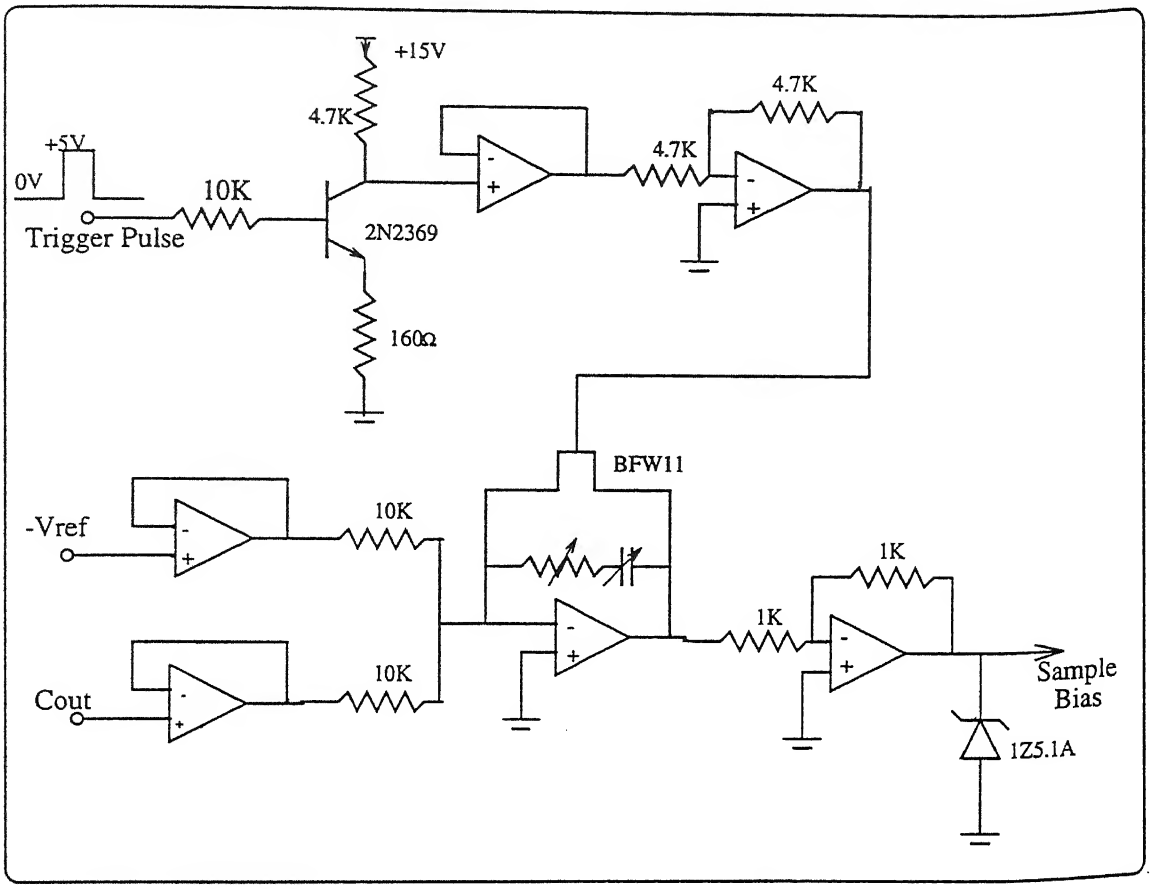

Figure 3.8: Schematic of the feedback circuit for constant capacitance control.

3.3.4 Voltage transient (constant capacitance) measurement

In general, by applying a voltage pulse across the device, one measures capacitance transient which carries trap information. However, to avoid nonexponential transient due to large trap concentration, capacitance is held constant during carrier emission measurements by dynamically varying the applied voltage during the transient response through a feedback circuit. Figure 3.8 shows the schematic for a constant capacitance feedback circuit. The analog output proportional to the capacitance (in the range 0-3V) was used as feedback. The reference was generated from PCL 718 AD card. Control was obtained using a proportional integral (PI) controller. To improve stability, all redun-

dant/unintentional poles in the feedback loop were eliminated. Zero biasing of the sample during filling is done by collapsing the feedback using a JFET for the desired duration. The relevant pulse is applied at the gate of the JFET for the desired duration. This scheme was essential for higher temperature transients as the C-V curve was nearly flat in the allowed voltage range.

The sample capacitance is a nonlinear function of temperature and bias voltage. The response time of the controller was kept usually within 1 ms to ensure stability over a large temperature range and for low noise. Fast response times up to 50 μs could be obtained by careful tuning of the parameters of the PI controller irrespective of choice of bias, filling and temperature. Filling time experiments are carried out using such fine tuning at a particular temperature.

The measurement steps are exactly identical to the steps of acquiring capacitance transient as described earlier.

3.3.5 Deep level transient spectroscopy (DLTS) & time analyzed transient spectroscopy (TATS) measurements

For deep level transient spectroscopy (DLTS) measurements the same setup as shown in Fig. 3.4 is used. The capacitance waveform (C-t) is digitized at each temperature during a temperature scan. Only one temperature sweep of the sample is required since the entire C-t waveform is obtained at different temperatures. Typically, a filling pulse of duration 50 ms was used in most of the DLTS measurements. The device is cooled under reverse bias and during heating cycle, at each temperature typically 10 transients are taken and averaged. This improves the signal to noise ratio dramatically. For this reason, temperature sweep is done at slow rate. Typically, DLTS signal corresponding to 7 different rate windows are stored in a single temperature scan for obtaining Arrhenius plot. On line plot of DLTS signal is done on the computer screen for a particular rate

window. One can store the entire waveform to check the exponentiality of the transient. Various signal processing functions can be performed on C-t data to improve signal/noise ratio, analyze nonexponentiality, resolve closely spaced peaks. Special care was taken to eliminate noise and electromagnetic interference as described in the next section.

Due to large change in capacitance during temperature scanning, DLTS is not performed in constant capacitance mode of operation. This would require high reverse bias to be applied through the feedback circuit to keep the capacitance constant.

For time analyzed transient spectroscopy (TATS) analysis, at a stabilized temperature the entire transient (C-t) is acquired with 30,000 data points and data in logarithmic time is extracted after proper filtering. Typically, only 600 data points are stored in logarithmic time scale. Signal is constructed in the way described in the previous Chapter. For obtaining an Arrhenius plot, transients at several temperatures are taken. Transients can be acquired for various filling times at one fixed temperature for capture cross-section measurement.

When the capacitance is held constant with the help of feedback circuit and isothermal voltage transient is taken to construct spectroscopic signal, that measurement is termed as constant capacitance (CC) TATS. In this work most lineshape analysis of spectroscopic data is carried out with CC-TATS measurements as the nonexponentiality due to large trap concentration is absent in such transients.

3.3.6 Thermally stimulated capacitance (TSCAP) measurement

In thermally stimulated capacitance (TSCAP) measurement, the device is cooled under reverse bias and at lowest temperature the traps are filled with majority carriers at zero bias or forward bias. Then the device is reverse biased, and heated at a constant rate to monitor the steady state capacitance as a function of temperature. Capacitance steps are observed as traps emit their carriers. Similar scans without the filling pulse at low

temperature are referred to as unfilled TSCAP curves and used as reference for isolating capacitance changes due to trap emission.

3.3.7 Current vs. voltage (I-V) measurement

For I-V measurements, programmable voltage is provided by PCL 718 card along with extra circuitry for obtaining both positive and negative voltage. Current is measured by a GPIB controlled Keithley picoammeter (Model 495). The sample is mounted in the cryostat (as described earlier) to monitor and control temperature. At a stable temperature, current and voltage data is taken for logarithmic/linear variation in voltage. The setup is computer controlled except for temperature control.

3.3.8 Impedance measurement

The implanted devices having large density of traps are tested for low frequency capacitance, impedance, loss, series resistance measurements. The measurement is done using a GPIB controlled Hewlett Packard impedance analyzer (Model 4192A) which can measure in the frequency range 5Hz-13MHz with test signal level 10mV-1V. At first, zero adjustment is done in open and close circuit configuration separately. Impedence and loss measurement at different temperatures was performed using an *ac* signal level of 10 mV at a frequency of 1 MHz. This set up is also computer controlled.

3.3.9 Noise elimination and filtration

The sensitivity of the transient measurement setup largely depends upon the degree of noise control and filtration. Despite large signal due to high trap concentration, stringent noise control was essential for higher order spectroscopy and lineshape analysis.

Two major sources of noise were electromagnetic interference leading to 50 Hz pickup, and high frequency noise from the computer. By appropriate shielding, grounding and

filtering, noise in the voltage bias/capacitance reference was reduced to less than 1 mV peak to peak. Heavy filtration dampens the response time and prevents fast switching of bias levels necessary for filling pulse. To overcome this problem, two heavily filtered bias levels were independently provided from PCL card and a multiplexer was used to switch between two levels as already described in section 3.3.2. The transient signal is processed using moving window averaging and further multi-point averaging whenever necessary. After filtration, the data set is reduced to 600 evenly spaced points in the logarithmic of time. This data is then subjected to the required spectroscopic operations to obtain the spectra.

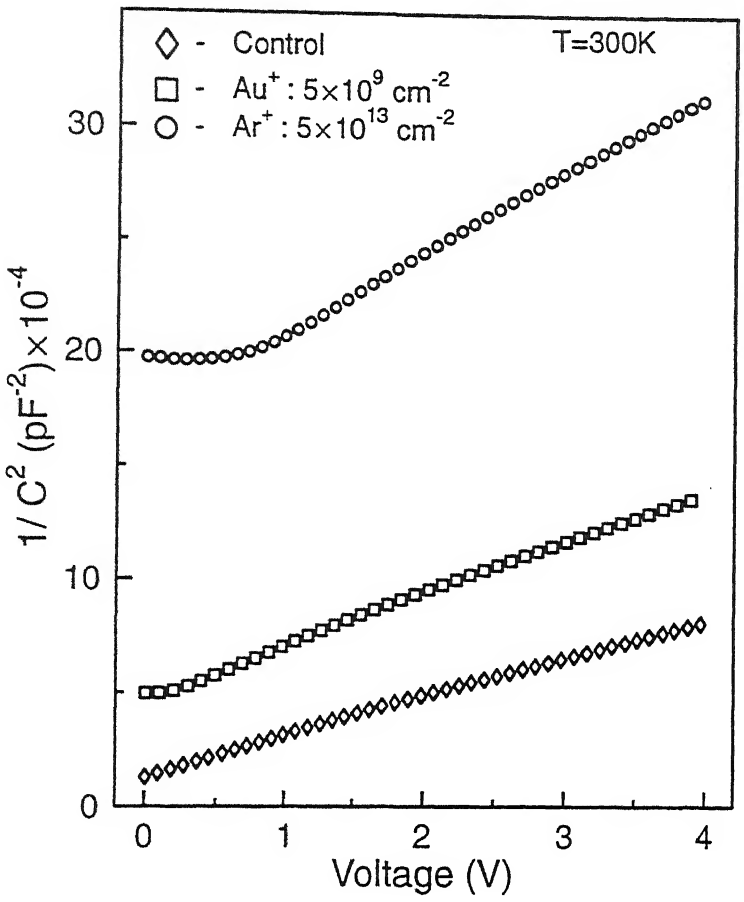

Figure 4.2: Comparison of C-V characteristics of unimplanted, Au^+ and Ar^+ implanted n-Si.

lower voltages. Since depletion width (W) is proportional to 1/C, the figure clearly shows that zero bias (or, even for any particular applied bias) depletion width systematically increases on increasing the dose of implantation.

Similar qualitative features, though to a lesser extent, are observed for Au^+ implanted silicon even though the doses used are only 10^9 cm^{-2}. Figure 4.2 shows comparison of C-V characteristics at room temperature for unimplanted, Ar^+ implanted and Au^+ implanted Si. As the range and dose of Au^+ ions are much smaller compared to Ar^+ ions in n-Si, one expects less effects of implantation on C-V characteristics for Au^+ ions.

Figure 4.3 shows $d(1/C^2)/dV$ vs. depletion width W, as is normally done to obtain conventional carrier concentration profiles, for unimpalnted and implanted samples ob-

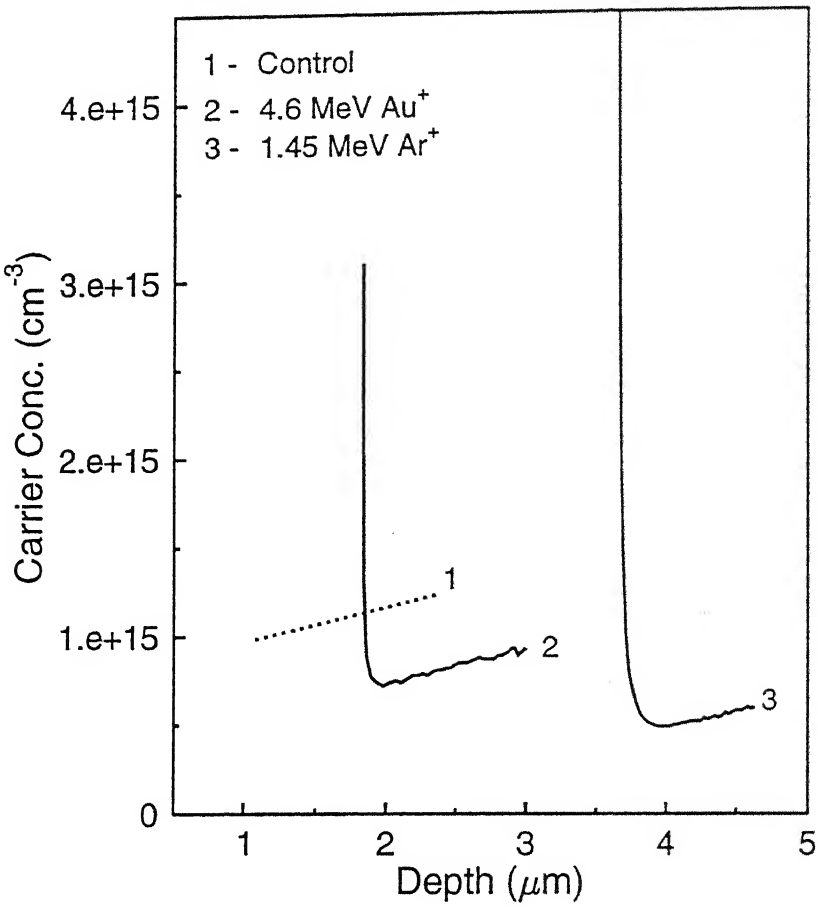

Figure 4.3: Apparent carrier concentration profile for unimplanted, Au^+ and Ar^+ implanted Si for different doses.

tained by differentiating the curves of Fig. 4.2. For unimplanted samples, carrier profile is seen to be uniform and in accordance with the background doping of the epitaxial layers. For implanted samples, the apparent carrier profiles show a sharp rise for the lowest W corresponding to flat region in the respective C-V characteristics. The depths at which these sharp rise occur are very large i.e. at about twice the zero bias width of the control diodes in case of Au^+ implanted Si and about 4 times in case of Ar^+ implanted Si. The sharp rise in concentration profile is due to presence of flat region in C-V characteristics. This feature in carrier profile is an artefact due to large trap density in a region of deple-

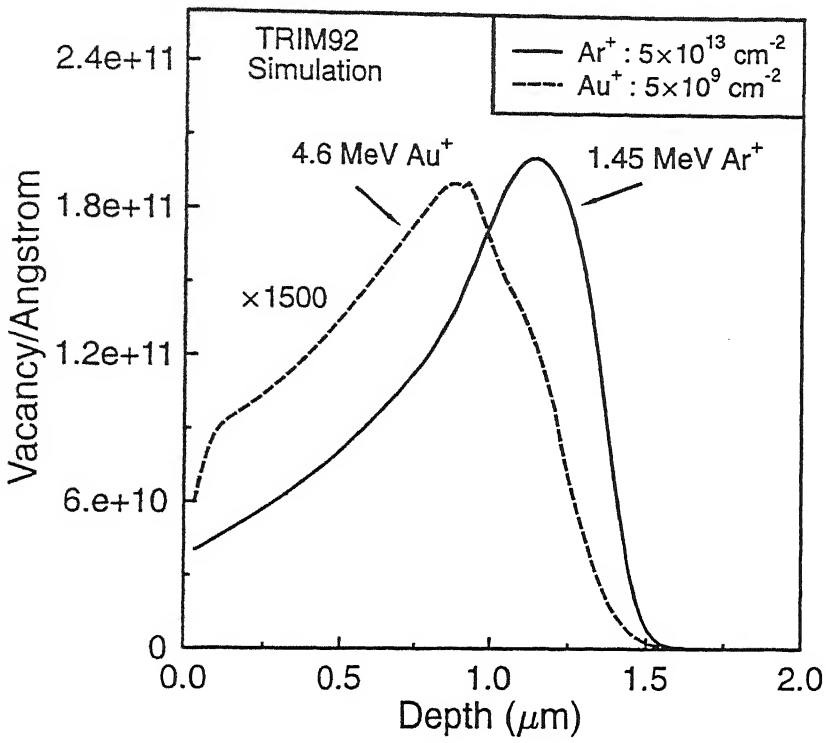

Figure 4.4: Vacancy distribution for 1.45 MeV Ar^+ (5×10^{13} cm^{-2}) and 4.6 MeV Au^+ (5×10^9 cm^{-2}) ions as predicted from TRIM simulation.

tion layer. The location of this trap dominated region lies far beyond the range predicted by TRIM [15] (Transport of Ions in Matter) which is only 1.23 μm. Large concentration of traps are expected to be present in as-implanted Si, but its location is unusual.

The TRIM predicted vacancy concentration profile for Ar^+ and Au^+ ion implantation are shown in Fig. 4.4. The peak concentration of the defect profile shows that for Au^+ ion implantation (dose 5×10^9 cm^{-2}) defect peak concentration is about 1500 times lesser than the Ar^+ ion (5×10^{13} cm^{-2}) case. Note that implanted dose of Au^+ ion is 4 orders of magnitude less compared to Ar^+ ion case. Being heavy in mass Au^+ ion produces significant amount of defect even for such a low dose. The damage peak positions are slightly shifted due to difference in the implant energy. However, this predicted position

of the peak defect concentration is quite shallower than the measured value as shown in Fig. 4.3. This is an important observation in the present work where defects are seen to be present at a place much larger than the expected range from TRIM simulation.

The flatness in C-V curve has been reported earlier in Mg^+ and Ni^+ implanted Si [132] and in He ion implanted Si [133, 134, 135] without a discussion of its origin. Singh *et al.* [136] have attributed occurrence of such flat regions to interface states in Ni/nCdF_2 Schottky diode using ideas suggested by Fonash [137]. High series resistance in the device can give rise to such feature [88] as it was shown with simulation in Chapter 2. Consequently, this yields wrong carrier concentration profile. However, independent measurement of dissipation factor ($\omega R_s C$ where R_s is series resistance and C is actual capacitance) at various temperature using an impedance analyzer showed no significant effect of series resistance in the capacitance measurement of irradiated device. The dissipation factor was found to be varying in the range of 0 to 0.17, larger value for higher temperature, in the temperature range of 100K-310K. The series resistance effect become significant when dissipation factor is comparable to or greater than 1. Moreover, as has been shown in the last chapter, large series resistance give rise to a minima in the $1/C^2$ vs. V curve rather than flatness as observed. Hence, this effect is a significant characteristics of the damaged region in the depletion width. We go on to present more parameters dependence on C-V curves in order to isolate the origin of these features.

4.1.2 Temperature Dependence

C-V measurements were carried out at various temperatures in the range 100K-310K. Figure 4.5 shows $1/C^2$ vs. V plot for low dose implanted Ar^+ ions in Si measured at various temperatures in the range 100K-310K. In these measurements, the sample is initially kept at steady state reverse bias at a constant temperature, and then C-V data is taken by changing the bias from high to low reverse bias. The change in capacitance

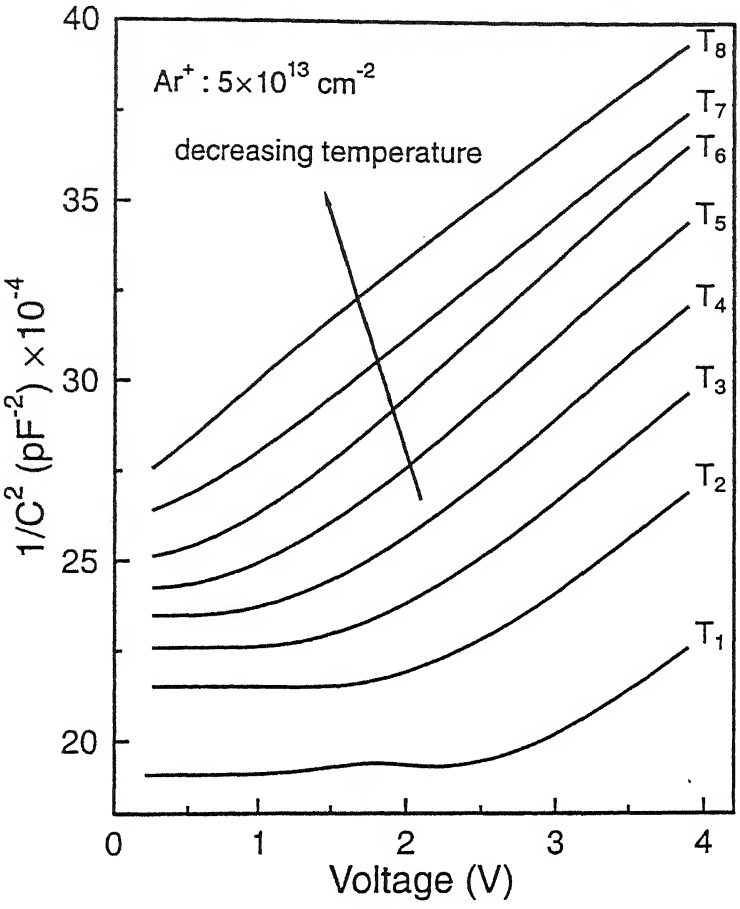

Figure 4.5: C-V characteristics of as-implanted n-Si measured at temperatures (T1) 303.9K, (T2) 278.3K, (T3) 257.4K, (T4) 237.9K, (T5) 217.2, (T6) 186.6K, (T7) 155.5K and (T8) 103.5K.

with temperature is seen to be large as shown in Fig. 4.5.

Note that as temperature is decreased from T_1 to T_8 in the figure, the depletion layer edge for any particular bias (say, zero bias) lies deeper in the sample. Further, the extent in voltage of flatter region gets reduced and the curves at the lowest temperatures are fully linear indicating constancy of carrier concentration. These distinct features taken together points to the involvement of traps on controlling the nature of the curves. Large changes in capacitances, say at zero bias, is an indicator of changes in the charged trap occupancy within the depletion layer with temperature. Clearly trapped charge is such

that the depletion width is large at lower temperature. For higher temperatures and lower voltages, the traps seem to affect the C-V curve, their occupancy being controlled by crossing of the Fermi level with trap level within the depletion layer. These systematics were observed in all our damaged samples. The increase in depletion width in presence of damaged region seems to be a consequence of acceptor nature of the dominant traps in the damaged region. These interpretation further gets supported by hysteresis measurements described in the next section.

4.1.3 Hysteresis Effect in C-V

The trap dominated nature of the damaged layer is confirmed by observation of hysteresis behaviour in the C-V measurement. Figure 4.6 shows $1/C^2$ vs. V plots at a certain low temperature for different voltage sweep rates in both directions of voltage change. A typical scan begins with decreasing reverse voltage from a steady state value. Note that the C-V characteristics depends on both sign and rate of voltage sweep clearly showing hysteresis effect. The occurrence of hysteresis can be easily understood in terms of presence of large number of trapping centers in concentration comparable or larger than the background doping. During C-V measurement, if the voltage sweep rate is made faster/comparable to the trap emission rate, one observes a difference in capacitance between decreasing and increasing voltage sweep. For the fastest sweep rate the difference between the two curves are maximum and for slow sweep rate upper curve approaches the lower curve as shown in Fig. 4.6. It can be noted that the C-V characteristics are identical for different sweep rates when the voltage is decreased owing to fast capture process at the traps, while it is different on increasing the voltage since it is now controlled by rate of emission. Thus it is clear that flat region or nonlinearity in C-V is due to trap filling during decreasing reverse bias. From transient measurement data presented later, we find that the sweep rates used here are comparable to the emission rate of a single

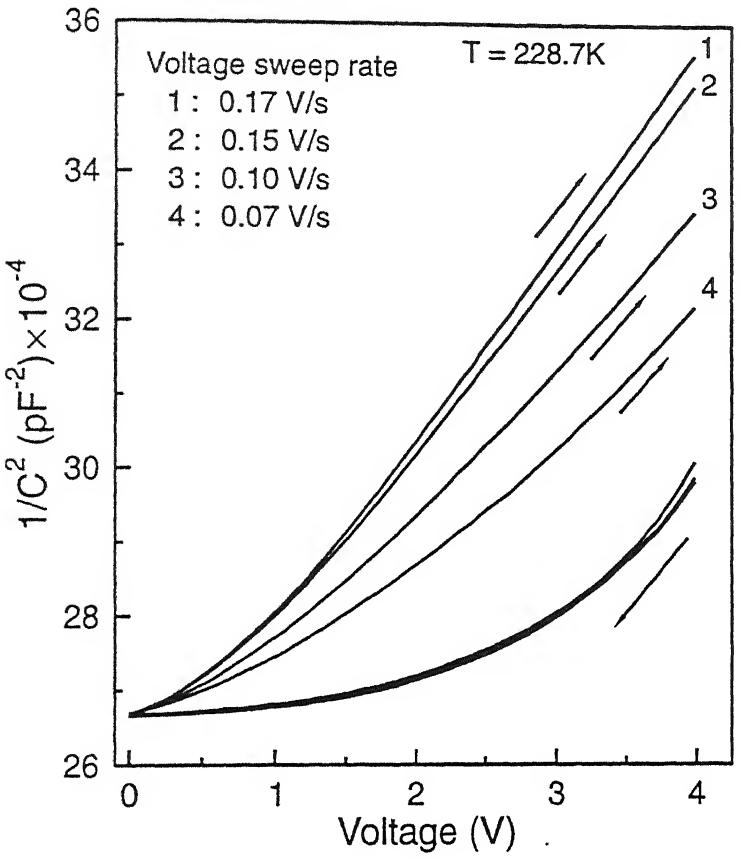

Figure 4.6: $1/C^2$ vs. V plot showing hysteresis behaviour for decreasing and increasing reverse bias with different voltage sweep rates. Arrows indicate the direction of voltage sweep.

major trap identified in this work. The zero bias depletion width of most devices having damaged layer are 2-3 μm larger than their corresponding undamaged device. Also note that the depletion width is larger when the reverse bias is increased after allowing capture during C-V measurements. This implies that after capture of electrons, the defects get negatively charged in so large number that the depletion region is widened to uncover required amount of positive background charge to maintain charge balance condition. Hence these traps play the role of dominant compensating center.

Similar hysteresis effect has been observed for Au^+ implanted Si as well. In Fig. 4.7, we choose to display such a behaviour with one difference. In this case the degree of forward biasing controls the degree of filling of traps. The sweep rate is kept constant for

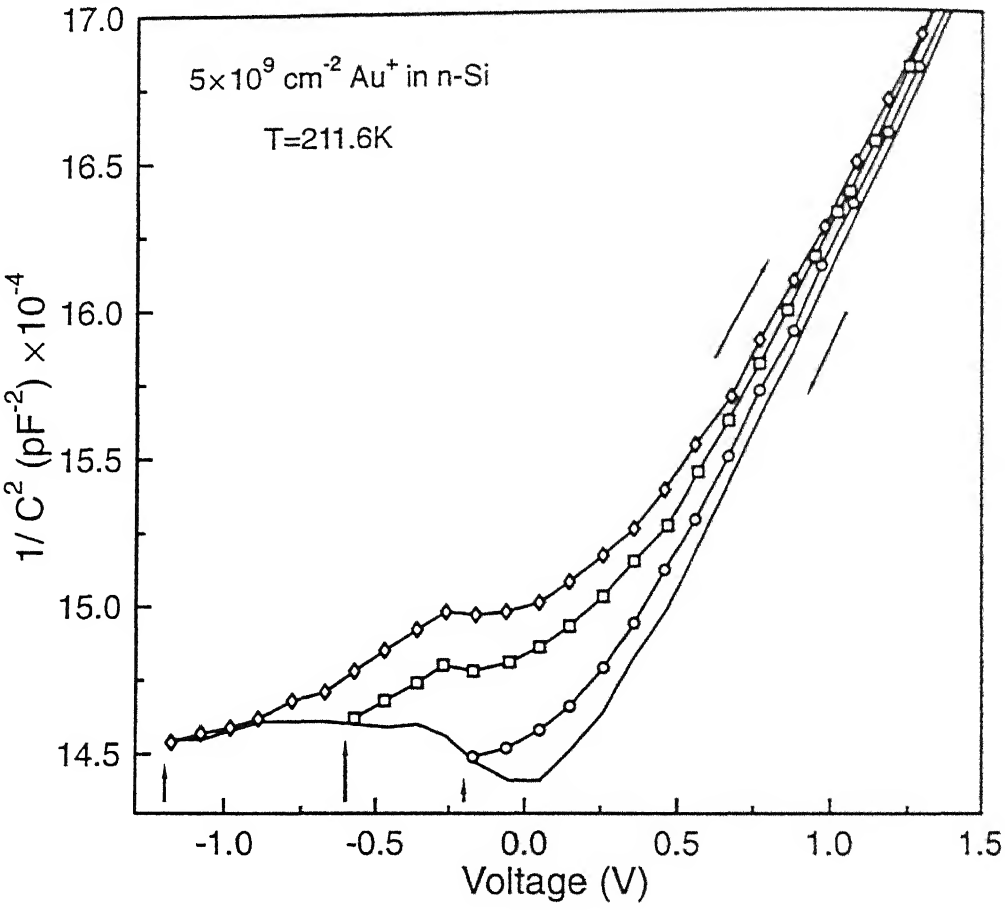

Figure 4.7: C-V characteristics with decreasing and increasing bias showing hysteresis effect in Au^+ implanted n-Si. Slanted arrow indicates the direction of voltage sweep, and different set of curves were obtained for different degree of forward bias injection. The forward bias voltage for each is indicated by vertical arrows above the voltage axis.

different cycles. During the decreasing voltage cycle we take the device to forward bias indicated as negative voltage in the figure. With increasing forward bias, we see larger hysteresis effect i.e. difference between curves corresponding to decreasing and increasing voltage cycle increases. The arrows in the figure indicate the voltage upto which the forward bias is applied before starting the increasing voltage cycle. It can be noted from the largest forward bias curve in Fig. 4.7 that initially the difference in capacitance between decreasing and increasing voltage cycle is negligible. This is partly due to sweep

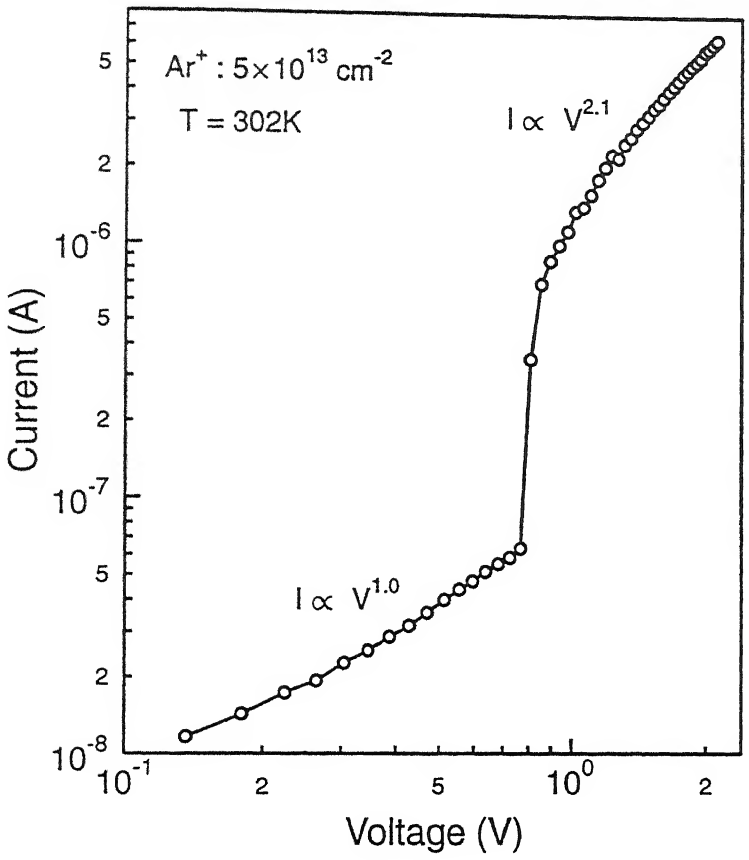

Figure 4.9: Forward I-V characteristics of 160°C annealed sample at 302K showing ohmic and space charge limited (SCL) current region. Voltage corresponding to nearly vertical section of the characteristics is trap filled limit voltage (V_{TFL}).

replaced by a metal and i-region is nearly intrinsic due to the above defect level. Transport behaviour on metal/implanted (amorphous) Si contacts have been earlier explained using a model of charge injection into a thin layer of trap rich amorphous Si [138]. Similar model has been proposed for proton bombarded GaAs [139].

4.2.2 Temperature Dependence

Temperature dependence of I-V characteristics for 160°C annealed (Ar^+ implanted) n-Si are shown in Fig. 4.10. The two distinct regions of current conduction are seen clearly for three different temperatures. The notable feature in these curves is decrease of V_{TFL}

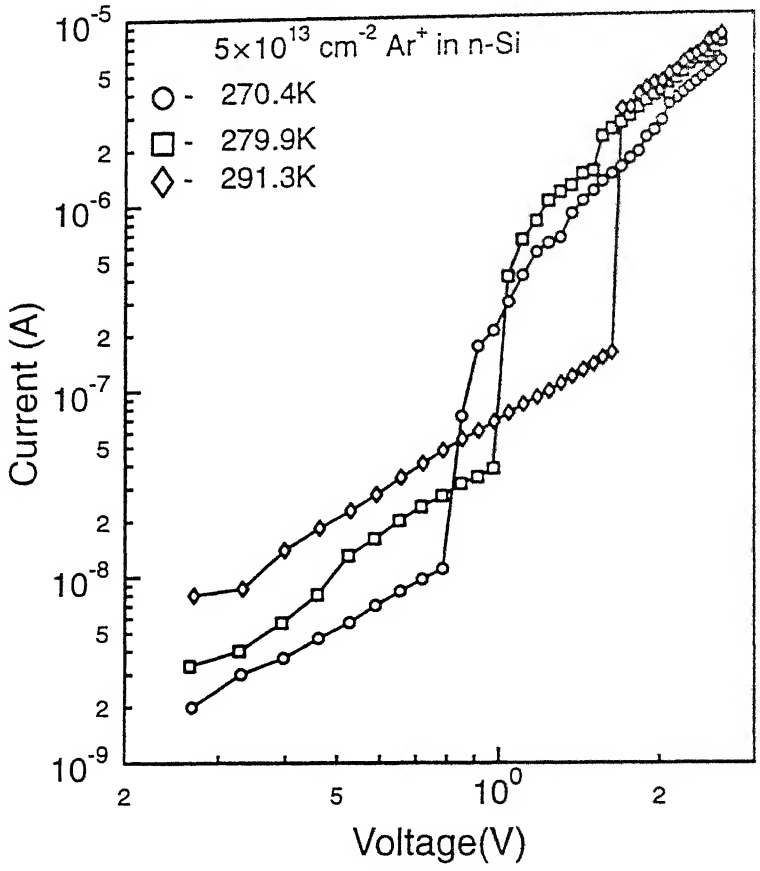

Figure 4.10: Forward I-V characteristics of Ar^+ irradiated (160°C annealed) Si measured at different temperatures showing shifts in V_{TFL}.

with decreasing temperature. The observed shift of V_{TFL} can be explained on the basis of trap filling with lowering temperature at a fixed bias. As the Fermi level moves closer to the conduction band in n-Si upon reduction in temperature, more traps get filled and thus number of unfilled fraction reduces with lowering temperature. Thus trap filled limit occurs for lower voltages at lower temperatures.

We will demonstrate in the next chapter similar effect in TSCAP spectra of Ar^+ ion implanted n-Si where trap filling is observed even without applying filling pulse. Thus unambiguous determination of space charge limited current in irradiated device proves the presence of fully trap controlled region in the depletion region of the irradiated diode.

Space charge limited current measurements have been used in the literature to determine energetic distribution and spatial profile of bulk traps in semiconductors [91, 140]. However, nonuniform spatial distribution of trap, voltage and temperature dependence of occupancy does not allow accurate determination of energetic distribution of traps from I-V characteristics. Nevertheless, for purposes of rough estimation, under the assumption of uniform trap distribution over the full depletion layer, we can use Eqn. 2.7 of Chapter 2 in this case. For V_{TFL}=1.7V (Fig. 4.10), estimated trap density is $N_T = 5.5 \times 10^{14}$ cm^{-3} for layer width of 2 μm. It is to be noted that the V_{TFL} measures that fraction of total trap that are empty in thermal equilibrium. Moreover, effective length over which trapping and detrapping is occurring during bias change is quite small compared to the total depletion width. Thus the trap concentration peak value is much larger than the value estimated above. For our purposes, it suffices to note that very large concentration of traps occur within the depletion layer controlling both its I-V and C-V characteristics. In the next section we present results on similar measurements for high temperature furnace-annealed samples.

4.3 Effect of Annealing on C-V and I-V Characteristics

We have annealed few irradiated samples at higher temperature prior to Schottky diode fabrication. The irradiated wafer pieces are annealed in vacuum ($\approx 2 \times 10^{-6}$ Torr) for 30 minutes at 400°C and 600°C respectively. The effect of annealing on C-V and I-V characteristics of the devices further help in relating trap activity to the degree of damage.

4.3.1 C-V Characteristics

Figure 4.11 shows $1/C^2$ vs. V plot for Ar^+ ion irradiated n-Si before and after annealing at

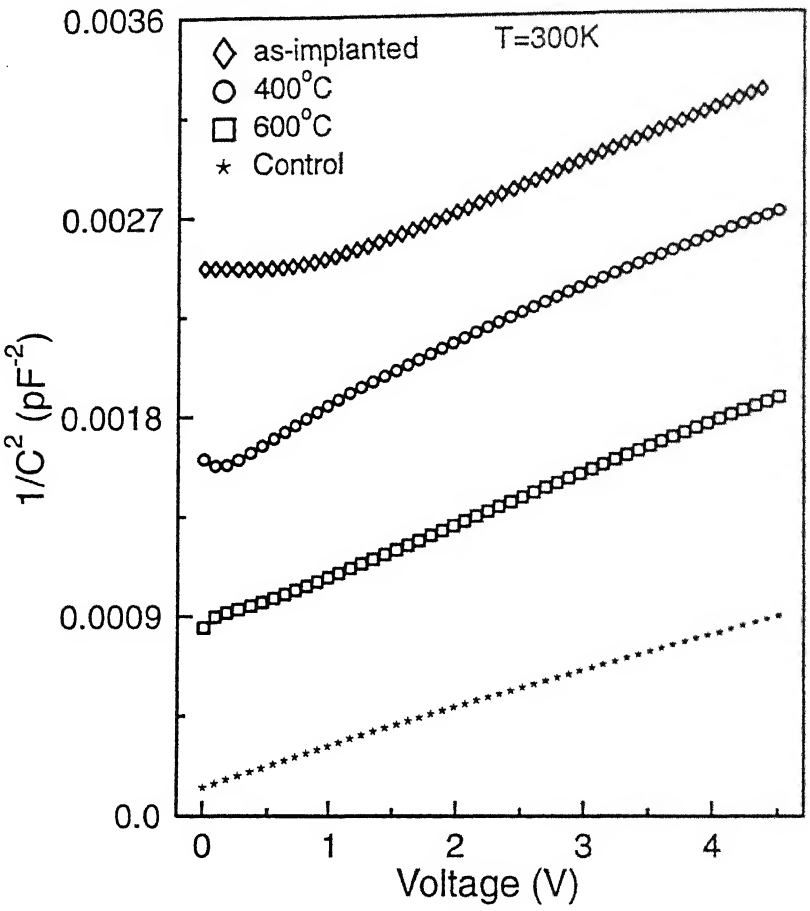

Figure 4.11: Comparison of C-V characteristics at 300K of unimplanted, as-implanted and annealed n-Si implanted with 5×10^{13} cm^{-2} Ar^{+} ions.

various temperatures. We have justified previously the cause of large depletion width in as-implanted device. It is clearly seen that high temperature annealing decreases the trap concentration. This leads to systematic changes in both the major features in $1/C^2$ vs. V curve. With increase in annealing temperature (i) the zero bias depletion width recovers towards the control samples, and (ii) the flat region for low bias reduces progressively. The temperature range of annealing (400°-600°C) itself suggests that the dominant defects controlling electrical behaviour are point defects, since extended defects begin annealing out only at temperatures above 1000°C. Comparison with unimplanted device shows that

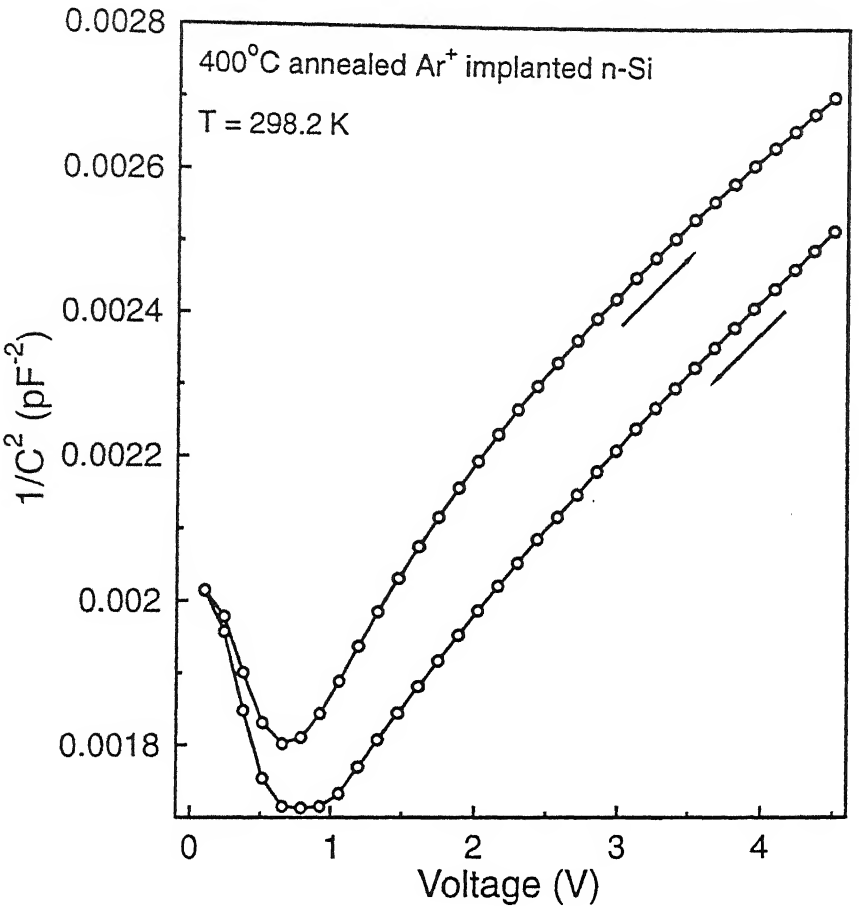

Figure 4.12: Hysteresis in C-V measurement at 298.2K during decreasing and increasing voltage sweep for 400°C annealed sample.

600°C is not sufficient to remove all the defects completely as the depletion width for the implanted samples is larger than the unimplanted case. The near parallel nature of the curves in Fig. 4.11 for high reverse bias region indicates absence of defects in the deeper region. For 400°C annealed samples, we could observe hysteresis effect in C-V measurements at room temperature as shown if Fig 4.12. It was obtained for fast sweep of voltage during decreasing and increasing bias voltage. This is also indicative of changed time constant of dominant defects controlling hysteresis. This indeed is further confirmed from transient measurements presented in the next chapter.

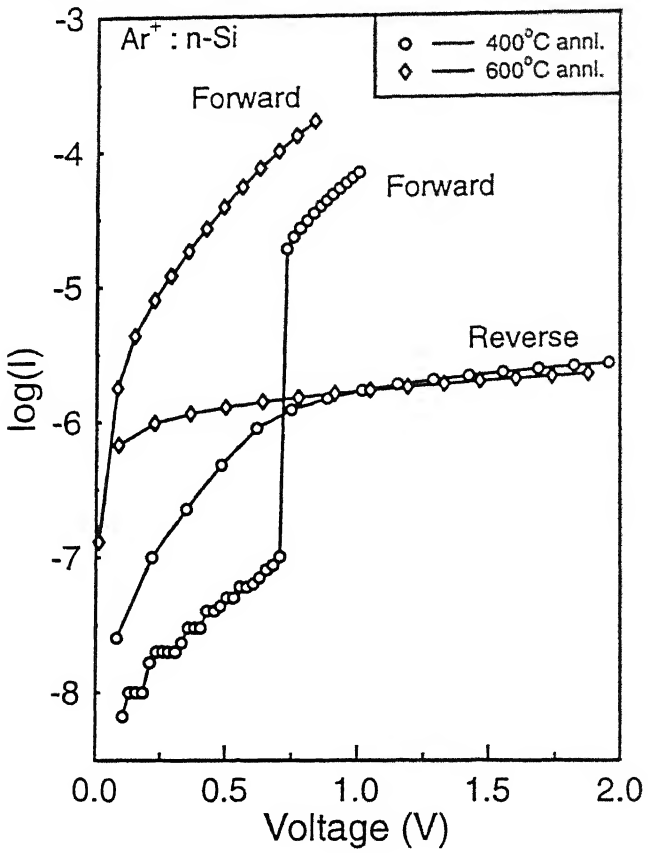

Figure 4.13: Forward and reverse I-V characteristics of Ar^+ implanted samples after 400°C and 600°C annealing.

4.3.2 I-V Characteristics

We show in Fig. 4.13, comparison of I-V characteristics at 300K for 400°C and 600°C annealed samples. The reverse saturation current is similar for these two samples. But the forward characteristics of 600°C annealed samples is considerably improved as compared to the case of 400°C annealed samples. For the later case space charge limited current above trap filled limit voltage is clearly seen. Though V_{TFL} is not so large as it was for as-implanted sample, presence of still large trap concentration is clear. It is expected that these defects can be annealed out by annealing above 600°C. These defects are anticipated to be due to point defect complexes rather than extended defect which forms after high temperature annealing in some cases.

4.4 Discussion

4.4.1 Summary of Major Experimental Features

It would be appropriate here to reiterate the salient features in the results presented in the preceding sections.

- High dose heavy ion irradiation causes damage which manifests in C-V and I-V characteristics of Schottky diodes made from these samples. Specifically, a very striking feature is that the capacitance does not change with bias for a voltage range in the low bias regime.

- The damaged layer is observed to be within the depletion layer with its width being much larger than control samples. The width is also larger than ion range or damage location predicted from TRIM simulations.

- Hysteresis and temperature dependence of C-V characteristics, are clearly indicative of involvement of traps in damaged layer embedded within the depletion layer. The observation of space charge limited conduction in forward bias also indicated the presence of a dominant trap in large concentration.

- The increase in irradiation dose increases the zero bias width. Annealing at temperatures in the range 400-600^{o}C reverses the effect to different degrees indicating recovery and damage relaxation.

4.4.2 Qualitative Explanation of Major Features

Let us first consider flatness in low-bias regime of C-V curves or bias independence of capacitance and consequent nonlinearity of $1/C^2$ vs. V curves. It is well known that a trap can be occupied in the transition region of the depletion layer where the trap level is below the Fermi level. Figure 4.14 shows a band diagram for a Schottky diode with

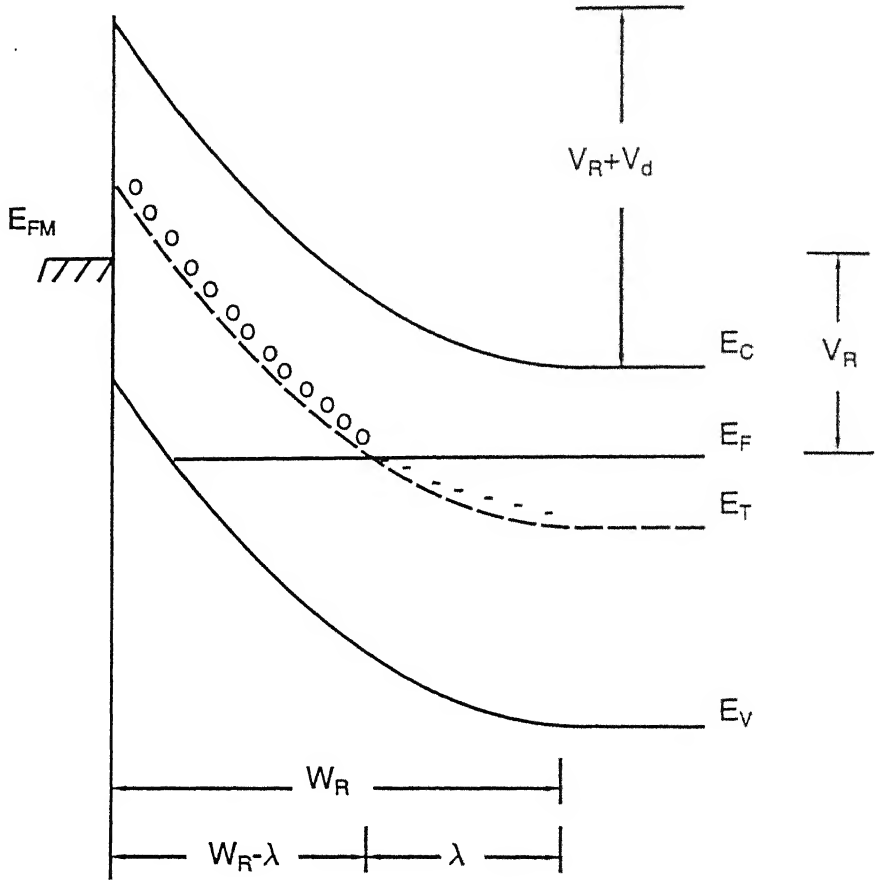

Figure 4.14: Energy band diagram for a Schottky diode with one acceptor trap level at energy E_T communicating with conduction band. V_R is applied reverse bias and V_d is built-in voltage.

one uniformly distributed deep level at energy E_T which gets negatively charged when occupied with electron. Changes in occupancy occur within depletion layer at the location where E_F and E_T cross each other due to band bending. In our case we are dealing with large concentration and nonuniform spatial distribution of traps. It is worth mentioning here that in standard cases of small trap concentration, band bending is mainly controlled by background shallow dopants. For this case, in contrast, trap concentration is so large that it controls band bending in the region of its presence and which in turn determines the crossing between E_T and E_F. Therefore, the location of the crossing is determined by

4.4.3 Model Simulations of C-V Characteristics

The purpose of model simulations is to arrive at the essential requirements on charge profile that would reproduce the major features of C-V characteristics. We seek to obtain reasonable estimates of concentration of charges and the distances at which they are located without attempting to provide numerical fit to the experimental data.

Several simplifying assumptions are required in order to keep the results of simulation transparent. To account for the presence of dominant trap indicated in the experiments, we assume that there exists only one midgap deep acceptor trap due to damage. The fact that its energy is in the middle of the bandgap would be shown to be fully justified on the basis of spectroscopic measurements in the next chapter. The region of depletion layer from the surface to the location of the damage induced trap is assumed to be uniformly compensated having low charge density. In reality, the degree of compensation would be varying over distance with a profile more or less similar to that predicted for damage distribution. Compensation would mainly be due to deactivation of shallow dopants and presence of deep defects in the region. However, the edge of the depletion layer is unable to penetrate into this layer during our capacitance measurements preventing changes in charge distribution in that region. Therefore an assumed effective compensation would suffice to take into account the voltage drop across this region. We also assume that the metal-semiconductor barrier height is same as that for control samples (i.e. standard value of 0.8eV for Au on n-Si Schottky). This value only appears as a constant in the magnitude of voltage.

One dimensional Poisson equation is solved numerically for a particular choice of trap profile to obtain the band bending in the semiconductor. The voltage dependence of capacitance is obtained by integrating over different widths of depletion layer. The trap occupation, band bending, and carrier concentrations are determined *self-consistently* during numerical integration. For the purposes of trap occupation, Fermi occupancy

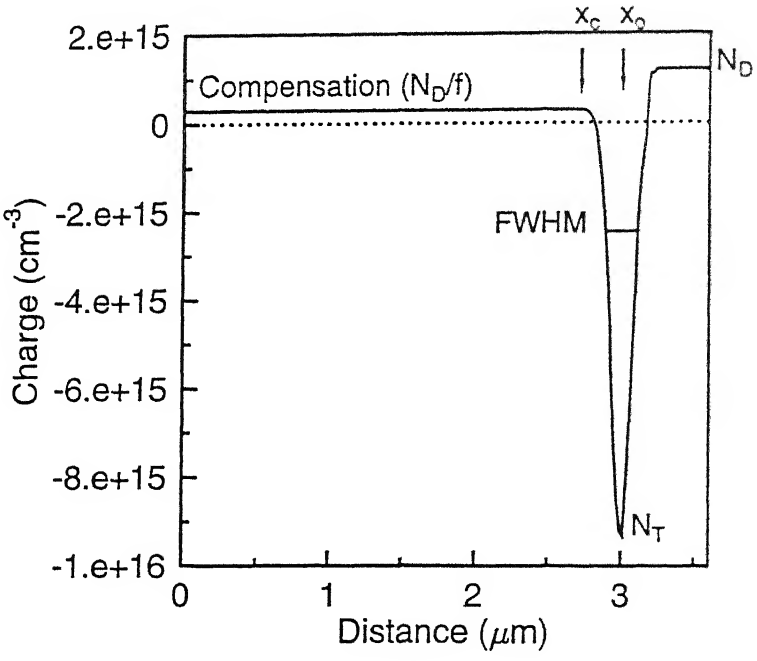

Figure 4.15: Charge profile due to trap concentration N_T and background doping N_D showing different parameters considered for simulations.

function is replaced with usual step approximation i.e. all traps lying below the Fermi level are considered to be occupied giving rise to a step in the occupancy at the E_T-E_F crossing point. Non-degenerate carrier statistics was only needed for all simulations. Depletion approximation was not explicitly assumed, though most of the results reported are well within the ambit of this approximation.

The parameters of simulation are specified in terms of a charge profile as depicted in Fig. 4.15. The relevant parameters are

1. the mean position (x_o) of trap profile (assumed to be a Gaussian),

2. the FWHM ($2\sqrt{2ln2}\,\sigma$) of the Gaussian distribution

3. the maximum concentration of trap N_T,

4. the width of the compensated layer (x_c) and the level of compensation specified in terms of fraction (f) of background doping (N_d).

The Poisson equation can now be written as

$$\frac{d^2V}{dx^2} = -\frac{\rho_t + \rho_d}{\epsilon} \tag{4.1}$$

where

$$\rho_t = -qN_T exp\left[-\frac{(x-x_o)^2}{2\sigma^2}\right]$$

$$\rho_d = \begin{cases} qN_d/f & \text{if } x < x_c \\ qN_d & x > x_c \end{cases}$$

Typical results of a simulation are shown in Fig. 4.16 where energy band diagram, trap concentration profile and the resulting $1/C^2$ vs. V are depicted in sequence. The C-V characteristics shown reproduced the major features in the experimental curves. The trap concentration and location are adjusted to obtain capacitance and voltage close to experiments. Recall that the flatness in the C-V curve is due to the fact that changes in trap occupation account for extra voltage drop without necessitating changes in depletion width.

In order to evaluate how the choice of parameters affect the calculated C-V curves, we perform simulations varying each parameter at a time holding others constant. Figure 4.17(a)-(d) shows the sets of C-V characteristics which clearly display different dependences. They can be summarized as follows:

- The sharpness of the transition from flat to linear region is controlled by FWHM of the trap distribution (Fig. 4.17(a)).

- The zero bias width is relatively insensitive to changes in trap concentration (Fig. 4.17(b)) but very sensitive to the choice of its mean position (Fig. 4.17(a)). The mean position largely controls the level of capacitance of the flat region without affecting the linear portion.

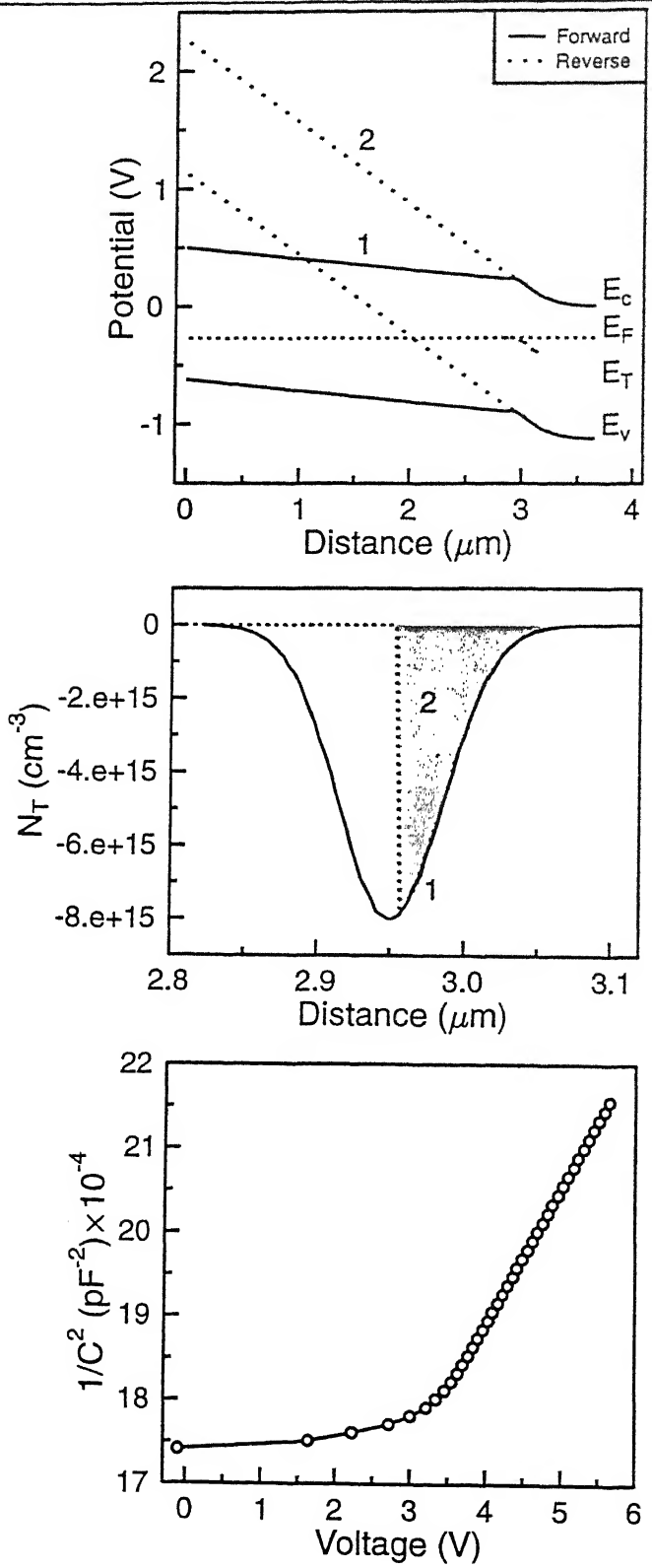

Figure 4.16: Calculated energy band diagram, trap occupancy profile and corresponding simulated C-V characteristics for a Schottky diode with one acceptor trap level at energy E_T. Two sets of energy band diagrams are shown corresponding to cases when : (1) all traps in the distribution are occupied, (2) only the shaded portion of the charge profile is occupied.

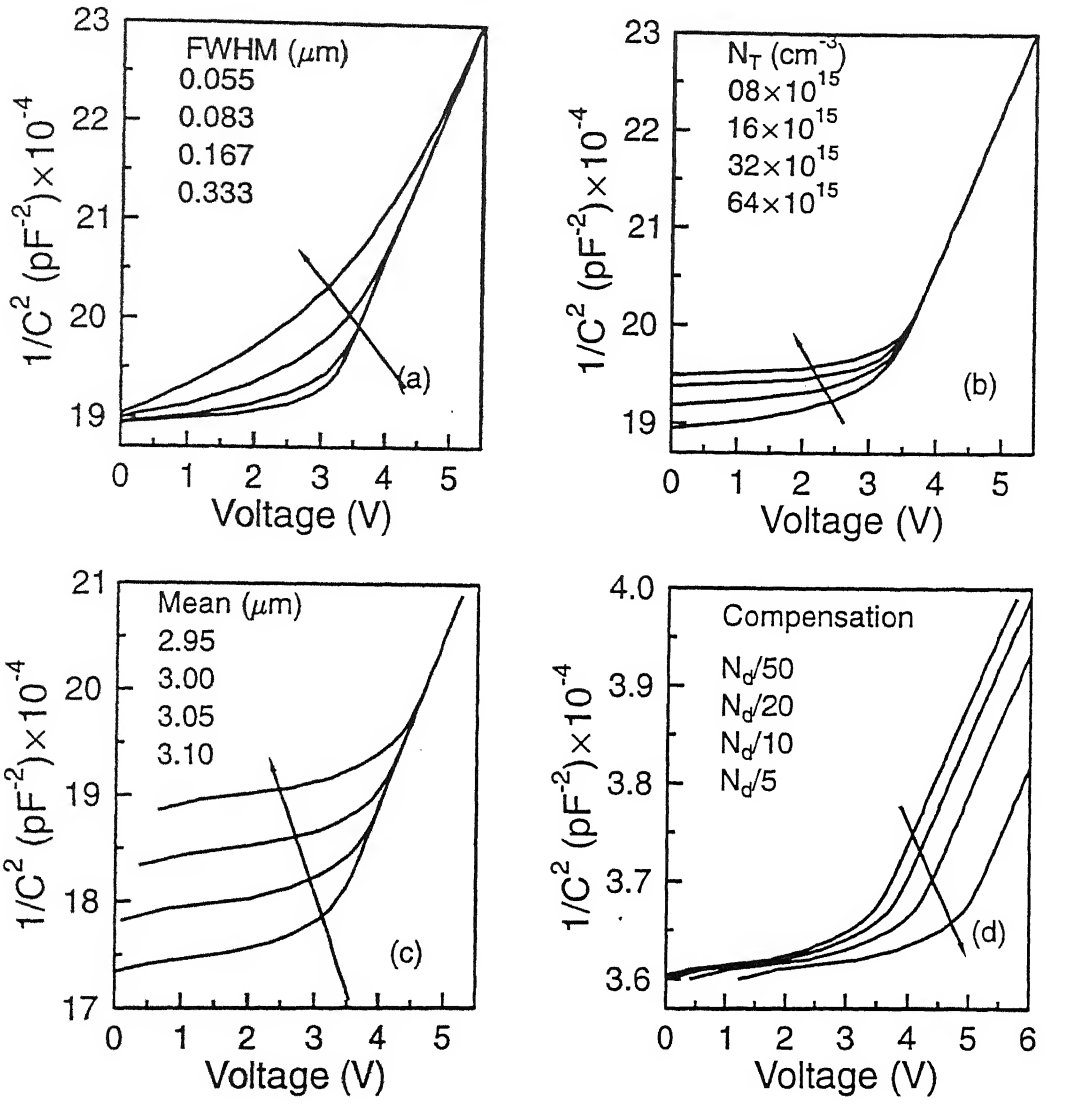

Figure 4.17: Different parameter dependence of simulated C-V characteristics for a Schottky diode with one acceptor trap level at energy E_T : (a) FWHM of Gaussian distribution, (b) trap concentration (N_T), (c) mean of trap profile (x_o), and (d) compensation (N_d/f).

ature is decreased the bulk Fermi level of the semiconductor moves up in relation to the metal Fermi level causing the crossing point to move towards the surface. This leads to increased occupation of the traps; hence increased negative charge forcing the depletion layer in turn to move out. At low temperature the traps filled in the process stay occupied leading to both larger zero bias depletion width, and linear $1/C^2$ vs. V curves.

Therefore, the information regarding electrically active defects would be from the E_T/E_F crossing point. In principle, by manipulating this crossing point in space one can obtain charge profile information. However, the problem of identifying the absolute location in space where this crossing occurs is not straightforward. The measurement of capacitance only gives the location of the edge of depletion layer and the crossing point relative to this edge would depend on the details of the profile inside. We have shown that the change of slope from the flat region to the linear region in $1/C^2$ vs. V curves is rather sharp as represented in apparent concentration profile (Fig. 4.3). The trap concentration profile at the crossing point is very sharp and can be treated as an "effective electrical interface" between trap-free and trap-dominated regions of the sample. The nature of this crossing point is distinctly different from that of a heterojunction or insulator-semiconductor interface capable of inversion. We have in course of our work ruled out these possibilities on the basis of C-V studies over extended region of bias. The doses used were below amorphization threshold and it was several orders of magnitude lower in case of Au^+ ion implantation. Yet the nature of characteristics are similar.

The deactivation of shallow dopants due to damage and charges due to electrically active traps produce a compensated region with low charge density till the end-of-range of the implanted ions. The degree of compensation would be expected to have a profile more or less similar to damage distribution as obtained from TRIM simulations.

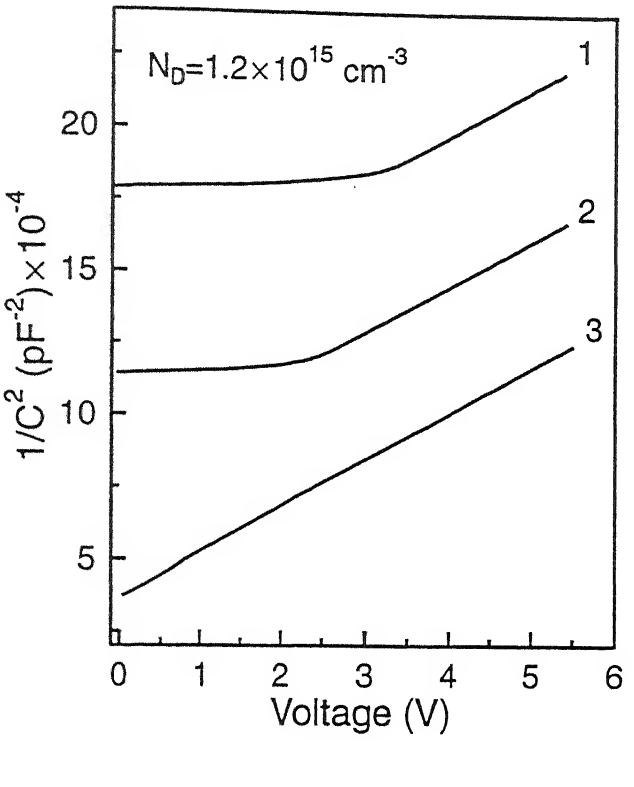

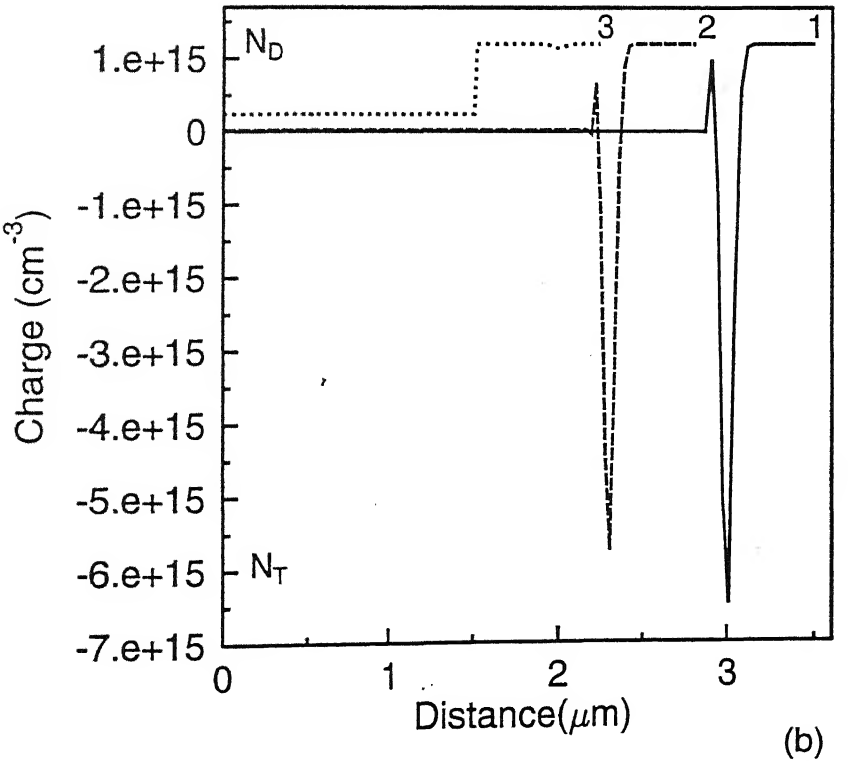

Figure 4.18: (a) Simulated C-V characteristics for irradiated device with different ion doses. (b) The corresponding charge profile is also shown.

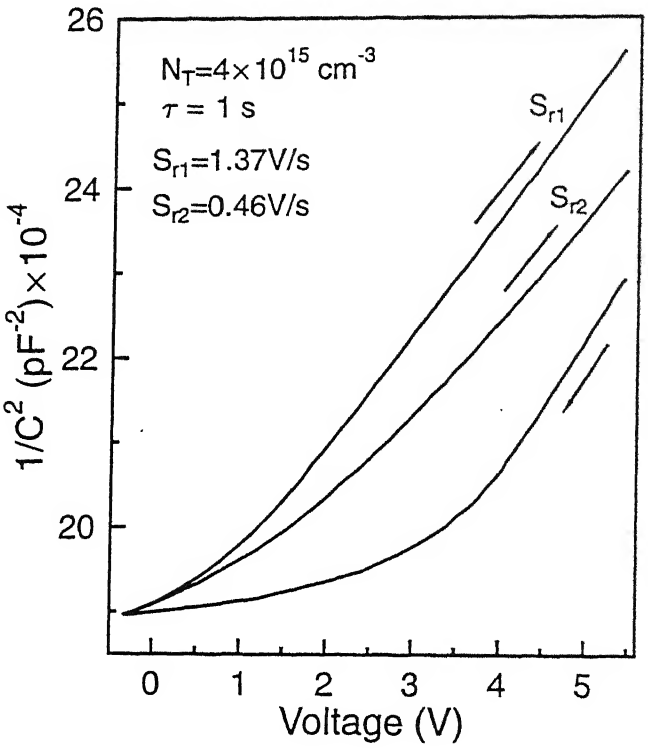

Figure 4.19: Hysteresis effect shown with simulated C-V curves assuming a fixed rate of emission from one acceptor trap level at energy E_T.

of emission of carrier from the trap into the simulations. A typical set of calculated curves demonstrating hysteresis in close agreement with experiment is shown in Fig. 4.19.

4.4.4 Physical Processes : Defect Migration & Clustering

Armed with insights from simulation, we are now in a position to discuss the most perplexing aspect of the results in this chapter. In the last section we have already seen that except for the last fraction of a micron, the depletion width is mostly due to the distance of the sharp edge of the trap profile. Typical depletion width in samples containing damage is between 2.5μm-4μm. In contrast, the prediction of TRIM simulations give an end-of-ion range of 1.23μm only. Hence the question arises as to why the trap profile extends so much beyond the location of the end-of-ion range damage. There is also the

the mechanism of recovery is unclear at this stage, it is most probably due to spatial variation of degree of clustering. It is known that binding energy for interstitial clusters increases with cluster size given by $E_{bi}(n) = 2.1 - 1.45(\sqrt{n} - \sqrt{n-1})$, where n is the number of interstitials in the cluster [52]. Hence higher temperature is needed to repair regions containing larger clusters which are closer to the damage. Though more detailed studies are required to pin down the mechanisms, our work demonstrates that capacitance based studies can serve as an important tool in such an endeavour.

4.5 Summary & Conclusions

In this Chapter we have presented results on steady state capacitance-voltage (C-V) measurements on Schottky diodes of n-Si containing damaged buried layers. It has been shown that characteristic features such as occurrence of bias independent capacitance region, hysteresis, strong temperature dependence of capacitance and space charge limited conduction are controlled by large concentration of a dominant acceptor trap within the depletion layer. The effective electrical interface between trap free and trap dominated region is defined by crossing between trap level and Fermi level. Model simulations of C-V characteristics were carried out to explain major features and to obtain essential requirements of the charge profile. A sharp trap profile is seen much beyond the ion range and its location is found to be dependent on irradiation dose and annealing temperature. The detection of sharp profile of traps at large distances has been explained on the basis of interstitial migration and clustering.

Chapter 5

Deep Level Spectroscopy of Defects in Deep Buried Layer

The essential physics of all forms of thermally stimulated space-charge spectroscopy is based on the thermal emission transient at some fixed temperature. In Chapter 2 we have discussed the formalism and analysis of transient signal and derivation of spectroscopic signal. One of the principal advantages of spectroscopic analysis, such as DLTS, is the presence of a flat baseline i.e. there is high common-mode rejection of the steady state capacitance variations in spectroscopic signals. Therefore, it is possible to obtain extremely high sensitivity e.g. $\Delta C/C \sim 10^{-5}$ for C$\sim$100 pF. Moreover, lineshape analysis in spectroscopic signal is extremely convenient for interpretation of related physics of defects in comparison to transient analysis. However, the task of extending use of these spectroscopic methods to the emerging class of defect dominated materials poses considerable challenge and MeV ion induced damage in buried layers is a case in point since validity of most standard analysis may be questionable.

In the previous Chapter, we have seen manifestation of various unusual features in steady-state capacitance and current measurements due to large density of defects in the damaged layer. In this Chapter, we will see more pronounced effect of these defects on the transient measurements. We carefully monitor capacitance transients and use a variety of spectroscopic techniques, identifying in the process sources of difficulties in standard interpretation. We have used TSCAP, DLTS as survey techniques. Having realized the problems of conventional DLTS based on capacitance transient measurements, we have

utilized the constant capacitance (CC) voltage transient measurements, and TATS has been used for spectroscopic analysis. Large change in capacitance with temperature does not allow implementation of DLTS technique in constant capacitance modes. Moreover, other advantages of isothermal spectroscopic technique as mentioned in Chapter 2 compared to thermal scan technique dictates the extensive use of TATS in CC mode for this work.

5.1 Capacitance Transients : Some Unusual Features

The basic step in all our spectroscopic measurements involves acquisition of capacitance or voltage transients. Hence it is worthwhile to concentrate on the features of transients at the outset. The transients are monitored at the end of a filling pulse across the test diode during which applied reverse bias is taken to zero to fill the traps with carriers. During the filling voltage pulse the time response of the capacitance is termed as capture transient, and its time dependence at the end of the filling pulse is termed as emission transient. In general capture of carriers at traps is faster than carrier emission rate at a particular temperature, though capture process can be thermally activated to make it slow enough at lower temperatures.

Figure 5.1 shows a set of typical capacitance response on application of a voltage pulse (from reverse bias -4V to 0V, for a filling time of t_f) to Schottky diodes which have damage embedded in the depletion layer. Following the application of zero bias, initially the capacitance increases sharply due to collapse of the depletion region but almost immediately it decreases to low capacitance value comparable to reverse bias capacitance thus showing a 'spike-like' behaviour in capacitance response during the filling pulse. Flat region towards the end of the filling pulse indicates no further change in depletion width for longer filling duration. This has been checked for long durations in many cases to

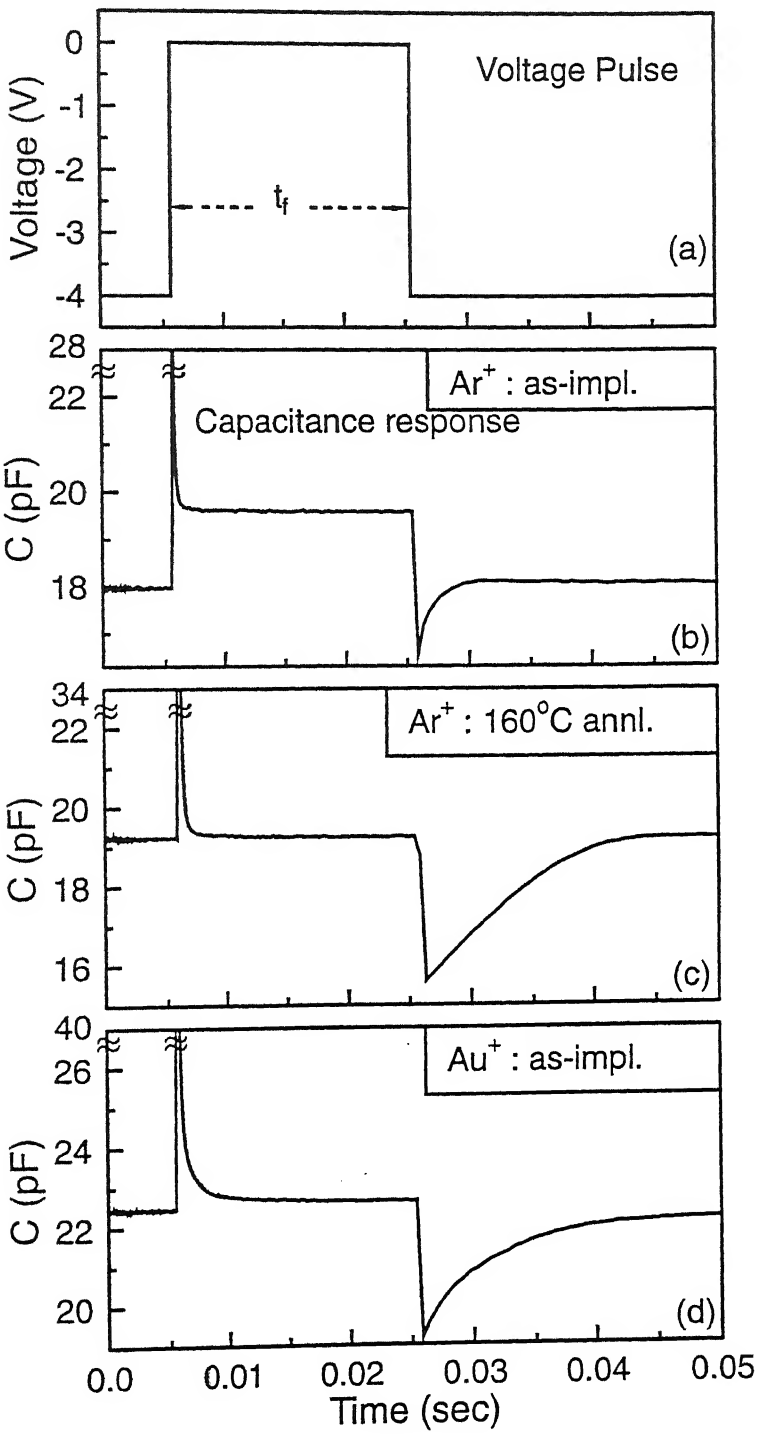

Figure 5.1: (a) Voltage filling pulse of duration (t_f) 20 ms on irradiated devices, (b) Capacitance transient response at room temperature for 5×10^{13} cm^{-2} Ar^+ as-implanted, (c) 5×10^{13} cm^{-2} Ar^+ and 160°C annealed and (d) 5×10^9 cm^{-2} Au^+ as-implanted samples.

detect any possible presence of slow components in capture transient. On reapplication of reverse bias voltage (V_R), a very large magnitude of capacitance change is observed due to emission of trapped carriers. Note that the transient magnitude is large in spite of the fact that the net change in capacitance at the end of filling pulse is very small.

In normal cases only an increase in capacitance corresponding to zero bias is expected, sometimes followed by a small transient due to filling of traps within the depletion layer from carriers in the Debye tail at the depletion edge. In our case the increase in capacitance is seen to be much larger than steady state zero bias capacitance indicating that the depletion edge does penetrate for a short while the beyond location of the apparent barrier observed through C-V measurements. The return of the depletion width is then clearly due to filling of traps leading to large decrease in positive charges within that period. Hence 'spike-like' response is direct consequence of encounter of the depletion edge with sharp trap profile with huge concentrations. As has been argued in the last Chapter, the dominant traps must be assuming negatively charged on capturing electrons in order to explain such a large depletion width. The occurrence of large magnitude majority carrier emission transient further proves beyond doubt that it is trapping within depletion layer which controls the observed response.

The magnitude of the capacitance spike is observed to be temperature dependent. At lower temperature, the spike height reduces and capacitance response increasingly resembles the normal case. This is also consistent with linearity of the $1/C^2$ vs. V plot at lower temperature as discussed in the last Chapter. The change in Fermi level with temperature increases steady state trap occupation and thus reduces the spike height as well as transient magnitude at lower temperature.

Form a closer look at the transient, it is apparent that the steady state of capacitance at reverse bias is achieved rather prematurely and suddenly before the characteristic time the transient ought to have taken to decay. In this sense, the transient behaviour is nonex-

ponential, and even taking into account nonexponentiality due to large trap concentration, such transient behaviour cannot be explained. A proper study of nonexponentiality requires use of spectroscopic techniques where lineshape analysis can reveal detail nature of the defect phenomena responsible for such unusual features. Since emission transient is of large magnitude, standard implementation of the DLTS analysis should be dealt with caution. In the next section we will present results from DLTS and thermally stimulated capacitance (TSCAP) measurements on these samples.

5.2 Broad Survey Using DLTS

The methodology and setup used for DLTS measurements are given in earlier chapters. The control diode was tested for any trap signature using DLTS measurements. No traps could be detected upto detection limit of 10^{-3} of background doping. This ensures that any traps detected in irradiated sample would be irradiation induced. The samples used for this study were irradiated prior to Schottky diode preparation i.e. irradiation was performed on bare silicon wafer pieces with back contact made by thick aluminum deposition. Devices were made on these wafers after proper etching/cleaning of surface oxide or any other contaminants.

A set of typical DLTS spectrum for samples irradiated with two different doses of Ar^+ ions and low dose Au^+ ions are shown in Fig. 5.2. For the chosen rate window, three majority carrier related peaks labelled A, V_2 and D1 are observed in the temperature range 90K-310K, irrespective of ion species and dose. The occurrence of a minority carrier peak H1 has been sample dependent. Though we do not study its systematics, appearance of minority carrier peak has been discussed later. Note that the doses used are considerably high so as to produce large concentration of defects. The peak A occurs in very small concentrations and it is due to well known A-center (oxygen-vacancy pair) [20]. This defect has an activation energy of E_c-0.17 eV with a electron capture cross-section of

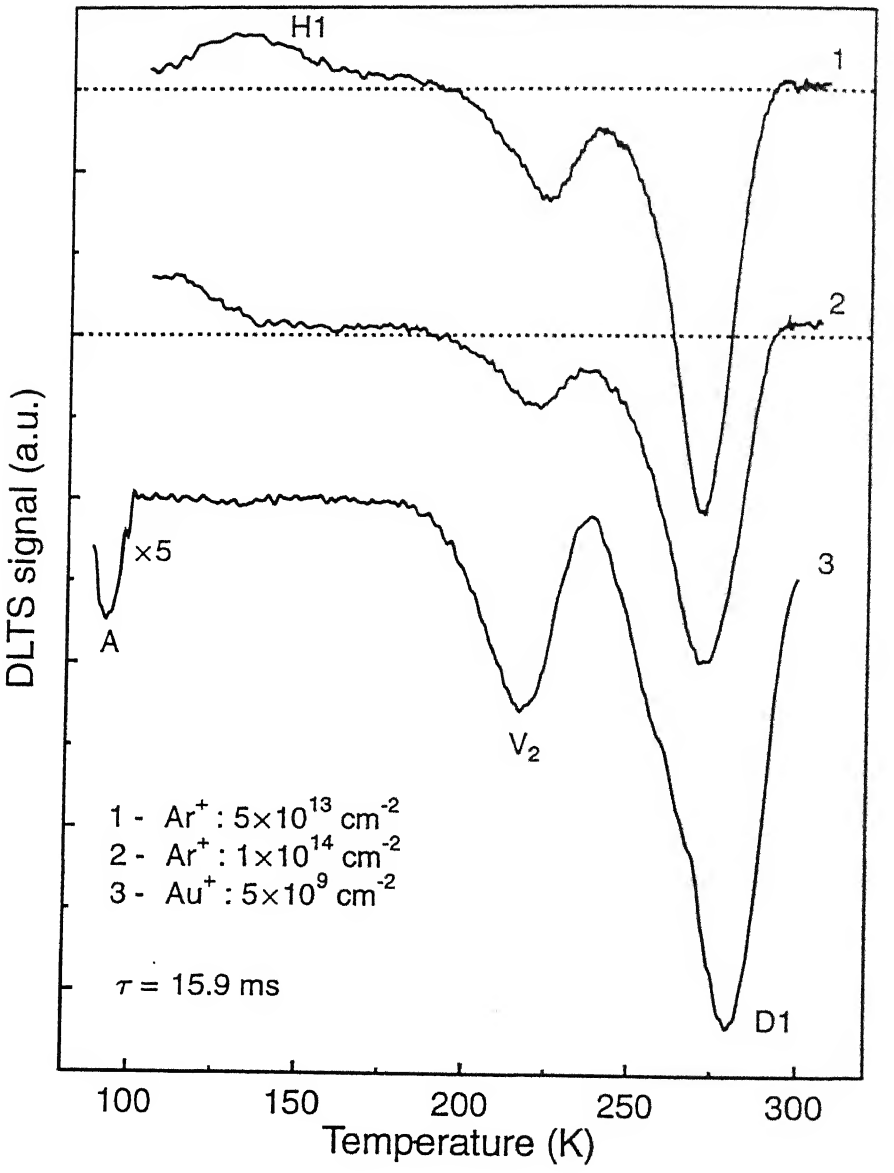

Figure 5.2: Typical DLTS spectrum of Ar^+ and Au^+ irradiated samples.

$\sim 2 \times 10^{-14}$ cm^2. This center is detected in most irradiation works with bulk silicon and has been extensively studied [83]. Since it is associated with oxygen, it is less likely in epitaxial wafers having low oxygen content. This justifies its very small peak height in our DLTS spectra. The peak labelled V_2 is a well known peak due to divacancy center ($V_2^{-/0}$) observed in all ion irradiation processes in n-Si [21, 24, 28, 142]. The peak labeled D1 is a newly observed feature and it is the most dominant among all other peaks shown in Fig. 5.2.

The concentration of V_2 related level as calculated from peak height is $\sim 5 \times 10^{13}$ cm^{-3}. This concentration ($N_T/N_D \sim 0.05$) is small compared to that expected due to high irradiation dose used in this work. In MeV Ge implanted Si with dose 1.2×10^9 cm^{-2}, much larger concentration ($N_T/N_D \sim 0.16$) of divacancy centers are reported by Svensson et al. [18]. The observed small concentration of divacancy centers even for such a high dose may be due to several reasons. Firstly, it may be due to incomplete filling of the traps using zero bias filling. As the zero bias depletion width is very high as concluded from C-V measurements, all the trap levels are not filled during application of filling pulse. This results in a peak height smaller than expected. Secondly, due to use of high dose rate ($\sim 10^{12}$ cm^{-2} s^{-1}) in our irradiation, divacancy production rate is smaller. Lower generation rate of point defects with increasing ion dose rate was reported by Svensson *et al.* [18]. Thirdly, evolution of defect complexes and clusters can be responsible for reducing divacancy concentration [19]. Comparatively, larger density of divacancy centers are observed in Au^+ implanted n-Si as can be seen in Fig. 5.2. The dose used for Au^+ implantation is 4 orders of magnitude lower than the dose used for Ar^+ implantation. However, due to heavier mass of the Au^+ ions, divacancy production rate is quite high. This is obviously smaller than the concentration expected from TRIM simulation as a large fraction of vacancies and interstitials recombine during the irradiation. In most of the low dose irradiation work, doubly negative charge state of the divacancy level ($V_2^{2-/-}$)

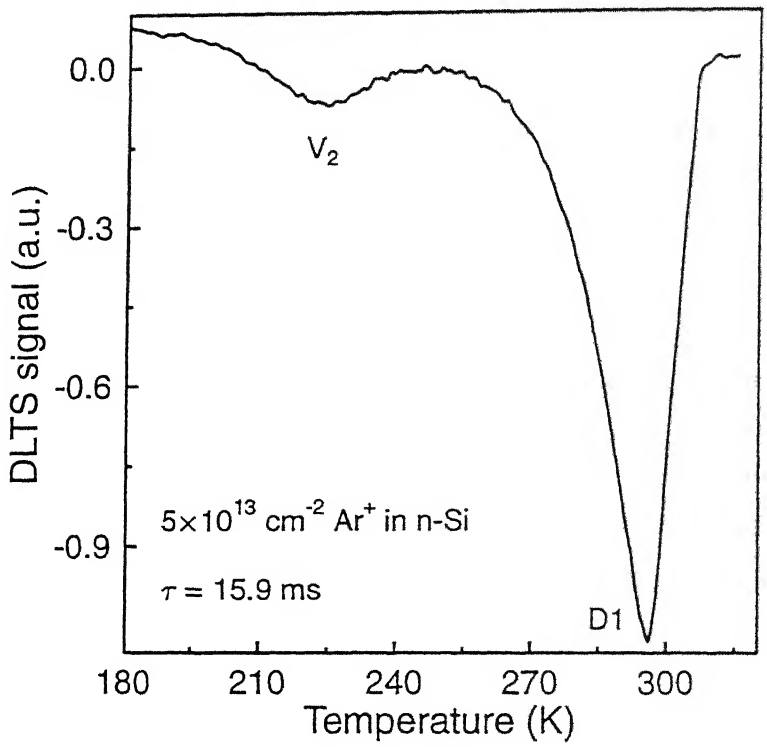

Figure 5.4: DLTS spectra of Ar^+ implanted sample annealed at 160°C showing large D1 peak. This peak shape is skewed at the right side of the peak.

centration in all our samples. This has not been observed so far mostly because, to our knowledge no other DLTS study uses unannealed samples with as high doses as in our case. An unusual feature in the DLTS lineshape of D1 is the sharp rise in the curve at the right side of the peak corresponding to premature end as previously pointed out in transients shown in Fig. 5.1. In the rate window implementation of DLTS, if the two times t_1 and t_2 are chosen such that t_1 fall in the normal region and t_2 falls in the prematurely flat region of the transient, such a narrow peak (or sharp rise) would be expected in DLTS spectrum. This particular spectrum shown in Fig. 5.4 corresponds to the transient shown in Fig. 5.1(b). In such a case, the peak position shown in Fig. 5.4 may not be the true peak position and hence use of Arrhenius plot for estimation of trap parameters will not

yield correct value. However, if one ignores the effect of such nonexponentiality on the Arrhenius plot, rough estimation of trap activation energy corresponds to a midgap level.

Note that nonexponentiality due to high trap concentration may affect the DLTS spectrum. Moreover, due to large change in steady state capacitance with temperature, the DLTS peak heights are strongly dependent on choice of rate window. In a temperature scanning method the spectral lineshape would be distorted in such cases. The temperature dependent peak height also seem to indicate different extent of filling at different temperatures. The superiority of a isothermal spectroscopic method has been demonstrated in Chapter 2 with a case study. We will see in the subsequent section the usefulness of such technique to isolate possible causes of nonexponentiality reinforcing its usefulness to defect phenomena. However, it is to be noted that the use of DLTS has enabled us to make a broad survey of defects present in such materials with ease, and it further dictates the necessity of using different spectroscopies for a particular defect of interest.

5.3 Detection of Defect Using TSCAP

TSCAP measurement is one of the simplest methods of detecting high density of traps in semiconductors. We have carried out TSCAP measurements for detection of dominant trap and for estimation of their concentrations. The measurement is done in constant voltage mode as large change in capacitance does not allow the measurement to be made in constant capacitance mode. Though this method has limitations as discussed in Chapter 2, we performed these measurements to get a better estimate of the density of traps. In these experiments reverse bias is applied only after cooling to low temperature and is hold at zero bias considerable amount of time for the filled case. Hence, filling of traps to a greater degree as compared to DLTS is ensured.

A typical TSCAP spectra for as-implanted (Ar^+ ions) Si is shown in Fig. 5.5 for zero bias filling and no filling case. The heating rate (β) was chosen to be 2K/minute and

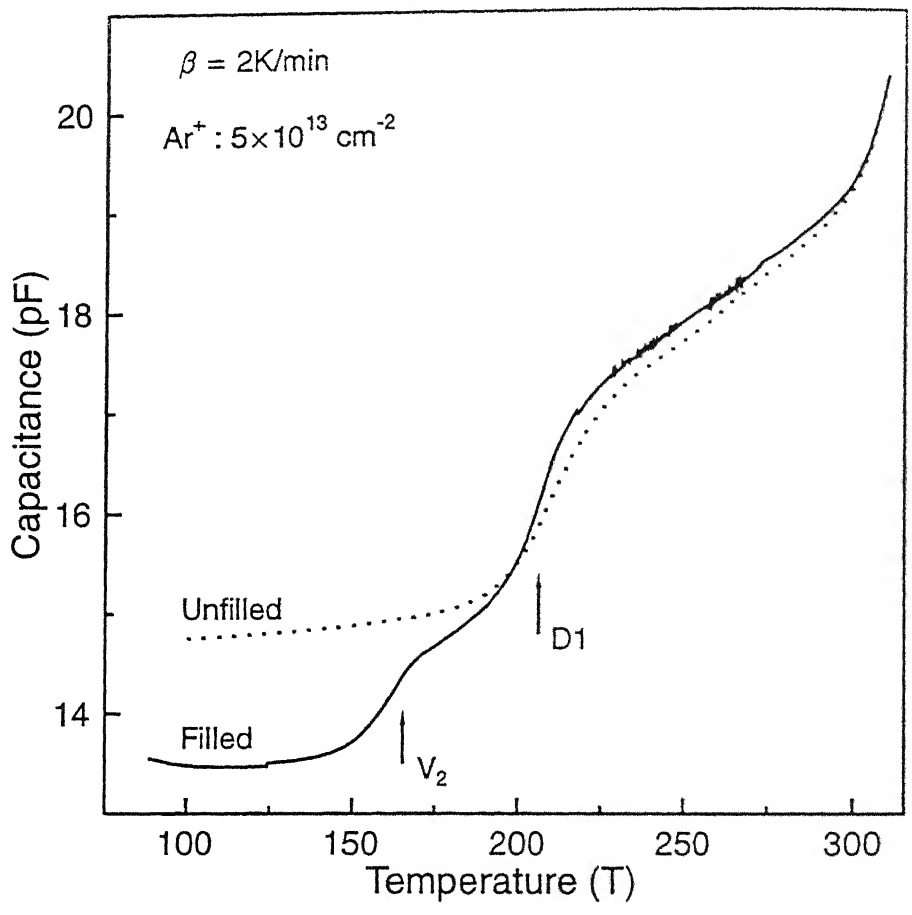

Figure 5.5: TSCAP signal for as-implanted Si with and without zero bias filling. Applied reverse bias V_r=4.5V. Arrows indicate capacitance step positions corresponding to V_2 and D1 levels.

both the curves are taken in heating cycle. The filled curve shows one extra capacitance step at lower temperature (165K) apart from the increased step height for the other one at 210K indicated by arrows. Thus, TSCAP spectra is dominated by two defect levels. The low temperature step is due to divacancy related level V_2 (E_c-0.42) eV which we have discussed earlier. Note that zero bias filling is essential for this trap to be seen in TSCAP spectra. It can also be noted that the change in capacitance corresponding to this step height is considerably large as compared to that found in DLTS measurement. The large step at 210K is due to damage related trap (D1) identified in this work. This step height

is a better indicator of the large magnitude of concentrations present in the as-implanted samples. From the step height in TSCAP, one can estimate the trap density using $N_d.\delta W$ where δW is change in depletion width due to capacitance step. For Fig. 5.5 this amount is $1 \times 10^{11}\ cm^{-2}$. Similar values were also estimated from C-V measurement at room temperature. With known heating rates and reasonable values of capture cross-section as found from transient measurement, we estimated the trap energy which confirmed that it is the same major trap as identified in DLTS measurement.

The large step height in *unfilled* curve of Fig. 5.5 indicates that traps are filled just by lowering the temperature and with zero bias filling these traps are additionally filled in larger amount. This can be explained on the basis of shift in Fermi level with temperature lowering which in turn causes occupation of large amount of additional trap at the E_F/E_T crossing. Due to large occupation of the traps, the band becomes almost flat over the distance such defects are present. This trap filling without application of filling pulse indicates that trap occupancy is controlled by quasi Fermi level which in turn is controlled by trap.

Figure 5.6 shows TSCAP spectra without zero bias filling for three different reverse biases. It is evident that for all these reverse biases, room temperature capacitance is almost identical indicating that C-V characteristics are flat around this temperature. This trap filling even at such high reverse biases indicates that trap occupancy is controlled by E_F movement with temperature. Note that such a behaviour is also in accordance with the temperature dependence of V_{TFL} as was shown in I-V characteristics of ion damaged Schottky devices.

Thus the TSCAP has been an useful tool to study such defects with large concentration. These unusual features including the dominance of D1 defect in damaged layer motivates us to study of this defect in detail using TATS.

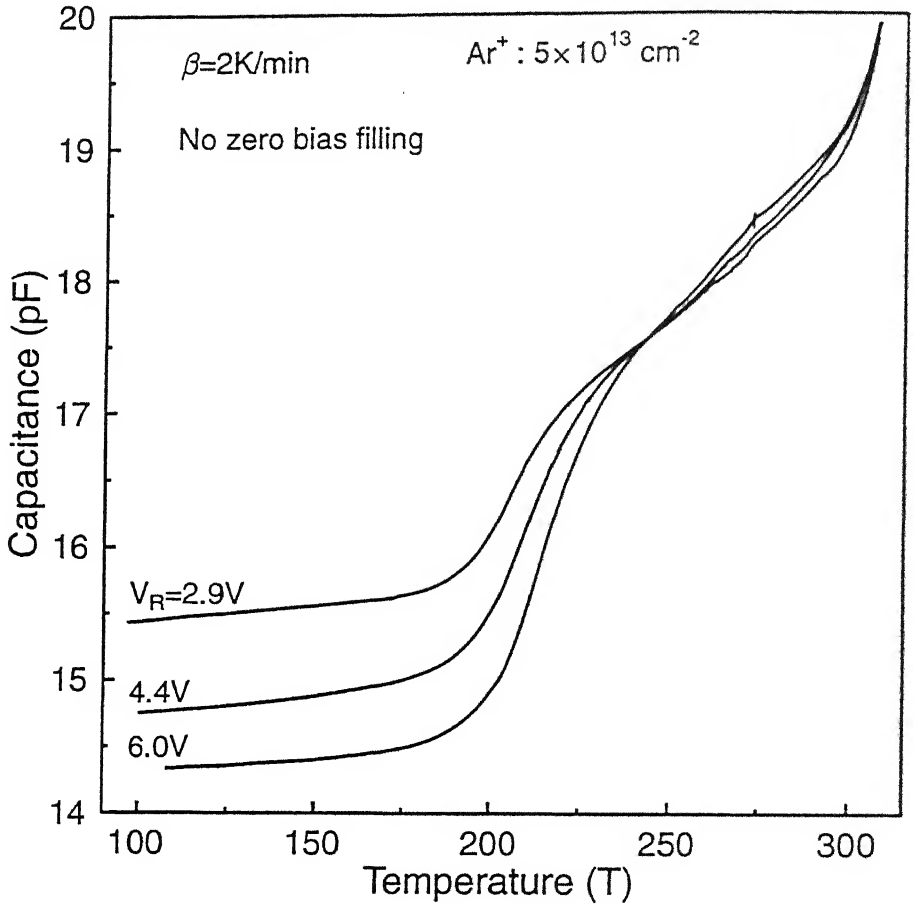

Figure 5.6: TSCAP signal for as-implanted Si taken under different reverse bias *without zero bias filling.*

5.4 TATS Measurements

In as-implanted (e.g. Ar^+) sample, because of large density of traps, nonexponentiality in transient is only to be expected. By performing the transient measurement in constant capacitance (CC) mode, we can avoid the nonexponentiality due to high trap concentration. Moreover, effect of series resistance on the capacitance transient can be severe causing ambiguity in conclusion regarding majority and minority carrier peaks in spectroscopic signal. Though independent measurement of dissipation factor ($\omega R_s C$) leads to the conclusion of negligible effect of series resistance on capacitance measurement, we

altogether overcome this effect by performing measurement in CC mode. In this mode, a feedback circuit controls the capacitance of the device to a predefined set value and corresponding voltage change is monitored as a function of time. Thus in CC mode, we measure the voltage transient instead of conventional capacitance transient.

As discussed in Chapter 2, TATS signal is constructed from the capacitance/voltage transient by varying the time window keeping temperature constant. For a chosen correlation, peak position in signal gives trap emission rate at a particular temperature. As the emission rate varies with temperature, TATS signal peak position also moves. It is also important to know the sign of the signal in TATS to differentiate between majority and minority carrier peaks. In CC-TATS method, a majority carrier related emission results in a positive peak whereas in conventional TATS (CV-TATS) it gives rise to a negative peak. Note that in conventional DLTS majority carrier related peak is negative. Henceforth, the terms positive peak and negative peak in TATS is to be understood with respect to particular methodology of analysis. Selection of suitable range of temperature for studying details of a particular defect is essential in TATS analysis. The detailed study of V_2 related peak will be discussed in the next Chapter where interesting features of this peak are revealed by performing transient experiments with varying filling times. In the next section, we will concentrate on the D1 level for improved determination of defect parameters.

5.4.1 TATS of dominant peak D1

In Fig. 5.7, CC-TATS signal is shown for transients taken at different temperatures for Ar^+ irradiated at two different doses. All the measurements are performed by keeping the depletion width (capacitance) constant corresponding to quiescent reverse bias. During filling, the device is taken to zero bias by special circuitry as described in Chapter 2. As the temperature is decreased, peak heights are reduced becoming undetectable at very

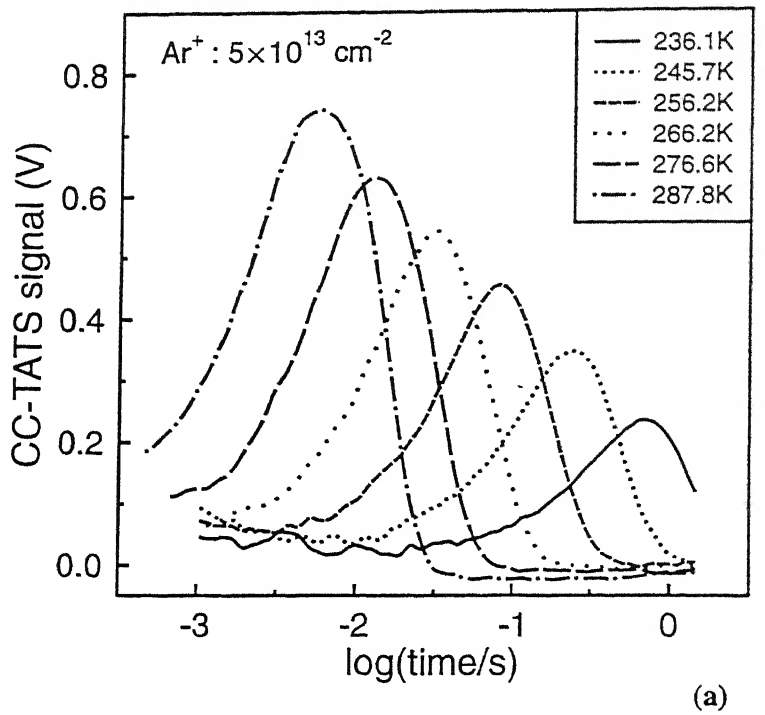

(a)

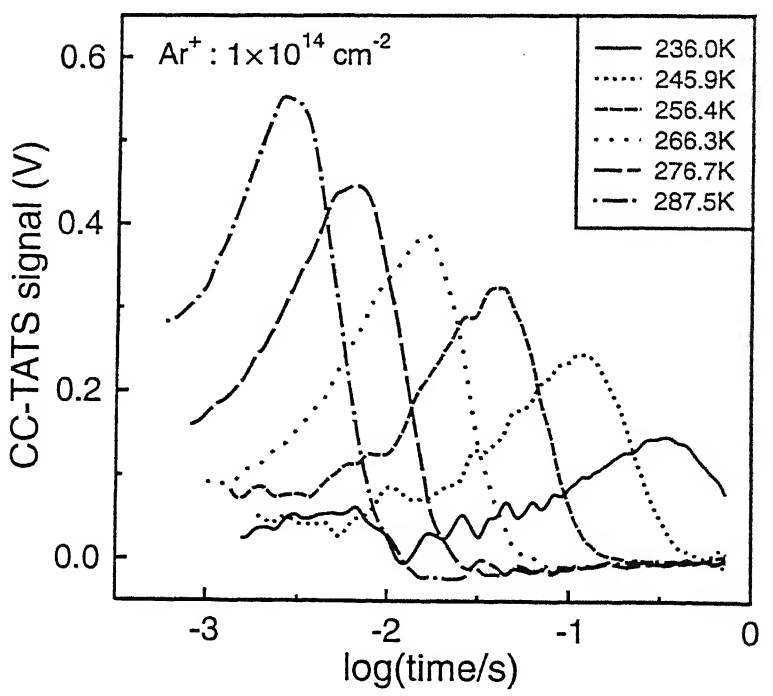

(b)

Figure 5.7: CC-TATS signal of defect D1 in as-implanted n-Si with (a) 5×10^{13} cm^{-2} and (b) 1×10^{14} cm^{-2} Ar^{+} at various temperatures for fixed depletion width.

low temperature. An inspection of lineshape in CC-TATS spectra shows that the peaks are distorted on the right, especially peaks corresponding to high temperatures. The reduction in peak height can be attributed to the fraction of trap filled or emptied being lesser at lower temperature. Similar features were also observed in I-V, C-V, TSCAP and DLTS characteristics. A temperature dependence of transient amplitude can give rise to lineshape distortion in a temperature scanning method such as DLTS. This in turn does not allow proper estimation of trap emission rate. In such cases superiority of isothermal spectroscopic methods such as TATS are clearly established. In both the samples with different doses, this temperature effect is pronounced.

As the defect is present in large concentration, this is expected to be responsible for carrier compensation in the damaged region which lies within the depletion region. As the measured depletion width is very large compared to the unirradiated sample, increase in depletion width is due to presence of high density of negatively charged traps (when occupied). Though these traps are located within the depletion layer, they are occupied due to unusual band bending at the defect location.

5.4.2 Nature of nonexponentiality

As mentioned in the previous section, lineshape of TATS peaks reveals that the peaks are not of proper symmetry as expected due to an exponential transient. For convenience of presentation from this point onwards, we would like to refer to peaks due to exponential transients as exponential peaks and that due to nonexponential transients as nonexponential peaks. As discussed in Chapter 2, inspection of the lineshape reveals that the peaks shown in Fig. 5.7 are narrower than exponential peaks. Narrow peaks can arise from transients whose emission rate is increasing with time as opposed to the case of an stretched exponential (stretching factor $\beta < 1$) transient where effectively emission rate is reducing with time. In no physical situation such narrowness is known to occur. Physical

peak is more distorted causing larger narrowness.

However, questions may be raised regarding the uniqueness of such a fit where both peak height and time constant are treated as free parameters in the fitting process. In order to test for the exponential character of the portion of the signal prior to apparent peak, we resort to method of point by point analysis of transient to evaluate time constant as described by Mangelsdorf [144]. We indeed find that within experimental errors a single time constant is involved till the time of the sudden cessation of the transient. Once the time constant is fixed, the peak height is adjusted to match the lineshape of the left side of the peak which would be unique. The nature and quality of fitting to more than thousand experimental points for each transient is convincing enough to consider that pair of parameters obtained are stable points in the solution space of fitting. The parameters so obtained shows that the time constant obtained from apparent peak position and peak amplitudes are both underestimates.

Figure 5.9 shows CC-TATS spectra with fitted exponential curves for two different samples implanted with different doses. Left peak marked P1 is due to divacancy related peak and it is seen to be broader than exponential peak. We will discuss more details about this peak later. The major peak (D1) height is seen to be smaller in case of samples implanted with high dose and lineshape is less skewed. Figure 5.10 shows Arrhenius plot for the major peak (D1) in four different samples prepared with different dose and annealing conditions. The estimated energy level and capture cross-section for the D1 defect are presented in Table 5.1. The energy level of the defect D1 is seen to vary between 0.49 eV to 0.56 eV depending on processing conditions. The magnitude of capture cross-section is typical of a deep neutral center [145] accepting an electron to become negatively charged. The variation in emission energy can be attributed to the defects' sensitivity to the degree of disorder in its environment or the degree of relaxation in the damaged layer. The relaxation of the damaged layer with relatively low temperature annealing will

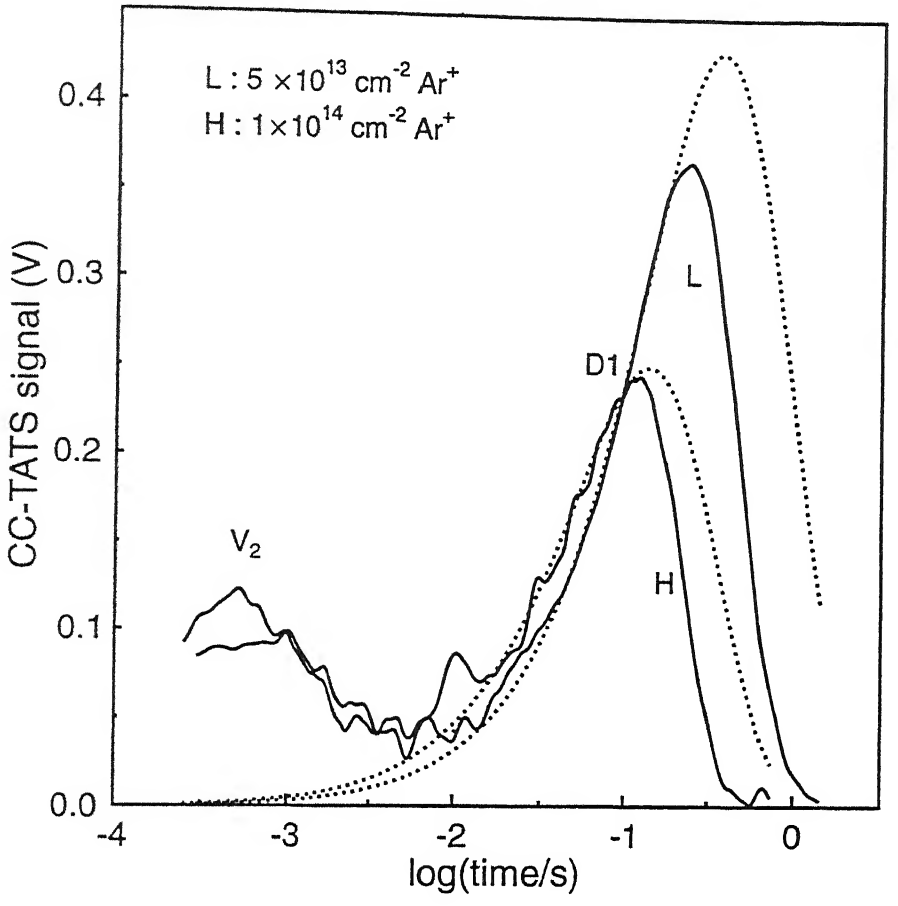

Figure 5.9: CC-TATS spectra of D1 with fitted exponential peaks for two different samples implanted with different doses. Left peak marked V_2 is due to divacancy related peak and it is not fitted.

Table 5.1: Trap parameters for the major peak (D1) for different set of samples.

Ar^+	as-implanted		160°C annealed	
Dose	E_c-E_T	σ_n	$E_c - E_T$	σ_n
(cm^{-2})	(eV)	(cm^2)	(eV)	(cm^2)
5×10^{13}	0.54	2.4×10^{-15}	0.56	7.4×10^{-16}
1×10^{14}	0.49	7.7×10^{-16}	0.52	1.1×10^{-15}

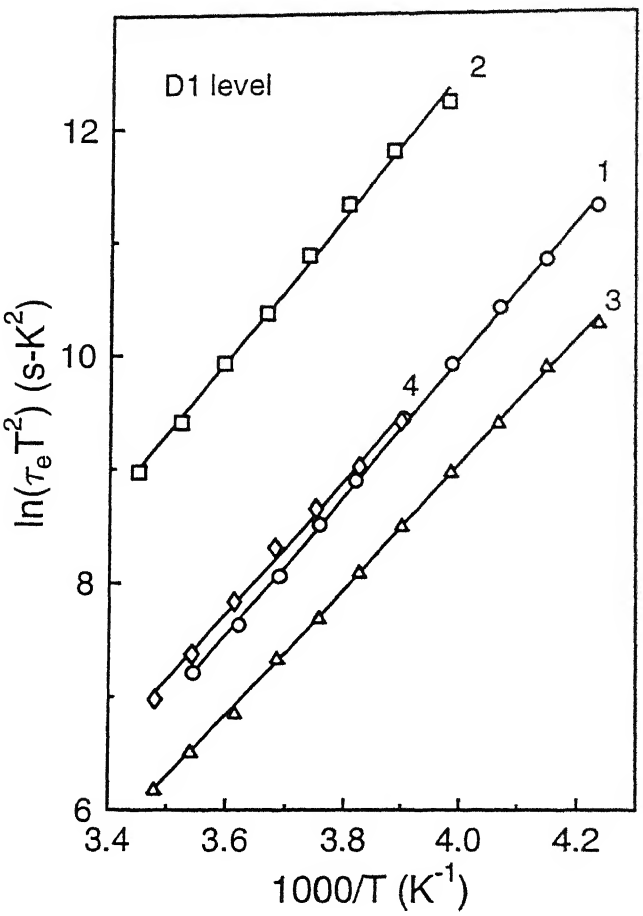

Figure 5.10: Arrhenius plot for the major trap (D1) in Ar^+ implanted four different samples : low dose (1) as-implanted, (2) 160°C annealed and in high dose (3)as-implanted, (4) 160°C annealed n-Si.

be discussed in a separate section. However, it is clear from the TATS spectra that the defect D1 stabilizes to deeper energy state for relaxed material in the case of low dose implantation or low temperature annealing. From fitting it has become clear that the peak height seen in DLTS or CC-TATS spectra is an underestimate. The actual peak height is shown with the fitted broken line in the CC-TATS spectra. For the spectra of Fig. 5.8 for 160°C annealed samples, the estimated trap concentration is $\sim 5.5 \times 10^{14}$ cm^{-3}. This concentration is sufficiently large to cause nonexponential transient in conventional

measurement. For high dose or as-implanted sample this concentration is smaller. This may be due to smaller extent of trap filling in those cases. Due to near intrinsic nature of the damaged layer, available carrier density for trap filling may be considerably low and thus a fraction of the traps show up in emission transient. Thus the observation of smaller peak in high dose implanted sample is an artefact of lesser extent of trap filling. Note that this concentration estimation is similar to that estimated from C-V hysteresis measurement or from I-V measurement.

The occurrence of sudden cessation of the emission transient leading to premature termination of peak in DLTS and CC-TATS spectra can be understood as follows. On restoration of reverse bias immediately after the filling pulse, the depletion width increases considerably owing to large increase in negative charge in the damaged layer, thus pushing the Fermi level down below the trap level in the damaged region. This leads to exponential emission of carrier from extra trapped charge till the quasi-Fermi level hits the trap level quickly bringing emission transient to an end. Note that the phenomena is crucially dependent on the fact that the emitting center itself controls the quasi-Fermi level in the damaged region and the overall band bending through its occupancy. Hence, in general premature termination is to be expected in a *p-i-n* like structure where the intrinsic *i*-region is compensated due to a deep level.

Since this phenomena occurs in time domain spectroscopies even in constant capacitance mode, it is a clear pointer to non-constancy of quasi-Fermi level in the region of large trap concentration in the damaged layer. It is the crossing of the quasi-Fermi level with E_T that decides trap occupancy. As emission proceeds the split in the quasi-Fermi level also keeps changing till it meets the trap level in the damaged region restoring quiescent reverse bias occupancy.

Observation of similar sudden termination of transients have been reported earlier in electron irradiated material and ascribed to reasons such as entropy driven metastability

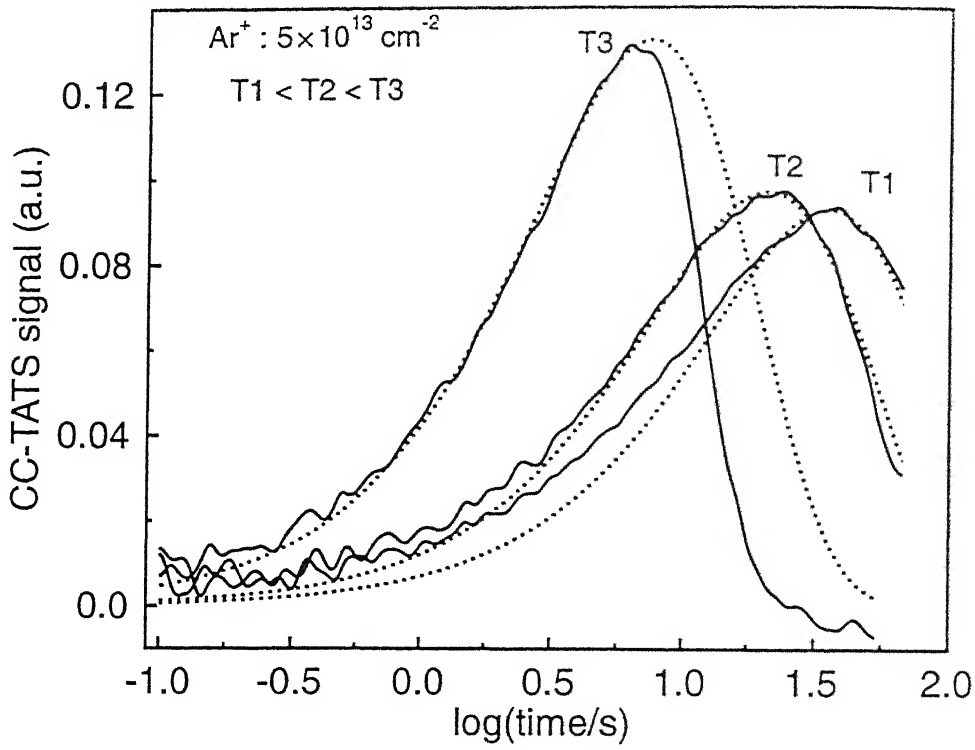

Figure 5.11: CC-TATS spectra (solid line) of D1 measured at temperatures (T1) 212.7K, (T2) 217.7K, and (T3) 228.6K. The dotted lines corresponds to peak fitted with exponential transients showing broad, exponential and narrow peaks respectively.

[146] or recombination currents [147]. In our opinion, mechanisms responsible for anomalous phenomena such as these are best understood when studied in the time domain using isothermal transient spectroscopies.

For this major peak, it is also observed that narrowness changes with temperature of measurement. Figure 5.11 shows the temperature dependence of the narrowness of this peak for Ar^+ implanted sample. With lowering temperature, peaks becomes less narrow and below certain temperature, it becomes broader than peak expected from exponential transient. We have already explained the cause of narrowness in peak shape. However, peaks broader than exponential is expected in such materials where defect are

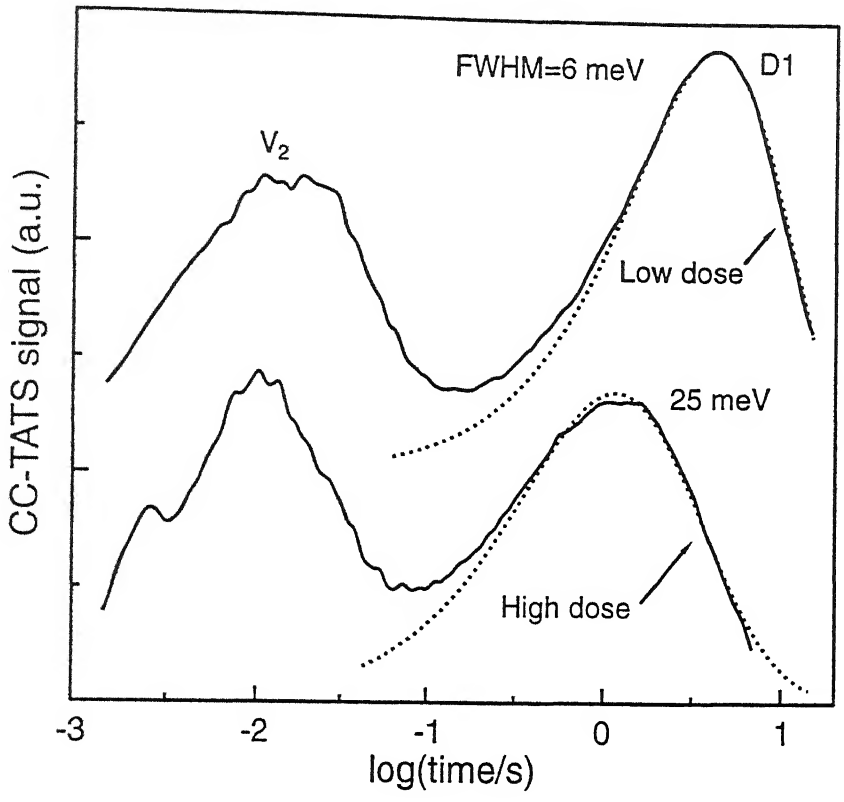

Figure 5.12: CC-TATS spectra of low dose and high dose implanted Si. Peak D1 is fitted (dotted line) with Gaussian broadened energy of different FWHM.

formed in a strained environment due to lattice damage. The degree of broadening in lineshape is a measure of degree of disorder in the immediate vicinity of these defects. A convenient measure of degree of disorder is in terms of spectroscopic lineshape broadening using Gaussian broadened activation energy of the trap level. CC-TATS measurements at lower temperature reveals a Gaussian broadening of trap energy with FWHM (full width at half maximum) of 25 meV for high dose (1×10^{14} cm^{-2}) Ar^+ implanted sample. This broadening is very small (6 meV) for low dose implanted sample. This is shown in Fig. 5.12 for as-implanted sample where experimental peak (solid line) due to D1 is fitted with a dotted line assuming Gaussian distribution in energy. Its sensitivity to strain and lattice disorder shows that it is possible to use it as a probe in the study of degree of

disorder for high dose implantations.

5.5 Annealing of Ion Damaged Layers

In order to understand the stability of the defects discussed above we annealed at 400°C and 600°C the irradiated samples prior to device fabrication. In some samples, devices fabricated from as-implanted wafers were annealed at relatively low temperature of 160°C for different durations. We have already discussed the effect of furnace annealing on the C-V characteristics in Chapter 4. From the depletion width measurement it was found that defects in the damaged layer get annealed under these heat treatments resulting in reduced zero bias depletion width. Note that the zero bias width was very large before annealing due to the presence of large number of negatively charged defects in the depletion layer of the junction. In this section we will examine the defect stability with respect to room temperature storage, relatively low temperature oven annealing and high temperature furnace annealing from spectroscopic measurements.

5.5.1 Room temperature usage and low temperature oven annealing

During the course of this work it was observed that for some high dose samples, there are minor, though noticeable, change in DLTS spectra with room temperature storage and usage. Figure 5.13 shows a set of DLTS spectra from high dose Ar^+ implanted n-Si. Curve 1 and 2 in the figure show the spectra taken under the similar conditions on the same sample in an interval of two weeks. Though the V_2 peak seen to be exactly matching for the two spectra, the damage related D1 peak is shifted towards higher temperature for the same rate window. The room temperature was in the range of 20°-35°C for this period and intermittently transient and steady-state capacitance measurements were performed on these sample. The increase in peak height and shift in peak position indicates that

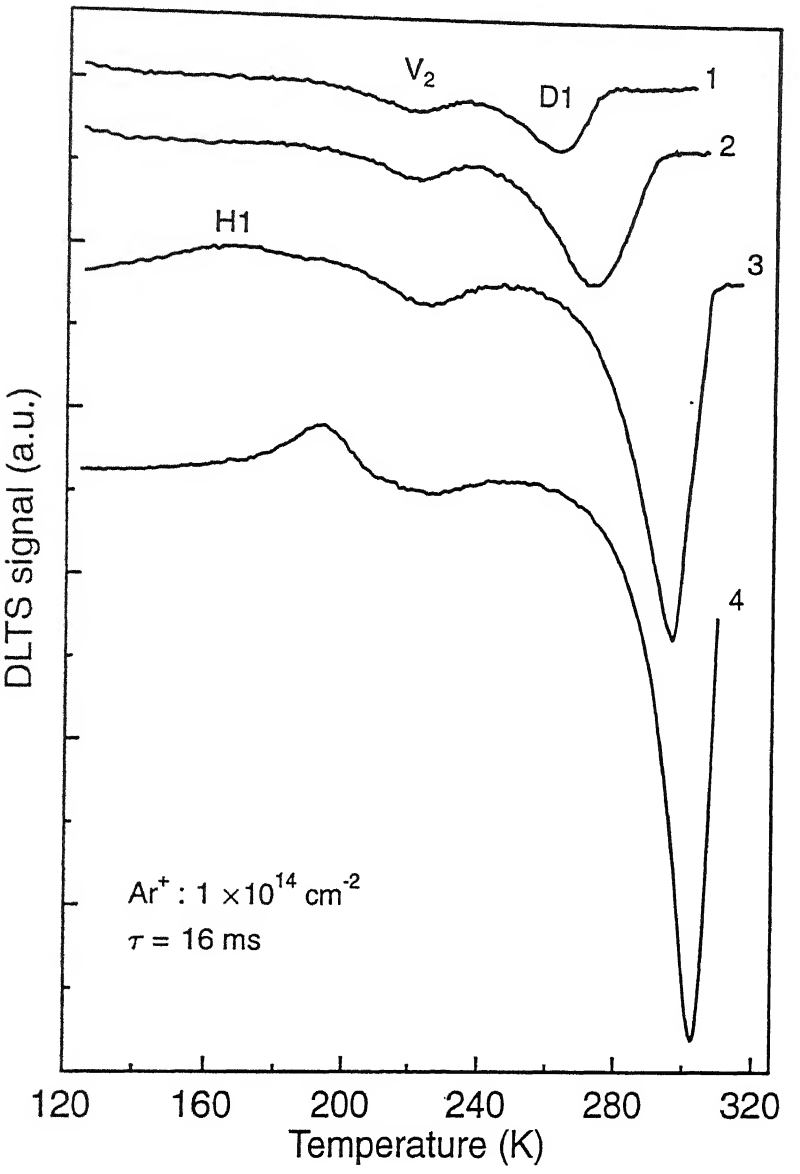

Figure 5.13: A set of DLTS spectra for (1) as-implanted, (2) after room temperature storage and usage of two weeks, (3) 160°C, 30 minutes annealed, and (4) 160°C, 3 hours annealed samples.

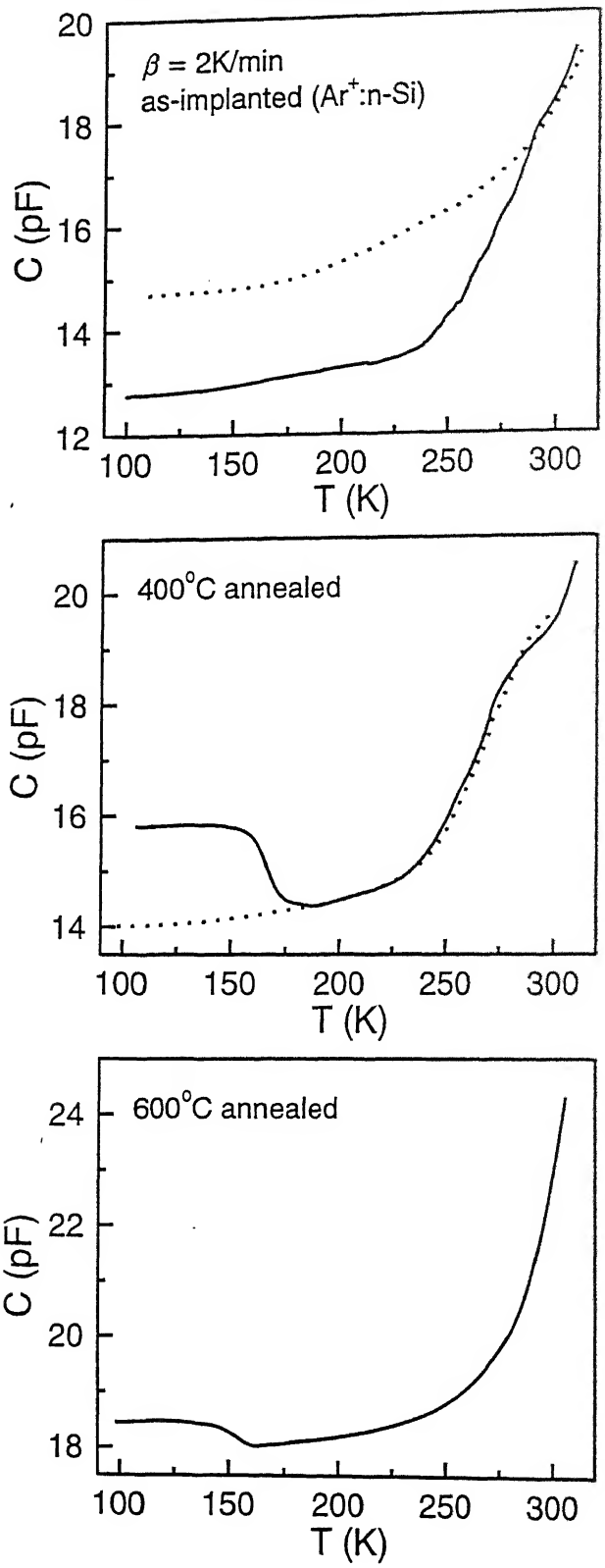

Figure 5.15: Comparison of TSCAP signal from as-implanted, 400°C and 600°C annealed samples taken under similar conditions. The dotted curves refers to signal *without* applying zero bias filling pulse.

for proper estimation of trap activation energy, nevertheless an approximate estimation refers to a midgap trap level. Hence, the major defect created in as-implanted samples are not annealed out by 400°C annealing, rather they form more stable defects complexes upon annealing. By 600°C annealing these defects are almost annealed out as shown in Fig. 5.14. Though the spectra corresponding to as-implanted and 400°C annealed sample showed apparent increase in peak height of the major peak along with growth of a minority carrier related peak (H2), C-V measurements on these samples indicated gradual decrease of defect density with annealing at 400°C and 600°C. With higher temperature annealing, the C-V behaviour approaches to that of unimplanted sample. It can be noted that though DLTS spectra shows negligible majority carrier related peak height in 600°C annealed sample, C-V characteristic showed a substantial difference between unimplanted and 600°C annealed samples. This indicates that all the defects beyond the effective electrical interface are not completely annealed out by 600°C annealing for 30 minutes. It has been reported earlier that damage related defects begin to anneal by about 600°C [149]. Our results are in agreement with this. The presence of positive peaks in DLTS spectra indicates that it may be due to minority carrier related trap levels. Note that the peak (H2) height is quite large in the spectrum. Though the definite origin of these are not clear at this moment, the appearance of minority carrier due to mild inversion in the damaged layer may cause such peak in DLTS spectra.

We have also studied the defect levels present in annealed samples using TSCAP measurements. A comparison of TSCAP signal from as-implanted, 400°C and 600°C annealed samples are shown in Fig. 5.15. The capacitance is monitored as a function of temperature in the heating cycle. The dotted curve corresponds to TSCAP signal without zero bias filling of the trap and the solid line corresponds to signal after zero bias cooling and subsequent heating at reverse bias. In as-implanted sample, difference between dotted curve and solid curve corresponds to trap filling. It is also seen that even

without application of zero bias, traps can be filled by simply lowering temperature due to shift in Fermi level. In 400°C annealed sample, a downward or negative step can be seen after zero bias filling of traps. This is again indicative of presence of minority carrier trap. corresponding to the positive peak in DLTS. The change in capacitance in as-implanted sample is quite large compared to other annealed samples. In 600°C annealed sample, only a smaller negative step is seen without any majority carrier related (positive) step.

5.6 Possible Origin of Defect D1

Though proper identification of a defect is rarely done on the basis of defect activation energy and capture cross-section, an attempt can be made on the basis of significant hints obtained otherwise from this study. Recall that this defect is present in a region much beyond the ion range predicted by TRIM calculation. According to TRIM simulation, the defect profile (mainly vacancies) lies close to the projected ion range. In our case, the ion range was expected to be about 1.23 μm with a range straggling of 0.18 μm. However, we have observed this defect at a depth of $\sim$ 3 μm from C-V studies. This is somewhat surprising that the defect profile can be so different from the TRIM predicted profile. Though very few studies are reported in the literature regarding the defect profile in high dose unannealed ion irradiated Si, preliminary studies by others with low dose MeV ions have indicated that defect profile is broad in the deeper region whereas its concentration is reduced near the surface. In most cases, it has been attributed to vacancy diffusion or field enhanced migration of vacancy type defects from the irradiated zone toward the deeper region [23].

In earlier works of low dose MeV heavy ion implanted Si, this defect is not found [20, 21]. However, in GeV Ar^+ irradiated and annealed Si many defects levels apart from divacancy level are found to be formed [25]. Most of those defects were believed to be formed during post-implantation annealing. As our sample did not undergo any high

temperature post-implantation annealing, the dominant defect level observed by us has a different origin.

The trap energy corresponds to a midgap level with capture cross-section typical of a neutral center. Occurrence of midgap levels has sporadically been noted in the literature in ion irradiated samples without assigning any particular origin [29, 150, 151]. In some cases such defects have been attributed to dislocation related levels in samples annealed after high energy implantation [25]. In some cases it has been referred to as damage related level without any further detailed studies [151]. In low dose implanted n-Si, electrical studies have normally revealed only vacancy-related defects namely oxygen-vacancy, phosphorus-vacancy, divacancy etc. These point defects are well characterized in the literature mainly in the study of electron irradiated silicon. Occurrence of other vacancy complexes are reported by Lee *et al.* through EPR studies [39]. In case of heavy ion implantation, point defect complexes are also likely apart from the above well known defects. Various defect reactions involving vacancies, interstitials and impurities lead eventually to more stable defects. As the vacancy and interstitials can migrate even at room temperature, survival of defect complexes are dependent on various factors. It is also known that many of the thermally stable defects may not be electrically active.

EPR study on ion implanted Si reveals presence of centers related to dangling bond, di-interstitials, planar tetravacancies etc. [34]. Dangling bond centers are believed to be most dominant in high dose implanted amorphous silicon [152, 153, 154]. Note that in our sample one major defect level (D1) is dominating the electrical signature. As we have worked with preamorphized silicon, it is tempting to attribute defect D1 to either dangling bond (D-center) or higher order complexes of intrinsic defects [155]. It has been shown recently that structural relaxation of amorphous silicon (a-Si) produced by MeV ion implantation is controlled primarily by point defect processes [69] and hence it would be interesting to investigate the role of accumulation of D1 defects for higher doses in

creation, relaxation and eventual regrowth of such layers.

More recently it has been shown from molecular dynamic simulations and high resolution electron microscopy observations that accumulation of di interstitial (D-D) pair occurs in heavy ion implanted layers leading to homogeneous amorphization beyond a threshold dose and only a defected material below that dose [55]. Di-interstitials has also been studied by Lee *et el.* [40] and by Tan [56] in ion irradiated Si. Further, Privitera *et al.* [51] have recently demonstrated long range migration of Si self interstitials. More recently, molecular dynamic simulation in conjunction with Monte Carlo simulation for defect process have predicted long range migration of defects and cluster formation even at room temperature [52]. In our case, since Ar^+ damage is a source of self-interstitials [45], the involvement of interstitial complexes such as di-interstitials are strongly indicated. The migration energy of the di-interstitial has been estimated to be 0.6 eV [40], and it is therefore immobile species at room temperature. Recent experimental study on electrical signature of point defect to extended defect evolution upon high dose implantation has indicated also interstitial cluster related defects [19]. Collating all these information together, there is a strong indication that the dominant defect D1 is related to di-interstitial pairs or similar interstitial clusters. Since we observe predominantly point defect signature, the defect responsible is probably a point defect participating in a cluster. Though di-interstitial itself is only observed by EPR in the +ve charge state, it may be driven to modified states, where it can bind electrons due to clustered environment. The fact that it's trapping parameters are sensitive to damage environment in term of dose used and annealing also suggested that it is a deep level whose relaxation state is strongly determined by the state of clustering. The energy level brodening is only moderate showing that it is the long range component of the defect potential that samples only an average disorder in the environment. Also recall that we are observing deep levels in a thin slice of damaged layer at the 'effective electrical interface' in our samples. The

sate of clustering may be fairly homogeneous within this slice, though it may be varying with distance from the damaged layer. The changes with annealing would then be due to ripening of cluster containing point defects.

The more definitive recognition with EPR would be helpful in such heavy dose implanted samples. However, several conditions must be satisfied for this complimentary supports. The damaged layer must be having sufficient number of defects for detection and the clustering should not broaden EPR signal beyond recognition. Electron occupation may have to be induced optically. Transient EPR studies analogous to DLTS would then be most convincing experiments provided one does detect EPR signals.

Photocarrier lifetime measurement in ion-implanted a-Si have shown the presence of midgap states with capture cross-section $\sigma_n \sim 6 \times 10^{-16}$ cm^2 [155] which is similar to the observed values shown in Table 5.1. The significance of defect D1 also lies in the observation that it is sensitive to strain and disorder in the environment. The observed disorder measured by Gaussian broadening parameter shows that we are still in the weak disorder limit.

5.7 Summary and Conclusions

In this chapter, we have studied the defects in the deep buried layers using a variety of junction spectroscopic methods. DLTS and TSCAP has been used as a general purpose survey technique to detect all possible defect levels in the band gap of Si in the temperature range 90K-320K. TATS measurements are made in constant capacitance mode to overcome problems due to high defect density, series resistance and strong temperature dependence of capacitance. Results and conclusions based on these spectroscopic measurements on as-implanted and annealed samples can be summarized as follows :

1. The DLTS spectra of the ion irradiated Schottky diodes with buried layers showed presence of peaks due to oxygen-vacancy (A-center), divacancy ($V_2^{-/0}$) and a damage

related *new* defect (D1) levels.

2. The DLTS and CC-TATS spectra is dominated by presence of D1 defects in very large concentration compared to V_2 related defect. The energy levels of the defect D1 corresponds to a midgap level with capture cross-section typical of a neutral deep level. The energy level position, varied from 0.49 eV to 0.52 eV, is sensitive to the degree of disorder and relaxation of the damaged layer.

3. The dominant defect related transient specially at high temperature shows premature termination of the transient leading to skewed peak shape in DLTS or CC-TATS spectra. The unusual capacitance spike during trap filling in the damaged layer is also associated with such observation.

4. Nonexponentiality of the transient was analyzed using CC-TATS spectra and showed that the measured peak height and time constant both are underestimated in the measured spectra. The process of sudden termination in transient is explained on the basis of quasi-Fermi level movement due to trap occupation change during emission.

5. Spectroscopic lineshape analysis showed energy broadening of about 25 meV for the major peak due to defect D1 for high dose implanted samples. Negligible broadening of lineshape was present for the low dose implanted sample.

6. Low temperature heat treatment of ion damaged sample showed relaxation of the damaged layer causing defect energy to go deeper in the band gap and more defect was accessible to the transient measurements.

7. Relatively higher temperature furnace annealing showed gradual change of the defect configuration indicating formation of more stable configuration of the same defect.

Most of these defects could be annealed out by vacuum annealing at 600°C for 30 minutes.

8. No electrical signature of extended defect formation is seen from annealing studies as doses used were below amorphization threshold and annealing temperatures were low.

9. The possible origin of the major defects (D1) are discussed on the basis of self-interstitial migration and formation of complexes like di-interstitials or their clusters. Possibility of dangling bond related center for this defect is not completely ruled out as specific orientation the defect complexes may give rise to unsaturated dangling bonds.

10. Minority carrier related peak is detected on annealed samples from DLTS and TSCAP studies. Occurrence of such a peak may be due to possible inversion in the damaged region causing minority carrier available for trap filling.

11. The detected majority carrier defects are seen to be present much beyond the predicted damage profile from TRIM calculation.

the Fermi level governs the energies at which formation of D defects occur [157, 158]. Alternative approaches have been to explain these differing energies by defect relaxation mechanism or even simply by occupation statistics of pre-existing distribution. Recently junction capacitance transient measurements or in other words, observations of charge relaxation mechanism have been used to seek the nature of defect relaxation in a-Si. A study of capture of carriers at gap states led Cohen and coworkers [159] to propose a novel hierarchical defect relaxation mechanism in which polarization around negatively charged defect cause relaxation driving its emission energy deeper into the gap. However, an alternate explanation of their transient data was proposed by Farmer and Su [160], who invoked a parallel mechanism of charge redistribution from shallower to deeper levels through multiple trapping at exponentially distributed gap states. In either case comparison with experimental transients required convolution with broad density of states and hence model distinction remain equivocal. The class of mechanisms in which a hierarchical relaxation is invoked can be viewed as serial mechanisms, whereas in contrast parallel mechanisms invoke participation of independent defects coupled through some common constraint. This difference in viewpoint has been central to many controversies in the defect literature, specially in the case of disordered semiconductors and compound semiconductor alloys. Controversies regarding distinction between hierarchical and parallel mechanism is common to many disorder systems and a succinct critique in this regard has been developed by Palmer *et al.* [161].

This brief introduction to the wider debate in disordered systems has been necessary since we present in this chapter unambiguous evidence of occurrence of both parallel and serial mechanisms of charge relaxation in the damaged layers in different regimes of sample conditions. We show that the study of defects in preamorphized silicon provides important conclusions about charge relaxation mechanism in amorphous silicon as these materials can be treated as precursor to the amorphous phase. It is possible to study

a variety of defect related phenomena more conveniently in these controlled disordered materials without having to take recourse to complex deconvolution procedure to compare theoretical predictions with observed experimental features. Apart from this, these studies are, of course, intrinsically important in understanding the nature of disorder in ion implanted material.

6.3 Design and Principle of Experiments

Experimentally our motive behind the measurements that we describe in this chapter was to monitor relative trap occupancies of multiple trap with different filling time duration, in order to investigate the nature of coupling between the trap levels observed in irradiated Si. In conventional cases where more than one deep level is present in the material under study, the occupancies of the deep levels (i.e as monitored by the magnitude of the TATS peak) increase monotonically with filling time and saturate for large filling times indicating its concentration. The sample is taken to zero-bias for a predetermined certain duration ranging from 100 μs to few seconds, and the resulting transient is monitored. One set of measurements constitute use of many different filling times at a fixed temperature. The temperature is chosen such that both peaks (peak V_2 and D1) occur within chosen time scale of measurements. In order to unravel any possible coupling kinetics of capture and to achieve sufficient resolvability, we resort to TATS. The implementation of higher order spectroscopy in transient analysis allows higher resolvability between closely spaced peaks. The choice of order of spectroscopy is guided by the required compromise between resolvability and signal to noise ratio.

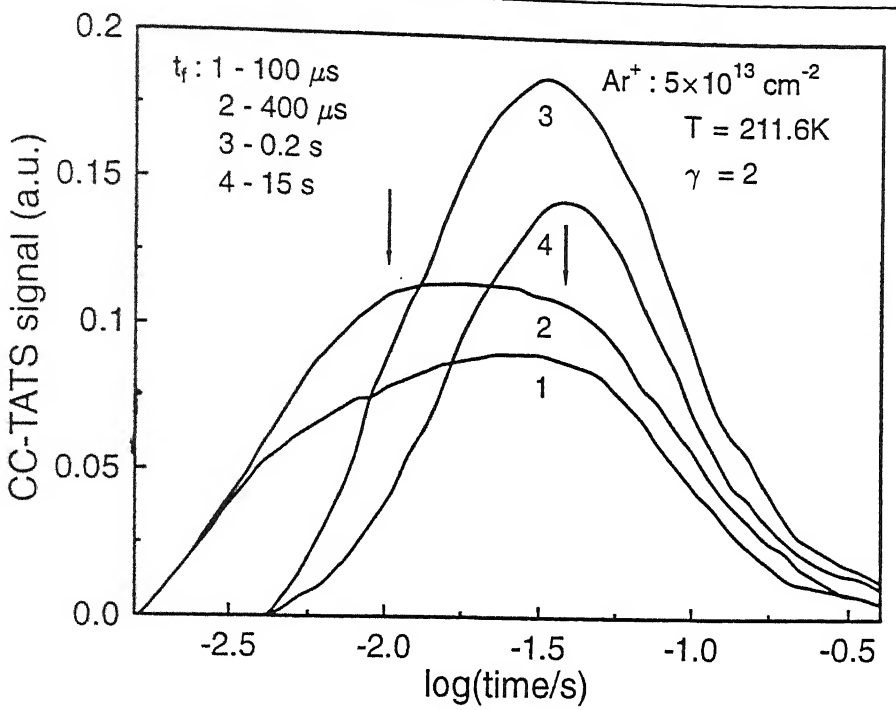

Figure 6.1: Second order TATS spectra of peak P1 for filling times varying from 100 μs to 15 s. Arrows indicate the apparent peak position for two different centers P1A, P1B.

6.4 Trapping Kinetics At Low Temperatures : Evidence For Charge Redistribution

6.4.1 Occupancy change with filling time

Since the divacancy peak ($V_2^{-/0}$) in the literature has been associated with two different defects, we use TATS in order to resolve possible multiplicity in its lineshape. Moreover, for very small filling time and large filling time, we found that the divacancy related peak (V_2) is apparently shifted. To resolve any closely spaced peaks which may cause such phenomena, we perform higher order TATS analysis on the emission transients due to different filling times. Figure 6.1 shows second order CC-TATS spectra of defect corresponding to peak V_2 for several durations of filling time. For convenience of nomenclature, we denote this peak as P1 in this chapter. This clearly shows that the lineshape is consti-

tuted of contributions from two distinct emitting centers for low filling times, and becomes progressively dominated by the slower peak for large filling times. This also shows that changes in occupancy of the constituent peaks with filling time is nonmonotonic. An unambiguous demonstration of the two peak nature of this spectra is clearly central to the understanding of carrier capture kinetics.

To quantitatively evaluate occupancy changes of all the three peaks P1A, P1B and D1, we use first order TATS spectra for filling times varying over five orders in magnitude. A typical set of such spectra is shown in Fig. 6.2 (frames (a) to (e)) for progressively increasing filling times. Note that peak D1 initially increases primarily at the expense of peak P1A and then saturates. The relative concentration of the constituents have been evaluated by fitting contributions from three different defects. The emission time constants of P1B and D1 have been obtained from their respective peak positions in the spectra in the high filling limit. The emission time constant (τ_e) of P1A is then estimated from experimental spectra. All time constants (τ_e) are kept fixed for varying filling times, while the relative concentrations of the peaks are treated as free parameters in the fitting. In the frame e of Fig. 6.2, a fitting to the peak D1 is also shown by dotted line. This required a Gaussian broadening with FWHM (full width at half maximum) of 25 meV in energy. However the amount of broadening needed for the same peak for the lower dose ($5 \times 10^{13}\ cm^{-2}$) sample was 6 meV. Peaks P1A and P1B show similar small broadening in the case of high dose samples. Similar feature of variations in trap occupancies with filling is also shown in Fig. 6.3 for low dose implanted sample. Larger peak heights are observed for this sample.

The relative occupancies obtained from the analysis have been plotted as a function of logarithm of filling time in Fig. 6.4(a) and (b) for samples irradiated with two doses. The occupancies of peak P1A initially increase going through a maximum, significantly enough, at filling times approximately equal to its emission time constant. The increase

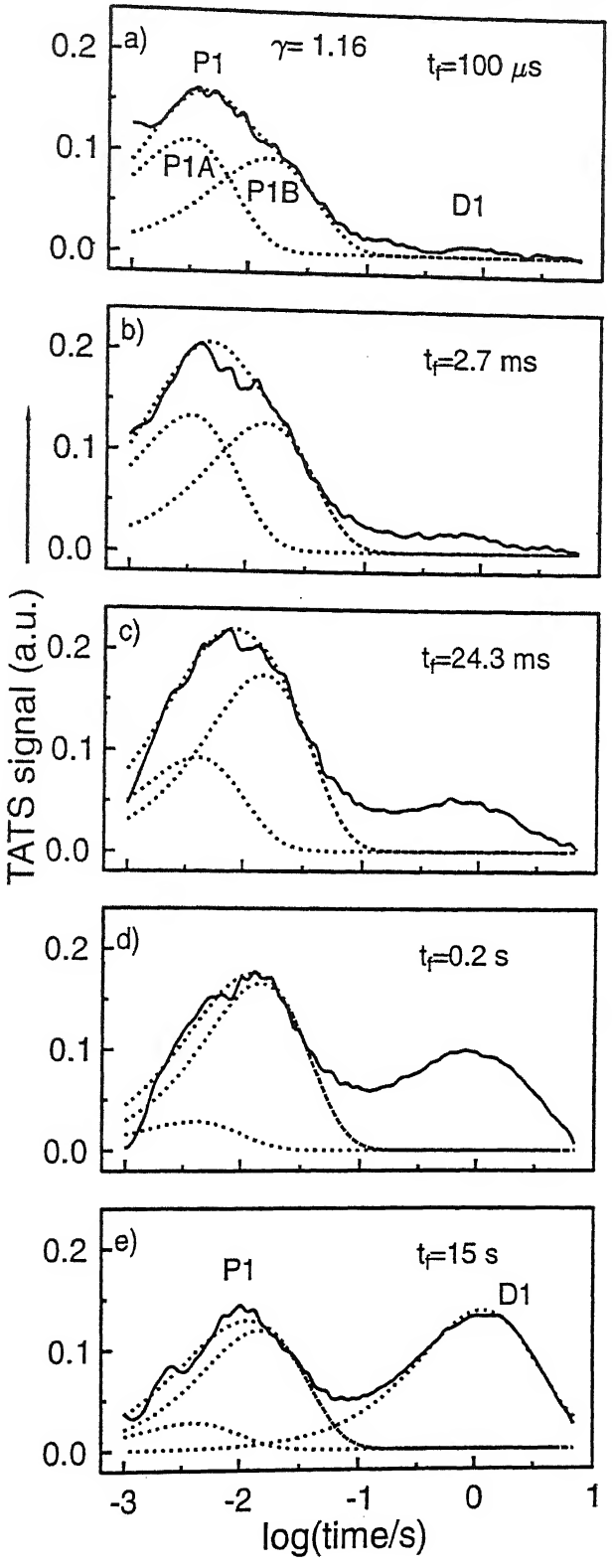

Figure 6.2: First order TATS spectra at 217.6K for different filling times (t_f) showing progressive changes in occupancy for high dose (1×10^{14} cm^{-2}) implanted sample. Peak P1 is fitted (dotted line) to two different centers P1A and P1B, and peak D1 is fitted to a Gaussian broadened peak with a FWHM of 25 meV and the fitting is shown by a separate dotted line in

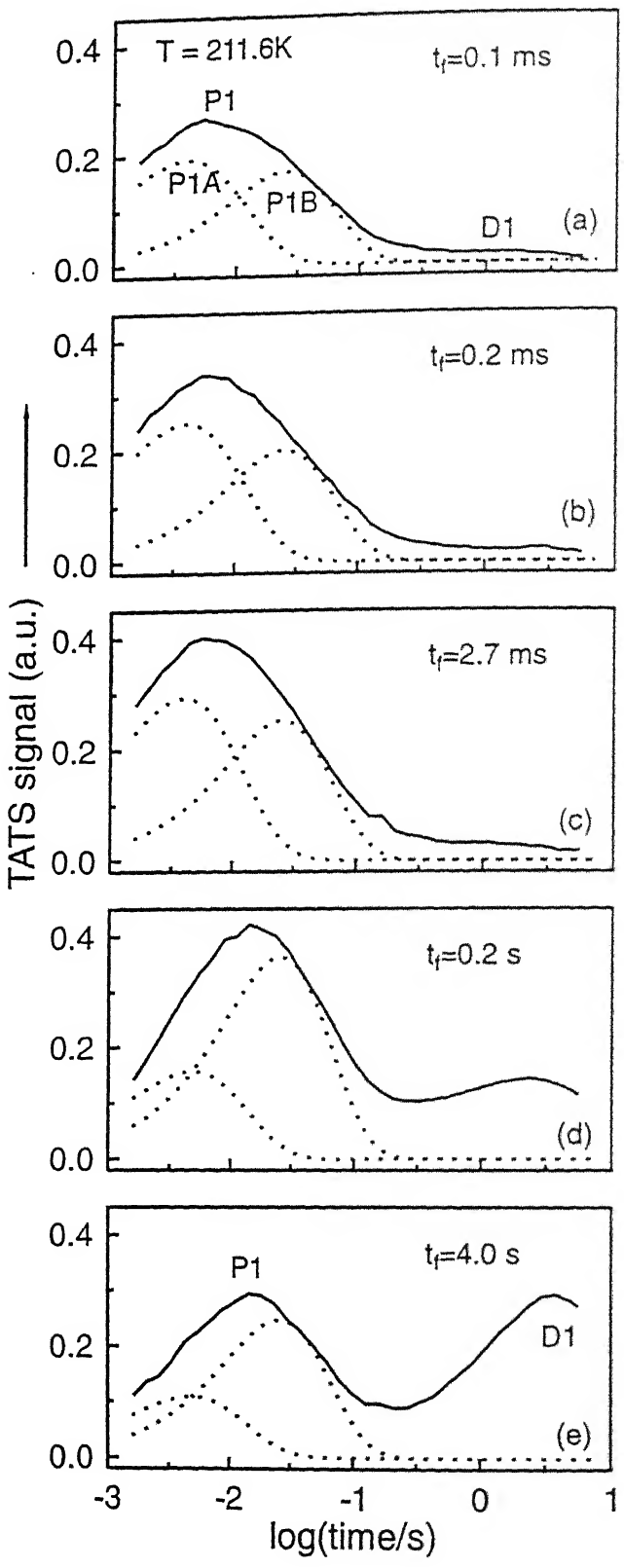

Figure 6.3: First order TATS spectra at 211.6K for different filling times (t_f) showing progressive changes in occupancy for low dose (5×10^{13} cm^{-2}) implanted sample. Peak P1 is fitted (dotted line) to two different centers P1A and P1B. Peak D1 can be fitted to a Gaussian [illegible] peak with a FWHM of 6 meV (not shown).

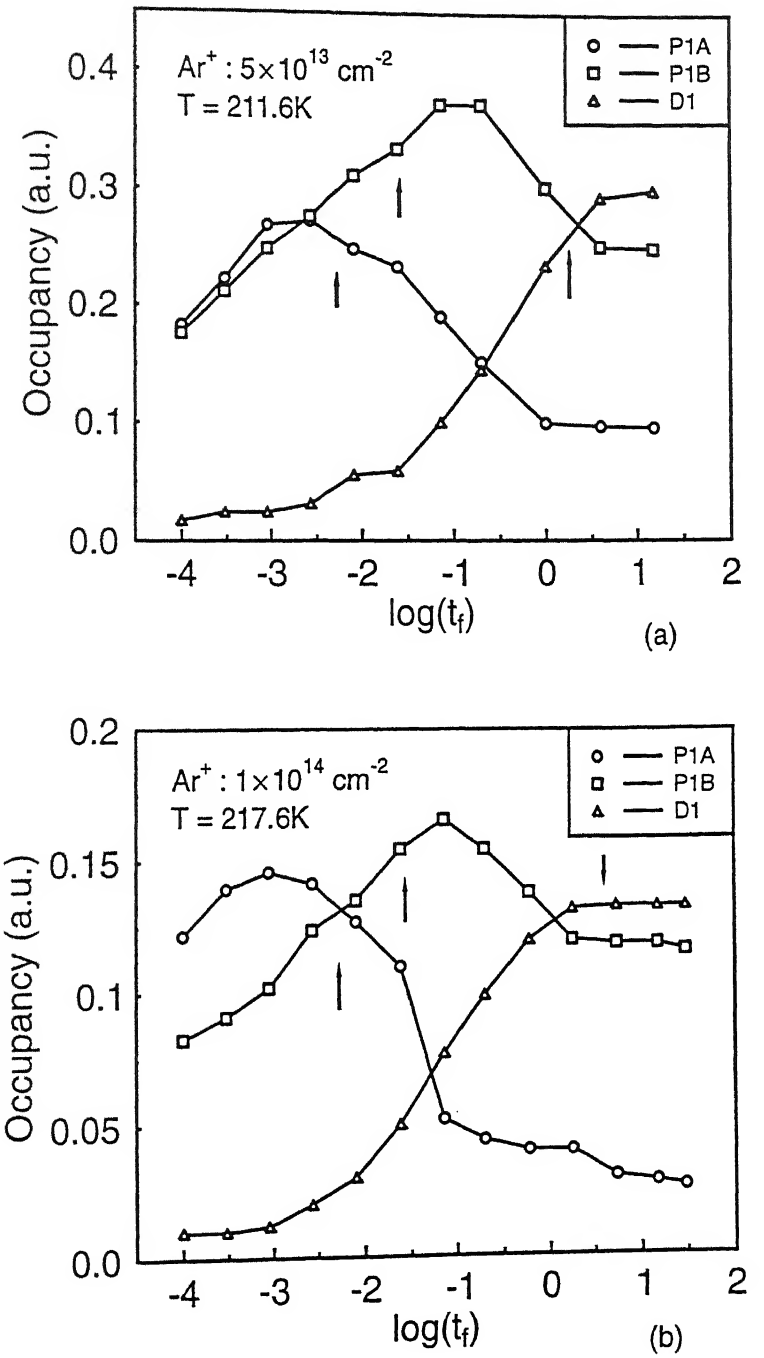

Figure 6.4: Occupancy of individual peak as a function of filling time for samples with two different doses of Ar^+ ions : (a) 5×10^{13} cm^{-2} and (b) 1×10^{14} cm^{-2}. Arrows indicate the measured emission time constants for the corresponding center.

of peak D1 occurs when P1A starts decreasing. Peak P1B also goes through a maximum and its contribution is small to the growth of peak D1. These broad features are common to both the samples irradiated to different doses.

Clearly this is a case of coupled carrier kinetics with multiple traps. There are *a priori* many possible mechanisms which can lead to such a coupling viz. multiple charge states of the same defect, internal conversion from a metastable to stable state or even some more elaborate defect relaxation process. The class of mechanisms in which hierarchical relaxation [161] is invoked can be viewed as serial mechanisms, whereas in contrast parallel mechanisms invoke participation of independent defects coupled through some common constraint. This difference in viewpoint has been central to many controversies in the defect literature, specifically in the case of disordered semiconductors and compound semiconductor alloys [162].

6.4.2 Simulating experimental features

In the present case, the key observation is that the shallower states lose charges to the deeper ones, and that too for filling times larger than their characteristic emission time. This in itself pins down the mechanism to redistribution of charges through multiple trapping. For filling times (t_f) shorter than time constant of emission (τ_e) of a particular level, the occupancy increases in proportion to the product of its capture constant and number density of empty states. For $t_f > \tau_e$, emitted electrons from a shallow trap is recaptured by deeper states with increase in filling time. The situation can be modeled simply by following rate equations for independent traps,

$$\frac{dn_{Ti}}{dt} = -e_i n_{Ti} + c_i n(N_{Ti} - n_{Ti}), \quad i = 1 \ to \ m \tag{6.1}$$

with the crucial constraint on number of electrons is,

$$n = \sum_{i=1}^{m} (N_{Ti} - n_{Ti}), \tag{6.2}$$

defect: for higher filling time D1 dominates. Note that in the experimental data, though the intermediate level P1B participates in the process of charge redistribution, its peak occupancy occurs for filling time larger than its emission time constant. This may be due to field enhancement of emission rate during the transient.

6.4.3 Discussion

The factors that made possible such an unambiguous observation of charge redistribution is worth listing and each of them has an important bearing on both phenomena and design of experiments.

- Firstly, a necessary condition for observation of the parallel mechanism of redistribution of electrons through conduction band is that the number of trapping sites available is much larger than the number of electrons available for capture. This condition is clearly satisfied in our experiment in the region of large damage. We not only have large number of traps, but also the region is converted to highly compensated region. Application of bias across the sample lets us control the number of carriers in the disordered region conveniently by raising or lowering the Fermi level in the crystalline region.

- The study of an embedded disordered region is also significant in another respect. The change in charges in the compensated region reflect in the width of the depletion layer, whose edge lies in the undamaged region. This allows convenient use of standard high frequency capacitance measurements to monitor charge relaxation in the damaged region.

- Also note that the time scale of dynamics varies from milliseconds to several seconds. For divacancy level whose capture cross-section is 3×10^{-15} cm^2, the filling time in normal case with carrier concentration of 1×10^{15} cm^{-3} would be of the order of

few tens of nanoseconds. In the damaged region however, the carrier concentration is down to near-intrinsic levels and hence the dynamics is considerably slowed down enabling clear observation of charge redistribution effect in a convenient time scale.

Charge redistribution among multiple traps have been observed in case of silicon related DX centers in AlGaAs [163, 125]. However, the dynamics is more complicated [125] in that case due to specific model of local alloy disorder, in which the same donor atom relaxes in a variety of local environments with distinct energy levels. In case of hydrogenated a-Si, model distinction was difficult since both the serial model of Cohen *et al.* [159] and the parallel model of Farmer and Su [160], used convolution with a broad density of states. Our results unambiguously confirm that it is not necessary here to invoke hierarchical relaxation to explain progressive deepening of energy levels leading to slowing down of emission transients with filling time. In our study we have been able to simulate conditions of those experiments without going over to the amorphization regime and thus avoiding the complexity of having to deal with any particular distribution of continuum of levels.

Note that the fully developed D1 peak was non-exponential to the extent that its density of states required a Gaussian broadening with FWHM of 25 meV as pointed out in Fig. 6.3e. On the other hand no significant broadening was observed for the same level in the sample irradiated with the lower dose. This broadening therefore provides a measure of inhomogeneities or disorder that the defect samples in its environment. It would require a more detailed study to track this level of broadening along with possible increase in multiplicity of levels to the full amorphization limit. It is important to point out the central role that a careful choice of spectroscopy plays in distinguishing between these two different effects of disorder i.e. increase in multiple levels and degree of energy broadening of these levels. The mean emission energy is the result of high degree of localization in real space provided by the short range part of the defect potential, whereas its broadening

can be viewed as resulting from the long, possibly Coulombic tail of the potential which samples a much larger volume of its environment. The existence of this broadening in our spectra for high dose sample can be considered as a *post facto* confirmation that we are indeed in the high disorder limit.

The defect level corresponding to peak P1B is located at $E_c - 0.42$ eV with capture cross-section of $\sim 3 \times 10^{-15}$ cm^2 as obtained by CC-TATS analysis at different temperatures. It is commonly attributed to divacancy V_2 (-/0). The peaks P1B is due to the divacancy related level. It is interesting to note that effects such as motional averaging of two configurations and sensitivity to damaged related strain have been invoked to explain DLTS lineshapes of V_2 (-/0) related peak [20]. The broadening of the individual peaks TATS spectra can be attributed to lattice strain in the damaged layer. Indeed it was found from DLTS study of heavy ion irradiated n-Si that the divacancy related defects with energy E_c-0.42 eV was formed in a region of lattice accommodating more strain.

The origin of the D1 defect is discussed in the previous chapter. It is confirmed from this study that these are responsible for carrier compensation in the damaged layer and less number of free carrier makes the carrier dynamics considerably slow to monitor such phenomena.

In summary, we have studied charge relaxation in severely damaged regions in silicon by embedding them in the depletion layer of otherwise crystalline material. Multiple trap levels, which have moderate broadening of energy for heavy damage, have been resolved. We have provided unambiguous transient based spectroscopic evidence of the occurrence of charge redistribution among multiple levels in the compensated regions.

6.5 Trapping Kinetics In Relaxed Materials : Evidence For Novel Defect Relaxation

During the course of filling time experiments, a novel phenomena was consistently observed in samples with either low dose implantation or those partially relaxed after annealing. It was most strikingly observed in (i) low dose Au^+ (5×10^9 cm^{-2}) implanted n-Si and (ii) Ar^+ implanted samples in which partial relaxation was induced by annealing at 400°C for 30 minutes. The presence of a preamorphized region with comparatively lesser degree of disorder is common to these set of samples.

Figure 6.6 shows CC-TATS spectra at room temperature for a series of filling times (t_f) varying from 20 ms to 1 minute. The feature of decreasing signal at the lowest emission of times (ms range) is due to the falling portion of the peak corresponding to the major trap studied in the previous chapter. Apart from that, the well formed peak shown in the figure is due to a new distinct peak whose time constant is strongly dependent on the filling time, becoming slower for longer duration of filling pulses. Note that the time constant of emission changes 4-5 orders of magnitude as does the filling time. Also note that the height of the new peak is approximately similar for all different filling times showing that the corresponding defect is located in the same region of peak and has nearly the same degree of occupancy irrespective of duration of pulse. Though the figure shows only a selection of curves, the time constant was observed to be continuously changing even when monitoring with small changes in filling time. In other words, the emission time constant of carriers from the defect progressively increased with filling time and hence this is not a case of a defect relaxing through discrete states in energy. At the same time, the lineshape analysis shows that the peaks are approximately exponential for lower filling times becoming slightly broad for largest filling time. This shows that for any particular filling time, we are observing emission from a discrete defect level. Had it one been from

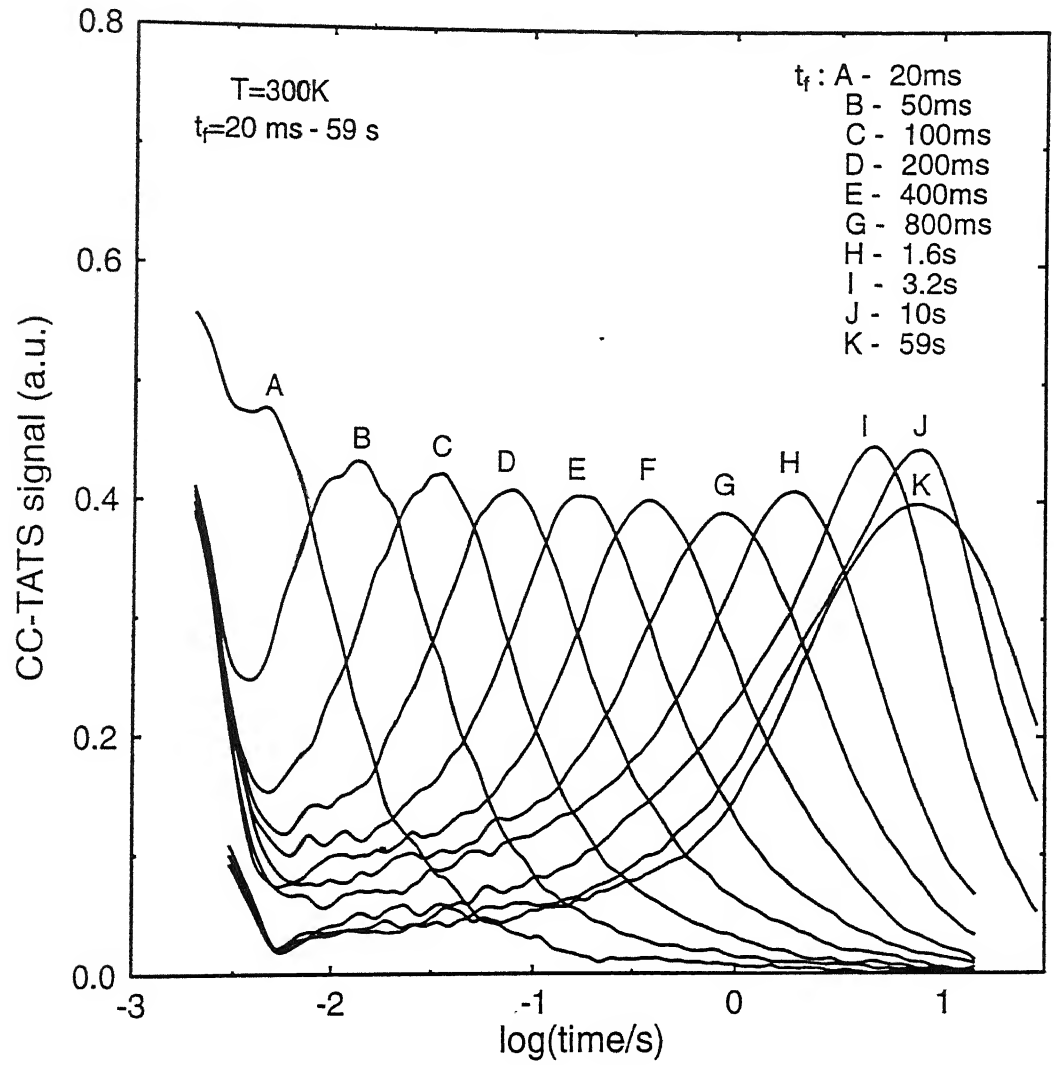

Figure 6.6: CC-TATS spectra for different filling time (t_f) at a fixed temperature showing evolution of a new peak whose time constant increases with increasing filling times.

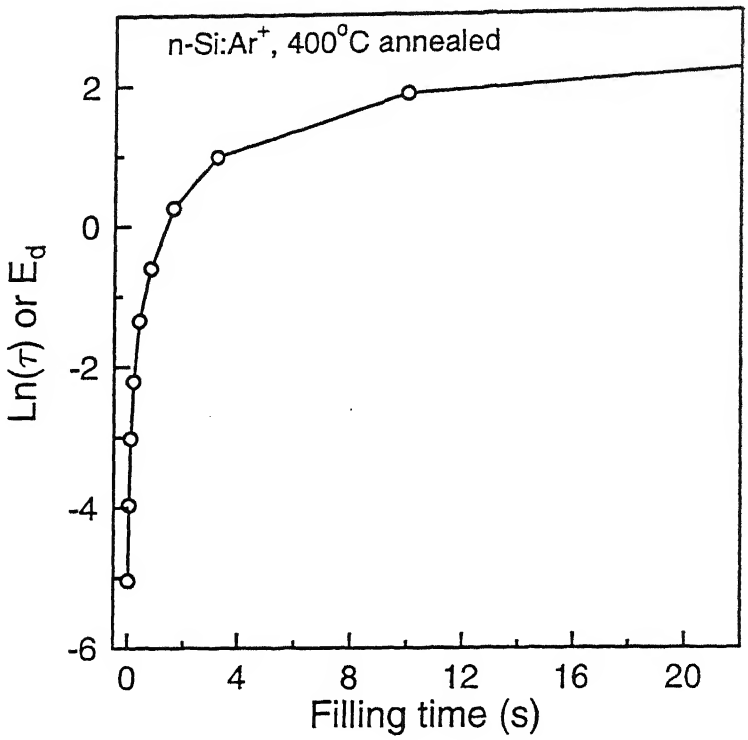

Figure 6.7: Change of emission time constant (τ) with filling time (t_f) for the evolved peak of Fig. 6.6. This shows stabilization of the relaxed state energy ($E_d \propto \ln(\tau)$) for longer filling times.

a part of broad density of states in energy, we would still have observed broadening for all the peaks. The peak evolves from a time constant of 6.5ms to 14s for filling times in the range 20ms to 59s at a particular temperature. This three orders of change in time constant would translate to about 180 meV change in terms of activation energy. Figure 6.7 shows log of time constant as a function of filling time. This is indicative of occurrence of hierarchical relaxation through continuous metastable states, stabilizing in a state with the longest time constant. This gradual slowing down (with τ and t_f obeying a power law) of emission or deepening of energy is typical of hierarchically constrained dynamics [161]. The emission time constant is dependent on resident time of electron in the defect site. This dependence on history and power law dependence are signature of *non-Markovian* process possessing a memory of the duration the electron spends at the

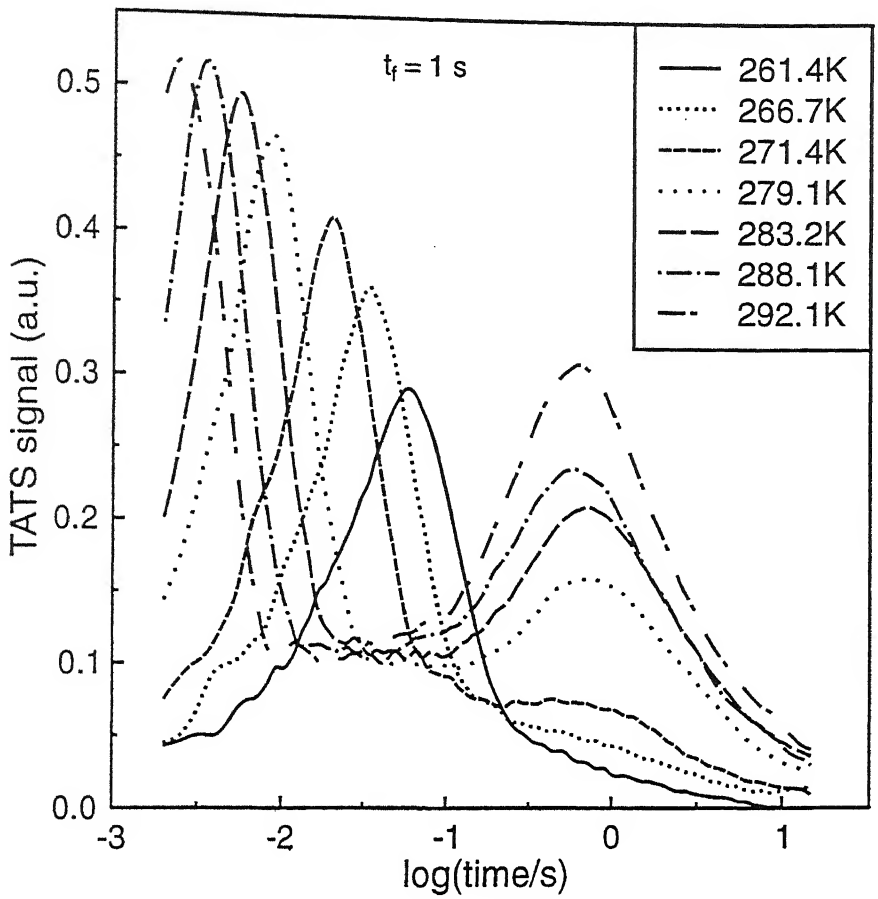

Figure 6.8: CC-TATS spectra at different temperature for a fixed filling time (t_f=1s) showing temperature independence of the evolved peak.

occupied defect [159].

Another intriguing feature of this phenomena is that the time constant is nearly temperature independent for any particular filling time, t_f. This is illustrated in Fig 6.8 where TATS spectra for a filling time of 1s are shown for different temperatures varying over 30K. The time constant of major peak on the left of the figure does indeed change as would be expected of a normal thermally activated process. However, the peaks that evolves with t_f, does not show shift in time constant with temperature. This shows that the process associated with the relaxation is nearly athermal. From the athermal nature,

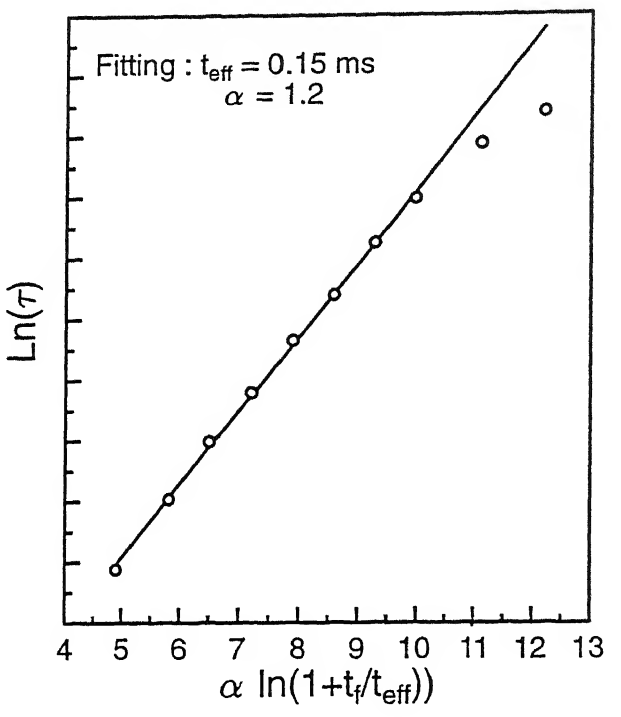

Figure 6.9: Power law dependence of τ and t_f for spectra shown in Fig. 6.6. Solid line refers to a best fit to relation : $\tau \sim (1+t_f/t_{eff})^{\alpha}$.

we conclude that the part of the free energy changing with defect relaxation can be considered to be proportional to temperature T. Incorporating the power law dependence of filling time (t_f) and emission time constant (τ), the effective energy associated with the relaxation can be written as

$$U_{eff} \sim K_b T ln[(1 + t_f/t_{eff})^{\alpha}] \tag{6.7}$$

where it is characterized by an effective time constant of relaxation t_{eff} and exponent α. In Fig. 6.9, we show such a dependence of τ and t_f where the linear portion of the plot can be fitted with t_{eff}=0.15 ms and α=1.2. The nature of this energy term also suggests that it can be viewed as an entropic term contribution to the measured enthalpy [146, 164]. Physically it would mean that traps undergoing relaxation during electron occupation, have a distinct entropy most probably owing to changes in degeneracy factor.

be dependent on the nature of damage which may allow multiple final configurations for

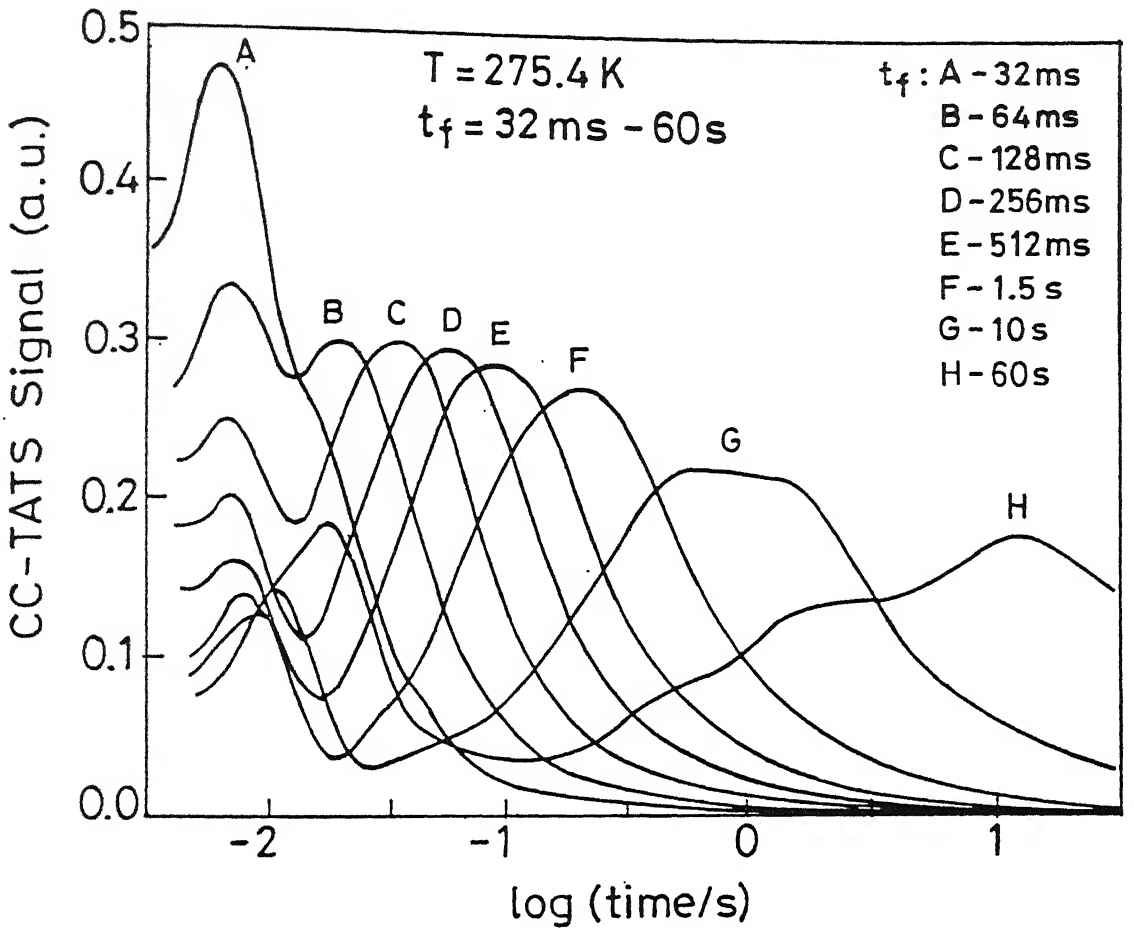

Figure 6.10: CC-TATS spectra with varying filling time at a fixed temperature for Au^+ irradiated (5×10^9 cm^{-2}) n-Si. Multiple peak structure in evolved peak for longer filling times can be noted.

long term filling of trap.

In summary, in ion damaged deep buried layers evidence for charge redistribution among multiple traps have been shown to occur through trapping kinetics studies over 5-6 orders of magnitude in time. At relatively higher temperature, for partially relaxed samples, a novel defect relaxation process is observed where defect energy progressively

deepens with trap filling time and this process is nearly athermal. It is important to reiterate here that isothermal spectroscopy such as CC-TATS is absolutely essential in study of phenomena such as described in this chapter. In a temperature scanning spectroscopy, such as DLTS, sensitivity to filling time and its temperature dependence on one hand, and possible occurrence of athermal process on the other can completely distort manifestation of such phenomena beyond recognition.

Chapter 7

Defects In Ion Irradiated p-Si

The previous three Chapters were devoted exclusively to n-type silicon. This chapter, in a nutshell, is devoted to similar studies on p-type silicon. The scope is limited to explore major differences and similarities with n-type case hoping to identify commonality of origin of traps and related phenomena. As pointed out in Chapter 1, a perusal of literature shows that irradiation induced defects has been studied to a lesser extent in p-type Si, in general. It is specially true for MeV heavy ions, where most of the studies have concentrated on evolution of defects observable by cross-sectional TEM with annealing. We focus on electrical characterization using C-V and deep level spectroscopies in samples irradiated with MeV Ar^+ and Au^+ ions. During the course of this work we have used both epitaxial and CZ p-type wafers.

We will keep this chapter brief by avoiding repetitions of explanations of similar effects already discussed in n-type case, and by focusing only on features specific to p-type samples.

7.1 C-V Characteristics

A number of Schottky diodes were made on unimplanted and implanted wafers. The control diodes (made on unimplanted wafer) are tested by C-V measurements at various temperatures. The plot of $1/C^2$ vs. V was seen to be linear indicating uniformity of shallow doping (boron) with concentration $1.5 \times 10^{15}\ cm^{-3}$ in the high voltage region. Figure 7.1 shows $1/C^2$ vs. V plots for Ar^+ ion irradiated p-Si at several temperatures

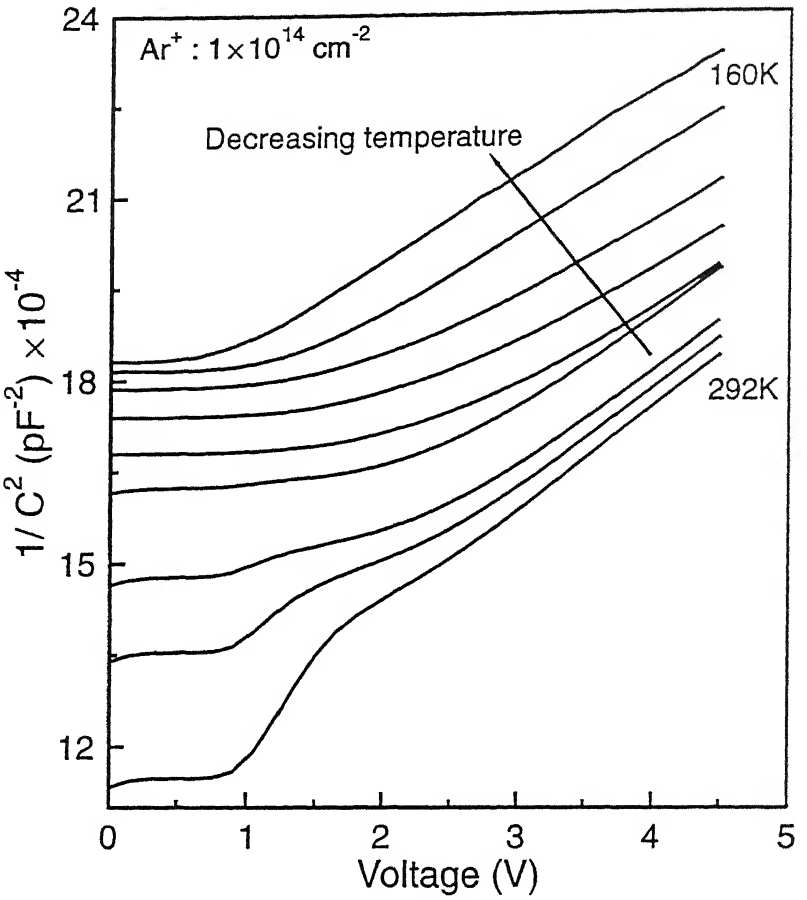

Figure 7.1: Temperature dependence of C-V characteristics of Ar^+ irradiated p-Si Schottky diode.

showing qualitatively similar features as in n-type case. Notable features that are common to in $1/C^2$ vs. V plots are :

- occurrence of flat region indicating large trap concentration at the crossing point between Fermi level and dominant trap level,
- transition to linear region at higher bias showing carrier concentration at the edge of the depletion layer.
- increase in depletion width with lowering temperature due to increased trap filling,
- increase in depletion width for higher doses

- occurrence of depletion layer edge much beyond the range of the ions and hence the damage location.

All these features indicate, as explained for n-type analysis, the occurrence of defect migration and clustering. The differences are only quantitative in nature. These are listed below on the basis of studies on several batches of samples :

- zero bias depletion widths are about 60% of that of n-type case though the doping concentration are similar.

- the transition from flat to linear region in $1/C^2$-V curve is consistently less sharp than n-type case or with non-linearity extending over larger bias range.

Figure 7.2 shows phenomena of hysteresis in C-V in close parallel to n-type case. This again indicates involvement of a dominant trap whose occupancy mainly controls C-V. The combinations of temperature and sweep rate needed to observe hysteresis are distinctly different from n-type case.

7.2 Deep Level Spectroscopies of Defects

7.2.1 Thermally Stimulated Capacitance (TSCAP) Measurements

As described in Chapter 2, TSCAP is an useful spectroscopic technique for detection of deep trap with high concentration. To find dominant traps in ion damaged buried layers in p-Si, we measured the capacitance as a function of increasing temperature after the traps are filled with zero bias pulse at low temperature. Figure 7.3 shows a differentiated TSCAP signal for Ar^+ ion implanted p-Si. Corresponding to the steps in capacitance values, two major peaks are detected in the temperature range 120K-230K. Though the detection sensitivity of TSCAP method is not so high as other transient spectroscopic

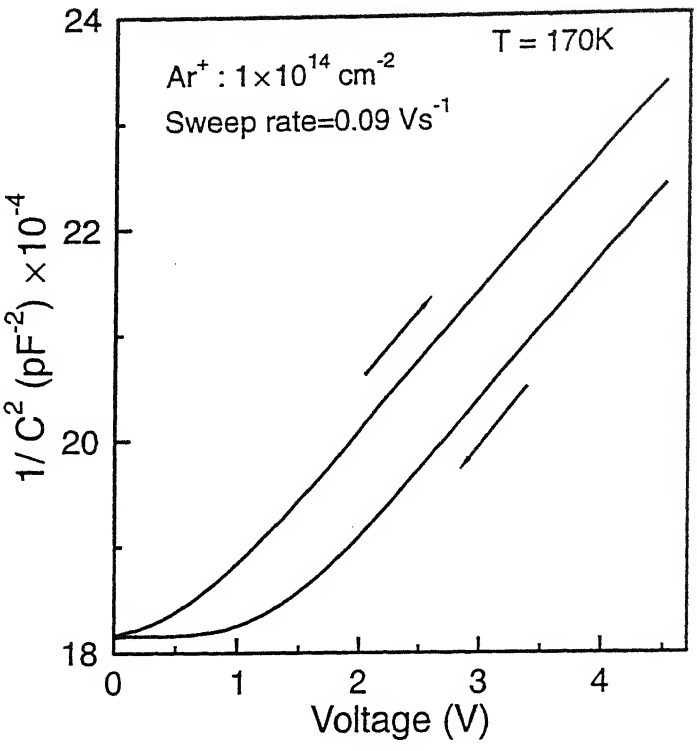

Figure 7.2: Hysteresis in C-V characteristics for decreasing and increasing reverse bias. Arrow indicates direction of voltage sweep.

methods such as DLTS, it was used as a survey technique to find the dominant traps. The trap parameter estimation was done from the DLTS and TATS methods. These parameters were used to simulate TSCAP in close agreement with experimental spectra using Eqn. 2.9 of Chapter 2.

7.2.2 Deep Level Transient Spectroscopy (DLTS) Studies

No traps could be detected using DLTS in control samples upto detection limit of 10^{-3} of background doping. This ensures that any traps detected in irradiated sample would be irradiation induced. The irradiated samples used for this study was irradiated prior to Schottky diode preparation i.e. irradiation was performed on bare silicon wafer pieces

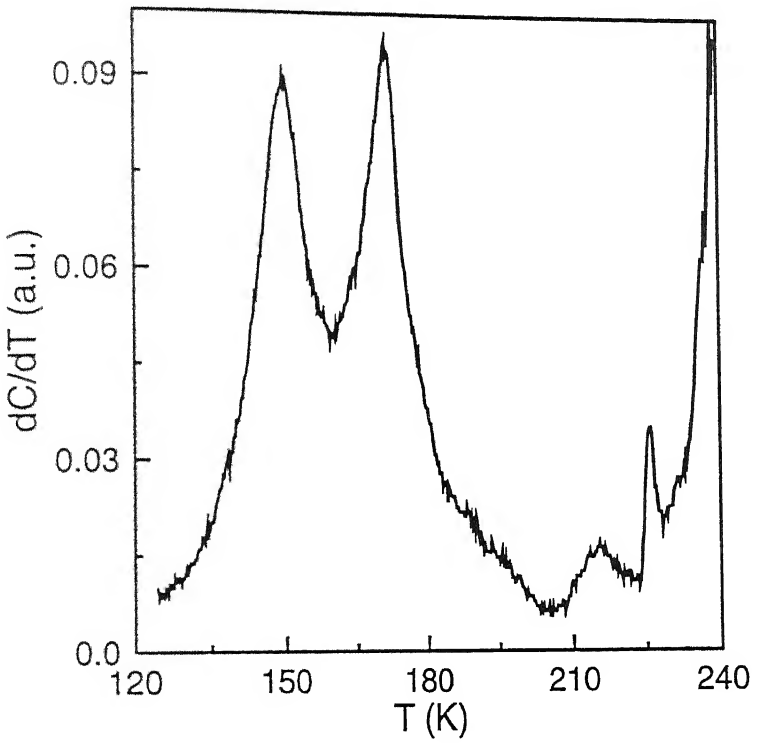

Figure 7.3: Differentiated TSCAP signal after zero bias filling of traps in Ar^+ ion irradiated p-Si. Heating rate was 2.0K/min.

with back ohmic contact made by thick aluminum deposition. Devices were made on these wafers after proper etching/cleaning of surface oxide or any other contaminants. A typical DLTS spectrum for sample irradiated with 1×10^{14} Ar^+ ions/cm^2 is shown in Fig. 7.4. For the chosen rate window ((2 ms)$^{-1}$), three majority carrier related peaks (P1, P2, P3) and one minority carrier related peak (P4) are observed in the temperature range 120K-310K. The small peak P1 has an activation energy of 0.37 eV and a capture cross-section of 4×10^{-15} cm^2 as estimated from the Arrhenius plot shown in Fig. 7.5. This peak corresponds to a hole trap commonly attributed to C_iO_i complex [171] in CZ substrates. We found this level in MeV Au^+ implanted p-Si as well. This trap is observed in small concentration in epitaxial layers since oxygen content in these layers are small.

The line shape of the DLTS peaks are fitted with peaks due to three exponential tran-

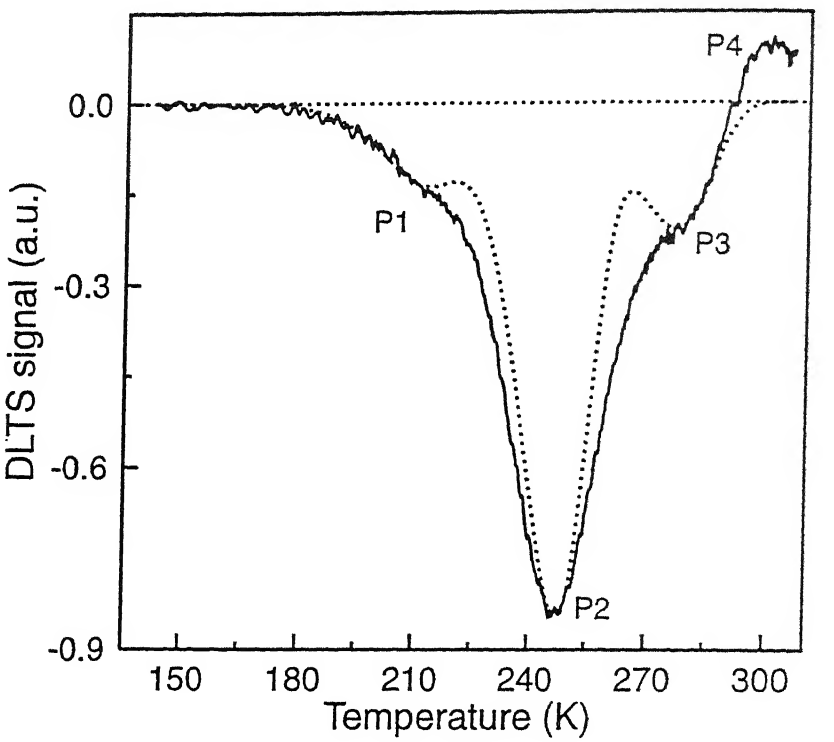

Figure 7.4: Typical DLTS spectrum of Ar^+ ion irradiated p-Si. Dotted line is a theoretical fit with three exponential transients corresponding to the three peaks P1, P2 and P3. Time constant corresponding to the chosen rate window is 2 ms.

sients as shown with the dotted line in Fig. 7.4. The trap parameters were chosen from Arrhenius plot obtained for each peak on the basis of DLTS results. Due to inherent nonexponentiality, Arrhenius plot may not yield accurate estimation of trap activation energies (E_T) and capture cross-sections (σ_p) and therefore, σ_p value was adjusted so as to get the peak position at the same temperature as seen in the experimental spectra. It is clear that major peak (P2) line shape is broader than the standard line shape expected from exponential transients. Such broadened line shape would correspond to a Gaussian broadened activation energy for the corresponding trap level. The line shape distortion may be due to several reasons. Since the concentration of traps is expected to be high

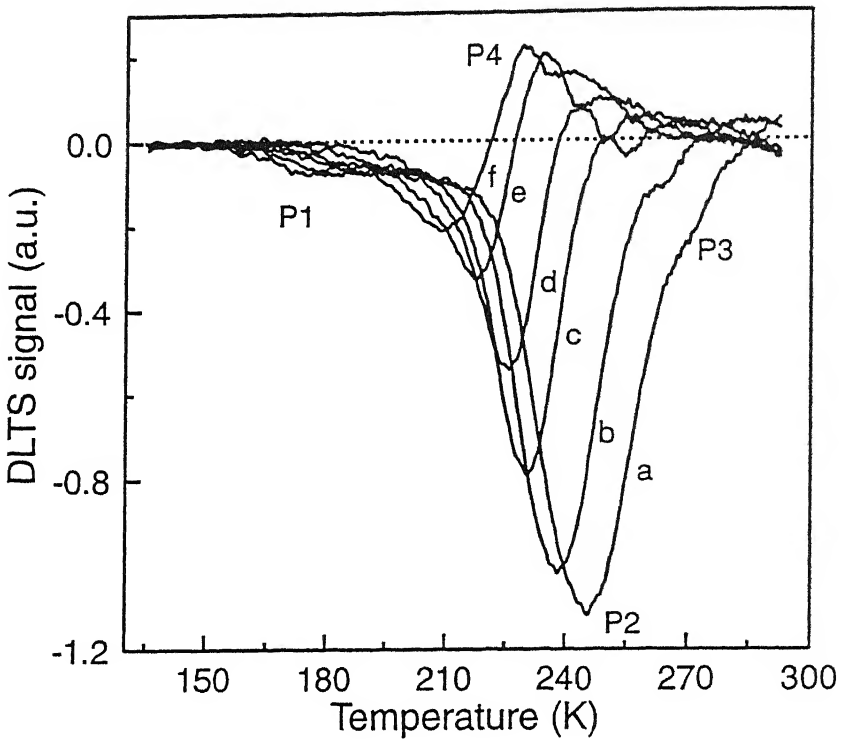

Figure 7.6: DLTS spectra of Ar^+ ion irradiated p-Si plotted for different rate windows (e_n): (a) $(2.2ms)^{-1}$, (b) $(5.1ms)^{-1}$, (c) $(15.2ms)^{-1}$, (d) $(30.1ms)^{-1}$, (e) $(75.0ms)^{-1}$ and (f) $(200.0ms)^{-1}$

corresponding to peak P3 are not possible since the peak is not so well resolved.

Figure 7.6 shows a set of DLTS spectra for different rate windows. The reduction in peak height for slower rate windows for the major peak (P2) is substantial and presence of feature P4 distorts the peak P2. It is known that a strong temperature dependence in capture rate and series resistance [101], can lead to such features in DLTS spectra. In our case strong temperature dependence of capacitance is primarily responsible for peak height reduction as well as nonexponentiality in DLTS peaks. Due to the above reasons DLTS results have not been used for trap parameters estimation, rather they have been used as a survey technique for detection of different traps. Proper evaluation of the trap parameters have been made using time analyzed transient spectroscopy which is presented

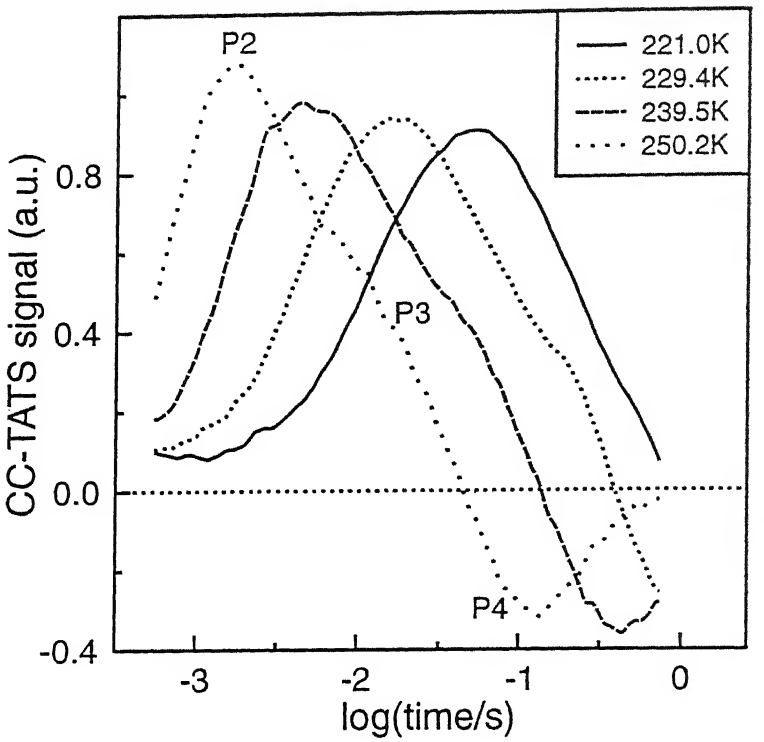

Figure 7.7: CC-TATS spectra at various temperatures showing three peaks (P2, P3 and P4) for Ar^+ ion irradiated p-Si in a convenient range of time scale.

as the problems due to high trap density and series resistance are sources of distortion in conventional TATS spectra, such conclusions may be in error. By using the technique in constant capacitance mode, it is possible to avoid the expected nonexponentialities due to large defect density in constant capacitance voltage spectroscopies [174]. Moreover, constant capacitance transients are not distorted due to any *dc* resistance present in the device.

Figure 7.7 shows a set of CC-TATS spectra at several temperatures for Ar^+ implanted p-Si. In the range of time scale shown in the figure, we see two majority carrier peaks (P2, P3) and the minority carrier related peak P4.[1] The minority carrier peak appears as a

[1]Note that a majority carrier peak in DLTS appears as a negative peak in conventional spectra whereas it appears as positive in CC-TATS spectra.

fully developed feature in contrast to DLTS spectra. The peak corresponding to peak P1 in DLTS spectra is too fast to appear for these temperatures. The lineshape analysis of the major peak (P2) in CC-TATS spectra for low temperature transients show that the peak is broader than corresponding exponential transient. Thus lineshape broadening is indeed due to inhomogeneous environment. However, CC-TATS peaks for higher temperature transients are seen to be narrower due to premature termination of transient as it was in the case of n-Si. But, parameter extraction at this temperature through fitting is not possible due to presence of another close peak slower in time constant. The reason for premature termination is same as was discussed in case of n-type Si.

Figure 7.8 shows Arrhenius plot for the major peak whose emission rates have been obtained from CC-TATS spectra using low temperature transients. For comparison, time constants obtained from conventional DLTS spectra which results in non-linear Arrhenius behaviour, is also plotted in the same figure. Data from CC-TATS is most reliable and gives an activation energy of E_v+0.52 eV with an unusually high capture cross-section of 9.9×10^{-14} cm^2. In Au^+ implanted p-Si, we also observe the same damage related trap. Good match in Arrhenius plot for this major trap (P2) in Ar^+ and Au^+ implanted p-Si has been obtained and shown in Fig. 7.9. For Au^+ implanted sample, activation energy and capture cross-section was found to be E_v+0.52 eV and 7.9×10^{-14} cm^2, respectively. A defect having similar parameters have been observed in heavy ion damaged Si and has been attributed to damage [21, 25]. However, such a level is not detected in damage created with light ions. Such high value of capture cross-section for this defect may be due to coulomb assisted trapping at the defect site. Similar high values of capture cross-section have been reported for grain boundary defects in Si [175].

As in the case of n-type Si, it is not possible to obtain the concentration profile of this defect since trap information is obtained only at the location of $E_T - E_F$ crossing. However, it is quite clear that the defect concentration is as high as in the case of n-type

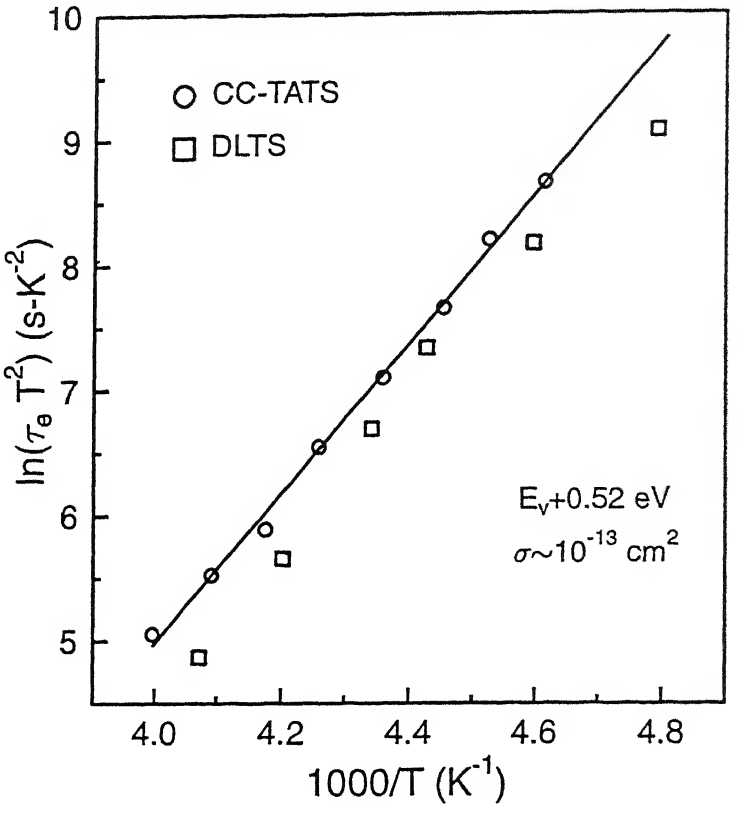

Figure 7.8: Arrhenius plot for the major peak (P2) obtained from CC-TATS and DLTS measurements. Solid line is a least square fit to the data from CC-TATS measurements.

at the effective electrical interface and a conservative estimate[2] would put it as 3×10^{15} cm^{-3}.

7.3 Capture Kinetics Of The Major Trap

7.3.1 DLTS and TATS of capture transient

The capacitance transients during capture are observed to be surprising slow. Capture transients are recorded at various temperatures and analysis shows that they are exponential in nature. As suggested by Ghosh *et al.* [176], for a straightforward measurement

[2]For estimation of trap concentration, total amount of defect charge corresponding to amplitude of transient is calculated and then divided by the approximate volume of the buried layer estimated from Gaussian damage profile.

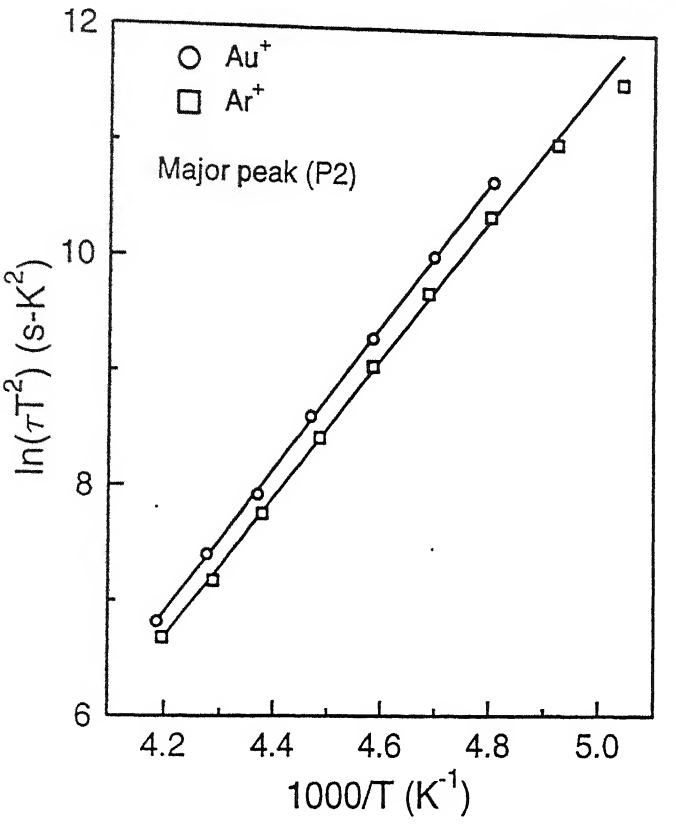

Figure 7.9: Arrhenius plot for major peak (P2) in Au^+ and Ar^+ implanted p-Si employing CC-TATS measurements.

of capture barrier, DLTS scans using capture transients were taken in the temperature interval of 175-300K. Typical capture DLTS peaks for different rate windows are shown in Fig. 7.10(a). Capture time constants have been obtained by both DLTS and TATS processing of capture transients and have been plotted in an Arrhenius plot in Fig. 7.10(b) yielding an activation energy of the 0.66 eV. Note that this is an unusually high activation energy for capture processes and this value is larger than the barrier for emission. Therefore, this barrier cannot be associated with the capture cross-section of the defect alone.

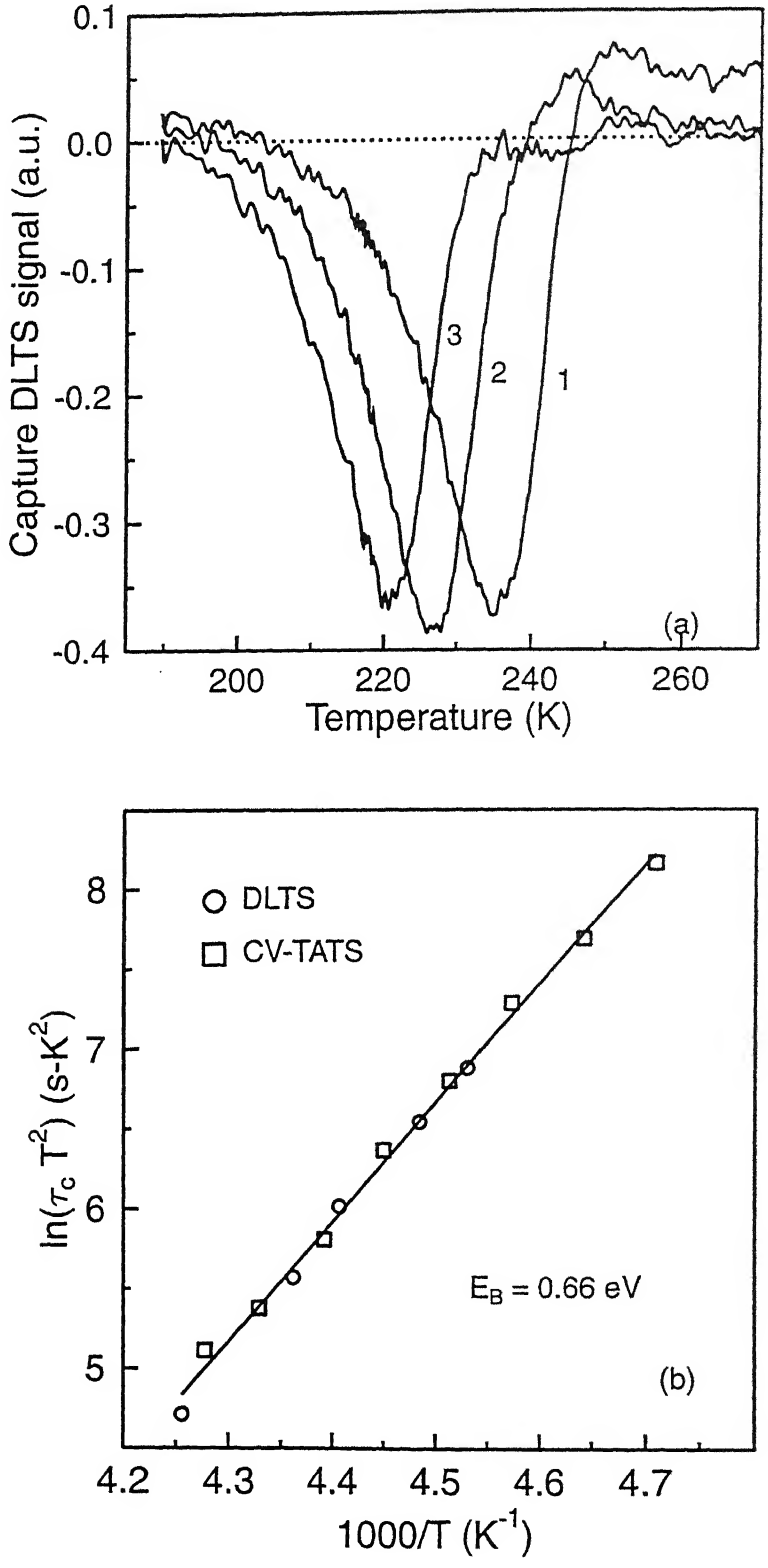

Figure 7.10: (a) DLTS spectra for *capture* transients with rate windows : (1) 500 s^{-1}, (2) 125 s^{-1} and (3) 50 s^{-1}. (b) Arrhenius plot obtained by DLTS and TATS analysis of capture

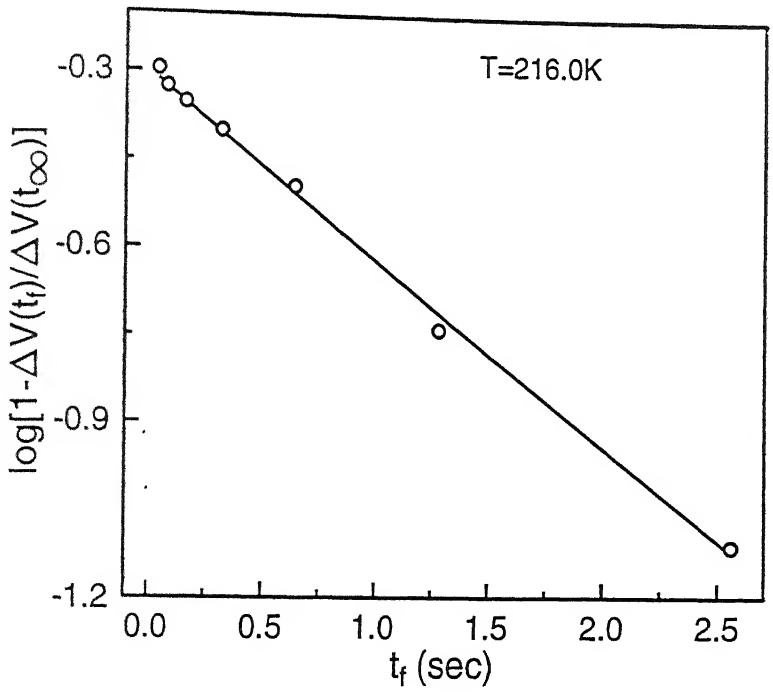

Figure 7.11: Filling time dependence of the occupancy of the major trap in Ar^+ implanted p-Si using varying pulse width technique in conjunction with CC-TATS

7.3.2 Variable filling pulse-width technique

For a more accurate measurement of the capture barrier, we performed the transient (capacitance/voltage) measurement using variable filling pulse width technique [177]. Figure 7.11 shows the filling time dependence of occupation of the major trap (peak P2) at 216K determined using constant capacitance varying pulse width technique. Capture is seen to be exponential from the point defect nature of the traps. However, for the same sample using constant voltage transients, trap filling during capture is observed to be slow and approximately logarithmic in time. Hence, we conclude that such slow filling is an artefact of nonexponentiality due to large trap concentration. Similar logarithmic time dependence of capture has been reported from conventional DLTS measurements

for plastically deformed silicon with dislocations [173]. Therefore, a conventional DLTS study can mislead one to conclude that defects are extended defects with time dependent capture barrier. A time dependent capture barrier will give rise to logarithmic filling time dependence as is the case for extended defects. In a recent study, Benton *et al.* [19] have reported in p-type ion irradiated sample a level at E_v+0.48 eV using conventional DLTS. They identify it to be due to extended defects {311} principally on the basis of logarithmic filling time dependence of occupancy. However, a more careful study of this level is required to resolve whether this is an extended or point defect.

In our samples annealed at 600°C, the major trap was found to have an activation energy of E_v+0.51 eV with capture cross-section of $\sim 10^{-12}$ cm^2. The peak related to this level in DLTS was found to occur at a lower temperature than the above level (for the same rate window) reported by Benton *et al.*.

Constant capacitance transient measurements using the variable filling pulse width technique at different temperatures reveal strong temperature dependence of capture kinetics of the major trap. Figure 7.12 shows an Arrhenius plot of capture time constant yielding an activation energy of 0.66 eV, which is unusually high. Note that this value is identical to that found from direct measurement of the capture DLTS/TATS. Since the activation energy for the emission is smaller than the observed barrier for capture, it cannot be associated with the capture cross section of the defect. It must be partially due to a macroscopic barrier for the carrier to be captured. In fact, since the buried layer always remains within the depletion layer, part of the observed barrier may be due to temperature dependence of limited supply of holes at the buried layer during filling pulse. In addition, this trap most probably has considerable lattice relaxation associated with it. Separating out the contribution to activation energy from lattice relaxation and macroscopic barriers is not simple in the present configuration of the samples.

Under such circumstances, defects in p-type Si seemed to have stabilized quicker than in n-type Si.

Figure 7.13 shows a set of TSCAP spectra for as-implanted and annealed samples. In each case, the dotted line curve is obtained for TSCAP spectra without zero bias filling of the traps and solid lines are after trap filling with zero bias. In both the cases, capacitance is recorded only during the heating cycle with controlled heating rate. For as-implanted and 400°C annealed samples, presence of multiples steps in TSCAP signal indicates the presence of several discrete traps. However, for 600°C annealed sample, only one large step is present indicating presence of one type of defect with large concentration. This study shows that in p-type Si, all the defects are not annealed out at 600°C in contrast to n-type Si where most of the damage related defects are annealed out

DLTS measurements are also done on these samples to survey residual/secondary defects after annealing. Figure 7.14 shows DLTS spectra for as-implanted, and for samples annealed at different temperatures (160°, 400°, and 600°C, 30 minutes). Clearly, all the spectra are different from each other for same rate window. This indicates formation of new defects/complexes even for low temperature annealing. The defect present after 600°C annealing occurs in very large concentration and thus causes large step in TSCAP spectra.

In this annealed sample, the major trap was found to have an activation energy of E_v+0.51 eV with capture cross-section of $\sim 10^{-12}$ cm^2. The peak related to this level in DLTS was found to occur at a lower temperature than a similar level reported by Benton *et al.* who studied defect evolution from point defect to extended defect with high dose implantation and subsequent annealing [19]. It is worth mentioning that in the report of Benton *et al.* for high dose implanted annealed sample DLTS peak occurring at lower temperature is not analyzed though it was distinctly clear. We believe that these defects are of same origin i.e. interstitial clusters.

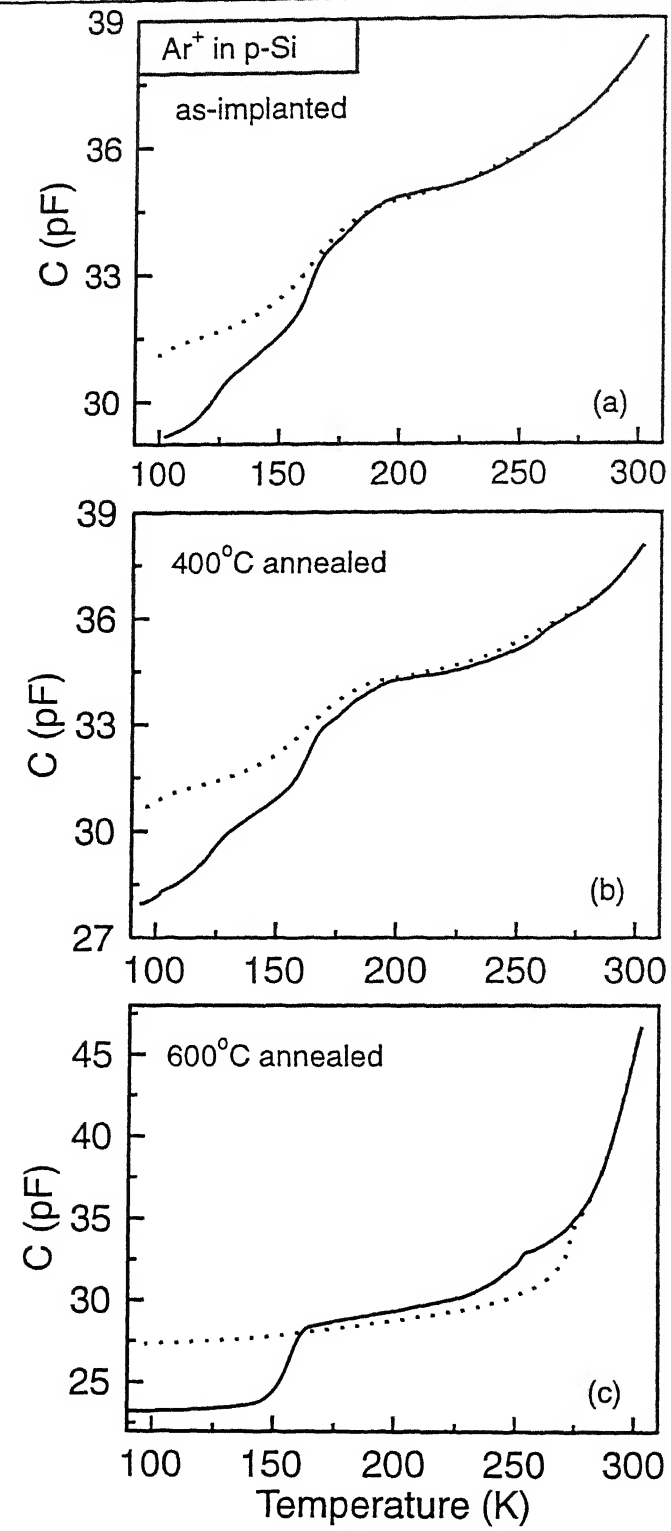

Figure 7.13: TSCAP spectra for (a) as-implanted, (b) 400°C annealed and (c) 600°C annealed samples with zero bias filling of traps (solid line). Dotted line represents spectra without zero bias filling.

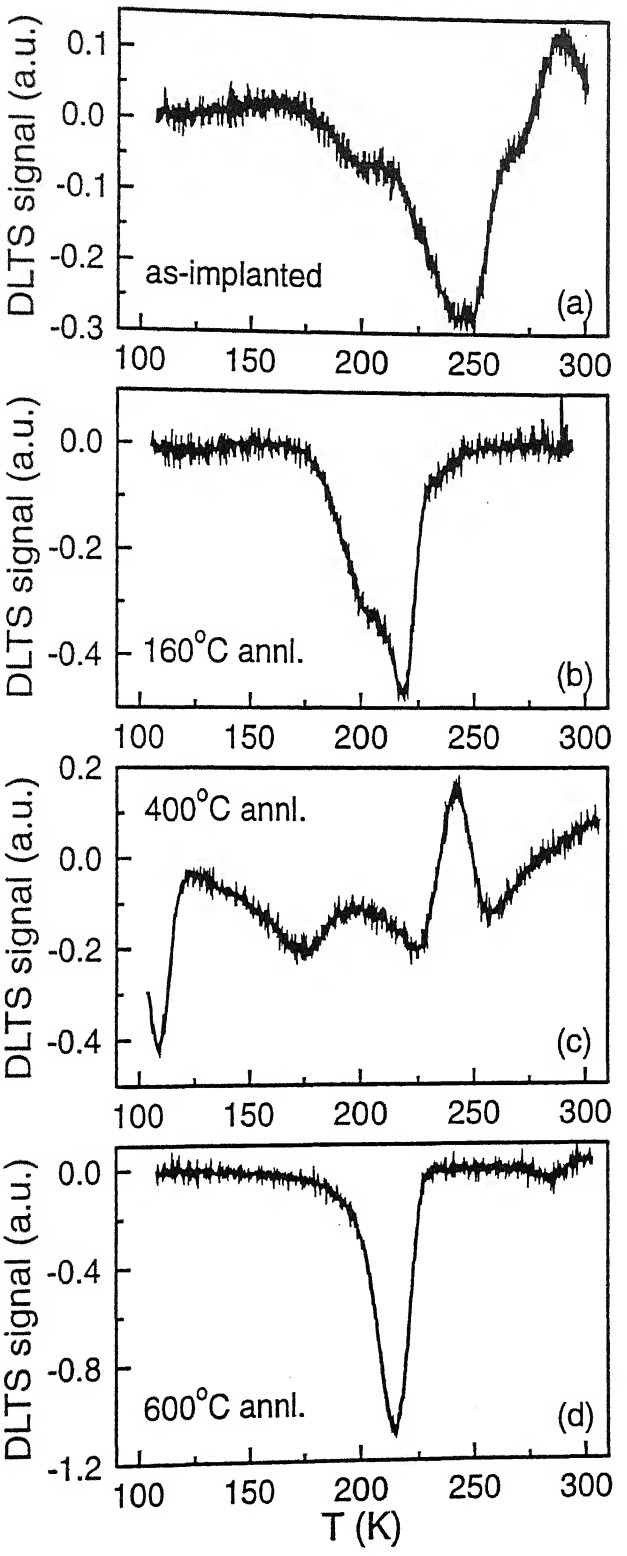

Figure 7.14: Comparison of DLTS spectra for (a) as-implanted, (b) 160°C annealed (c) 400°C annealed and (d) 600°C annealed Ar^+ irradiated p-Si. The annealing time is 30 minutes in each case.

In the literature, formation of secondary defects upon annealing has been reported [179] for implanted p-Si. Such continuous change in DLTS spectra for different annealed samples is indicative of formation of defect clusters of varying size. The evolution of point defect cluster is only beginning to be studied at present and Benton *et al.* [19] term it as the study of "missing links" between intrinsic point defects and extended defects that they finally give rise to on annealing. In a study of low temperature annealing of defects in electron irradiated p-Si, formation of vacancy-oxygen complexes was reported. We have not seen any divacancy related level in our heavy ion irradiated p-Si. Moreover, temporal changes in DLTS spectra with minority carrier injection related effects has also been reported [180]. We have not observed any such effect.

7.6 Discussion

The electrical defect signatures described in preceding sections are different from those point defects normally associated with complexes of vacancies and interstitials with impurities observed for low dose ion or electron irradiation. The difference could be ascribed to possible agglomeration of defects leading to distinct electrical signatures in case of high fluence irradiation. There have been extensive TEM studies in the fluence regime ¿10^{12} cm^{-2} of ion irradiation in Si after high temperature annealing [56, 58]. These studies reveal formation of interstitial chains and related extended defects commonly referred to as {311} defects. At very high doses, the formation of amorphous region and the kinetics of amorphous/crystalline interface has been explained on the basis of accumulation of di-interstitial pairs [55]. Though the involvement of interstitial agglomeration has been beyond doubt from these studies, the electrical signatures of defects arising from such clustering have not been studied except for a recent report by Benton *et. al.* [19]. In our case, the fact that these defects are detected much beyond the ion range is in itself a strong indication that interstitial clusters are responsible for the observed defect spectra.

Studies on cluster formation using molecular dynamics predict formation of clusters of varied sizes which in principle should reflect in broadening of electrical activation energies. Our results show that most spectra is dominated by point-defect-like trap signatures with relatively small amount of broadening in energy, which could be either due to narrow distribution of stable cluster sizes or inhomogeneous environment in the vicinity of the defect. The defect spectra goes through complex changes with annealing, and finally yielding a stable defect with large concentration after 600°C annealing as described in the previous section. The process of agglomeration seems to be more complicated in this case. In contrast, for the n-type case the major defect only displayed progressive deepening of activation energy with annealing. We do not observe signatures of extended defects either in terms of broad structures in the defect spectra or logarithmic filling of occupancy. The annealing temperature of 600°C may not be sufficient for the formation of extended defects.

The major defect is found to be responsible for compensation in the damaged region. Origin of the minority carrier trap peak can be explained on the basis of mild inversion occurring within depletion region. From analysis of minority carrier trap related peak, it was found that the time constant of emission of this peak and of the major trap in n-type are identical at same temperature. Thus it can be concluded that the dominant majority carrier trap in ion damaged n-Si and the minority carrier trap in as-implanted p-Si are of common origin and it acts as an efficient recombination center. The dominant majority carrier trap in p-type Si is in all likelyhood related to di-interstitial or higher order interstitial clusters.

7.7 Summary and Conclusions

In this chapter, we have studied defects in high dose ion implanted p-type Si using a variety of steady state and transient spectroscopic techniques. As compared to n-type Si

case, the ion induced defects in p-type Si manifest slightly different features in spite of many commonalities. Results and conclusions based on C-V, DLTS, TSCAP, CC-TATS measurements on as-implanted and annealed samples can be summarized as follows :

- C-V studies show presence of damage induced defects at a depth larger than that predicted by TRIM calculations. However, this depth is not as large as in n-type case. Migration and subsequent formation of defect cluster at a larger depth can explain such observation.

- The DLTS spectra of as-implanted sample shows three distinct majority carrier trap related peaks and one minority carrier trap related peak. Well known C_iO_i center occurs in small concentration. The new major damage related trap has small energy broadening which has been ascribed to narrow distribution of stable cluster sizes or inhomogeneous environment in the vicinity of the defect. Minority carrier related trap peak is explained on the basis of availability of electrons in the depletion layer due to inversion or near intrinsic character of damaged layer.

- By using CC-TATS, the activation energy of the dominant trap has been found to be E_v+0.52 eV with a large capture cross-section ($\sigma \sim 10^{-13}$ cm^2).

- Capture transient was found to be extremely slow and thermally activated. Using both capture DLTS and varying filling-pulse-width techniques a macroscopic capture barrier of 0.66 eV was found. This is partly due to large lattice relaxation associated with the state and partly due to macroscopic barrier limiting hole supply.

- The defects in p-Si are less stable thermally. They form new secondary complexes upon annealing. No signature of extended defect formation is observed upon annealing upto 600°C.

- Estimation of time constant for the negative peak in CC-TATS spectra reveals that this peak is same as found in n-type Si. Thus the damage related major defect is an efficient recombination center.

Chapter 8

Summary and Conclusions

8.1 Summary and Conclusions

Traditionally electrically active defects induced by irradiation in semiconductors have been studied for light particles and, to a lesser extent, for ions with (i) energies in the keV range, (ii) low dose, or (iii) after removal of damage through annealing. However, there has been a recent thrust, motivated by technological applications, in studies of defects due to *high dose* irradiations of MeV *heavy ions*. This thesis deals with several aspects of electrically active defects in deep buried layers in Si produced by MeV heavy ions using mainly capacitance based techniques. The work has involved critical evaluation of existing spectroscopic techniques and their suitable extension needed for studying heavy ion damaged semiconductors. These studies reveal several significant aspects concerning defect migration and clustering, electrical identification, effect of degree of disorder, and defect relaxation mechanisms.

In order to separate out effects due to heavy ion damage alone from electrical activity of implanted species, we have used noble gas Ar^+ ions, with energies around 1.45 MeV and doses 10^{13}-10^{14} cm^{-2} to produce buried layers in both n and p-type epitaxial silicon. Samples implanted with heavier Au^+ ions at 4.5 MeV and dose 5×10^9 cm^{-2}, but not annealed to avoid electrical activation, have also been studied for comparison. Irradiation doses are chosen to be below amorphization threshold but comparatively higher than used by most other workers. Conventional Schottky barrier diodes are fabricated for characterization using capacitance based techniques. Both as-implanted and low temperature

carriers, large magnitude emission transient and its premature termination. These features are shown to be consequences of trap filling giving rise to large negative charge density within the depletion layer and are discussed in the light of crossing between quasi-Fermi level and the major trap controlling these phenomena. DLTS, in spite of its inadequacy in this situation to provide reliable defect parameters through standard analysis, has been useful as a survey technique, and does provide helpful guide to further experimentation. In case of n-Si, both DLTS and thermally stimulated capacitance (TSCAP) spectra in the range 90K-320K reveal occurrence of mainly two discrete trap levels of which one is the well known divacancy center ($V_2^{-/0}$, E_c-0.42 eV) and the other is a newly found midgap trap. This new trap level is the dominant trap occurring in very large concentrations in all our MeV irradiated samples and is responsible for controlling hysteresis in C-V and space charge limited conduction in forward I-V characteristics.

(ii) Nonexponentiality : Isothermal Spectroscopic Study

Transient measurements for time domain analysis (as in TATS) performed in constant capacitance mode were found to be most useful since they overcome known sources of nonexponentiality due to large trap concentration and series resistance. TATS lineshape corresponding to the major trap is seen to be broad for low temperatures and, narrow and skewed at high temperatures. The peak shape narrowness is linked to occurrence of premature termination of transients which in turn is explained on the basis of time evolution of quasi-Fermi level and its crossing with the trap level within the depletion layer. It is possible to estimate the true time constant and peak height associated with these skewed peaks from a careful fitting of the useful part of the lineshape. The signature of the dominant trap is obtained from such analysis for various samples. The emission energy of the dominant trap is observed to vary from E_c-0.49 eV to E_c-0.56 eV depending on processing conditions such as low temperature oven annealing and irradiation dose. This sensitivity

of the defect parameters seem to be characteristic of preamorphized regions and is due to varying degree of relaxation of disorder in its environment. At low temperatures, in the absence of skewness in lineshape due to premature termination, the damage related peak for high dose samples shows a Gaussian broadening in energy with FWHM of 25 meV. This broadening is disorder induced since it is observed to be only 6 meV for low dose samples. The capture cross-section values are typical of neutral trapping center. The possible origin of this defect has been discussed, most likely candidates being dangling bonds, higher order vacancy complexes or interstitial clusters. However, consistent with our observation of involvement of migrating species and in accordance with mounting evidence from recent studies on involvement of interstitials, di-interstitials or their clusters seem to be responsible for the dominant damage related trap. High temperature furnace annealing studies show near complete removal of the dominant trap on heat treatment at 600°C for 30 minutes. In annealed samples minority carrier related traps could also be observed possibly due to mild inversion in the damaged layer.

D. Charge Redistribution

Trapping kinetics of multiple traps has been studied by monitoring relative occupancies of multiple traps after allowing filling of traps for different duration over 5-6 orders of magnitude in time. Surprisingly we observe two distinct mechanisms which could be isolated at different temperature regimes in different group of samples. At lower temperatures, filling time dependence of TATS peaks corresponding to multiple traps show nonmonotonic change in trap occupancy. With filling time evolution, it was possible to recognize that the peak attributed to divacancy alone, in reality, constitutes contributions from two distinct emitting centers. The resolution of peak structure has been clearly demonstrated using higher order implementations of TATS. The progressive evolution of occupancies over many orders of magnitude in time reveals coupling in capture kinetics.

We show that this coupled kinetics is due to *charge redistribution* among multiple traps, in which deeper states gain at the cost of shallower states with time. Broad experimental features in occupancy as a function of filling time could be reproduced by solving coupled rate equations for three independent traps with charge redistribution constraint. However, closer match with experiment is obtained when in addition a configurational interdependence of two traps is assumed. The mechanism of charge redistribution had been invoked earlier to explain charge relaxation in amorphous silicon, though it was considered controversial in that context due to lack of unambiguous experimental proof. This mechanism is expected to be operative whenever number of trapping sites are larger than availability of carriers for capture.

E. Novel Defect Relaxation

Evidence of a novel defect relaxation mechanism was found by studying filling time dependence of occupancies for low dose implanted samples (Au^+ at dose 5×10^9 cm^{-2}) and for partially relaxed (400°C annealed) Ar^+ irradiated samples - presence of a preamorphized region with comparatively lesser degree of disorder being common to these set of samples. The observed phenomenon could most conveniently be studied for temperatures above 270K. When filling time is increased at a particular temperature, TATS emission spectra shows a distinct new peak whose time constant is strongly dependent on the duration of filling. The time constant of emission shows a power law dependence on filling time. This dependence of emission characteristics on history, in terms of waiting time, is a strong indicator of a non-Markovian process of relaxation occurring during capture. The height of the new evolving peak remains almost constant for all filling times. Further, changes in ionization energy seem to involve an entropy-like term since the emission time constant is nearly temperature independent for a particular filling time. All these features suggest that the relaxation mechanism follows a hierarchically constrained dynamics sim-

ilar to those proposed for glassy systems. A closely similar defect relaxation mechanism has been invoked to explain capacitance transient data in hydrogenated amorphous silicon though it is more involved in that case due to presence of broad density of states.

F. Comparison With p-type Silicon

Studies on p-type Si with high dose irradiation showed qualitatively similar features as that of n-type Si. From spectroscopic analysis, in addition to well known traps a new major trap and a minority carrier related trap were found. Major peak in this case is due to damage related trap and the DLTS lineshape is broader than peak expected from exponential transients due the strain in lattice. Proper evaluation of trap emission time constants, capture cross-section, trap concentration and spectroscopic lineshape were carried out using constant capacitance TATS analysis. The major trap is found to be located at E_v+0.52 eV having a large capture cross-section of $\sim 10^{-13}$ cm^2.

Carrier capture rate at this major trap is seen to be surprisingly slow and thermally activated. From DLTS-like processing of capture transients as well as from variable filling pulse width TATS measurements, capture barrier was estimated to be 0.66 eV which is quite large compared to the emission barrier mentioned above. A part of capture barrier may be due to a macroscopic barrier for holes to reach the trap levels at the damaged layer. With a high macroscopic barrier, a mild inversion or injection from near-intrinsic region are probable sources of filling of minority carrier traps which show up as negative peak in CC-TATS spectra. The time constant of the negative peak matches with that of damage related majority carrier peak in n-Si. Thus the dominant majority carrier defect in n-type and the minority carrier trap in p-type Si seem to be of common origin acting as an efficient midgap recombination center in heavy ion damaged Si. The majority carrier peaks in p-type also seem to have origin in interstitials and their clusters.

In contrast to the case of n-Si, high temperature furnace annealing of damaged p-Si

upto 600°C showed considerable change in defect spectra with appearance of new traps. The evolution of defects would require more systematic studies than envisaged in this work.

8.2 Recommendations For Further Work

Our work may be viewed as an attempt to lay a foundation for studies in defect dominated materials, such as heavy ion damaged Si, by overcoming several hurdles in the use of suitable techniques and interpretational difficulties. There are several obvious extensions of our work some of which are listed below.

1. Many of the interesting questions of damage and defect mechanisms require complimentary characterization techniques. Particularly, use of structural tools such as transmission electron microscopy (TEM), Rutherford backscattering spectrometry (RBS) channeling and positron annihilation spectroscopy (PAS) would give more coherent understanding of the damage related defect. Similarly, magnetic resonance studies such as EPR, ENDOR along with electrical studies would give details of the defect structure and symmetry for proper identification.

2. Optical characterization techniques such as photocapacitance based spectroscopy would simultaneously be useful for such compensated material to develop better understanding of the defect.

3. More systematic study of the defect in buried layers using our electrical characterization techniques should be done by varying different parameters (ion dose, implantation temperature etc.) for ion implantation. Also, a more systematic and thorough study of evolution of defects with annealing is required to understand relationship between clustering of defects and their corresponding electrical activity.

During the course of this work, it was found that forward biasing of diodes sometimes led to changes in defect spectra. This aspect needs further systematic and controlled studies. This may reveal that relaxation of the damaged layer could be induced by recombination events.

4. During implantation, changes in defect spectra can be monitored in-situ to study defect kinetics at shorter time scales following irradiations into finished devices.

We believe that extension of this work along these directions would open up many more possibilities in this regime of defect clustering in ion-implanted semiconductors and similar defect dominated materials.

Bibliography

[1] E. Chason, S.T. Picraux, J.M. Poate, J.O. Borland, M.I. Current, T.D. de le Rubia, D.J. Eaglesham, O.W. Holland, M.E. Law, C.W. Magee, J.W. Mayer, and A.F. Tasch, *J. Appl. Phys.* **81**, 6513 (1997).

[2] D. Stivenard and J.C. Bourgoin, *Ion Implantation in Semiconductors* (Trans Tech, Switzerland, 1988).

[3] J.S. Willaims, R.G. Elliman, M.C. Ridgway, C. Jagadish, S.L. Ellingboe, R. Goldberg, M. Petravic, W.C. Wong, Z. Dezhang, E. Nygren, and B.G. Svensson, *Nucl. Intrum. Methods* **B80/81**, 507 (1993).

[4] J. F. Zeigler, *Handbook of Ion Implantation Technology* (North Holland, Amsterdam, 1992).

[5] J.O. Borland and R. Koelsch, *Solid State Technol.* **36**, 28 (1993).

[6] S.J. Pearton, *Duffusion and Defect Data B : Solid State Phenonema* **1** & **2**, 247 (1988).

[7] S. Kalbitzer, *Nucl. Intrum. Methods* **B63**, 1 (1992).

[8] S. Dhar, T. Som, Y.N. Mohapatra, and V.N. Kulkarni, *Appl. Phys. Lett.* **67**, 1700 (1995).

[9] J.M. Parsey, Jr., in *Materials Science and Technology* edited by R. W. Cahn, P. Haasen, and E.J. Kramer (VCH, Geinheim, 1996), Vol. 16, p476.

[10] H. Ennen, J. Schneider, G. Pomrenke, and A. Axmann, *Appl. Phys. Lett.* **43**, 943 (1983).

[11] A. Polman, *J. Appl. Phys.* **82**, R1 (1997).

[12] B. Zheng, J. Michel, F.Y.G. Ren, L.C. Kimerling, D.C. Jacobson, and J.M. Poate, *Appl. Phys. Lett.* **64**, 2842 (1994).

[13] J.L. Benton, J. Michel, L.C. Kimerling, D.C. Jacobson, Y.-H. Xie, D.J. Eaglesham, E.A. Fitzerald, and J.M. Poate, *J. Appl. Phys.* **70**, 2667 (1991).

[14] H. Ryssel and I. Ruge : *Ion Implantation* (Wiley and Sons, NY 1986), Chap. 1.

[15] J.F. Zeigler, J.P. Biersack, and U. Littmark, *The Stopping of Ions in Solids* (Pergamon, New York, 1985).

[16] M.T. Robinson and I.M. Torrens, *Phys. Rev. B* **9**, 5008 (1974).

[17] T.E. Seidel, Chapter 6 in *VLSI Technology*, ed. S.M. See (McGraw-Hill, NY 1983).

[18] B.G. Svensson, C. jagdish, and J.S. Williams, *Phys. Rev. Lett.* **71**, 1860 (1993).

[19] J.L. Benton, S. Libertino, P. Kringhoj, D.J. Eaglesham, J. M. Poate, and S. Coffa, *J. Appl. Phys.* **82**, 120 (1997).

[20] B.G. Svensson, B. Mohadjeri, A. Hallen, J,H. Svensson, and J.W. Corbett, *Phys. Rev. B* **43**, 2292 (1991).

[21] J.R. Troxell, *Solid State Electron.* **26**, 539 (1983).

[22] A. Hallen, B. U. R. Sundqvist, Z. Paska, B. G. Svensson, M. Rosling, and J. Tiren, *J. Appl. Phys.* **67**, 1266 (1990).

[23] L. Palmetshofer, J. Reisinger, *J. Appl. Phys.* **72**, 2167 (1992).

[24] H. Indusekhar, V. Kumar, and D. Sengupta, *Phys. Stat. Sol. (a)* **93**, 645 (1986).

[53] de Kock A.J.R., *Appl. Phys. Lett.* **16**, 100 (1970).

[54] R. G. Rhodes, *Imperfections and Active Centers in Semiconductors* (Pergamon, 1964), p13.

[55] T. Motooka, S. Harada, and M. Ishimaru, *Phys. Rev. Lett.* **78**, 2980 (1997).

[56] T. Y. Tan, H. Foll, and W. Krakow, *Appl. Phys. Lett.* **37**, 1102 (1980).

[57] G.H. Gilmer, T. D. de le Rubia, D.M. Stock, and M. Jaraiz, *Nucl. Intrum. Methods B* **102**, 247 (1995).

[58] K. S. Jones, S. Prussin, and E. R. Weber, *Appl. Phys. A* **45**, 1 (1988).

[59] P. Kringhoj, J.S. Williams, and C. Jagadish, *Appl. Phys. Lett.* **65**, 2208 (1994).

[60] R.J. Schreutelkamp, J.S. Custer, J.R. Liefting, W.X. Lu, and F.W. Saris, *Mater. Sci. Rep.* **6**, 1 (1991).

[61] H. Alexander and H. Teichler, in *Materials Science and Technology* edited by R. W. Cahn, P. Haasen, and E.J. Kramer (VCH, New York, 1991), Vol.4, p249.

[62] Martin D. Giles, *Appl. Phys. Lett.* **62**, 1940 (1993).

[63] G.H. Kinchis and R.S. Pease, *Rep. Prog. Phys.* **18**, 1 (1955).

[64] A. Battaglia and S.U. Campisano, *J. Appl. Phys.* **74**, 6058 (1993).

[65] A. Claveri, C. Vieu, J. Faure, and J. Beauvillain, *J. Appl. Phys.* **64**, 4415 (1988).

[66] F. F. Morehead, Jr. and B. L. Crowder, *Radiat. Eff.* **6**, 27 (1970).

[67] M.L. Swanson, J.R. Parson, and C.W. Hoelke, *Radiat. Eff.* **9**, 249 (1971).

[68] O. W. Holland, M. K. Ei-Ghor, and C. W. White, *Appl. Phys. Lett.* **53**, 1282 (1988).

[69] S. Roorda, W. C. Sinke, J. M. Poate, D. C. Jacobson, S. Dierker, B. S. Dennis, D. J. Eagleshman, F. Spaepen, and P. Fuoss, *Phys. Rev.* B 44, 3702 (1991).

[70] S. Roorda, R. A. Hakvoort, A. van Veen, P. A. Stolk, and F. W. Saris, *J. Appl. Phys.* **72**, 5145 (1992).

[71] D.V. Lang, *J. Appl. Phys.* **45**, 3023 (1974).

[72] S. T. Pantelides, *Rev. Mod. Phys.*, **50**, 797 (1980).

[73] *Deep Centers in Semiconductors*, ed. S. T. Pantelides, (Gordon and Breach, New York, 1986).

[74] *Electronic Structure and Properties of Semiconductors*, ed. W. Schroter, Vol. 4, Materials Science and Technology (VCH, New York, 1991).

[75] M. Jaros, *Deep Levels in Semiconductors*, (Adam Hilger, Bristol, 1982).

[76] P. T. Landsberg, *Recombination in Semiconductors*, (Cambridge University Press, Cambridge, 1991).

[77] R.R. Senechal and J. Basinski, *J. Appl. Phys.* **39**, 3723 (1968).

[78] C. T. Sah and G. V. K. Reddi, *IEEE Trans. Electron Devices* **ED-11**, 345 (1964).

[79] G. I. Roberts and C. R. Crowell, *J. Appl. Phys.* **41**, 1767 (1970); *Solid-State Electron.* **16**, 29 (1973).

[80] Y. Zohta and Y. Ohmura, *Appl. Phys. Lett.* **21**, 117 (1972).

[81] E. P. EerNisse, *Appl. Phys. Lett.* **18**, 183 (1971).

[82] M. Bleicher and E. Lange, *Solid-State Electron.* **16**, 375 (1973).

[83] L.C. Kimerling, *J. Appl. Phys.* **45**, 1839 (1974).

[84] W.C. Johnson and P.T. Panousis, *IEEE Trans. Electron Dev.* **ED-18**, 965 (1971).

[85] M. Schulz, *Appl. Phys. Lett.* **23**, 31 (1973).

[86] K. Nagai, T. Sekigawa, and Y. Hayashi, *Solid State Electron.* **28**, 789 (1985).

[87] A.M. Goodman, *J. Appl. Phys.* **34**, 329 (1963).

[88] J.D. Willey and G.L. Miller, *IEEE Trans Elevtron Dev.* **ED-22**, 265 (1975).

[89] P. Kramer, C. de Vries, and l.J. van Ruyven, *J. Electrochem. Soc.* **122**, 314 (1975).

[90] E.H. Roderick, *Metal-Semiconductor Contacts* (Clarendon, Oxford, 1978).

[91] M.A. Lampert and P. Mark, *Current Injection in Solids* (Academic, New York, 1970).

[92] M. G. Buehler and W. E. Phillips, *Solid-State Electron.* **19**, 777 (1976).

[93] C.T. Sah, L. Forbes, L.L. Rosier, and A.F. Tasch, *Solid State Electron.* **13**, 759 (1970).

[94] A.F. Tasch, Jr., C.T. Sah, *Phys. Rev. B* **1**, 800 (1970).

[95] Alex C. Wang and C.T. Sah, *J. Appl. Phys.* **55**, 565 (1984).

[96] G. Goto, S. Yanagisawa, O. Wada, and H. Takanashi, *Appl. Phys. Lett.* **23**, 150 (1973).

[97] N. Link, S. Bauer, and B. Ploss, *J. Appl. Phys.* **69**, 2759 (1991).

[98] J.A. Pals, *Solid State Electron.* **17**, 1139 (1974).

[99] N.M. Johnson, *J. Vac. Sci. Technol.* **21**, 303 (1982).

[100] N.M. Noras, *Phys. Stat. Sol.* **69a**, K209 (1982).

[101] A. Broniatowski, A. Blosse, P.C. Srivastav, and J.C. Bourjoin, *J. Appl. Phys.* **54**, 2907 (1983).

[102] E.V. Astrova, A.A. Lebedev, and A.A. Lebedev, *Sov. Phys. Semicond.* **19**, 850 (1985).

[103] P.K. Giri, S. Dhar, V.N. Kulkarni, and Y.N. Mohapatra, *Nucl. Instr. Methods* B **111**, 285 (1996).

[104] S. Anand, S. Subramanium, and B. M. Arora, *J. Appl. Phys.* **72**, 3535 (1992).

[105] P.K. Giri, S. Dhar, V.N. Kulkarni, and Y.N. Mohapatra, *J. Appl. Phys.* **81**, 260 (1997).

[106] K. Dmowski, B. Lepley, E. Losson, and M. El Bouabdellati, *J. Appl. Phys.* **74**, 3936 (1993).

[107] M.C. Chen, D.V. Lang, W.Ç. Dautremont-Smith, A.M. Sergent, and J.P. Harbison, *Appl. Phys. Lett.* **44**, 790 (1984).

[108] N.M. Johnson, D.J. Bartelink, R.B. Gold, and J.F. Gibbson, *J. Appl. Phys.*, **50**, 4828 (1979).

[109] S. Weiss and R. Kassing, *Solid State Electron.* **31**, 1733 (1988).

[110] D.C. Look and J.R. Sizelove, *J. Appl. Phys.* **78**, 2848 (1995).

[111] D.V. Lang, *J. Appl. Phys.* **45**, 3014 (1974).

[112] D.K. Schroder, *Semiconductor Material and Device Characterization* (John Wiley & Sons, Singapore, 1990), Chapter 7.

[113] H. Okushi and Y. Takumaru, *Jpn. J. Appl. Phys.* **19**, L335 (1980).

[114] P.M. Henry, J.M. Meese, J.W. Farmer, and C.D. Lamp, *J. Appl. Phys.* **57**, 628 (1985).

[115] Sandeep Agarwal, Y.N. Mohapatra, and V.A. Singh, *J. Appl. Phys.* **77**, 3155 (1995).

[116] P.K. Giri and Y.N. Mohapatra, *J. Appl. Phys.* **78**, 262 (1995).

[117] G. Williams and D.C. Watts, *Trans Faraday Soc.* **66**, 80 (1970).

[118] L. E. Benatar, D. Redfield, and R.H. Bube, *J. Appl. Phys.* **73**, 8659 (1993).

[119] A.C. Campbell and B.G. Streetman, *Appl. Phys. Lett.* **54**, 445 (1989).

[120] P. Omling, L. Samuelson, and H.G. Grimmeiss, *J. Appl. Phys.* **54**, 5117 (1983).

[121] B.M. Arora, *Solid State Comm.* **61**, 105 (1987).

[122] M.S. Hodgart, *Electron. Lett.* **14**, 388 (1978); **15**, *ibid.* 724 (1979).

[123] C.R. Crowell and S. Aliphani, *Solid State Electron.* **24**, 25 (1980).

[124] K. Dmowski, *Rev. Sci. Instrum.* **61**, 1319 (1990).

[125] Sandeep Agarwal, *Ph.D. Thesis*, IIT Kanpur, India, 1995.

[126] R.K. Singh, V.A. Singh, J.W. Corbett, and A. Das, *J. Phys. C, Solid State Phys.* **19**, 2177 (1986).

[127] Ch. Hurtes, M. Boulou, A. Mitinneau, abd D. Bois, *Appl. Phys. Lett.* **32**, 821 (1978).

[128] Maria J.S.P. Brasil and P. Motisuke, *J. Appl. Phys.* **68**, 3370 (1990).

[129] J. Morimoto, T. Kida, Y. Miki, and T. Miyakawa, *Appl. Phys. A* **39**, 197 (1986).

[130] L. Young, W.C. Tang, S. Dindo, and K.S. Lowe, *J. Electrochem. Soc.* **133**, 609 (1986).

[131] S.R. Blight and H. Thomas, *J. Appl. Phys.* **65**, 215 (1989).

[132] J. Bollman and H. A. Klose, *Solid State Phenomena* Vols. 6 & 7, 461 (1989).

[133] V. Raineri, G. Fallica, and S. Libertino, *J. Appl. Phys.* **79**, 9012 (1996).

[134] C. H. Seager, S. M. Myers, R. A. Anderson, W. L. Warren, and D. M. Follstaedt, *Phys. Rev. B* **50**, 2458 (1994).

[135] Rajnish Kumar Gupta, *M.Tech. Thesis*, IIT Kanpur, India (1997).

[136] A. Singh, *Solid-State Electron.* **28**, 223 (1985).

[137] S.J. Fonash, *J. Appl. Phys.* **54**, 1966 (1983).

[138] A. Golan, R. Fastow, and M. Eizenberg, *J. Appl. Phys.* **67**, 1940 (1990).

[139] J. E. Ejimania, *Solid. State Electron.* **29**, 841 (1986).

[140] S. Nespurek and J. Sworakowski, *J. Appl. Phys.* **51**, 2098 (1980).

[141] S. Coffa, V. Privitera, F. Priolo, S. Libertino, and G. Mannino, *J. Appl. Phys.* **81**, 1639 (1997).

[142] L.C. Kimerling, *IEEE Trans. Nucl. Sci.* **NS-23**, 1497 (1976).

[143] B.G. Svensson, C. jagdish, and J.S. Williams, *Nucl. Instr. Methods* **B80/81**, 583 (1993).

[144] P.C. Mangelsdorf, Jr., *J. Appl. Phys.* **30**, 442 (1959).

[145] J. Bourgoin and M. Lanoo, in *Point Defects in Semiconductors II* (Springer, Berlin, 1983), p196.

[146] Bruce Hamilton, Anthony R. Peaker and Sokrates T. Pantelides, *Phys. Rev. Lett.* **61**, 1627 (1988).

[147] M. Zazoui, J. C. Bourjoin, D. Stivenard, D. Deresmes, and G. Strobl, *J. Appl. Phys.* 76, 815 (1994).

[148] R. S. Germana and S. U. Campassino, *Appl. Phys. Lett.* **60**, 1726 (1992).

[149] F. Richou, G. Pelous, and D. Lecrosnier, *Appl. Phys. Lett.* **31**, 525 (1977).

[150] Y. N. Erokhin, J. Ravi, C. W. White, and G. A. Rozgonyi, *Nucl. Instr. Methods* B **96**, 223 (1995).

[151] O. Kumagai and K. Kaneko, *J. Appl. Phys.* **52**, 5143 (1981).

[152] B. L. Crower, R. S. Title, M. H. Brodsky, and G. D. Pettit, *Appl. Phys. Lett.* **16**, 205 (1970).

[153] B. R. Gossick, *J. Appl. Phys.* **30**, 1214 (1959).

[154] J. R. Dennis and E. B. Hale, *J. Appl. Phys.* **49**, 1119 (1978).

[155] P. A. Stolk, F. W. Saris, A. J. M. Berntsen, W. F. van der Weg, L. T. Sealy, R. C. Barklie, G. Krotz, and G. Muller, *J. Appl. Phys.* **75**, 7266 (1994).

[156] See, e.g. P. G. LeComber and W. E. Spear, *Philos. Mag. Lett.* **53**, L1 (1986).

[157] Y. Bar-Yam and J. D. Joannopoulos, *Phys. Rev. Lett.* **56**, 2203 (1986).

[158] S. C. Deane and M. J. Powell, *Phys. Rev. Lett.* **70**, 1654 (1993).

[159] J. David Cohen, Thomas M. Leen, and Randall J. Rasmussen, *Phys. Rev. Lett.* **69**, 3358 (1992).

[160] J.W. Farmer and Z. Su, *Phys. Rev. Lett.* **71**, 2979 (1993).

[161] R. G. Palmer, D. L. Stein, E. Abraham, and P. W. Anderson, *Phys. Rev. Lett.* **53**, 3358 (1984).

[162] J. R. Mcdonald, *J. Appl. Phys.* **62**, R51 (1987).

[163] Z. Su and J.W. Farmer, *Appl. Phys. Lett.* **59**, 1746 (1991).

[164] Sokrates T. Pantelides, *Phys. Rev. B* **36**, 3462 (1987).

[165] Fan Zhong and J. David Cohen, *Phys. Rev. Lett.* **71**, 597 (1993); J. D. Cohen and Thomas M. Leen, Comments, *Phys. Rev. Lett.* **73**, 366(1994).

[166] A. Chantre and D. Bois, *Phys. Rev. B* **31**, 7979 (1985); A. Chantre, *ibid.* B **32**, 3687 (1985); L. Song, X. D. Zhan, B. W. Benson, and G. D. Watkins, *Phys. Rev. Lett.* **60**, 460 (1988).

[167] A. Chantre, A. Vincent, and D. Bois, *Phys. Rev. B* **23**, 5335 (1981).

[168] V. Heine and J. A. Van Vechten, *Phys. Rev. B* **13**, 1622 (1976).

[169] Howard M. Branz and Richard S. Crandall, *Appl. Phys. Lett.* **55**, 2634 (1989).

[170] G. E. Jellison, Jr. and F. A. Modine, *Phys. Rev. B* **14**, 3539 (1976).

[171] J. Vanhellemont, A. Kaniava, E. Simoen, M.A. Trauwaert, C. Claeys, B. Johlander, R. Harboe-Sorensen, L. Adams, and P. Claus, *IEEE Trans. Nucl Sci.* **41**, 479 (1994).

[172] H. Sayama, A. Kinomura, Y. Yuba, and M. Takai, *Nucl. Instrum. Methods Phys. Res B* **80/81**, 787 (1993).

[173] P. Omling, E.R. Weber, L. Montelius, H. Alexander, and J. Michel, *Phys. Rev. B*, **32**, 6571 (1985).

[174] J.A. Pals, *Slid-State Electron.*, **17**, 1139 (1974).

[175] A. Broniatowski, *Phys. Rev. B* **36**, 5895 (1987).

[176] S. Ghosh and V. Kumar, *J. Appl. Phys.* **75**, 8243(L) (1994).

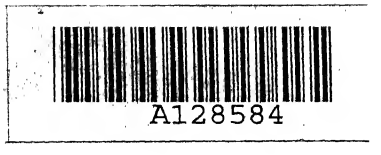

heavy ions. There are several simulation packages such as TRIM (Transport of Ion in Matter) [15], MARLOWE (based on Binary collision approximation programs) [16] which work remarkably well for low energies in predicting range and profile of ions and displaced atoms. Such computer programs normally use ballistic regime approximation and do not take into account defect processes.

1.4 MeV Implant Induced Damage and Defects : A Brief Review

The energy lost by the ions can be sufficient in displacing host atoms, which in turn can displace others resulting in collision cascades. Normally only a nuclear interaction result in displacement of host atoms. A host of different types of defects can results starting from simple point defects to their clusters, complexes and amorphized zones due to agglomeration. Radiation damage is produced only if the energy loss is larger than the displacement energy of the lattice atom (typically $\sim$ 15 eV for silicon). Therefore, the damage distribution can be expected to lie closer to the surface than that of the ion profile. An example of the difference is shown in Fig. 1.2, where vacancy and ion profiles are obtained using TRIM simulations. For low energy implants, the peak of damage profile generally occurs at $\sim$ 0.7-0.8R_p with standard deviation of $\sim 0.75\Delta R_p$, where R_p and ΔR_p are ion range and straggling respectively. It has been observed that a simulation package such as TRIM normally yields ion profiles in close agreement with experiments, but the damage profile can be very different than predicted for heavy ion implants in MeV range. The final damage profiles in these cases is dependent on details of defect processes such as diffusion and agglomeration, in addition to cascade geometries. This is the reason why the results of the simulational packages cannot be taken at their face value at present for heavy ion implants in the MeV range.

As described by Seidel [17], an implanted ion comes to rest in $\sim 10^{-13}$ s, which is

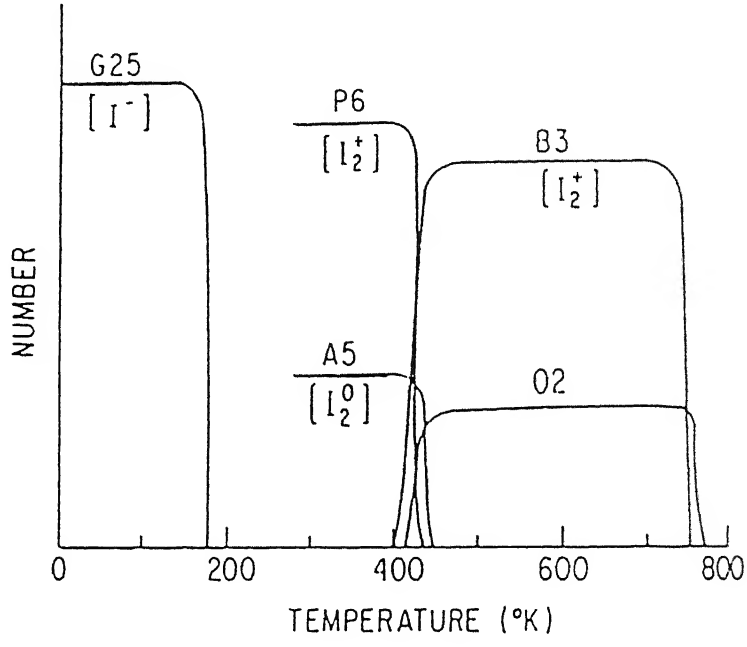

Figure 1.4: Schematic of the recovery of several interstitial related defects as studied by EPR (after ref. [44] and references therein). The relative intensity (number) is irrelevant between defects as annealing data are from different sources.

in this thesis, we note that silicon interstitial generated by Ar^+ ion implantation has been shown to cause an order of magnitude increase in coefficient of phosphorus diffusivity at temperature less than 800°C . Argon ion implantation were shown to be source of long lasting silicon interstitials [45]. The current views on the life of an interstitial from the time of its generation has been succinctly summarized in a recent paper [46]. It has been shown that for sufficiently high damage levels, the resulting excess number of interstitial atoms are approximately equal to the imbalance in the interstitial vacancy concentrations resulting from an extra, implanted silicon atom. This is commonly referred to as '+1' model [47] which suggest that recombination of interstitials and vacancies is the dominant process operative at the initial stages of their generation.

mechanisms in presence of disorder. By studying such phenomena in a regime of disorder below amorphization, one hopes to avoid difficulties encountered in the more complex situation of amorphous silicon.

Our aim in this work has not been to carry out comprehensive comparative studies through variation in implantation parameters, rather the attempt has been to lay down a foundation for such studies using capacitance based techniques by exploring basic phenomena and possible interpretational hurdles. In other words our effort has been to hone the capacitance based electrical characterization techniques to study electrical manifestation of defect phenomena due to MeV heavy ion implantation notwithstanding complexities due to heavy damage. More generally, these studies would be helpful in the study of complex inter-relationships between defects, damage and disorder. MeV heavy ion damaged silicon provides a challenging setting for such studies.

scheme extensively in transient measurements to keep the sampling volume same and to avoid non-exponentialities in transients due to large concentration of traps. Necessary instrumentation for implementation of this circuit is discussed in the next chapter.

In practice, series resistance can be temperature dependent also. In a subsequent section, we will discuss way of overcoming such problems for analyzing capacitance transients.

2.2.3.2 Excess leakage current

Schottky barrier devices occasionally show large leakage current. After ion implantation, the device may become more leaky due to presence of recombination centers. The assumption in the conventional profile equation is that the voltage is measured across the space charge region only. If, however, excess leakage current flow an appreciable voltage can be developed across the quasi-neutral regions. This voltage is automatically included in the recorded voltage introducing errors in measured C-V characteristics [89].

2.2.3.3 Minority carrier and interface trap

When a Schottky barrier diode is reverse biased, the thermally generated electron-hole pairs are swept out of the space charge region and leave through the ohmic contact of the device. In case of MIS devices, thermally generated minority carriers drift to the insulator/semiconductor interface to form inversion layer. The device is unable to remain in deep depletion and doping profile measurement will be in error. When the voltage is varied rapidly, inversion charge do not get time to appear. Cooling the device to low temperature works well to reduce the effect of minority carrier generation. Effect of interface traps is also of major concern in case of MIS structures. Its contribution is also reduced when the device is cooled.

2.6.2 Effect of series resistance and leakage current

We have already discussed the effect of series resistance on the capacitance transients. This can be extended to DLTS as well. Using Eqn. 2.12, measured DLTS signal ΔC_m can be writen as

$$\Delta C_m = \Delta C\{\frac{1-Q^2}{(1+Q^2)^2}\} \tag{2.22}$$

where $Q = \omega r_s C$. This simple form of equation is valid for small change of Q with time.

According to Eqn. 2.22, DLTS signal would vanish for $Q = 1$ and its sign is reversed for $Q > 1$. Broniatowski *et al.* [101] have proposed a method of detecting the presence of series resistance in DLTS and a correction scheme, based on varying circuit impedance by means of additional series resistance. In practice, this is cumbersome to implement due to variation of r_s and C with temperature. The distinction between negative peak due to minority carrier trap and peak due to series resistance can be made by noting the change in crossover point in temperature due to extra series resistance added [109, 102]. If no change is observed, the sign reversed DLTS peak can be attributed to the presence of a minority carrier trap.

The lineshape distortion in DLTS due to series resistance gives modified trap parameters. Lineshape analysis of DLTS for different Q values show that larger the Q value, FWHM and peak height of DLTS will go down and peak will be shifted to higher temperature side for chosen window. Figure 2.4 shows a set of simulated DLTS spectra for different Q values. For Q>1, peaks of opposite signs can be noted. This may be mistaken as minority carrier trap related peak. For temperature dependent series resistance, peak height will be a complicated function of resistance.

Reduction in DLTS peak height with smaller rate window can be due to leakage current effect [107] as well as series resistance effect. As discussed in section 2.3.2, time constant will be changed and extracted trap parameter can be very different from actual parameter.

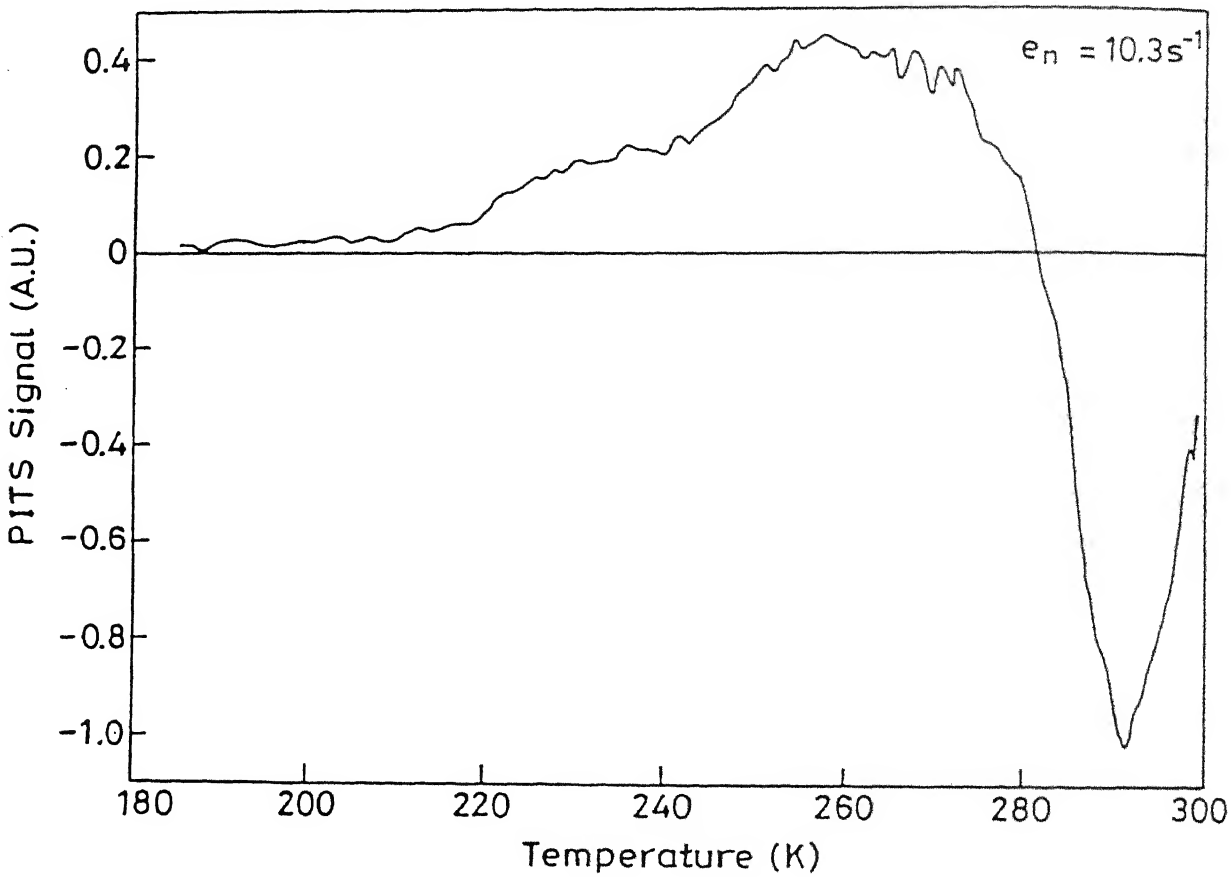

Figure 2.8: Typical PITS spectrum of SI-GaAs sample with t_1=0.141 s, t_2=0.279 s, showing negative peak along with broad positive peak.

a broad positive peak prior to the negative peak and has been seen in most samples. The shape of the negative peak in PITS spectra is highly distorted owing to the presence of this broad positive peak. However, significance of this feature in relation to the negative peak has not been discussed in the literature. We also see a well formed positive peak at lower temperature in the PITS spectra which is discussed later in this section.

In our experiments, as do other reports, we have seen that the strength of the transients is highly dependent on temperature for a constant filling time leading to distortion of PITS spectra. Moreover, most transients are non-exponentials to varying degrees making

Chapter 3

Experimental Details : Sample Preparation and Measurements

3.1 Introduction

In this chapter, details of sample preparation, diagnostic techniques and experimental set-up made in house are given. The diagnostic studies involve capacitance and current based steady-state or transient measurements in the temperature range of 77K-330K. Most experimental setups and their automations for various measurements were developed in house using a few commercial instruments as basic modules. Flexibilities of in-house developments in the hardware and software were important for this work, since many designer experiments were needed to be carried out to decide suitable mode of characterization and for thorough appraisal of cross-sensitivities.

3.2 Sample Preparation

A typical sample preparation process involves following steps : (i) surface cleaning of Si wafers, (ii) irradiation with MeV ions (Ar, Au) on Si wafers and finished Schottky devices, (iii) vacuum annealing of implanted wafers or oven heating on finished devices for low temperature annealing, (iv) Schottky diode formation with back ohmic contact, (v) mounting the device on a header for taking epoxy contacts. Most of the studies in this work were done on as-implanted sample where step (iii) mentioned above is omitted. The 2 MeV Van de Graaff accelerator facility here at IIT, Kanpur, India, was used for Ar^+

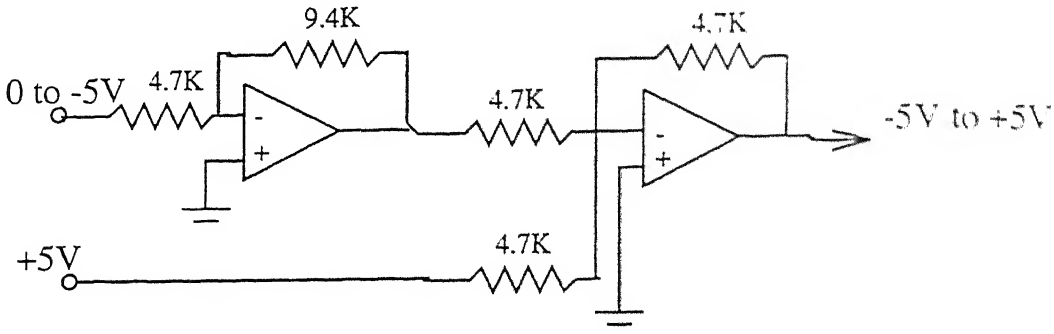

Figure 3.6: Biasing circuit for application of both forward bias and reverse bias.

3.3.2 Capacitance vs. voltage (C-V) measurement

A Boonton capacitance meter (Model 72B with 50 μs response time) operated at 1 MHz with a 15 mV test level was used for all capacitance measurements. Programmable voltage is generated with the help of a plug-in AD/DA card (Model PCL 718). It is a high performance, high speed, multi-function data acquisition card for IBM PC/XT/AT. It has two analog outputs (range 0 to +5 V, with a resolution of 12 bit and 5 μs settling time). For changing the polarity of the voltage, an opamp inverting circuit is implemented. A simple adder circuit whose schematic is shown in Fig. 3.6, is used to get voltage in the range of -5V to +5V. In most of the cases, voltage is changed from high value to low value while monitoring capacitance at each voltage. This prevents effect due to dynamical change of capacitance due to trap de-occupation at a temperature where trap emission time constant is comparable to the voltage sweep rate. For all C-V hysteresis measurements. voltage is swept at a predetermined rate from high voltage to low voltage and then from low voltage to high voltage. The diode is kept under reverse biased condition to start with. The applied voltage and capacitance meter analog output are digitized through two input channels of Keithley high speed voltmeter (K194A) which can store 64 KB data. Different ranges of capacitance meter gives different analog output which is 1V or 3V maximum if

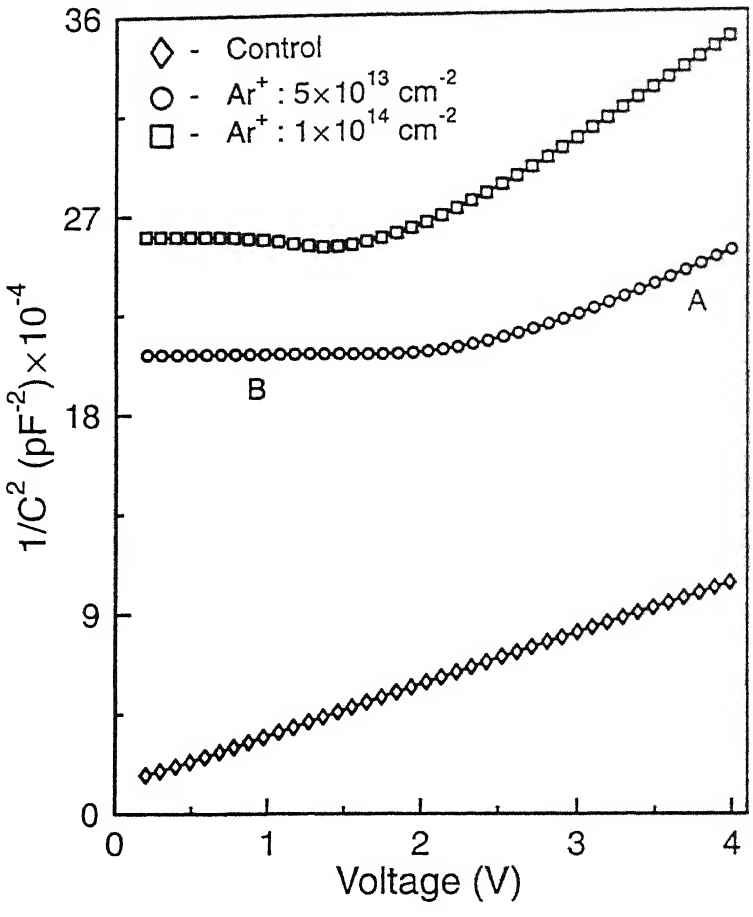

Figure 4.1: Typical C-V characteristics at T=300K for n-Si Schottky diode irradiated with various doses of Ar^+ ions.

have been irradiated at room temperature with various implant doses in the range of 5-10×10^{13} cm^{-2} of Ar^+ ions and 5×10^9 cm^{-2} of Au^+ ions. Typically in a C-V measurement, bias voltage is changed from high reverse bias to zero bias so that time dependence of trap occupancy, if any, does not affect the steady state capacitance measurements assuming that carrier capture rate is very fast compared to rate of change of voltage.

Figure 4.1 shows a typical $1/C^2$ vs. V plot at room temperature for unimplanted and Ar^+ ion implanted samples with two different doses. It can be noted that for unimplanted samples, the curve is linear in the measured voltage range indicating uniformity of shallow doping concentration. However, for implanted samples there are distinctly two regions of which the linear region (A) occurs for higher voltages and the flatter region (B) occurs for

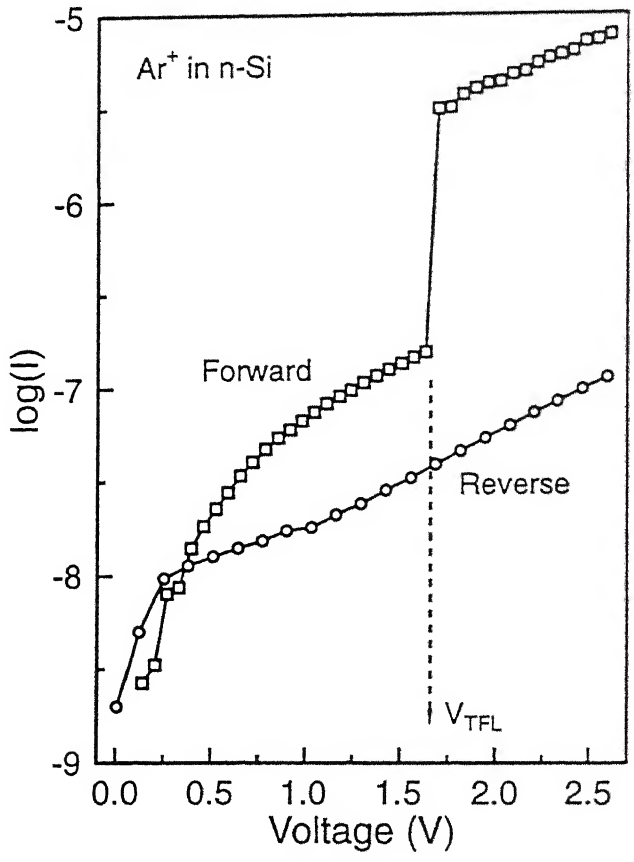

Figure 4.8: Forward and reverse I-V characteristics of Ar^+ implanted Si at room temperature.

is low enough for unproblematic capacitance measurements as shown in the last section. However, note the sudden jump of forward current at a particular voltage.

In Figure 4.9, we have plotted the log(I) vs. log(V) for Ar^+ ion implanted sample annealed at 160°C for 30 minutes. This plot shows a near ideal case of crossover from ohmic conduction ($I \propto V$) to square law space charge limited conduction ($I \propto V^2$) regime at the voltage corresponding to trap filled limit (V_{TFL}). The nearly vertical rise in current accompanying the trap filling is an indicator that the associated defect is a discrete level [91]. In this case, the same defect controls hysteresis in C-V measurements due to its large concentration and this is the dominant level in ion damaged buried layer which acts as a near intrinsic region. Thus the structure under study is akin to *p-i-n* diode where *p* is

dynamic simulational studies of combined processes of defect generation, migration and clustering during and after implantation. Their atomistic simulation show migration of free interstitials and clustering at room temperature even several hours after initial fast recombination processes have died out. They also show that the depth distribution of remnant interstitials peak at approximately twice the implant range. Defect clustering is known to be more favourable in heavy ion irradiation due to occurrence of high density of collisional cascades in comparison to light ions. Similar effects are also expected for high dose implants [19] . Therefore there is a growing body of evidence showing that the ion induced damage acts as a source of migrating interstitials which can combine to form clusters at distances beyond the damage location. Though the electrical activity of *point* defects and *extended* defects in implanted material have been studied in detail, there is a lack of similar studies on *defect clusters*. Its only recently, Benton *et al* [19] have reported electrically active traps associated with second and higher-order interstitial clusters in residual damage of Si implanted with high fluences. It appears reasonable to conclude that the dominant electrically active traps observed in our experiments also originate from interstitial clusters. We postpone a discussion on origin of the major defect till the next chapter where we report spectroscopic characterization of electrically active defects. The sharp trap profile at distances much larger than ion range would be fully consistent with the mechanism of migration and eventual cluster formation of interstitials. In fact, our results constitute a direct experimental evidence of such a mechanism.

The fact that the effective electrical interface moves with changes in process variables such as dose and annealing also supports occurrence of a mechanism involving migration and clustering. With increase in irradiation dose, the interface between trap dominated and trap-free regions is expected to move deeper into the sample as there would be more abundant supply of interstitials from the damaged region. Similarly, the effective interface is observed to move towards the surface with increase in annealing temperature. Though

Though large concentration of defects are produced in ion-atom collisions, most of the primary defects, namely vacancies and interstitials, are unstable at room temperature and they form divacancy and other higher order complexes. Divacancy is known to have three charge state configurations which introduce different energy levels (E_c-0.42 eV, E_c-0.23 eV and E_v+0.25 eV) in the bandgap of semiconductor. However, we do not observe the peak corresponding to E_c-0.23 eV related charge state configuration in the DLTS spectrum. This is mainly due to low production rate of $E_c - 0.23$ level as compared to the $E_c - 0.42$ level in heavy ion irradiated n-Si. Note that the presence of a broad peak H1 may cause suppression of other majority carrier related peaks which are of smaller concentration. In a detailed study of divacancy acceptor level profile in MeV ion irradiated n-Si, Svensson *et al.* [20, 143] reported that concentration of E_c-0.23 eV level is significantly lower than that of E_c-0.42 eV for high dose and heavier mass implants. They observed that concentration of the two levels are identical in tail region towards the surface while it is very different in the damage peak region. They argued that for heavy ions the rate of energy deposition is higher and V_2 centers occur in lattice regions which accommodate lattice strain. This lattice strain causes broadening in the DLTS spectra. Inspection of the lineshape of the peak V_2 reveals that it is broader than the peak expected from exponential transient. Detailed analysis of the lineshape in the context of capture kinetics is carried out using isothermal spectroscopic technique and is presented in the next Chapter. It is also known that a defect level with similar trap parameters i.e. E-center (P-V complex) may contribute to the observed broadening. We have examined possible contribution of this level from lineshape analysis of as-implanted and low temperature (160°C) annealed samples. In principle, for silicon with large phosphorus doping, contribution of this defect may become significant. Normally it is recognized by studying its annealing behaviour since the defect anneals out at temperature of $\sim$ 300°C.

The defect responsible for peak D1 shown in Fig. 5.4 occurs consistently in large con-

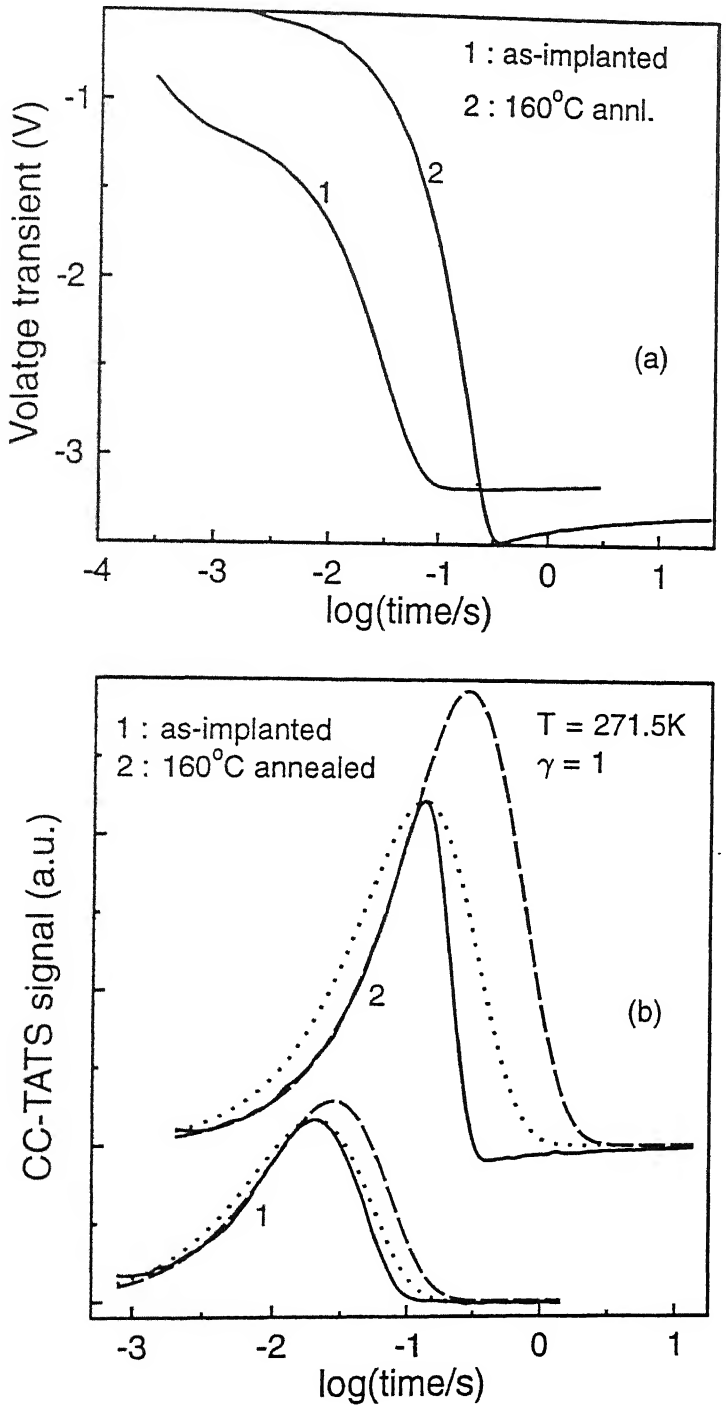

Figure 5.8: (a) Isothermal voltage transient measured in CC mode for as-implanted and 160°C annealed sample, (b) Corresponding CC-TATS spectra (solid line), with exponential peak fitting (dotted line) assuming apparent peak as the true peak. The broken line is fitted with an exponential transient considering only left side of the peak.

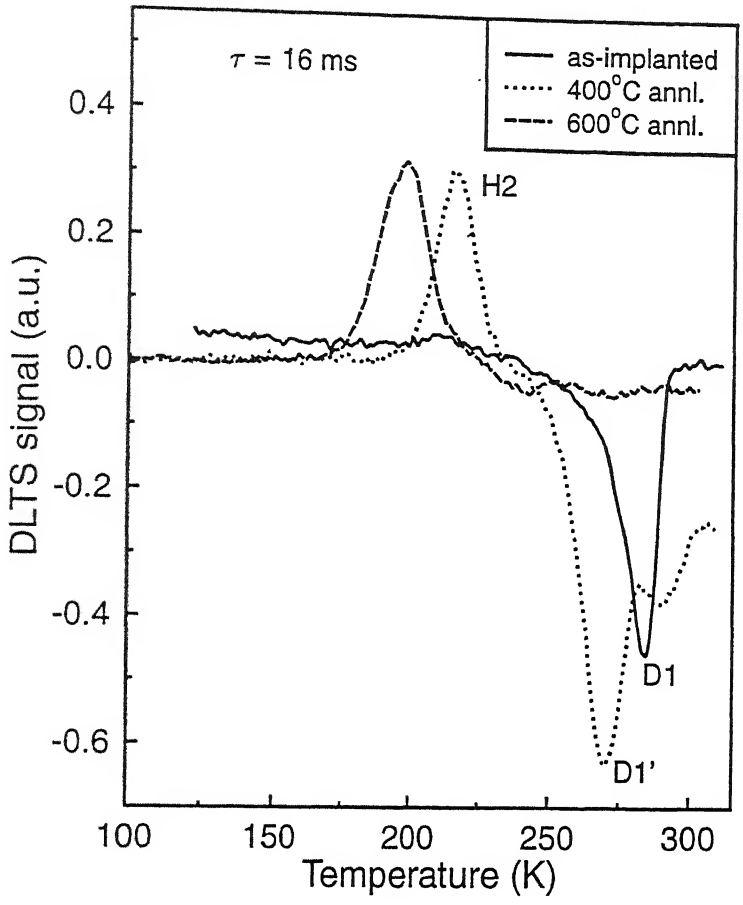

Figure 5.14: Comparison of DLTS spectra on as-implanted, 400°C and 600°C annealed samples for same rate window.

low temperature annealing is most probably due to changing sizes of clusters.

5.5.2 Furnace annealing

Effect of vacuum annealing of the irradiated Si at higher temperatures are shown in Fig. 5.14. In contrast to as-implanted sample which showed V_2 related peak and D1 peak (solid line), 400°C annealed sample shows a different DLTS spectrum consisting of two majority carrier peaks and one minority carrier related peak. The absence of V_2 related peak is expected since they anneal out at $\sim$ 350°C. The peak position of the major defect D1 is shifted towards lower temperature side. Though DLTS analysis can not be relied

laboratory for dealing with similar questions asked in the context of amorphous silicon. This is mainly because the defect density of states remain discrete in our samples while other conditions prevailing in amorphous silicon such as large concentration of defects and presence of disordered environment are still satisfied.

Before we present our results, we provide in the next section a brief background to the above mentioned debate and the perspective in which our results must be viewed. We go on to provide experimental evidence for two distinct mechanisms of charge relaxation in varying sample conditions and different temperature regimes of measurements.

6.2 Models of Charge Relaxation in Disordered Silicon

The presence of continuously distributed states over wide energies is one of the characteristic feature of electronic properties of disordered semiconductor .There is a vast and rich literature in relation to the determination of density states, origin, effective correlation energies, and mechanisms of charge relaxation in these materials. These studies have been most intensive in hydrogenated amorphous silicon (a-Si:H) where the energy distribution is attributed to the dominant deep defect 'D' associated with dangling bond [156]. It is also appropriate here to mention that , in contrast to a-Si:H, there has been very little studies on DOS (density of states) in the gap of pure amorphous silicon created by MeV ion implantation [155]. Without going into the details of these studies, which have been reviewed from time to time, it suffices to state here that a principal source of most controversies have been the necessity of using complex deconvolution procedures to extract information from measured quantities.

There have been several approaches to resolve inconsistencies in connection with differing density of states in a variety of samples both doped and intrinsic a-Si:H. There have been attempts to explain such a variation in DOS using the 'defect pool model' in which

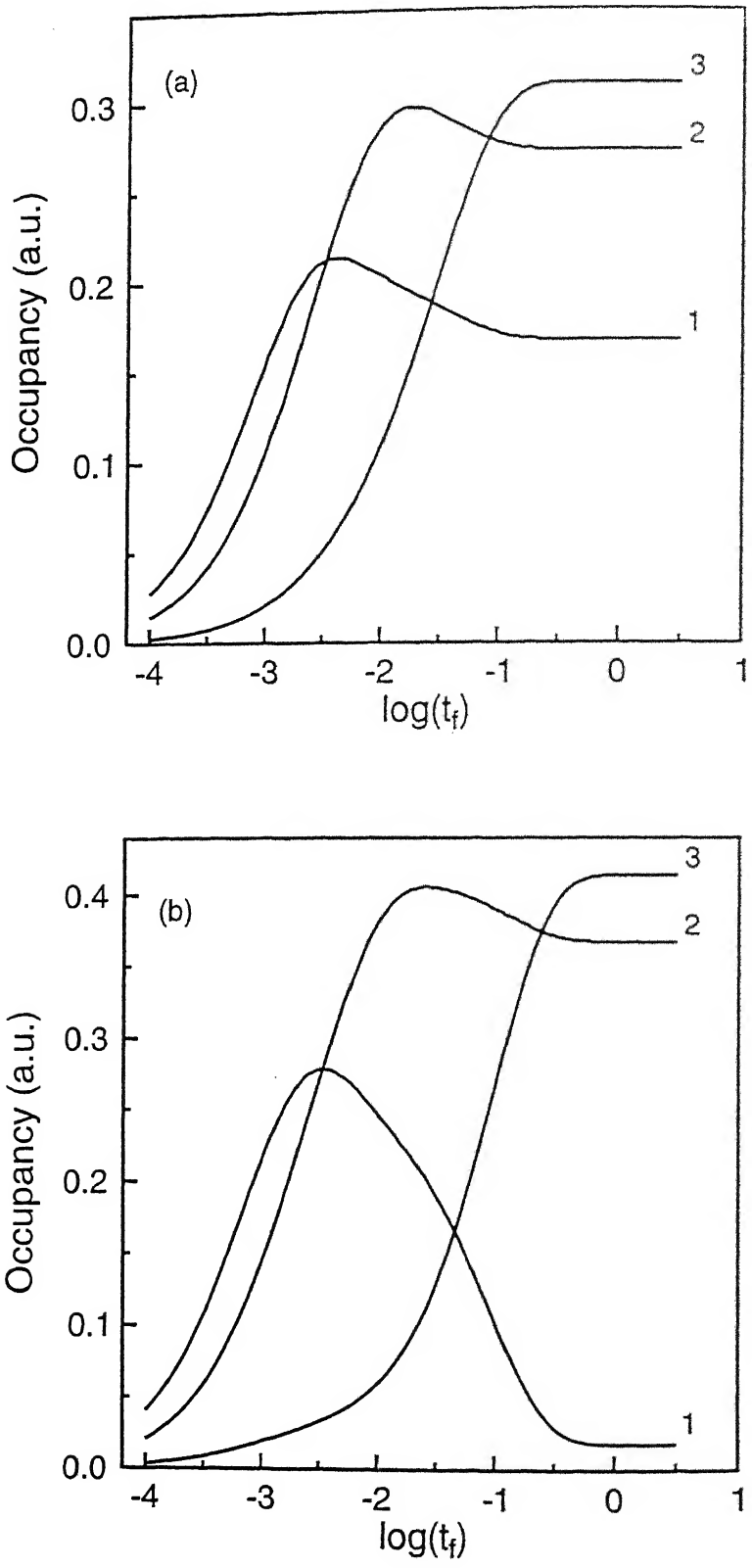

Figure 6.5: Simulated occupancy behaviour of three trap levels by solving rate equations under the condition $N_T \geq n$, (a) assuming three independent trap levels, (b) assuming that fastest and slowest sates are two configurations of the same defect. Parameters of simulation are given in

During the capture pulse, successive emission and capture events can drive the defect to relax continuously to more stable states if the polarization cloud is unable to follow this process rapidly. In other words a relaxation process much slower than emission or capture processes would have the memory of net duration of occupation.

The driving force, in fact, can be due to entropic variations in configurational space. Such entropy driven metastabilities have been invoked in the past in the context of several defects in semiconductors known to have metastable configurations which can be accessed by charge state change, optical excitation and rapid heating and cooling cycles [146, 166, 167]. Hamilton *et al.* [146] have used such an argument to explain the existence of a critical temperature at which certain configuration becomes unstable giving rise to a discontinuous DLTS spectrum. Though that case is distinct from the ones described here, the significance of entropic terms in determining relaxation is to be noted. Further, it is also significant that most of such observations have been reported in electron or ion irradiated semiconductors. This is to be attributed to occurrence of multiple or continuously varying configuration for an electrically active point defect in the environment of irradiation induced damage. The temperature dependence of electronic ionization energy has in the past been conveniently represented by associating an ionization entropy resulting from electron-phonon interaction [168]. The estimates of entropy change on ionization from a deep defect varies between $3-4k$ in the temperature range of our observations [169, 170]. Hence entropic contribution to ionization can be well in the range of 100 meV at room temperature. The net free energy change of 180 meV in our case can indeed be due to changes in ionization entropy. It is to be noted that samples used in this work provide a convenient laboratory for further studies on details of this relaxation mechanism. In a group of samples, studied in this context, we observe qualitatively similar behaviour, as described here, but with the difference that multiple traps evolve with filling time. An example of Au^+ irradiated sample is shown in Fig. 6.10. These show that relaxations may

forward bias, only a small percentage of the current is due to injected electrons, so minority carriers are not usually seen. However, in the present study, there is a large damage due to heavy ion implantation. As the major trap (P2) causes carrier compensation and changes the band bending depending upon the trap occupancy, we ascribe this negative peak to changes in occupancy of minority carrier traps in presence of mild inversion caused by band bending in the damage region. A simple calculation of band bending at zero bias shows that the interface at the damaged region would be mildly inverted. This seems to indicate that a minority carrier trap can indeed be filled within depletion layer.

Another possible mechanism of small minority carrier generation may be due to the nearly intrinsic nature of the damaged region where a large concentration of traps can effectively pin the Fermi level to a position near the middle of the energy gap. Such an effect has been reported previously [28] to occur in ion damaged Si. The equilibrium electron concentration in the damaged region acts as a source of electron to fill the minority carrier trap. The slow rate of carrier capture in the damaged region is due to the presence of small majority carrier concentration. Minority carrier trap related peaks were observed by Jackson and Sah [178] in boron implanted n-Si after annealing at $\sim$ 400°C and observation was justified by possible intrinsic hole concentration in the damaged region.

7.5 Thermal Stability Of The Defects

In order to carry out a preliminary study of thermal stability of these damage related defects, we have annealed the irradiated wafers at 400°C and 600°C for 30 minutes in vacuum, and subsequently fabricated Schottky diodes on them. Some finished devices (irradiated) are annealed at 160°C for 30 minutes in oven to study low temperature annealing effects. It is also important to mention that no room temperature transformation of the defects has been seen in p-Si, in contrast to n-Si case. Note that, our samples were stored at room temperature for few months before carrying out electrical measurements.

materials.

B. Evidence for Defect Migration and Clustering

Unusual features observed in steady-state C-V studies on Schottky diodes of n-Si, containing damaged buried layers, strongly indicated trap controlled nature of the damaged layer. The damaged layer is found to be extended to several microns beyond the range of the ions or damage profile predicted by Monte Carlo simulations using TRIM. The experimental features in C-V curves have been simulated using model charge profiles taking into account crossing of Fermi level with a midgap trap within the depletion layer. The simulations suggest that the irradiation damage seem to produce two regions : (i) a compensated region with most dopants being deactivated, and (ii) a sharp negatively charged defect profile with large concentration close to the depletion edge, with the depletion layer being much larger than expected range of ions. Our experimental observations lend support to recent results of molecular dynamic simulations according to which primary defects such as vacancies and interstitials migrate and form clusters and complexes. Occurrence of a single dominating trap in the damaged region is established from C-V and I-V studies. Dopant activation and annealing of the major defect was found to occur in the damaged region by 600°C vacuum annealing. The nature of variations in charge profile with annealing shows that the effective electrical interface moves progressively towards the surface.

C. Spectroscopies of Defects

(i) Conventional DLTS : Survey and Limitations

Transient response of diodes containing damaged layer showed interesting and unusual features which include occurrence of a 'spike' in capacitance response during capture of

[40] Y. H. Lee, N. N. Gerasimenko, and J. W. Corbett, *Phys. Rev. B* **14**, 4506 (1976).

[41] G.D. Watkins and J.W. Corbett, *Phys. Rev.* **134**, A 1359 (1964).

[42] G.D. Watkins, in *Materials Science and Technology* edited by R. W. Cahn, P. Haasen, and E.J. Kramer (VCH, New York, 1991), Vol.4, p.107.

[43] See Ref. No. 8, 9, 10, 11, 12 of the preecding reference.

[44] J.W. Corbett, J.P. Karins, and T.Y. Tan, *Nucl. Intrum. Methods* **182/183**, 457 (1981).

[45] G.B. Bronner and J.D. Plummer, *Appl. Phys. Lett.* **46**, 510 (1985).

[46] P. A. Stolk, H.-J. Gossmann, D.J. Eaglesham, D.C. Jacobson, C.S. Rafferty, G.H. Gilmer, M. Jaraiz, J.M. Poate, H.S. Luftma, and T.E. Haynes, *J. Appl. Phys.* **81**, 6031 (1997).

[47] M.D. Giles, *J. Electrochem. Soc.* **138**, 1160 (1991).

[48] M. Lannoo and J. Bourgoin, in *Point Defects in Semiconductors I* (Springer, Germany, 1981), Chap. 7, p.219.

[49] U.M. Gosele and T.Y. Tan , in *Materials Science and Technology* edited by R. W. Cahn, P. Haasen, and E.J. Kramer (VCH, New York, 1991), Vol.4, p.197.

[50] K. K. Larsen, V. Privitera, S. Coffa, F. Priolo, S. U. Campisano, and A. Carnera, *Phys. Rev. Lett.* **76**, 1493 (1996).

[51] V. Privitera, S. Coffa, F. Priolo, K. K. Larsen, and G. Mannino, *Appl. Phys. Lett.* **68**, 3422 (1996).

[52] M. Jaraiz, G. H. Gilmer, J. M. Poate, and T.D. de le Rubia, *Appl. Phys. Lett.* **68**, 409 (1996).